1-1-2003

Experimental and theoretical studies of composite multiple-box girder bridges

Anwar Androus
Ryerson University

EXPERIMENTAL AND THEORETICAL STUDIES OF COMPOSITE MULTIPLE-BOX GIRDER BRIDGES

BY

Anwar Androus, B. Eng

Ryerson University, 2001

A Thesis

Presented to Ryerson University

In partial fulfillment of the

Requirements for the degree of

Master of Applied Science

In the program of

Civil Engineering

Toronto, Ontario, Canada, 2003

Your file Votre référence
ISBN: 0-612-87149-5
Our file Notre référence
ISBN: 0-612-87149-5

AUTHOR'S DECLARATIONS

I hereby declare that I am the sole author of this thesis.

I authorize Ryerson to lend this document to other institutions or individuals for the purpose of scholarly research.

Anwar Androus

I further authorize Ryerson University to reproduce the document by photocopying or by other means, in total or part, at the request of other institutions or individuals for the purpose of scholarly research.

Anwar Androus

BORROWERS PAGE

Ryerson University requires the signatures of all persons using or photocopying this thesis.

Please sign below, and give address and date.

ABSTRACT

Experimental and Theoretical Studies of Composite Multiple Box Girder Bridges

Anwar Androus
2003, MASc, Department of Civil Engineering Ryerson University

Due to their high torsional and wrapping stiffness as well as economic and aesthetic reasons, multi spine composite concrete-deck steel-box girder bridges became a very popular choice in highway bridges. Currently, North American Codes of Practice have recommended some analytical methods for the design of curved multiple-box girder bridges, providing a geometrically defined criterion to establish when horizontally curved may be treated as a straight bridge. To meet the practical requirements arising during the design process, a simple design method is needed for straight and curved composite box girder bridges in the form of load distribution factors. This study consisted of an experimental and a theoretical investigation. The experimental investigation included testing up-to-collapse three bridge models. While the theoretical investigation used a finite element software to examine the behavior of 225 different bridges to extract stress distribution factors for maximum bending stresses that occur at the mid span.

ACKNOWLEDGEMENTS

I wish to express my deep appreciation to my advisor Dr. K. Sennah at Ryerson University, for his constant support and valuable supervision during the development of this research. Dr. Sennah devoted his time and effort to make this study a success. His most helpful guidance is greatly appreciated.

To my colleagues and friends, thanks for the memorable times we had over the past six years.

The author wishes to thank N. Jalouk and D. Peneff for their assistance in the experimental work.

The author is also very grateful to his parents and brothers for their great support and encouragement during the course of this study.

DEDICATION

TO MY FAMILY

TABLE OF CONTENTS

NOTATIONS

A	bridge width
B	Box width
C	steel top flange width
D	total depth of the steel boxes
[D]	constitutive matrix or elasticity matrix
DLA	dynamic load allowance
D_σ	stress distribution factor for straight bridges
E	modulus of Elasticity
F	total depth of composite bridge
I	moment of inertia
[K]	structure of global stiffness matrix
L	centre line span of simply supported bridge
M	applied moment
N_b	number of boxes
N_L	number of lanes
N	modular ratio
[P]	applied loads vector at the nodes
R	radius of curvature of center span of any bridge
t_1	thickness of steel top flange
t_2	thickness of steel web
t_3	thickness of steel bottom flange

t_4	thickness of concrete deck slab
[U]	Displacement vector at the nodes
W1	Outer web of outer box girder in any bridge model
W2	Inner web of outer box girder in any bridge model
W3	Outer web of inner box girder in any bridge model
W4	Inner web of inner box girder in any bridge model
y_b	Distance to neutral axis from bottom of composite beam
y_t	Distance to neutral axis from top of composite beam
α	The generalized coordinates
φ	displacement function
υ	the internal displacement vector of the element
Φ	Rotation (degree of freedom)
$(\sigma_b)_{max}$	maximum stress in bottom flange fibers obtained from finite element analysis
σ_b	maximum stress in bottom flange fibers obtained from simple beam theory

LIST OF TABLE

LIST OF FIGURES

CHAPTER I

INTRODUCTION

1.1 General

In structural design it is necessary to obtain an appropriate geometric shape for the structure so that it can safely carry the loads imposed on it. In densely populated cities elevated freeways and multi-level interchange structures are necessary. Nowadays, horizontally curved bridges became an important component in highway bridges, especially where tight geometric restrictions are often encountered. Curved bridges allow smooth traffic flow and create a painless directional transition at interchanges. This directly results in fewer traffic jams, less air pollution due to idle-car emissions, and less road rage. However, the older types of curved bridges such as beam bridges were not economical for long spans because of the rapid increase in the ratio of dead load to total design load as the span length increases. In dealing with this problem, the hollow concrete and concrete-steel composite bridges usually referred to as box-girder bridges were developed. Because of its well-known structural advantages such as light dead weight (compared to similar I-girder bridges), having shallower depth of cross-section, and having significant longitudinal bending and torsional stiffness, the box girder bridges became a popular solution for medium- and long-span bridges in modern highways and even in railway bridges. Also, box girder bridges have more resistance to vibration effects caused by live load than classical bridges. In addition to their obvious structural benefits, the surface inside the box girder bridges is closed from the outside environment. Theses boxes can be used to carry the required utilities which are aesthetically more pleasing and at the same time this minimizes the surface area vulnerable to environmental conditions compared to open-section bridge. In

this manner maintenance costs could also be minimized throughout the life of the structure. Due to their advantages, curved box-girder bridges became widely popular in modern highway bridges and interchanges in large urban areas. Due to their increasing use in modern highways, the impact of curved bridges, both socially and economically is just cause for the intense research, which has been performed in previous years and its continuation today.

Generally, bridges can be constructed entirely from reinforced concrete, pre-stressed concrete, steel, or composite concrete deck-steel girders. These bridges may be comprised of a concrete slab deck or steel deck on concrete or steel box girders or I-girders. Steel box girders are constructed as segmented cantilevers, they are prefabricated in long lengths and in most cases lifted into position by climbing jacks and connected together. The slabs could be of steel or reinforced concrete. In the case of curved steel plate girders, as shown in Fig. 1.1, there are two fabrications methods that are usually employed. The first method involves cutting curved flanges from straight plates to the required curvature and then welding them on the mechanically bent plates or webs which are curved. The second method involves prefabrication of straight webs followed by either cold-bending or heat-curving in which a straight girder is curved to the stipulated radius by applying heat to the edges of the flanges to achieve the required curvature. This actual curving of girders has allowed greater span lengths, fewer piers, and more aesthetically pleasing structures than straight girders used as chords in forming a curved alignment. Concrete box girders are usually cast in-situ or precast in segments which are erected on falsework or launching frame and prestressed.

A box girder bridge is supported by abutments and piers in the same way as a simple or continuous beam bridge. The span may consist of a top and a bottom flange plates in the case of steel box girders or otherwise top and bottom concrete slabs connected together by a series of cylindrical or conical webs to form the closed structure. This creates voids or "boxes". Box girder cross-section may be composed of one or a few cells which are either continuous or separated. In most cases the interior cells have a rectangular shape while an edge cell has vertically inclined or rounded outside webs. Box girder bridges may have one cell (one box) or many cells (separate boxes) or even or multi-cell with a common bottom flange (contiguous cells or cellular shape). Examples of this can be seen in Fig 1.2. In shorter spans, the box girder is usually of uniform depth. In longer spans, the depth is usually variable, as shown in Fig 1.3, and is accomplished by varying the depth of the webs to provide a curved surface under the bridge.

A two box girder bridge cross-section is shown in Fig. 1.4, while a view of a prototype twin-box girder bridge is shown in Fig 1.5. It consists of composite construction of concrete deck and steel boxes. The steel box consists of two top flanges and common bottom flange connecting to the top flanges by webs. Shear connectors connecting the steel top flanges with the concrete deck slab ensure full interaction between them. Solid end-diaphragms are used at the support lines. While cross-bracings and top chords (lateral ties to the steel top flanges) made of steel are used between the support lines.

1.2 The Problem

Currently, the Canadian Highway Bridge Design Code, CHBDC, (66) recognizes plan curvature as a factor affecting the structural behavior of bridges. However, the North American Codes of Practice recommend only analytical methods for the design of straight composite multiple-box girder bridges and provide a geometrically defined criterion to establish when horizontally curved may be treated in a similar way as straight bridges. In both cases, there is no practical design method in the form of expressions for moment and shear distributions factors. Also, since the structural response of curved bridges is different from the straight ones, different design considerations and expressions are needed for curved composite multiple-box girder bridges. Therefore, to meet the practical requirements arising during the design process, a simple design method is needed for straight and curved composite multiple-box girder bridges in the form of load distribution factors for stresses, shear, deflection and reactions as well as expressions for the dynamic load allowance.

On the basis of the literature review on curved multiple-box girder bridges, experimental test data up-to complete-collapse on curved composite multiple-box girder bridges is yet unavailable.

1.3 Objectives

The objectives of this study are:

1. To provide experimental data up-to-complete collapse on curved and straight

composite multiple box girder bridges. This data will include results from free-vibration testing to obtain bridge natural frequencies.

2. To develop simplified design method of straight and curved composite multiple box girder bridges in the form of load distribution factors for longitudinal bending moment.

In this thesis, a detailed analytical and experimental study on straight and curved composite multiple box girder bridges is presented. Analysis was based on the finite-element method. The main key parameters studied were: bracing system, bridge aspect ratio, number of lanes, number of boxes, degree of curvature and loading conditions.

1.4 Scope

The scope of this study includes the following:

1. A literature review of the experimental and theoretical research work, field testing, and codes of practice for straight and curved box girder bridges.
2. An experimental study on three composite concrete deck-steel twin-box girder bridges of different curvatures and, number of cross-bracings between boxes.
3. Comparison of the experimental findings and the analytical predictions using finite-element method with the commercially available "ABAQUS" software, and
4. Using ABAQUS software, an extensive parametric study on 180 curved and 45 straight composite box girder bridges was conducted, the analysis was performed to evaluate their load distribution factors for longitudinal bending stress under dead and live CHBDC truck loading.

1.5 Contents and Arrangement of this Study

In chapter 2, some previous work and literature review on box girder bridges is presented. Chapter 3 shows the experimental program conducted on three composite twin-box girder bridge models. This chapter includes the model details, setup of the testing performed, instruments used to load and obtain the resulting data. Chapter 4 includes a description of the finite element program "ABAQUS", the linear static analysis, and idealization and modeling of the composite bridge components. Chapter 5 presents the discussion of the results obtained from the experiment program as well as from the finite element verification including free-vibration analysis for the experimental bridge models. Chapter 6 provides a description of the prototype bridges used in the parametric study as well as the loading cases considered in the study. It also includes description of the parametric studies performed in this research work. Chapter 7 shows the results of the parametric study performed. Chapter 8 summarizes the findings of this research, outlines conclusions reached, and recommendations for further future research.

CHAPTER II

LITERATURE REVIEW

2.1 General

In the past, a significant amount of research was conducted to predict the behavior of different types of box girder bridges in the elastic range. However, only few teams have undertaken experimental studies to investigate the accuracy of existing design methods. Due to the curvilinear nature of box girder bridges, along with the complex deformation patterns and stress fields developed form different boundary conditions and loading cases, approximate and conservative methods for static and dynamic analysis posed a challenge for designers. The literature survey conducted is presented in the following manner:

1. Box girder bridges during the construction phase
2. Experimental studies on elastic response of box girder bridges
3. Ultimate response of box girder bridges
4. Dynamic response of box girder bridges
5. Load distribution and codes of practice for box girder bridges.

2.2 Box Girder Bridges during the Construction Phase

During the construction phase of box girder bridges, under variable construction loads high distortion or twist can occur due to the flexibility of the bottom webs and flanges in torsion. In straight right-angled bridges, cross frames and diaphragms act as secondary members to maintain structural integrity of the bridge. However, in horizontally curved bridges, due to their interaction between the webs and bottom flanges, cross frames and

diaphragms become major load-carrying elements (primary elements) under the torsional and bending loads. Up to date, very little experimental and analytical studies have been conducted on the behavior of curved bridges during the construction phase.

In the past, bridge such as the Yarra Bridge in Australia, the Rhine River Bridge in Koblens, the fourth Danube Bridge in Vienna, the Milford Haven Bridge in Wales suffered damages or failures during the construction phase (12). Such failures led to questioning the basis for the design of box girder bridges. In 1976, elastic experimental testing was performed by MacDonald et al. (56) on two single-cell steel girder models under concentric and eccentric loading. These models had top lateral bracing and varied the number of cross-bracings. Open cross section models with top lateral bracing were analyzed as equivalent closed box section with a top steel plate by using a concept introduced by Dabrowski (28) in 1968. The experimental findings were very close to the analytical results. In 1978, the United State Steel USS (91) reported some problem that are faced during the construction phase of steel box girder bridges, some of theses problems included excessive rotation of the girders before and during the placement of the concrete slab deck. In 1985, Branco & Green (13) performed experimental work on a series of simply supported scale models single cell and interconnected box girder bridges. The main purpose of their work was to study the effects of construction loading, bracing configuration and overall stability and deformation on torsionally open and quasi-closed box girder bridges. Results from this work were compared with analytical studies based on both the torsion-bending analysis of open and quasi-closed sections and finite-strip method. In 1989, Schelling et al. (76) performed an analytical study to examine the response of curved multi-I-girder system subjected to its

self-weight loading and the weight of the concrete deck before hardening. His study included three-dimensional space frame modeling. Results from his work included general dead load distribution factors, which may apply to various popular erection schemes, in order to prevent over-stress during the construction phase when shoring is not required. In 1996, Davidson et al. (29) used the finite element method to conduct a study on the warping stresses encountered in the horizontally curved steel I-girder bridges, however his study only examined the influence cross bracings effect on minimizing the wrapping stresses developed in the steel flanges just after pouring of the concrete deck.

2.3 Experimental Studies on Elastic Response of Box Girder Bridges

In general, the objectives of the experimental work mentioned in this section were mainly to verify and validate the accuracy of computer programs and available methods adopted to investigate the structural behavior of box girder bridges. Till now, reported elastic field testing of box girder bridges remains limited to a few.

In 1975, Kissane and Beal (50) performed a test on a horizontally curved composite concrete deck-steel bridge located on the Avoca-Bath section of the Southern Tier Expressway, carrying it over the Genes-see Expressway, in Steuben County, New York. The bridge was a three-spine two-span continuous box bridge. One year later, Yoo et al. (96) conducted similar testing on a three-span continuous curved composite concrete deck-steel twin-spine box girder bridge located in the I-695 and I-83 interchange near Baltimore. In 1975, Evans and Rifaie (32) performed an experimental work on box girder bridges. In this work, eighteen simply-supported single-cell models of different curvatures were tested elastically to validate results obtained from the finite-element method. Most of these models

were built of steel plates and the rest were built of the sand/araldite material. Rigid end-diaphragms were provided only at the models ends. Also, Aslam and Godden (7, 8) conducted experimental work on a series of aluminum small scale straight, skew, and curved four-cell box girder bridge models. By applying a single point load at different locations along the span, these models were tested elastically both with and without a mid-span radial diaphragm. In 1979, Brennan and Mandel (14) tested elastically small-scale horizontally curved I-girder and composite concrete deck-steel multi-spine bridge models. Data from this work was collected for possible future analysis and comparisons. Using this data and based on folded plate method, finite-strip method, and finite-element method Scordelis (81) summarized five representative bridge models to verify the elastic solutions. Scordelis et al. (74, 75, 76) also performed tests on three (straight, curved, and skewed) large scale reinforced concrete, two-lane, four-cell box girder models. These models were continuous over a central column support. Dead and live loads at working stress, and ultimate loading level to failure were applied on these models. Also in 1982, Buckle and Hood (17) tested a curved two-span continuous, single cell, laboratory scale model under point load in different locations at the mid-span cross-section. The tested model consisted of segments of filled-epoxy resign and of diaphragms over the supports. The model was prestressed with a draped parabolic profile.

In 1972, Heins and Bonakdarpour (39) performed elastic testing on a small scale curved three-spine box girder bridge model made of plexiglass. His work examined the applicability of the slope deflection theory that is based on the Vlasov's thin-walled beam theory, considering neither cross-section distortions nor warping. In 1976, Fam and Turkstra

(34) conducted an investigation on two, single-cell, plexiglass models having high curvature to investigate the effects of intermediate diaphragms and the adequacy of the three-dimensional finite-element modelling of curved single-cell structures. In 1987, Xi-jin and De-Rong (94) tested elastically a prespex model of three span continuous curved, two-cell, box girder bridge model to verify the accuracy of the finite-strip method in predicating the behavior of curved multi-cell bridges. In 1988, Siddiqui and Ng (85) tested elastically two straight plexiglass, single cell, box girder bridge models to determine the effect of transverse diaphragms on the behavior of the box section under concentric and eccentric point loading. In 1990, Mirza et al. (58) performed static and dynamic tests on two 1/7 scale model bridges. Both of these models were simply supported prestressed concrete bridges, the first had one-cell and the second had two-cells, the main purpose of his work was to provide experimental data on the linear and non-linear response of concrete box girder bridges at different levels of concrete cracking damage. In 1992, Ng et al. (61) conducted experimental study on 1/24 linear scale model of the Cyrville Road bridge overpassing the Queensway, east of Ottawa. The model was a curved four-cell box girder bridge made of concrete and aluminum. The model was continuous over the central support and was tested elastically under various OHBD truck loading conditions.

2.4 Ultimate Response of Box Girder Bridges

In all pervious mentioned experimental and theoretical work done on box girder bridges, only few dealt with the non-linear behavior to collapse as well as the local buckling of individual steel plates of straight and curved box girder bridges. In 1973, Abdel-Sayed (2) investigated the problem of the critical limit of loading and pre-buckling behavior for webs

of curved girders under combined loading due to shear and normal stresses. In 1979, Heins and Humphreys (40) performed up to failure testing on a series of box beam models; the models were loaded using a combination of increasing torsional and bending forces. These models were composed of top steel flanges, steel webs, steel bottom flange, and cross-bracings. Only some of the models had a concrete deck slab. Results of this work were used to verify the classical torsional theory in the elastic range and to develop a non-dimensional equation to expedite the load factor design of curved steel box girders.

In 1984, Seible and Scordelis (81) developed a numerical method and a computer program to trace the nonlinear response of multi-cell reinforced concrete box girder bridges under increasing static loading. The non-linearities considered were concrete material non-linearities such as cracking of concrete, yielding of the reinforcement, formation of plastic hinges due to shear and moment, and crushing of concrete. A three-dimensional grillage model has been used in order to minimize the computer effort. The results from the this technique were compared well with results from a two-span, four-cell, reinforced concrete box girder bridge, tested to collapse by Scordelis et al. (80). In 1985, Perry et al. (70) and Pinkney et al. (71) tested to complete collapse a 1:12 scale prestressed concrete bifurcated box girder bridge model. The model represented a four-lane carriageway bifurcating into three- and two-lane spans, and was of typical single and two-cell box girder construction, incorporating large scale cantilevers. The bridge, highly curved in plan, was continuous over the central supports and torsionally restrained at the three outer supports. Similar study was conducted by Owens et al. (69) but on curved composite concrete-deck steel multi-spine box girders assemblage.

In 1986 and 1988, Choudhury (25) and Choudhury and Scordelis (26) combined the Bazant-El Nimeiri, and Zhang-Lyons models to develop a curved non-prismatic thin-walled single-cell box beam element for nonlinear analysis of reinforced and prestressed concrete box girder bridges. In 1988, Mari et al. (55) developed a straight box-beam of non-deformable cross-section composed of concrete panels with steel layers to model curved prestressed box girder bridges. In 1989, Razaqpur and Nofal (73) constructed a finite-element computer program to predict the materially non-linear behaviour up to collapse of structures made of plain concrete, reinforced concrete, prestressed concrete, steel, and composite concrete-steel. 1/7 Scale models of single-cell and two-cell prestressed concrete box girder bridge models, tested to destruction by Mirza et al. (59) were analyzed using the proposed nonlinear technique. In 1989, Lopez and Aparicio (54) developed similar mathematical model for nonlinear analysis of reinforced and concrete structures. A Prestressed concrete curved, double-trapezoidal-cell, curved bridge, located at the Santamarca junction in La Paz Highway in Madrid, Spain, was used to present the application of the proposed model. The bridge consisted of five-span continuous construction with radius of 103.5 m and total length of 155.56 m. In 1993, Ng et al. (62) developed similar finite-element program to trace the nonlinear response of only reinforced concrete structures. A two-span, four-cell, reinforced concrete box girder bridge, previously tested by Scordelis et al. (80), was used to compare with this analysis.

In 1994, Soliman and Elmekaway (87) conducted a nonlinear finite-element analysis to investigate the effect of bottom slab provided near the intermediate support region on the deformation behaviour of reinforced concrete girder type bridges. In 1994, Soliman and Ghali (86) extended the theoretical study using a nonlinear finite-element technique to examine the effect of the intermediate diaphragms and end-diaphragms on the behaviour of short, medium, and long span, single-cell, box girder bridges. In 1995, Yabuki et al. (95) presented a numerical method for predicting the influence of local buckling in component plates and distortional phenomenon on the nonlinear behaviour and ultimate strength of thin-walled, welded steel box girders curved in plan and stiffened by intermediate diaphragms. The theoretical predictions obtained using the proposed method were compared to experimental test results of two large-scale curved steel box girders with different numbers of interior diaphragms. On the basis of the literature review on curved bridges, experimental test data up to complete collapse on curved composite box girder bridges is as yet unavailable.

2.5 Dynamic Response of Box Girder Bridges

With rcent advancements in materials over the past three decades, the development of newer high strength materials such as high strength steel has lead to the use of more slender members in bridges. Along with the benefits of longer spans that can be achieved with theses new materials, excessive dynamic deflections and or vibrations can occur due to heavy truck loading, wind or seismic excitations. This can be a discomfort to riders and pedestrians traveling on such bridges. To solve this problem, analytical and experimental studies have been and still are being conducted to study the dynamic response of box girder bridges.

In 1967 and 1972, Culver (27) and Shore and Chaudhuri (84) used a closed form-solution of the equation of motion to study the effect of transverse shear deformation and flexural rotatory inertia on the natural frequencies of a horizontally circularly curved beam. Such a study used the differential equation of motion for a freely vibrating horizontally circular curved beam. In 1968, Tan and Shore (89, 90) used the differential equations that represent the out-of-plane vibrational motion of a horizontally curved beam to model a simply-supported horizontally curved girder bridge by idealizing the bridge as a slender, prismatic curved beam subjected to a moving force of constant magnitude. In 1966 and 1970, Komatsu and Nakai (52,53) used the fundamental equation of motion along with the Vlasov's thin-walled beam theory to conducted several studies on the free-vibration and forced-vibration of horizontally curved single-box, and twin-box girder bridges. They also used results of experimental data from tests on existing simply-supported and continuous

box bridges in Japan to verify their theoretical analysis. In 1972, Cheung and Cheung (24) described the application of the finite-strip method to determine the natural frequencies and mode shapes of vibration of straight and curved box-girder and beam-slab bridges.

In 1972 and 1973, Tabba (88) and Fam (33) used the finite-element method to apply dynamic loads in order to determine the behavior of curved box section bridges. They also performed experimental work on two curved two-cell box girder plexiglas models which confirmed the reliability of the proposed analysis methods. In 1975, Rabizadeh and Shore (72) presented a finite-element method for the dynamic analysis of curved multiple box girder bridges, which formed the basis for the previous impact factor adopted by the American Association of State Highway and Transportation Officials (AASHTO, Guide Specification 1980) (5). In their research, Rabizadeh and Shore used two sets of concentrated forces to simulate a moving vehicle; the moving vehicle had component forces in the radial and transverse directions and moved with constant angular velocity on circumferential path of the bridge. In 1981, Heins and Lee (42) presented the experimental results obtained from vehicle-induced dynamic field testing of a two-span continuous curved composite concrete deck-steel single cell bridge, located in Seoul, Korea.

In 1984, Billing (11) summarized the results of dynamic testing done in 1980 on 27 bridges of various configurations and span lengths. Results from this study formed the basis for the dynamic load allowance adopted by the Canadian Standard Association, CAN/CSA-S6-88, (18) and the Ontario Highway Bridge Design Code, OHBDC second edition 1983, (67). This dynamic load allowance, DLA, was calculated on the basis of the flexural beam

theory and depends on the bridge first flexural frequency. However, this dynamic load allowance/frequency relationship was revised in the third edition of the OHBD code, 1992, (67) as well as the CHBD code, (66). The new DLA was to be a constant value depending on the number of axles. In 1997, Akoussah et al (3) questioned this new revision. Using three-dimensional finite element modeling, Akoussah et al. investigated the interaction between vehicle and the bridge and then the dynamic amplification factor of simply-supported reinforced concrete bridges of spans of 20 to 32 m. The bridge code of the American Association of State Highway and Transportation Officials, AASHTO 1996, (6) has traditionally applied an impact factor depending only on the bridge span.

In 1985, based on the predetermined mode shape function, Chang et al. (19) used a method developed by Rayleigh-Ritz to predict the seismic response of a single, two, three and four-span continuous curved girder bridges, supported on single pier bents. In 1985 and 1986, Mirza et al. (59) and Cheung and Mirza (23) conducted both a theoretical and experimental investigation on the influence of bracing systems on the dominant frequency of composite concrete steel model bridge. The theoretical part was based on using the finite-element method. The experimental part was performed by building one straight composite twin box girder bridge model. The model was continuous over two spans, with varying depth at the intermediate support. The study investigated only the bridge's fundamental frequency. In 1987, Inbanathan and Wieland (47) presented an analytical investigation on the dynamic response of a simply-supported box girder bridge due to a moving vehicle over a rough deck surface. They found that the stresses developed by a heavy vehicle moving over a rough surface at high speeds exceed those recommended by

current bridge design codes. In 1988, Abdel-Salam and Heins (1) presented the results of a comprehensive study of the seismic response of curved continuous composite concrete-steel multiple box girder bridges. The El Centro earthquake ground motion acceleration record and its corresponding response spectrum were used as dynamic input and the bridge was modeled using three-dimensional space frame elements in which special elements were introduced to account for the curved geometry and boundary conditions. The study showed that the higher modes of vibration have a significant effect on the seismic response of this type of bridges.

Based on a planar grid finite-element analysis, in 1988, 1990, and 1992, Galdos (36), Galdos et al. (37), and Schelling et al. (75) studied the dynamic response of horizontally curved multi-spine box girder bridges, of different spans. In their work, a moving vehicle is represented by two constant forces, with no mass, traveling with constant angular velocity along the same curvature as the bridge. From their findings, the current impact factors currently used by AASHTO (Guide specification for horizontally curved highway bridges, 1993) for curved multi-spine box girder bridges were developed (5). In 1990, Mirza et al. (58) conducted free-vibration tests on two prestressed concrete simply-supported bridge models. The first model was one-cell and the second was a two-cell box girder bridge model. In this study, the fundamental frequency of vibration and damping ratios of the bridge models at different levels of cracking damage, were examined. These dynamic characteristics could be used to estimate the cracking damage in the bridge. In 1991, Cheung and Magnount (22) used the finite-element method to investigate the influence of diaphragms, cross-bracings, and bridge aspect ratio on the dynamic response of a straight

twin-box girder bridge of 45 m span. In 1990 and 1992, Kashif and Humar (50), and Kashif (49) developed a finite-element technique to analyze the dynamic response of simply-supported multiple box girder bridges considering vehicle-bridge interaction.

In 1993, Richardson et al. (74) presented the results of a field test, using simulating earthquake loads, on a curved highway overpass of box girder cross-section. In the test, large horizontal loads were applied to the superstructure of the bridge and quickly released, causing the bridge to vibrate. The vibration modes were used to verify the analytical model of the bridge dynamic response. The model was verified using only the fundamental vibration mode, which was primarily a horizontal vibration mode.

In 1995, Huang et al. (45) studied the dynamic response of curved I-girder bridges due to truck loading. In this work, Huang et al. (46) presented a method for obtaining the dynamic response of thin-walled box girder bridges subjected to truck loading. The box girder is divided into a number of thin-walled beam elements. Both warping torsion and distortion were considered in the study. Four different classes of road-surface roughness generated from power spectral density function for very good, good, average, and poor roads were used in the analysis. The analytical results show that the dynamic response is greatly affected by the higher modes. In 1996, Wang et al. (92) studied the free-vibration characteristics and the dynamic response of three-span continuous and cantilever thin-walled single-cell box girder bridge when subjected to multi-vehicle load moving across a tough bridge deck. Results showed that the continuous-and-cantilever bridge with only one hinge at mid-span is much more susceptible to vibration than that with middle suspension

span. In 1997, Senthilvasan et al. (82) investigated the bridge-vehicle interaction in curved box girder bridges. In their investigation Senthilvasan et al. combined the spline finite-strip method of analysis and a horizontally curved folded-plate model to perform the analysis.

2.6 Load Distribution and Codes of Practice for Box girder bridges

Due to their larger torsional stiffness, bridges of concrete deck over steel boxes are more efficient and economical than those of composite steel-concrete I-girders. Composite box girder bridges exhibit better transverse load distribution than the usual composite steel-concrete I-girders. Below is a summary of the research work done on load distribution of different composite bridge types.

The effect of cross-bracing on the warping and bending stresses of curved I-girders were first studied by Yoo and Littrell (97) in 1985 by using a full three-dimensional finite-element model. In 1986, Brockenbrough (16) also used the finite-element modeling to reach load distribution factors, including warping effects, of curved composite I-girder bridges as a function of the span length, radius of curvature, girder spacing, and cross-bracing spacing. In 1967, and 1968, Johnston and Mattock (47), and Fountain and Mattock (35) studied the lateral distribution of load in simple span composite multiple box girder bridges without transverse diaphragms, they used a computer program for the analysis of folded plate structures. Also, experimental work was done to verify the analysis and computer program. In the experimental work, two bridges were built, the first is a one-quarter scale, two-lane, 80 ft span bridge supported by three box girders, the second is a fifth scale model of a two-lane, 100 ft span bridge supported by two box girders. Both bridges were built and tested under concentric and eccentric AASHTO truck loadings. Results from their work were used to develop expression for the only live load bending moment distribution factor for each box girder as a function of the roadway width, and number of boxes. The summary of their

results formed the basis for the lateral distribution of loads for bending moment currently used by AASHTO, 1996 (6) and the first two editions of the Ontario Highway Bridge Design Code (OHBDC 1979; OHBDC 1983) for multi-spine box girder bridges. However, this expression did not take into account the beneficial effect of the cross-bracing inside and between the boxes. It also limited the application to bridges where the number of spines was the same as the number of lanes. The AASHTO LRFD, 2000 (4) provides another expression for load distribution at ultimate limit state to obtain the live load bending moment and shear force in each box of the multiple box girder bridge cross-section.

In 1985, and 1992, Bakht and Jaeger (9, 10) proposed a load distribution factors for bending moment and shear, which forms the basis for live load distribution used by the third edition of the OHBDC, 1992, (68) for multi-spine bridges. Their work was based on multi-spine bridges having at least three spines, zero transverse bending stiffness, and load transfer between the various spines through transverse shear. In 1994, Normandin, and Massicotte (63) determine the distribution patterns in multi-spine box girder bridges with different characteristics and geometry by using the results of a refined finite-element analysis. In their work, they considered parameters such as: the type of live load, the use of external bracing, and the presence of the internal diaphragms. Their investigation proved that internal diaphragms, inside boxes, are essential components in box girder since they largely reduce distortion of the cross-section under different loading. They also found that in the case of a fully loaded bridge, the external bracing between boxes does not significantly influence the distribution characteristics for bending moments and shear. Their results also indicated that, in some cases, both OHBDC, 1992, and, AASHTO, 1996, distribution factors under predict

the live load effects by a significant amount. However, the proposed method is also limited to bridges having the same number of spines as lanes.

In 1978, Heins (38) proposed a modification factor which would extend the applicability of the straight multiple box girder moment distribution equation provided by Fountain and Mattock (35) to horizontally curved composite multiple box girder bridges. The modification factor proposed is a function of the radius of curvature only in the case that cross-bracings are used inside the boxes. In 1980, Mukherjee and Trikha (60) used the finite-strip method and developed a set of design coefficients for moment, shear, transverse moment, and vertical deflection under webs for twin cell curved box girder reinforced concrete bridges. The coefficients served as an aid to practical design of such bridges. However, they were limited only to concrete bridges of two-lane, span length between 20 and 40 m, and radius of curvature between 45 and 150 m.

The AASHTO (Guide Specification for Horizontally Curved Highway Bridges, 1993) (5) is pertained to both curved composite concrete deck-steel I-girder bridges and multiple box girder bridges. The specifications for load distribution for both curved I-girders and multiple box girders were based on a design-oriented research work done by Heins and Jin in 1984 (41) on live load distribution of single and continuous curved composite I-girder bridges by a space frame idealization. The space frame modeling has incorporated the interaction of diaphragms (cross-bracing in the radial direction) and bottom lateral bracing in some or in all bays. Appropriate design equations were presented for use in conjunction with a plane grid solution. For both curved I-girders and curved multiple box girders, the AASHTO (Guide Specification for Horizontally Curved Highway Bridges, 1993) specifies

that the moments and shears required to proportion the individual members shall be based on a rational analysis of the entire structure which takes into account the complete distribution of loads to the various members. Moreover, if the rational analysis considers the system as a plane gird and not as a space frame and bottom lateral bracing is specified in some bays or in all bays, the code modifies the resulting maximum live load stresses, using Heins-Jin design equation, considering additional warping stresses beside the normal bending stresses.

In 1981, Davis and Bon (30, 31) presented correction factor for curvature for load distribution in concrete and prestressed concrete multi-cell box girder bridges. For the outmost girder (farthest from the centre of curvature), they proposed straight bridge load distribution just as it is without any modifications. For all other girders, this factor is a ratio of the distance from the centre of curvature to the girder-to-radius of curvature. However, this method did not consider the beneficial effect of the transverse diaphragm. In 1988, Nutt et al. (65) proposed a set of equations for moment distribution in straight, reinforced and prestressed concrete, multi-cell box girder bridges as a function of number of lanes, cell width, span length, and number of cells. In 1989, Ho et al. (44) used the finite-strip method to analyze straight simply-supported, two-cell box girder and rectangular voided slab bridges without intermediate diaphragms. Empirical expressions for the ratio of the maximum longitudinal bending moment to the equivalent beam moment were formulated. The span lengths of the bridges in this study were up to 40 m in case of two-lane, 50 m in case of three-lane, and 67 m in case of four-lane. However, the empirical expressions were developed only for straight two-cell bridge section made of either concrete or steel. In 1995,

Cheung and Foo (21) used the finite-strip method to develop expressions for the relative behaviour of curved and straight multiple box girder bridges as a function of span length, number of lanes, box spacing, and radius of curvature. In his study, there was no consideration made for the effect of number of boxes and dead load distribution. Also the beneficial effect of diaphragms inside the boxes and cross-bracings between boxes were neglected.

Using specified load distribution factors suggestions made by California design engineers in 1959. The AASHTO, 1996, (6) refined the specified load distribution factors for bending moment in straight reinforced concrete box girder bridges (S/8 for one-lane traffic and S/7 for two or more traffic lanes where S is the cell width). However, these distribution factors do not give any indication on the structural behavior of the bridge or the parameters influencing the response of the bridge. In 1991, Zokaie et al. (97) proposed other moment and shear distribution factors for reinforced and prestressed concrete multi-cell bridges. Their findings formed the load distribution factors for moment and shear currently used in AASHTO LRFD, 1994 (4) for straight concrete multi-cell bridges. In 1996, Brighton et al. (15) described a study to determine a live load distribution factor for a new type of precast concrete double cell box girders that was proposed for a prefabricated bridge system for rapid construction of short-span bridges.

The Canadian high bridge design code (66) provides no specifications or aids for the design of horizontally curved bridges including those of multiple box-girder cross-sections. Because of its high torsional-to-bending stiffness when compared to other I-girder cross-

sections, the multi-spine box girder bridge cross-section is one of the best solutions in sharply curved alignments to allow better load distribution characteristics and reduce material content in a structure. The American Association of State Highway and Transportation Officials, AASHTO 1996 (6) states that the curved bridge may be designed as a straight bridge if the central angle $\leq 12^{\circ}$. On the other hand, the Canadian Highway Bridge Design Code, CHBDC 2000, (66) states that for horizontally curved bridges, the effect of curvature may be neglected in structural design calculations as long as the L^2/bR ratio is less than 1.0, where L is the curved span length, b is half the bridge width, and R is the radius of curvature. These limitations are questioned in case of moment and shear in case of curved composite multi-cell bridges. Therefore, due to the lack of knowledge about the distribution of moment and shear in composite concrete-steel straight and curved box girder and multi-cell, research work is required.

Chapter III

EXPERIMENTAL STUDY

3.1 General

In curved box girder bridges, torsional moments and deformations are of great importance even for concentric loading. In order to develop a better understanding of the ability of behavior of box girder bridges under these loading conditions, an experimental work was performed at the Structural laboratory at Ryerson University. The experimental program was undertaken to investigate the behavior of curved and straight box girder bridges under static and free-vibration loading conditions, and the influence of curvature on the structural response. In the experimental program, bridge models were built and loaded up to failure. Results such as deflections and strains were recorded.

The main purpose of this experimental study was:

1. To use the experimental data collected in order to verify the structural response of the type of bridges predicted by the analytical modeling using the commercially available finite element "ABAQUS" software;
2. To obtain data related to the free-vibration response of such bridges;
3. To examine the nonlinear up-to-failure behavior of box girder bridges.

In this chapter a detailed description of the bridge models is presented including the geometry, material properties, construction of the models, instrumentation, test equipment,

and experimental setup. An outline of test procedure is later listed.

3.2 Description of the Bridge Models

The experimental program was carried out on Three 1:10 linear-scale composite concrete deck-steel twin-box girder bridge models under free-vibration, elastic and up-to-collapse loadings. All of the three models were simply-supported. Two of the models (M1 & M2) were curved in plan while the third one (M3) was a straight bridge. To study the effect of the presence of cross-bracing between boxes on the structural response, the first model M1 had five cross-bracing and top-chord systems between the radial support lines inside and between boxes, while the second model M2, of the same curvature as the first model, did not have any bracing systems between the boxes except at the support lines. To study the effect of curvature on the structural response, both the second and third bridges, had the same number of cross-bracing with the exception that the second model was curved while the third one was straight in plan. The details of the geometry are shown in some of the following sections.

3.2.1 Simply-Supported Curved Bridge Model (M1)

The first bridge was a 1:10 linear-scale twin-box girders bridge model; it was built and tested under three loading conditions. The bridge was simply-supported with composite construction of concrete deck and steel box girders. The cross-sectional dimensions are shown in Fig. 3.1. The concrete deck was 800 m wide, 35 mm thick, and was supported by two 111 mm deep steel box girders. The box girders consisted of two top flanges each 38×3 mm, four webs each 111×3 mm, and a common bottom flange 200×3 mm thick. Two

diaphragms, 3 mm thick, were placed at the extreme end sections in the radial direction of each box girder. Access holes measuring 50×50 mm were provided in each diaphragm. This model contained five braces inside the box girders equally spaced to section the girder into six equal sections, from support to support along the span. All braces had a top chord and two diagonal members crossing form corner to corner on a diagonal angle. This bridge model was also braced between the boxes dividing the span into six equal sections from support to support, and thus seven braces similar to the ones inside the boxes were used starting from one support to the other. Finally stiffeners were added at and between the support and the location of the first brace line on each side of the box girder, plan details of the locations of all the braces, stiffeners and diaphragm locations are shown in Fig. 3.2.-a. To fasten the concrete deck and the girders together, channel shear connectors were used with length of at 25 mm, and spaced at 125 mm, along each top flange. Two meshes of steel reinforcement, 100×100×3.2 mm directed tangentially and radially, were used in the concrete deck slab.

3.2.2 Simply-Supported Curved Bridge Model (M2)

The second simply supported bridge model M2 was very similar to bridge model M1. Both M1 and M2 models had the same overall dimensions and curvature. The only difference here is that no bracing was provided between the boxes except at the supports for bridge model M2. Figure 3.2-b shows the plan view details of the model.

3.2.3 Simply-Supported Straight Bridge Model (M3)

The last bridge model constructed was a straight composite concrete deck-steel twin-

box girder model. Just like the curved models, this one spanned 3000 mm from support to support at center, this model was the same as those for model M2 with the exception that it is straight in plan. It had braces between the boxes only at the supports and the rest of its details in terms of locations of stiffners, shear connectors, diaphragms and concrete deck were exactly the same as those for model M2. Plan view details of this model are show in figure 3.2-c.

3.3 Materials

Local available materials were used to construct all the bridge models used in this study.

3.3.1 Steel

All the steel plates were provided in sheets. Three coupon specimens were cut from the sheets and tested up-to-failure using a Universal Testing Machine. Figure 3.3 shows the dimensions of the specimens tested. Average stress-strain relationship for the tested coupons are shown in Fig. 3.4. The 3-mm plates had yield strength of 260 MPa, with a modulus of elasticity of 200 GPa.

3.3.2 Reinforcing Steel

The concrete deck slab for all the bridge models was reinforced by using two meshes of stainless steel reinforcement, 100×100×3.2 mm directed tangentially and radially. Three specimens of 300 mm long were tested in tension up-to-failure. The average stress-strain relationship for the tested specimens is shown in Fig. 3.5. The yield strength was

found to be 820 MPa, with a modulus of elasticity of 200 GPa.

3.3.3 Concrete

A ready mixed concrete having a 28 day minimum specified strength of 35 MPa was used for the concrete deck slabs of all bridge models. The cement was normal-strength Portland cement, CSA Type 10, manufactured by Canada Cement Company. Since the slab was only 35 mm thick, the aggregate used in this concrete mix had a maximum nominal size of 10 mm to ensure low air gaps between the concrete and steel mesh. Natural tap water was used in the concrete mix. The water-cement ratio of the mix was 0.45. Three standard cylinders were cast concurrently with the casting of the concrete deck slab of each model. The cylinders were kept beside the model bridges to ensure the same curing conditions after casting. The concrete cylinders were tested on the same day the bridge model was tested to determine the compressive strength. Table 3.1 shows the average compression strength of the concrete cylinders for each model.

3.3.4 Shear Stud Connectors

The channel shear connectors were welded to the top steel flange of the box girders at 125 mm spacing. The channels were welded on both sides of the contact area between it and the flange over the channel length of 25 mm. The channel was of 19 mm height, 3 mm flange width, 3 mm web thickness, and 25 mm web depth. Figure 3.6 shows a view of a channel stud welded on top of the flange in one of the bridge models.

3.3.4 Construction of the Bridge Models

Using the commercially available AutoCAD software, all the steel parts were plotted with one to one scale on 910 mm wide role of paper, then cut and taped onto the steel sheets. This was done to make the cutting boundaries of the different elements accurate. An electric cutter available at the workshop of the Civil Engineering Department was used to cut the plates and strips. To form the steel grid of each model, the webs, end-diaphragms, cross-bracings, and top flanges were first clamped in position and then spot welded to each other at first. They were then moved to a local steel welding and fabrication shop off campus to apply the welds along the full span. To minimize the heat generation problem that was encountered in the welding process, proper clamping and stabilization before welding were ensured. Also, the welds were applied in 50 mm increments and staggered along the span of the girders by careful utilization of 2 mm continuous welds using a medium-heat welding machine. The bottom flange plate of each model was then clamped to the steel grid and welded to the webs. Channel shear connectors, along the top flanges, were then welded. Views of all the bridge models after completion of the welding (non composite stage) are shown in Figs. 3.7 to 3.9.

Styrofoam insulation sheets measuring 2438 x 1219 x 25 mm are shown in Fig. 3.10. These sheets were used for the concrete stay-in-place formwork between the cells and on the outside of the cells. Small cubes of Styrofoam were placed inside the cells to support the Styrofoam sheets. Views of the formwork for the bridge models are shown in Figs. 3.11 to 3.13. After the forms were prepared, duck tape was put on all area to prevent leaking of the concrete mix between the form work and steel. Then, two meshes of steel reinforcement,

100×100×3.2 mm directed tangentially and radially, were placed over the formwork as shown in Figs 3.13 to 3.15. These steel meshes were formed by using common thin gauge tie wire to strap them at 100 mm spacing and were held apart by using bobby pins (Fig. 3.16) around the reinforcing steel mesh to keep the top mesh erected while the bottom mesh rested just on top of the flanges.

In the concrete slab pouring process, the concrete was poured from one end to the other for each bridge model. As the concrete was poured the top of the concrete slab was worked with a wooden 2x4" to obtain a level surface. The top surface of the concrete slab was then given smooth final finish by trowelling. Figures 3.17 to 3.20 show photos taken during the casting and finishing of the concrete work. Since it was not possible to continuously moist cure the concrete after it was poured and set, it was sprayed with water for the following four days to ensure a better hydration and prevent evaporation. After that, the bridge models were left to be air-cured till the testing time.

3.5 Instrumentation

3.5.1 Strain Gauges

To measure the strain on the top surface of the reinforced concrete slab of the bridge models, electrical strain gauges, type KFG-30-120-C1-11, were used. The concrete strain gauges had a length of 30 mm, a resistance of 120±2% ohms, and a gauge factor of 2.11±1%. In order to measure the strain on the outer sides and bottom of the steel box girders bridge models, electrical strain gauges, types EA-13-250BG-120 and in certain cases EA-06-240LZ-120, were used. The first type of the steel strain gauges had a length of 13

mm, a resistance of 120.0 ohms, and a gauge factor of 2.09±0.5% (figure 3.21). While the second type of the steel strain gauges had a length of 6 mm, a resistance of 120.0 ohms, and a gauge factor of 2.045±0.5%. However, it is important to note that the second type of strain gauges used (EA-06-240LZ-120) were only as a replacement in case of a defected gauge problem. These second type gauges were used only on three locations in bridge model M1 because the original stain gauges were not working properly. All the strain gauges were placed at the mid span of each bridge model. Figure 3.22 shows the locations of the concrete and steel strain gauges on the tested bridge models.

3.5.2 Linear Variable Displacement Transducers, LVDT's

Linear variable displacement transducers (LVDT's), of 50 mm electrical stroke, were used at various locations to measure deflections in all the models. In the case of the first two bridge models (M1 & M2) four LVDT's were mounted under the steel girders to collect deflection data for the determination of the natural frequency, and three LVDT's were mounted at three different locations at the mid-span locations to measure deflections during the loading stage. In the case of the third bridge, four LVDT's were mounted under the girders to measure displacements. In all cases, LVDT's were placed in locations at 0.25 and/or 0.5 of the span length. These locations for all bridge models are shown in Figs. 3.23 to 3.25.

3.5.3 Mechanical Dial Gauges

Where LVDT's were not possible to mount due to physical limitation, mechanical dial gauge having a travel sensitivity 0.01 mm were used to measure the deflections at mid-

span section. This was the case for the first two model bridges at the most outer web. The dial gauge readings were manually taken at each increment of loading throughout the test procedure.

3.6 Testing Equipment

3.6.1 Hydraulic Jack

A hydraulic jack having a capacity of 200,000 lbs was used for the application of the load. The jack was mounted on a w-shape steel member supported by a rigid portal frame as shown in Fig. 3.26.

3.6.2 Load Cells

One loading cell was used in this experimental work. A universal flat load cell, of 900 kN capacity, was used to measure the applied loads on all bridge models. Figure 3.26 shows loading cell mounted on the bottom of the hydraulic jack.

3.6.3 Automatic Strain Indicator

Automatic strain indicator supplied by Intertechnology was used to record the strain during the application of the loads. The strain indicator consisted of two devices: the V1E-21 switch balance and ten digital strain indicator SB-10. The SB-10 strain indicator unit was used to measure strains on top of the concrete surface in all bridge models.

3.6.4 Data Acquisition System

During natural frequency testing, the data from the LVDT sensors were captured by

a test control software (TCS) using a SYSTEM 6000 data acquisition unit. The test control software, TCS, is a powerful tool developed specially for acquiring; reducing and analyzing the dynamic analog data captured using the SYSTEM 6000. It simplifies the process for collecting and converting data captured by strain gauges and LVDT's. The TCS was adjusted to sample the data at a rate of 500 readings per second for the LVDT's during the natural frequency test and 10 readings per second during the loading process.

3.7 Experimental Setup and Testing Procedure

Each bridge model was supported at its ends by a simple system under each web. Figure 3.27 shows the details of the support under the web ends. A tie-down system was used over each support line to prevent any possible torsional uplift. The supporting system was firmly tied down to the supporting beams that the model bridges rest on to ensure that there is no uplift during loading. Figure 3.28 shows the testing setup. Figure 3.29 shows view of the tie down system of the bridge support line, while Fig. 3.30 shows a view of the tie down system to the bridge supporting beam. Each model was tested in three stages as follows:

3.7.1 Stage (1), Free-Vibration Tests on the Bridge Models

The free-vibration tests on all bridge models were performed by first mounting the LVDT's under the girders as described earlier. A round bowling ball, weighing 4.53 kg, was then dropped from a height of 0.5 m over the concrete deck along the centre line at 300 mm from the mid span. The LVDT's data captured by the SYSTEM 6000 data acquisition unit was fed into the test control software (TCS) for reduction into a ASCII format data file.

Using data analysis and display software called DADiSP, (DSP Development Corporation, www.dadisp.com), the ASCII files were fed into a Fast Fourier Transform, FFT. The FFT analyzer gave the spectrum response of the bridge in the frequency domain from which the natural frequencies of the models were deduced. The DADiSP software also yielded the magnitudes and phase angles for the mode shape.

3.7.2 Stage (2), Two point Concentrated Elastic Loading

In this stage of loading, the bridge models were tested elastically under two different cases of concentrated point loading applied at the mid span of all models. In the first case (Case I), two concentrated loads were applied on top of the webs of the outer girder. In the second case (Case II), two concentrated loads were applied on top of the webs of the inner girder. In both cases, the initial load applied was approximately at 2225 N then was moved up to 4500N. Figure 3.31 summarizes the above mentioned loading cases for all bridge models.

3.7.3 Stage (3), Loading the Bridge Models up-to-complete-collapse

Finally, each model was tested to failure using a four point loading arrangement (case III). In this case, four concentrated point loads were applied at the mid span, one at the top of each web, this type of arrangement can be seen in Fig. 3.31. For all the models, the load was applied at a constant rate in increments of 2.5 KN. After each increment, the load was maintained constant during recording of the deflections and strains. Moreover, the crack propagations in the top of the concrete deck slab were traced. After failure of each bridge model, the applied load was released slowly.

Chapter VI

FINITE ELEMENT ANALYSIS

4.1 General

The finite-element method is one of the most powerful methods of analysis available today. Because of recent development in finite-element method, it is now possible to model a bridge in a very realistic manner and to provide a full description of its structural response within the elastic and post-plastic stages of loading. One of the most important advantages of the finite-element method is its ability to deal with problems that have arbitrary arrangements of structural elements, material properties, and boundary conditions. Therefore, the finite-element method is very suitable for the analysis of curved composite box girder bridges. This chapter includes descriptions of the modeling of the different components of the composite box girder bridges. The finite element model includes the reinforced concrete deck slab, top steel flanges, steel webs, bottom steel flange, the solid end-diaphragms, the cross-bracings, and the top chords as described in subsequent sections in this chapter. The finite element program ABAQUS (43) was used throughout this study to determine the structural behavior as well as the free vibration response of the curved composite box girder bridges. A general description of this program is presented later in this chapter. The finite element method of structural analysis described herein was also employed to perform the parametric study on the static response of both straight and curved composite box girder bridges.

4.2 Finite Element Approach

The finite-element method is a numerical method for solving problems in engineering and mathematical physics. In structural problems, the solution is typically concerned with determining stresses and displacements. Finite element model give approximate values of the unknowns at discrete number of points in a continuum. This numerical method of analysis starts by discretizing a model. Discretization is the process where a body is divided into an equivalent system of smaller bodies or units (elements) interconnected at points (nodes) common to two or more elements and/or boundary lines and/or surface. An equation is then formulated combining all the elements to obtain a solution for one whole body. Using a displacement formulation, the stiffness matrix of each element is derived and the global stiffness matrix of the entire structure can be formulated by the direct stiffness method. This global stiffness matrix, along with the given displacement boundary conditions and applied loads is then solved, thus that the displacements and stresses for the entire system are determined. The global stiffness matrix represents the nodal force-displacement relationships and is expressed in a matrix equation form as follows:

$$[P] = [K][U] \tag{4.1}$$

Where:

[P] = nodal load vector;

[K] = the global stiffness matrix;

[U] = the nodal displacement vector;

The steps for deriving the above equation can be summarized in the following basic relationships:

(a) $\upsilon(x, y) = [\Phi(x, y)][\alpha]$ (4.2)

where:

υ= the internal displacement vector of the element.

φ= the displacement function.

α= the generalized coordinates.

(b) $[U] = [A][\alpha]$ *then,* $[\alpha] = [A]^{-1}[U]$ (4.3)

Where [A] is the transformation matrix from local to global coordinates,

(c) $[\varepsilon(x, y)] = [B(x, y)][\alpha] = [B(x, y)][A]^{-1}[U]$ (4.4)

Where:

[B(x,y)]= the strain-displacement matrix.

[ε(x,y)]= the strain matrix.

(d) $[\sigma(x, y)] = [D][\varepsilon(x, y)] = [D][B(x, y)][A]^{-1}[U]$

Where; [D] is the constitutive matrix or the elasticity matrix. From the principle of minimization of the local potential energy for the total external work equal to 1/2 $[U]^T[P]$, then

(e) (i) $W_E = [u']^T[P]$

(ii) $W_I = \int_{vol.} [\bar{\varepsilon}]^T [\sigma] = [u']^T [A]^{-1} [k'][A]^{-1}[U]$ (4.5)

Where:

W_E = the external virtual work;

W_I = the internal virtual work;

[u'] = the vector of virtual displacement;

[k'] = the element stiffness matrix.

where $$[k'] = \int_{vol.} [B(x,y)]^T [D][B(x,y)] \tag{4.6}$$

(f) From the principle of virtual work, $W_E = W_I$. By taking one element of virtual nodal displacement vector [u'] equal to unity successfully, the solution becomes:

$$[P] = [K][U] \tag{4.7}$$

Where $[K] = \Sigma[k']$, so the global structural stiffness matrix is an assemblage of the element stiffness matrix [k'].

(g) The solution of the resulting system of equations yields the values of nodal displacement [U] and the internal forces for each element can be obtained from equation (4.4).

In the case of a liner (elastic) structural problem, loads are first applied on a model and the solution is obtained directly. In a nonlinear case, the analysis follows a numerical method to obtain a solution. However, such analysis is beyond the scope of this thesis and is not discussed.

4.3 The Finite Element Program 'ABAQUS'

ABAQUS is a multi-purpose finite-element program developed initially for nuclear power and offshore engineering communities, who needed a tool for studying complex,

nonlinear engineering problems. Widespread adaptation across many industries during the 1980's and 1990's made ABAQUS a popular choice for demanding finite element analysis. The program is used world-wide to estimate structural responses of power plant structures due to accident and operating stresses. However, it is used on a much wider scale to solve all types of structural problems. ABAQUS runs as a batch program to assemble a data deck which describes a problem so that an analysis can be performed. A data deck for ABAQUS contains model data and history data. Model data defines a finite-element model which includes: the nodes, elements, element properties, material definitions, nodal constraints or boundary conditions, and any data that specify the model itself. Data decks for complex simulations can be large but can be managed without too many difficulties by using the convenient feature built into the program's input structure. History data defines what happens to the model such as the sequence of events or loadings in which model was subjected to. In ABAQUS, this data history is divided by the user into a sequence of steps. Each step is a period of response of a particular type such as static loading or dynamic response. The definition of a step includes the procedure type, the control parameters for time integration for non-linear solution procedures, loading, free-vibration procedure, forced vibration procedure, and output requests.

All data definitions in ABAQUS are accomplished with option blocks which are sets of data describing a part of the problem definition. The user chooses these options that are relevant for a particular application. Each option is introduced by a keyword card. If the option requires data cards, then the data should be placed after the key words. One of the most useful features of the ABAQUS data definition method is the availability of sets. A set

can be a set of nodes or a set of elements. The user provides a name for each set. That name then provides a means of referencing all of the members of the set. Sets are the basic reference throughout ABAQUS and the user of sets is recommended. Choosing meaningful set names makes it simple to identify which data belong to which part of the model. Where global and local coordinates are not aligned such as in the ends of the curved bridges, ABAQUS provides a TRANSFORM option to specify a local coordinate system at nodes by setting up rotated direction for displacements and rotations at individual nodes and node sets. This option was used to rotate the two horizontal displacements (U_x and U_y) to radial and tangential displacement to apply the boundary condition in the radial supports of curved bridges.

4.4 Finite-Element Modeling of Composite Multiple Box Bridges

A three dimensional finite-element model was used to analyze all composite bridges included in this study. A convergence study was conducted to choose the finite-element mesh. The finite-element mesh is usually chosen based on pilot runs and is a compromise between economy and accuracy. In the finite element modeling process, the structure is first divided into several components. In this case, the bridges were divided into: concrete deck slab, steel top flanges, steel webs, steel bottom flange, steel solid-end-diaphragms and cross-bracing and top-chords. Several element types were attempted at first as trial until a suitable one is found. Also several trial runs proved that the effect of vertical web stiffeners on the structural behavior was insignificant. Therefore, they were not included in the finite-element model. In this chapter, different element types and material used for modeling the elastic loading stage are presented. The analysis results presented in this chapter were verified by

loading cases on three different composite laboratory bridge models discussed in chapter 3.

4.4.1 Geometric Modeling

(a) Modeling of Deck Slab, Webs, Bottom Flange, and End-Diaphragms

For these components, shell elements were used. From the many types of shell elements available in the ABAQUS library, the four-noded shell element named S4R was chosen. Depending on its nodes, this type of element can have either straight or curved boundaries depending on nodes definitions; this makes it suitable for the curved bridges. The S4R element had six degrees of freedom at each node, these were (U1, U2, U3) and three rotations (Φ1, Φ2, Φ3). A detailed diagram of the shell element S4R is shown in Figure 4.1.

(b) Modeling of Steel Top Flanges, Top-chords, and Cross-bracings

For these components, two-node three-dimensional beam element, called B31H in ABAQUS library, was used to model the steel top flanges, top-chords, and cross-bracings. This element has two nodes having six degrees of freedom at each node. They are three displacements (U1, U2, U3) and three rotations (Φ1, Φ2, Φ3). A detailed diagram of the beam element B31H is shown in figure 4.2.

4.4.2 Boundary Conditions

Two different nodal constraints were used in the analysis; these were boundary constraints and multi-point constraints. For the boundary conditions, two different constraints were set in modeling the simply supported bridges. First the roller support at one

end of the bridge was restricted to both vertical and radial displacements at the lower end nodes of each web. Second, the most inner hinged support at the other end of the bridge was restricted to all possible translations at the lower end node, however the rest of the support end nodes were restricted only to radial and vertical translations. In summary, the boundary conditions for all end support nodes in the finite-element models were as follows: (1) one interior support fixed against tangential, radial, and vertical displacements; (2) all other supports were free to move tangentially but fixed against radial and vertical displacements.

The multi-point constraint option in the ABAQUS software, type BEAM, was used to model the presence of the shearing stud between the shell nodes of the concrete deck and the beam element nodes of the steel top flanges, the beam type element allows for constraint between different degrees of freedom and thus, ensures full interaction between the concrete deck slab and the steel cells as intended in the design. In this type of constraint, the finite-element modeling software ABAQUS uses a linear constraint equation, where beam elements are placed between the concrete deck and the flanges act as rigid links. This way, all forces and moments experienced by the shearing studs are transferred directly to the steel flanges by the beam element. In this manner, the nodal degrees of freedom of the nodes of element are transferred to those of another element node which that it is attached to. The multi-point constraints between the concrete deck and the top steel flanges, shown in figure 4.3 were used with the proper spacing based on the comparative study between the experimental study and theoretical results.

4.4.3 Material modeling

It is important that the material properties are defined so that ABAQUS (43) can provide suitable properties for those elements. Also, the material properties can highly affect the results of the analysis. Structural material properties include elastic modulus and yield stress, must be input to ABAQUS for accurately predicting the behavior of the model.

4.5 Dynamic Analysis using the Finite-Element "ABAQUS" Program

There are several methods for performing dynamic analysis using the ABAQUS software. Usually, modal methods are chosen for linear analyses instead of direct integration methods. This is because, in direct integration dynamics, the global equations of motion of the system must be integrated through time, which makes direct integration methods more expensive than modal methods. For linear problems, dynamic response is determined by using the eigenmodes of the system. In such cases, modes and frequencies are calculated first in a simple frequency (free-vibration) procedure step in ABAQUS.

4.5.1 Free-Vibration Analysis

To obtain the natural frequencies and the corresponding mode shapes of an object, the FREQUENCY command is used in ABAQUS. ABAQUS obtains the frequency using the eigenvalue technique. The eigenvalue for the natural frequencies for a finite element model is as follows:

$$(-\omega^2 M^{MN} + \omega C^{MN} + K^{MN})\phi^N = 0 \qquad (4.8)$$

Where:

M^{MN} = mass matrix (which is symmetric and positive definite);

C^{MN} = damping matrix (neglected during the eigenvalue extraction);

K^{MN} = stiffness matrix;

Φ^{N} = eigenvector (the mode of vibration);

ω = frequency value;

M & N = degrees of freedom.

Also, densities of materials must be defined. Using the DENSITY option in ABAQUS, the user can define the different densities of all materials used to form the structure. The users need to specify the number of eigenvalues required. In ABAQUS, the analysis process normalizes the eigenvectors so that the largest displacement entry in each vector is unity. Also, using the eigenvectors, the program automatically calculates the participation factor which indicates how strong the motion was in the global x-, y-, and z-direction or rigid body rotation about one of these axes.

4.6 Finite-Element Analysis of the Bridge Models and the Prototype Bridges

The above mentioned finite element method was employed to study the elastic and free-vibration response of the three tested bridge models described earlier in Chapter 3. In the finite element modeling, pilot runs were performed to determine the least number of possible elements in the mesh discritization without a loss in accuracy. As a result, for the elastic and vibrational load verifications, it was sufficient to vertically use six elements for

each side of the web and four elements between webs for the concrete slab bottom steel flanges, 72 elements in the longitudinal direction. For the purpose of consistency, the discritization for the all finite elements models was kept the same per box girder. Figure 4.3 shows the finite element discritization of the cross-section of the bridge model M1. Pilot runs were also performed to investigate the effect of vertical stiffeners and concrete steel reinforcement on the structural response of the finite element models. It was found that the vertical stiffeners had an insignificant effect on the structural response of the finite element model, so they were omitted in the modeling. Also, the steel reinforcement in the concrete deck had no significant effect on the model elastic or dynamic response, and therefore, the steel reinforcement were also excluded from the finite element models.

The finite element modeling was first verified and substantiated by testing three bridge models with different number of cross-bracing. The finite element modeling was then used to conduct a parametric study on the structural response of curved and straight composite box girder bridge prototypes. A list of ABAQUS input data decks used in elastic, free-vibration analysis is shown in appendix A7. Figure 4.4 shows view of bridge model M1, with concrete deck slab, while Fig. 4.5 shows the same model without the concrete slab. Figures 4.6 and 4.7 shows view of the finite element models for the straight bridge model M3 with and without the concrete deck slab, respectively.

Chapter V

RESULTS FROM THE TESTED BRIDGE MODELS

5.1 General

The main objective of the experimental study was to substantiate and verify the linear finite element analysis. The experimental study was also used to:

1. Study the effect of curvature on the behavior of simply-supported curved composite twin-box girder bridges;
2. Study the effect of the presence of cross-bracing system between the support lines on the behavior of curved twin-box girder bridges;
3. Investigate the effect of different cases of loading on the elastic behavior of such bridges.

In order to achieve the above objectives, experimental tests were conducted on three simply supported composite concrete-steel box girder bridge models, where, the first two were curved having a different number of cross bracing between the boxes while the last was a straight bridge model. This chapter summaries and compares the results of the experimental and finite element analysis for the three different bridge models. These results include: natural frequencies and mode shapes deflections, longitudinal strains, and failure modes of the bridge models.

5.2 Free-Vibration Test Results

Free-vibration tests were conducted on all three bridge models. Using two different LVDT setups as described earlier in Chapter 3, each bridge model was excited to set it under free-vibration. Displacement data captured from the LVDT sensors were fed into a Fast

Fourier Transformation Analyzer to give the spectrum response of the each bridge in the frequency domain from which the highest frequencies as well as the mode shape were extracted. Figures 5.1 to 5.24, 5.26 to 5.29, 5.11 to 5.14, 5.16 to 5.19, 5.21 to 5.24, and 5.26 to 5.29 show the displacement-time histories at certain locations as explained in Chapter 3 for all bridge models. While Figures 5.5, 5.10, 5.15, 5.20, 5.25, and 5.30 show the frequency spectra for all bridge models. The experimental natural frequencies were extracted from the data obtained from the deflections of the bottom flanges at each LVDT location. However, due to limitations in the experimental work, only the most reliable data that revealed the full spectrum was used for the final natural frequency results. Table 5.1 summarizes the natural frequencies and the mode shapes for all bridge models. In general, a good correlation between the experimental and theoretical findings was observed. However, it was noticed that theoretical frequencies were generally higher than those obtained experimentally.

For the straight bridge model M3, only the first natural frequency was captured due to error made during the ball drop testing. The first natural frequency of vibration using the finite-element model was 34.9 Hz which is close to the frequency of 30 Hz obtained from the experimental data collected. Also, the corresponding mode of vibration was purely flexural for both the theoretical and experimental frequencies.

From Table 5.1, it can be observed that the experimental value of the first frequency was the same for the first and second model bridges. Both of these models have the same curvature and dimensions with the exception that the first model has external bracing between the box girders. Also the finite element results for the first frequency were almost identical for both models. From this observation, it seemed that the external bracing did not have any effect on the dominant frequency of the models. However, in the case of the second natural frequency, only the experimental values were different, where the second

bridge model M2 had a 5.2% higher value than the first bridge model. In the case of the third natural frequencies, the theoretical values were higher than the experimental values by 17.4 % and 18.7 % for the first bridge models. However, here the first bridge M1 had higher theoretical and experimental frequencies values than M2. Judging by the dominant first natural frequency, it seems that the presence of the bracing in the first bridge model M1 did not contribute to any enhancement in its torsional stiffness.

5.3 Results from Loading the Composite Bridge Models up-to-Collapse

After the free vibration testing, each model was loaded eccentrically in the elastic range. Two concentrated loads were applied over the outer webs and the mid-span section, as shown in Fig. 5.31. Then two concentrated loads were applied over the inner webs as shown in Figure 5.32. Figure 5.37 shows similar loading for model M3.

Each model was tested to failure using the four point load configuration described earlier in Chapter 3. In all model bridges, four concentrated loads were applied over the webs at mid-span. Figure 5.33 shows view of bridge model M1 during loading to collapse. The load was applied at a constant rate in increments of 2225 N (500 lbs) approximately. After each increment, the load was maintained constant during recording deflections and strains. Moreover, the cracks in the top surface of the concrete deck slab were traced. After failure of each bridge model, the applied load was released slowly. A bridge model was considered failed when it could not carry any further load.

The testing up-to-collapse of bridge model M1 began by applying the load in increments. When the loading reached approximately 31 KN (7000 lbs), the first concrete crack line was observed extending closely along the center line from the quarter length on the left side to near the mid span. From that point on, as the load increased, other cracks

developed until the bridge reached its ultimate load. Figure 5.34 shows view of the deflected shape of bridge model M1 after failure. While a view of the crack pattern for models M1 is shown in Fig. 5.35. It is important to note that the cracks were observed visually only. The test was terminated at an ultimate applied load of 89.4 kN. After the bridge collapsed, it can be seen that the cracks were inclined to the supporting line where the model bridge was restrained. From the pattern of the cracking lines it can be shown the cracks were mostly attributed to the high torsional moment associated with the curvature of the bridge model. It should also be noted that the crack lines around the mid-span area lined up closely on top of the webs 1, 2 and 3. Figures 5.41 show the load-deflection relationships of the bottom-web points at the mid-span. It can be observed that the outer web (Web1) deflected more than the inner web (Web4).

The testing up-to-collapse of bridge model M2 started by applying the load in increments of 2225 N (500 lbs) approximately. The first concrete crack was noticed on the top surface of the deck slab close to the support lines on one side of the bridge at a load of 22 kN. Other major diagonal cracks appeared at the top surface of the concrete deck slab at higher load increments. These cracks propagated far towards the mid-span section with the load increase. Just like the behavour of Model M1, these cracks were closely lined up on top of the webs location at the mid area of the bridge model. However, in this case, due to the absence of the cross bracing between the box girders, only the outer two webs (Web1 and Web2) had longitudinal cracks on top of the concrete deck. The test was terminated at a load of 82.1 kN. View of the crack pattern for models M2 is shown in Fig. 5.36. Again, theses cracks were inclined to the supporting line and may be attributed to the high torsional moment associated with the curved bridge model. Figures 5.42 show the load-deflection relationship of the bottom-web points at mid-span. It can be observed that the outer web deflected more that the inner web.

The testing up-uo-collapse of straight bridge model M3, with no cross-bracings between the support lines, started by applying the load in increments of 2225 N (500 lbs) approximately. In this case, there were no visible cracks observed on the surface of the concrete until the bridge model collapsed. The test was terminated at a load of 114.8 kN. It should be noted that at failure, crushing of the concrete deck slab was observed at the top surface all-over the mid-span cross-section only. These cracks were due to the effect of bending only with no torsion. Figures 5.38 and 5.39 show the deflected shape of the bridge model M3 during and after failure respectively. Figure 5.43 shows the load-deflection relationships of the bottom-web points at mid-span.

Comparison of bridge model M1 of five cross-bracing systems between the supporting lines and bridge model M2 of the same curvature as bridge model M1 but without cross-bracings, showed that the presence of cross-bracings increased the load carrying capacity of the curved composite thee-cell bridge model by 5.5%. Moreover, cracks detected at the top surface of the concrete deck slab close to the support lines of bridge model M1 were suppressed due the presence of cross-bracings. These cracks in the second model were more progressive and more localized over the outer webs, (web1 and web2) than those in the first model due to the absence of cross-bracings. These cracks resulted from the higher torsional effect near the supporting line and propagated, with the increase of the applied load, towards the mid-span section.

Figures 5.44, 5.45, 5.46 and 5.47 show a comparison between the load-deflection relationships at the bottom of each web of the mid-span section for all bridge models. It can be observed that at the same load, the deflection readings were higher for the curved models. Also, when the two curved bridge models are compared separately, it can be seen that the presence of the external cross bracing in model M1 did not reduce the deflection. Finally,

from the ultimate loading capacity of all the bridge models, it was verified that the curvature reduces the load carrying capacity of the bridge models.

Table 5.2 presents a summary of the collapse loads of the tested bridge models obtained experimentally. The experimental load carrying capacity of bridge model M1 was 21% less than that of the straight bridge model M3. While bridge model M2 with no external cross bracing had a 28% less ultimate load capacity than that of straight bridge model M3. Therefore, it can be said that: (i) the presence of external bracing between box girders enhances the ultimate load capacity of curved bridges, and; (ii) curvature decreases the load carrying capacity of box girder bridges.

From all the failed bridge models, it can be observed that the concrete crack lines in models M1 and M2 had cracks along the span which were inclined to the support lines. This supports the idea that the failure was due to torsional effect. Also both of these models had longitudinal concrete cracks in the middle of the bridge along the web line. In model M1, these longitudinal cracks were present on top of all but the inner web. In Model M2, the longitudinal cracks were only present on top of the outer girder webs; the reason for this could be that the torsional moments were more evenly distributed over the two box girders due to the presence of the external bracing between the boxes in the first model. In case of bridge model M3, there were no observed cracks along the span. Only when the bridge failed, the concrete slab was crushed exactly at the mid span of the bridge model. Here, the failure was due to bending moment only.

5.4 Elastic Loading Results on the Composite Bridge Models

In this analysis, there were three different loading cases applied to all bridge models. In the first and second case, a pair of concentrated loads was applied on the outer box girder

and then on the inner girders to a stage where the behavior is still in the elastic stage. Figure 3.31 in chapter 3 shows the positions of the applied loads on each of all tested bridge models. This chapter uses a combined pair of concentrated loads equaling 10 kN when different loading cases loads are mentioned. Due to limitation of accuracy in the equipment used to apply the loading, the actual applied loads in the experimental work conducted were less than 10 kN, and thus the corresponding deflections would be less than the ones presented in deflection figures mentioned later. However assuming a linear behavior in the elastic stage, the loads and the corresponding deflections were scaled up to 10 kN. This was done so that a proper comparison and assessment can be shown when presenting the results of the different model bridges.

For bridge model M1, a pair of concentrated loads was first applied on the outer lane, then on the inner lane at the mid span of the bridge. Figures 5.48 and 5.49 show the resulting deflections obtained experimentally and theoretically for elastic combined loading of 10 kN. This model having an L/R=1 and external bracing between the box girders, showed generally an agreement between the theoretical and experimental results. However, the theoretical results underestimated the experimental deflection in a range between 14% and 21% in the case of outer loading case; and 9% and 16% in the case of inner loading case.

For bridge model M2, the deflection results are shown in Figures 5.50 and 5.51. In the case of outer loading, again, the theoretical deflections underestimated the actual deflections except below web1. It is important to note, that the deflection reading under web1 was measured using a mechanical dial, while the rest were performed using the accurate LVDT instruments. For that reason, it was thought that this could have been probable cause for loss in accuracy. The highest difference in this case was 15 %. In the case of the inner loading (Fig. 5.51), the theoretical deflections showed the same trend as the

actual deflections, but underestimated the measured deflections by a range between 5% and 30%.

For straight bridge model M3, the deflection results are shown in Figures 5.52 and 5.53. This model had a closer agreement between the experimental and theoretical deflections than the rest of the models. In this case of outer loading, the maximum difference between the theoretical and actual deflection was 6%, while the difference was almost 15% for all the readings in the case of inner loading. In both loading cases the experimental deflections were either the same or higher than the theoretical deflections.

In most cases, there was a trend agreement between the experimental and the theoretical results for all bridge models. However, in certain cases, the theoretical deflections were higher or lower than the experimental deflection. The theoretical results from the finite element modeling seemed to under predict the actual deflections. In the worst case this difference was 30%.

A comparison of the deflections of the bridge models due to the two different loading cases are presented in Figures. 5.54 and 5.55. In these graphs only the finite modeling results for the three bridge models were compared. In Fig. 5.54, for the case of outer lane loading, it was surprising to see that bridge models M1 and M2 had almost identical deflection behavior; this behavior was also very similar in the case of inner lane loading for both these bridge models. Such a behavior suggests that the presence of the external cross bracing system used in the first model M1 did not increase its deflection resistance capacity. However, in the case of the inner lane loading (Fig. 5.55), web1 in model M1 seemed to deflect slightly more that in model M2, but without reducing the deflection under the bottom of the inner girder, this slight difference is thought to be

attributed to the presence of the external cross bracing system but without any beneficial effect in terms of deflection.

The behavior of straight bridge model M3 was generally more predictable than the curved bridge models. Here it was noticed the maximum deflections occurred below the bottom flange of the lane where the pair of concentrated loads was applied regardless of which loading case. Unlike straight bridge model M3, the maximum deflection for the curved bridge models occurred when the pair of concentrated loads was applied over the outer lane. Also, for the same loading cases, the deflections were higher for the curved models M1 and M2 when compared with model M3, therefore the curvature of the bridge increased the deflections

In all, even that the theoretical results for deflection were not identical to the actual deflections, the theoretical results generally possessed the same trend of behavior as the measured deflection and could if necessary be altered by a factor to match the actual deflections, and would be relied on for the rest of this work.

5.7 Summary of Findings

The structural behavior of the curved composite box girder bridge models was examined analytically through the commercial finite element computer program "ABAQUS" and experimentally. Comparison between the two schemes was made in terms of vertical deflections and natural frequencies. The correlation between the analytical and experimental findings in this chapter had the following:

1- The good trend agreement between the experimental and theoretical results supports the reliability of using the finite element modeling to predict the elastic response and free-vibration response of box-girder bridges.

2- The presence of cross-bracing systems used between the boxes in a curved box girder bridge did not have a significant effect on the bridge natural frequencies, or maximum deflection. However, it increased the load carrying capacity of the curved bridge models.

3- The curvature in composite concrete-deck steel-box girder bridges increases the downward deflection while decreases the ultimate load capacity.

4- When comparing only the outer or inner loading cases, the outer loading case in a curved bridge causes the maximum design deflection.

5- The dominant mode of vibration of a curved bridge is a combined flexural and torsional mode.

6- Curvature in composite concrete-deck steel-box bridges decreases the natural frequency.

Chapter VI

PARAMETRIC STUDY

6.1 General

Currently, there is no proper method for the design of curved box girder bridges. In the current practice it is common for design engineers to increase the design moment of a straight box girder by 5% to 20% for a curved box girder. Therefore, the parametric study was conducted in this chapter to obtain information about box girder bridges that could aid in its design and also to extract stress distribution factors for bending moment. To conduct the parametric study, many finite element prototype bridges were modeled for straight and curved box girder bridges. Theses bridges were fully loaded according to the CHBDC in order to provide useful information for bridge designers. Thus, the objectives of this parametric study were to:

1. Investigate the influence of major parameters affecting the straining actions of composite multiple-spine box-girder bridges.
2. Generate a data base for the maximum longitudinal stresses developed in the bridges due to the bending moment.
3. Summarize bending stress distribution factors, average mid-span deflections and maximum axial force in bracing members.

6.2 Description of the Bridge Prototypes Used in the Parametric Studies

To predict the structural response of straight and curved composite multi-cell bridges, it is important to define the geometric parameters that correspond to the box girder bridges.

These parameters include: span length, number of boxes, number of lanes, and span-to-radius of curvature ratio. In this study 5 sets of 45 different composite concrete-deck steel box girder bridges were loaded according to CHBDC specifications. The first set was made of all straight bridges while the rest have different curvatures. Table 6.1 summarizes the different basic prototypes of the straight box girder bridges used in this study. The symbols used in the first column in Table 6.1 represent designations of the bridge types considered: *l* stands for lane; *b* stands for box; *ss* stands for simply-supported and straight and *sc* stands for simply-supported and curved; and the number at the end of the designation represents the span length in meters. For example, 1*l*-2*b*-*sc*-20 denotes a bridge of 1 lane, 2 boxes, simply-supported and curved, and of 20 m span. Figure 6.1 shows the basic cross-sectional configurations and symbols as presented in Table 6.1.

In the parametric studies, the span length of the bridges ranged from 20 m to 100 m and the number of lanes were taken as 2, 3, and 4. The CHBD Code (65) recommends that each lane width for bridges and ramps of two or more lanes should be 3.75 meters. According to these recommendations plus the additions of a side walk on each side of a bridge, the bridge widths were: 9.30 m in the case of two-lane, 13.05 m in the case of three-lane, and 16.80 m in the case of four-lane bridges. The number of box girders ranged from 2 to 4 in the case of two-lane, 3 to 5 in the case of three-lane, 4 to 6 in the case of four-lane. To change the number of box girders for the same lane width, the thicknesses of the steel top flanges, webs, and bottom flange were changed to maintain the same shear stiffness of the webs and overall flexural stiffness of the cross-section. Figure 6.2 shows the different number of box girders considered for each lanes width in the parametric studies.

For each bridge included in the parametric study, the transverse geometry and the radius of curvature were changed to study their effects on the structural response. The number of cross-bracings between support lines and the top-chords were varied depending on the span length and the CHBDC recommendation of bracing between intervals having at least 7.5 meters minimum spacing. The number of internal bracing between supports was maintained at 3 for 20 meter spans, 5 for 40 meter spans, 7 for 60 meter spans, 11 for 80 meter spans and 17 for 100 meter spans. The number of external bracing was always two more than the internal due to the fact that a brace is placed between the box girders at the supports where there is normally a diaphragm in the case of internal bracing.

All curved bridges in this study were assumed to have constant radii of curvature and concrete decks with constant elevations. The degree of curvature was defined by the span-to-radius ratio, L/R, where, L, is the arc length along the centre span line of the cross-section and the radius of curvature, R, is the distance from the origin of the circular arc to the centre line of the cross-section. The L/R ratios used in were 0.0 in the case of a straight bridge and 0.4, 1.4, 1.0 and 2.0 in the case of the curved bridges. The higher values of L/R along with the lower value of the span length, 20 m, are theoretically possible to analyze but practically uncommon for curved highway bridges since the Geometric Design Standards for Ontario Highways, 1985, (56) only allow using curved bridges when the radius of curvature $\geq$ 45 m. However, the inclusion in this study of a smaller radius of curvature serves to show the trend of the structural response of curved bridges within certain limits of L/R.

The ranges of the parameters considered in this study were based on an extensive

survey of actual designed bridges [Johanson et al., 1967, (46); Chapman et al., 1971, (20); Heins, 1978, (37)]. For the parametric studies, the material properties (modulus of elasticity, poission's ratio, and mass density, etc.) for the concrete deck, steel boxes, diaphragms, and bracing systems were taken to be the same for all the cases studied. Complete listing of the geometries of the bridge prototypes used in the parametric studies is shown in Appendix A.8.

6.3 Loading Conditions of Composite Multiple box girder Bridges at Service

In this section, the different loadings considered on all bridges are outlined; the main intention is to determine the load distribution factors on the straight and curved box girders due to dead or truck loading. The North American Codes of Practice (4, 5, 6, 65, 66, 67) provide load distribution factors for only truck loading on straight bridges but not dead load since the dead load is considered distributed equally between girders. However, in curved bridges, the curvature affects the uniform distribution of the dead load. Highway truck loading considered in this study are according to the CHBDC truck loading. The highway truck loading includes a highway truck and lane loading. The lane loading, which governs the design live load longitudinal moments for spans greater than about 45 m, is provided merely as a convenience to avoid the placing of more than one truck in one lane in bridges with large spans.

6.3.1 Dead Load

In order to simulate the effect of the dead load due to self-weight, the densities of the materials were used. The self weight option in ABAQUS was used to calculate the dead

weight of individual components forming the box girder bridge using the assigned material density.

6.3.2 Live Load

For live loading, the Canadian Highway Bridge Design Code, CHBDC 2000, (62) proposes a truck with a gross weight of 625 kN (CL-625) with impact. In the case of bridges spanning more than 45 meters, the CHBD lane loading consists of a truck reduced to 80% of the specified gross weight and a uniformly distributed live load of 9 kN/m with impact applied centrally on a 3.0 m wide area. Figure 6.3 summarizes the truck loading and lane loading proposed by the CHBD code.

According to the CHBDC, two types of live load (the truck loading and the equivalent lane loading) were first applied on a straight girder to determine which case produces the maximum effect in bridges of 20, 40, 60, 80, and 100 m span. When studying moment distribution in the bridge prototypes, the trucks were placed at the mid span in accordance with the CHBDC. The CHBD code suggests that the maximum moment stresses are produced when the mid span of the bridge is lined up at half the distance between the centriod of the truck and its largest loading axle, this configuration is shown in Figure 6.4. Initially, all four loading cases were considered for each bridge prototype: three different truck loading (or equivalent lane-loadings) are shown in Fig. 6.5. The fourth case of loading was the dead load of the bridge. In the two partial loading cases, Fig. 6.5.b and 6.5.c, the wheel loads close to the curbs were applied at a distance of 0.6 m from the inside edge of the curbs. However, due to findings in initial simulation runs that the case of fully

loaded bridge produced the maximum moment in the live loading stage, the other truck loading cases were omitted for the rest of the study.

6.4 Parametric Study

This parametric study examined the effects of bridge spans, number of lanes and number of boxes on the maximum bending stress distribution factors, deflection at the mid span and maximum axial force in bracing members.

The parametric study was conducted on the simply-supported curved composite concrete deck-steel box girder bridge prototypes to:

1. Investigate the influence of major parameters affecting the mid span stress distribution, deflections and maximum axial force throughout the bridge cross-section;
2. Generate a database for stress distribution factors, mid-span deflection and maximum axial force in bracing for both dead and live load cases.

In this study, the chosen parameters were: number of lanes, number of boxes, span length, and span-to-radius curvature ratio. The parametric study was based on the following assumptions:

1. the reinforced concrete slab deck had complete composite action with the top steel flange of the cells (100% shear interaction);
2. the bridges were simply-supported;
3. all materials were elastic and homogenous;
4. the effect of road superelevation, outer-web-slope, and curbs were ignored;

5. Solid end-diaphragms were used in the radial direction and their material and thickness were taken to be the same as those of the webs;
6. Bridges had constant radii of curvature between support lines.

Regarding superelevation in curved bridges, it was observed (6) that the live load applied to composite I-girder bridges produced essentially the same moments, twisting moments, and deflections for any angle of bridge superelevation between 0 and 10 percent. The details of the parametric study are described in the following sections.

6.4.1 Stress Distribution in Simply-Supported Straight and Curved Composite Multi-Box Girder Bridges

The box girder cross-section may be idealized as an I-beam shaped girders as shown in Fig. 6.6. Each idealized girder consists of the web, steel top flange, concrete deck slab, and bottom flange. For any given girder, the width of concrete deck slab is twice that of the web spacing, and the bottom flange width is taken to be the same as the web spacing. It is important to note that the extra length in the concrete slab due to the curbs and the parapet wall for the cases of the outer and inner girders was ignored, and thus, all the idealized girders for the same bridge have the same cross sectional dimensions. In order to determine the stress distribution factor, D_σ, carried by each curved girder, the maximum stress, σ, was calculated in a simply-supported girder when subjected to wheel loads of a CHBDC truck in the case of 40m and 20 m bridges, or wheel loads of an CHBDC truck with lane load as a line load per meter long of the bridge in the case of 60, 80 and 100 m bridges. From the finite element modeling, the distributions of maximum stresses of the bottom flange at mid-

span section were obtained. From these stresses the maximum mid-span longitudinal stresses carried by each girder, σ_{max}, was calculated for all the prototype bridges. Using the obtained σ_{max} and σ, the stress distribution factor, D_σ, was calculated as follows:

$$D_\sigma = \frac{\sigma_{max}}{\sigma} \tag{5.1}$$

Pervious work done by Sennah (82) revealed that changing the type of cross bracing system had an insignificant effect on stress distribution. In practice, X-type bracings as well as top-chords (lateral ties to the steel top flanges) are made from single or back-to-back angles. Such work showed that replacing the angle cross-section by rectangular one, or changing the bracing cross-section from 25×25 mm to 150×150 mm, has no effect on moment distribution. Therefore, it was decided to conduct the parametric study with X-bracings and top-chords having a 100×100 mm rectangular cross-section.

In terms of bracing effect, pervious work done by Nour (63) showed that having internal bracings improved the ability of the cross section to transfer loads from one girder to an adjacent one. Further more, the wrapping stresses due to torsion and distortion were significantly reduced. However, the addition of external bracing (between boxes) did not have a significant effect on the stress distribution. Based on such findings, even that the presence of external bracing was insignificant, for consistency reasons, this parametric study used internal and external bracing in accordance with the minimum spacing required by CHBDC for all bridges.

6.4.2 Part (2), Deflection Distribution in Simply-Supported Straight and Curved Composite Multiple-box Bridges

The CHBD code of Practice (65) limits deflection of a straight bridge by limiting the ratio of the span length or by limiting the span-to-depth ratio. In the case of curved bridges, the curvature increases the deflection more than that in straight bridges and also increases the cross-section slope. The output files of all the finite element analysis performed on moment distribution in the parametric study were set up to provide the deflection under the bottom flanges in all loading conditions. The effects of the same parameters, adopted for stress distribution at the mid-span of the simply-supported bridge prototypes, were also studied for deflection distribution.

6.4.3 Axial Forces in Bracing System in Simply-Supported Straight and Curved Composite Multiple-box Bridges

Bracing systems were placed inside and between the box girders to enhance the torsional resistance against curvature and eccentric loads. The output files of all the finite-element analysis were also setup to provide the axial force in each bracing and top-chord members. The same key parameters used for moment distributions were also used to study the effect of the maximum tensile and compressive forces in the bracing system.

CHAPTER VII

RESULTS FROM THE PARAMETRIC STUDY

7.1 General

This chapter presents the results from an extensive parametric study, using the finite-element modeling, in which 45 prototypes totaling 225 different simply-supported composite multiple-box girder bridges were modeled and analyzed to evaluate their structural response for moment distribution of dead and fully loaded cases. The parametric study conducted herein presents the: (i) moment distribution in simply-supported straight and curved composite multiple-box bridges; (ii) deflection distribution in simply-supported curved composite box girder bridges; (iii) axial forces in the bracing members. A data base was generated from the parametric study, to further derive a simplified design method for straight and curved simply-supported composite multiple-box bridges. Due to the large amount of different bridges considered in this study, it will not be possible to graphically illustrate each observation for all the different bridge prototypes, and thus a variety of different choices of bridge configurations will be used to illustrate different comparisons and observations in the parametric study.

7.2 Moment Distribution in Simply-Supported Straight and Curved Composite Multiple-Box Bridges

This parametric study proposes stress distribution factors to estimate the flexural response of bridge girders. The bottom flexural stress distribution factor will be calculated

as follows:

$$D_\sigma = \frac{(\sigma_b)_{\max}}{\sigma_b} \tag{7.1}$$

Where $(\sigma_b)_{max}$ is the maximum mid-span flexural stress in the outside fibers of the bottom girders obtained from the finite elements analysis, and σ_b, is the bottom flexural stress of a straight simply supported idealized girder, this value is obtained from the simple beam analysis using:

$$\sigma_b = M\frac{y_b}{I} \tag{7.2}$$

Where M is the resulting bending moment from an applied CHBDC truck or dead load on simply supported straight idealized girder; y_b is the distance of the idealized girders neutral axis to from the bottom surface, and I is the moment of inertia of the idealized girder. It should be noted here, that the simply supported straight idealized girder is formed of a typical box girder forming the multiple box section of the real bridge, where the width of the deck slab is the spacing between the steel boxes. In a similar manner, the flexural stress distribution factors for the concrete deck can be obtained by using the stresses in the top fibers of the concrete deck. The compressive stress at the top of the concrete slab can be obtained as follows:

$$(\sigma_t)_{\max} = D_\sigma\left(\frac{y_t}{ny_b}\right)\sigma_b \tag{7.3}$$

Where: D_σ is the value obtained from Eq.(7.1), y_t is the distance of the neutral axis from the

top of the composite beam, n is the modular ratio and σ_b is the value obtained from Eq.(7.2). However, sensitivity analysis performed by Nour (63) on very similar bridges revealed that the maximum tensile stresses in the bottom steel flange are much higher in absolute value than the maximum compressive strength in concrete. Furthermore, the composite beam is designed in a manner where the bottom steel flange is supposed to reach its yield point before the concrete deck reaches its maximum compressive strength. Also, pervious work done [Nutt et al. (64)], proved that neither the thickness of the concrete slab thickness or bottom flange had a significant influence on the moment distribution in case of straight reinforced and prestressed concrete multi-cell bridges. This was also confirmed by Sennah (82) and Nour (63) in case of composite concrete-deck steel-girders in multi-cell bridges and multiple box bridges, respectively. Based on such findings from pervious work, this parametric study considered only the tensile stress in the bottom steel flange in determining the stress distribution factors for multi-box girder bridges.

Other work done by Heins (39,40 ,41,42), also revealed that changing the span-to-depth ratio between the practical range of 20 to 30, has insignificant effect on moment distribution. Based on the facts mention above, it was decided to conduct the parametric study using span-to-depth ratio of 25 and a constant number of cross bracing for each bridge span. The key parameters investigated were: degree of curvature, number of lanes, number of boxes and span of the bridges considered.

7.2.1 Effect of Curvature

The effect of curvature on moments carried by the outer, central, and inner girders

was investigated. Figures 7.1 and 7.2 show the stress distribution factors for each box girder of the four-box, four-lane, bridge of 100m span with different curvatures and when subjected to dead load as well as CHBDC truck loading in all lanes, respectively. It can be observed that the outer box girder, the furthest from the center of curvature carry the greatest stresses distribution factors. Moreover, these stresses seem to increase with increase in curvature. Similar behavior was also observed in case of two and three-lane bridges with different number of box girders.

Figures 7.3 and 7.4, present the effect of span-to-radius of curvature ratio, L/R, on the moment carried by the inner and outer box girders of 4 lane, 80 m span bridges under dead load. While Figure 7.5 shows the effect of span-to-radius of curvature ratio on the stress carried by the outer box girders of a 4 lane, 80m bridge under full CHBDC truck loading. It is observed that the stress distribution factor for the outer and inner girders increases with the increase in the L/R ratio. However, in the cases of dead load on curved bridges having the same width, increasing the number of box girders seemed to decrease the stress distribution factor slightly for the inner box girder and increase it for the central and outer box girders. Such behavior can be explained by the fact that, in the geometry of curved bridges, the outer girders have a longer self-center span that the inner girders, and thus the volume and area are larger resulting in higher dead load when compared to an equivalent straight bridge of the center same span. For the case of fully loaded lanes, the stress distribution factors increased with an increase in curvature and decreased with the increase of number of boxes. Similar behavior was observed in the cases of two and three lane bridges of different span under CHBDC full loading.

7.2.2 Effect of Bridge Span Length

In examining this effect on the bridge response, the bridge width was kept constant while changing the span length. Figure 7.6 shows the effect of span length on the stress distribution factor of the central girder of four-lane, five box girder bridges under full CHBDC truck loading. It was observed that varying the span length did not have any impact on the stress distribution factors. This can be explained by the fact that, with the increase of bridge span, the load distribution among girders tends to become uniform. However in bridges of spans 20 and 40 meters, the stress distribution factors were considerably higher than the longer span bridges. This is most likely due to the fact that in smaller span bridges, plate action is significant and the load distribution among girders tends not to be uniform. In general, it was also noticed that in all the curved bridges, the stress distribution factors increased with the increase in curvature for all spans. Similar behavior was also observed for all the bridges in the parametric study.

7.2.3 Effect of Number of Boxes and Number of Lanes

The variation in the number of steel box girders for the same bridge span length was studied for different number of lanes. Figures 7.7 shows the effect of both the number of steel box girders and the number of lanes on the stresses due to bending carried by the outer girders of straight bridges of 40 m span due to full CHBDC loading. While Fig. 7.10 shows this effects on the bending stresses of central girders of bridges, of 100 m span and span-to-radius of curvature ratio of 1, under the condition of fully loaded lanes. It is observed that the stresses carried by a girder decrease significantly with increase in the number of steel box girders. It is also revealed that for the same number of steel boxes, these moment

distribution factors increase with the increase in the number of traffic lanes.

7.3 Deflection Distribution in Simply-Supported Curved Composite Box Girder Bridges

7.3.1 Effect Number of Boxes and Number of Lanes on Curvature and Deflection

The effect of number of steel box girders, traffic lanes and degree of curvature on deflection was examined under dead load as well CHBDC truck loading conditions. Figure 7.9 shows the effect of number of steel box girders and span-to-radius of curvature ratio on the average mid-span deflection of four lane bridges of 100 meter span under dead load. It can be observed that for the case of the straight bridges the number of box girders has no effect on the deflection. However, in the case of curved bridges, increasing the number of boxes and/or curvature increased the deflection. Figure 7.10 shows the effects of the number of traffic lanes and curvatures on the deflection for the case of four box girder bridges of 80 meter span under dead and CHBDC full truck loading. It can be seen that for the same number of traffic lanes, deflection increases with curvature. It can also be seen that while maintaining the same curvature, the increase in number of lanes also increases the deflection as well.

7.3.2 Effect of Bridge Span

To examine the effects of aspect ratio and curvature on the mid-span average deflection, another bridge prototype was used. Here, the bridge width was kept constant while changing the span and ratio of curvature. Figure 7.11 shows the effect of span length on the mid-span average deflection for different four-lane, five box girder bridges subjected

to full CHBDC truck and while Fig. 7.12 shows the effect of span length on mid span deflection for the same bridge but under dead load conditions. It was observed that the mid span average deflection increased with the increase in aspect ratio (increase in span) or increase in curvature or both. Similar trend was observed for all other bridge loading cases when the width is fixed while the span or curvatures were varied.

7.4 Axial Forces in Bracing Members

The effects of curvature and span length, number of steel boxes and curvature were examined for the maximum axial forces in the bracings. This parametric study used a minimum spacing of at least 7.5 meters between external or internal bracings in any given bridge. Figure 5.13 shows the effect of the span length and degree of curvature on the maximum compressive force in bracing members of two lane two box girder bridges of different spans subjected to dead load conditions. It can be observed that the maximum compressive force increases with the increase in span or curvature or both. Similar behavior was also observed for the CHBDC full truck loading conditions. Figure 5.14 shows the effects of curvature and number of boxes on the maximum compressive bracing force in four-lane, 100 meters span bridges of different curvatures subjected to CHBDC full truck loading conditions. It can be seen that for the case of straight bridge, increasing the number of boxes had no effect on the maximum axial compressive force in bracing members. However in the case of the curved bridges and with the exception of the L/R=0.4 it was observed that the increase of any or both the curvature or number of boxes, the maximum compressive axial force increased in the bracing members. Similar behavior was noticed for the same bridges under dead load conditions. Figure 7.15 shows the effect of number of

boxes on the outer maximum compressive force in bracing of four-lane bridges of 100 m span under dead load. Figure 7.16 presents the effects of the traffic lanes and curvature on the response four-box, 60 meter span bridges under dead load conditions. It can be observed generally that the axial force increased with the increase of either curvature or number of lanes. However, this effect was more noticeable in the case of curvatures when L/R was equal to or larger than 1.0.

CHAPTER VIII

SUMMARY AND CONCLUSIONS

8.1 Summary

In this study, experimental and theoretical studies were conducted to investigate the static structural behavior of straight and curved composite concrete deck-steel multiple box girder bridges. A literature review was conducted in order to establish the foundation for this study. It was observed that there is lack of information regarding the load distribution. While the current design practices in North America recommend few analytical methods for the design of straight composite multiple-spine box girder bridges, practical requirements in the design process requires a need for a simplified design method in the form of stress distribution factors expressions for moment and shear distribution factors for such bridges.

Three composite concrete deck-steel twin-box bridge models, two curved and one straight simply-supported, models were fabricated, and elastically tested under free vibration condition and under increasing load to collapse, and analyzed throughout the experimental program performed in this study. For its analytical versatility, the finite-element method was used throughout this study to describe linear responses of such bridges. The experimental effort that covered the three tested bridge models and was extended to conduct a parametric study on prototype bridges subjected to dead load and CHBDC truck loading.

8.2 Conclusions

The most important conclusions drawn from the theoretical and experimental results in this study are summarized below. They are presented in the following two areas: behavior

and load distribution characteristics of straight and curved composite multiple box girder bridges.

8.2.1 Experimental behavior and load distribution characteristics of straight and curved composite concrete deck steel-box girder bridges

1- The presence of external cross bracing system between the steel boxes had no significant difference on the natural frequency or deflection. However these external bracings increased the load carrying capacity in the case of curved bridges by 8.9%. Further more, from the concrete crack pattern observed; the presence of external cross bracing ensured better distribution of the stresses under ultimate loading conditions.

2- The curvature in composite bridges decreases the ultimate load capacity while increases the downward maximum design deflection.

3- The dominant mode of vibration of a curved simply-supported bridge is a combined flexural and torsional mode, with the bridge frequency decreasing with an increase in the degree of curvature. On the other hand, it is purely flexural for the straight bridge model.

8.2.2 Behavior and Load Distribution Characteristics of Straight and Curved simply supported Composite box girder Bridges

1- Curvature is the most critical parameter that influences the design of girders and bracing members in multiple-box bridges. Increase in the degree of curvature increases the bending stress and deflection distribution factors as well as the maximum axial force in a bracing member.

2- For the same number of lanes, the bending stress distribution factors decrease with the increase in number of box girders. On the other hand, while holding the number of lanes constant, increasing the number of boxes increases the maximum axial force in the bracing members as well as the mid-span deflections.

3- Increasing the bridge span increases the bending stress distribution factors for the outer and inner girders. It also increases the deflection distribution factors and maximum axial force in bracing members.

8.3 Recommendations for Future Research

It is recommended that further research efforts be directed towards the following:

1- The study of load distribution in curved continuous composite box girder bridges when subjected to CHBDC truck loadings.

2- From the data base resulting from this study, a set of empirical expressions for stresses and deflection distribution factors can be developed.

3- The study of the economics of number of boxes on a given number of lanes.

4- The study of shear distribution in simply supported curved composite box girder bridges when subjected to CHBDC truck loadings.

REFERENCES

1. Abdel-Salam, M. N., and Heins, C. P. 1988. **Seismic response of curved steel box girder bridges**. ASCE Journal of Structural Engineering, 114(12): 2790-2800.

2. Abdel-sayed G. 1973. **Curved webs under combined shear and normal stresses**. ASCE Journal of Structural Division, 99(ST3): 511-525.

3. Akoussah, K. E., Fafard, M., Talbot, M., and Beaulieu, D. 1997. **Parametric study of dynamic load amplification factor for simply-supported reinforced concrete bridges**, in french. Canadian Journal of Civil Engineering, 24(2): 313-322.

4. American Association of State Highway and Transportation Officials, AASHTO. 2000. **AASHTO LRFD Bridge Design Specifications**. Washington, D.C.

5. American Association for State Highway and Transportation Officials, AASHTO. 1993. **Guide specification for horizontally curved highway bridges**. Washington, D.C.

6. American Association of State Highway and Transportation Officials, AASHTO. 1996. **Standard specifications for highway bridges**. Washington, D.C.

7. Aslam, M., and Godden, W. G. 1975. **Model studies of multi-cell curved box girder bridges**. ASCE Journal of the Engineering Mechanics Division, 101(EM3): 207-222.

8. Aslam, M., and Godden, W. G. 1973. **Model Studies of curved box-girder bridges**. California University, Berkeley / Department of Civil Engineering, Report No. UC/SESM 73-5.

9. Bakht, B., and Jaegor, L. G. 1992. **Simplified methods of bridge analysis for the third edition of OHBDC**. Canadian Journal of Civil Engineering, 19(4): 551-559.

10. Bakht, B. and Jaegor, L. G. 1985. **Bridge deck simplified**. McGraw-Hill, New York, N.Y.

11. Billing, J. R. 1984. **Dynamic loading and testing of bridges in Ontario**. Canadian Journal of Civil Engineering, 11(4): 833-843.

12. Branco, F. A. 1981. **Composite box girder bridge behaviour**. Thesis presented to the University of Waterloo, Waterloo, Ontario, Canada, in partial fulfilment of the requirements for the degree of Master of Science.

13. Branco, F. A., and Green, R. 1985. **Composite box girder bridge behaviour during construction**. ASCE Journal of Structural Engineering, 111(3): 577-593.

14. Brennan, P. J., and Mandel, J. A. 1979. **Multiple configuration of curved bridge model studies**. ASCE Journal of the Structural Division, 105(ST5): 875-890.

15. Brighton, J., Newell, J. and Scanlon, A. 1996. **Live load distribution factors for double cell box girders**. Proceeding of the 1st Structural Specialty Conference, Alberta, Canada, 419-430.

16. Brockenbrough, R. L. 1986. **Distribution factors for curved I-girder bridges**. ASCE Journal of Structural Engineering, 112(10): 2200-2215.

17. Buckle, I. G., and Hood, J. A. 1982. **Testing and analysis of a curved continuous box girder model.** Department of Civil Engineering, University of Aucland, New Zealand, Report No. 181.

18. Canadian Standard Association. 1988. **Design of highway bridges (CAN/CSA-S6-88)**. Rexdale, Ontario, Canada.

19. Chang, P. C., Heins, C. P., Guohao, L., and Ding, S. 1985. **Seismic study of curved bridges using the Rayleigh-Ritz method**. Computers & Structures, 21(6): 1095-1104.

20. Chapman, J. C,, Dowlind, P.J., Lim P. T. K., and Billington, C. J. 1971. **The Structural behavior of steel and concrete box girder bridges**. The Structural Engineer, 49(3):111-120.

21. Cheung, M. S., and Foo, S. H. C. 1995. **Design of horizontally curved composite box girder bridges: a simplified approach**. Canadian Journal of Civil Engineering, 22(1): 93-105.

22. Cheung, M. S., and Magnount, A. 1991. **Parametric study of design variation on the vibration modes of box girder bridges**. Canadian Journal of Civil Engineering, 18(5): 789-798.

23. Cheung, M. S., and Mirza, M. S. 1986. **A study of the response of composite concrete deck-steel box girder bridges**. Proceedings of the 3rd International Conference on Computational and Experimental Measurements, Porto Caras, Greece, 549-565.

24. Cheung, Y. K., and Cheung, M. S. 1972. **Free vibration of curved and straight beam-slab or box-girder bridges**. International Association of Bridges and Structural Engineering, 32(2): 41-52.

25. Choudhury, D. 1986. **Analysis of curved non-prismatic reinforce concrete and prestressed concrete box girder bridge**. Ph.D. Thesis, University of California, Berkeley, CA.

26. Choudhury, D., and Scordelis, A. C. 1988. **Structural analysis and response of curved prestressed concrete box girder bridges**. Transportation Research Record, Highway Research Board, 1180: 72-86.

27. Culver, C. G. 1967. **Natural frequencies of horizontally curved beams**. ASCE Journal of the Structural Division, 93(2): 189-203.

28. Dabrowski, R. 1968. **Curved thin-walled girders, Theory and analysis**. Springer, New York.

29. Davidson, J. S., Keller, M. A., and Yoo, C. H. 1996. **Cross-frame spacing and parametric effects in horizontally curved I-girder bridges**. ASCE Journal of Structural Engineering, 122(9): 1089-1096.

30. Davis, R. E., Bon V. D., and Semans, F. M. 1982. **Live load distribution in concrete box girder bridges**. Transportation Research Record, Transportation Research Board, 871:47-52.

31. Davis, R. E., Bon V. D. 1981. **Transverse distribution of loads in box girder bridges (Volume 7): Correction for curvature**. California Department of Transportation, Socramento, CA, Report No. FHWA-CA-5D-81-16 Final Report.

32. Evans, H. R., and Rifaie, W. N. 1975. **An experimental and theoretical investigation of the behaviour of box girders curved in plan**. Proceedings of Institute of Civil Engineers, 59(2): 323-352.

33. Fam, A. R. M. 1973. **Static and free-vibration analysis of curved box bridges**. Structural Dynamic Series No. 73-2, Department of Civil Engineering and Applied Mechanics, McGill University, Montreal, Quebec, Canada.

34. Fam, A. R., and Turkstra, C. J. 1976. **Model study of horizontally curved box girder.** ASCE Journal of the Structural Division, 102(ST5): 1097-1108.

35. Fountain, R. S., and Mattock, R. S. 1968. **Composite steel-concrete multi-box girder bridges.** Proceedings of the Canadian Structural Engineering Conference, Toronto, 19-30.

36. Galdos, N. H. 1988. **A theoretical investigation of the dynamic behaviour of horizontally curved steel box girder bridges under truck loadings.** Thesis presented o the University of Maryland at Collage Park, Md., in partial fulfilment of the requirement for the degree of Doctor of Philosophy.

37. Galdos, N. H., Schelling, D. R., and Sahin, M. A. 1990. **Methodology for the determination of dynamic impact factor of horizontally curved steel box girder bridges**. ASCE Journal of Structural Engineering, 119(6): 1917-1934.

38. Heins, C. P. 1978. **Box girder bridge design-State-of-the-Art.** AISC Engineering Journal, 2: 126-142.

39. Heins, C. P., Bonakdapour, B., and Bell, L. C. 1972. **Multi-cell curved girder studies.** ASCE journal of the Structural Division, 98(ST4): 831-843.

40. Heins, C. P., and Humphrey, R. 1979. **Bending and torsion interaction of box girders.** ASCE Journal of Structural Division, 105(ST5): 891-904.

41. Heins, C. P., and Jin, J. O. 1984. **Live load distribution on curved I-girders.** ASCE Journal of Structural Engineering, 110(3): 523-530.

42. Heins, C. P., and Lee, W. H. 1981. **Curved box-girder bridge: field test.** ASCE Journal of the Structural Division, 107(2): 317-327.

43. Hibbitt, H.D., Karlson, B. I., and Sorenson, E. P. 1996. ABAQUS version 5.6, finite element program, Hibbitt, H. D. & Sorenson, Inc, Providence, R. I.

44. Ho, S., Cheung, M. S., Ng, S. F., and Yu, T. 1989. **Longitudinal girder moments in simply supported bridges by the finite strip method.** Canadian Journal of Civil Engineering, 16(5): 698-703.

45. Huang, D., Wang, T., and Shahawy, M. 1995. **Dynamic behaviour of horizontally curved I-girder bridges.** Computers & Structures, 57(4): 703-714.

46. Huang, D., Wang, T., and Shahaway, M. 1995. **Vibration of thin-walled box-girder bridges exited by vehicles.** ASCE Journal of Structural Engineering, 121(9): 1330-1337.

47. Inbanathan, M. J., and Wieland, M. 1987. **Bridge vibration due to vehicle moving over rough surface.** ASCE Journal of Structural Engineering, 113(9): 1994-2008.

48. Johanston, S. B., and Mattock, A. H. 1967. **Lateral distribution of loads in composite box girder bridges.** Highway Research Record, Highway Research Board, 167: 25-33.

49. Kashif, A. M. 1992. **Dynamic response of highway bridges to moving vehicles.** Ph.D. dissertation, Department of Civil Engineering, Carleton University, Ottawa, Canada.

50. Kashif, A. M., and Humar, J. L. 1990. **Analysis of the dynamic characteristics of box girder bridges.** Proceedings of the Third International Conference on Short and Medium Span Bridges, Toronto, Ontario, 2: 367-378.

51. Kissane, R., and Beal, D. B. 1975. **Field testing of horizontally curved steel girder bridges.** Research Report 27, The U.S. Department of Transportation.

52. Komatsu, S., and Nakai, H. 1966. **Study on free vibrations of curved girder bridges.** Transactions, Japan Society of Civil Engineers, Tokyo, Japan, (136): 35-60.

53. Komatsu, S., and Nakai, H. 1970. **Fundamental study on forced vibration of curved girder bridges.** Transactions, Japan Society of Civil Engineers, Tokyo, Japan, 2(I): 37-42.

54. López, A. and Aparicio, A. C. 1989. **Nonlinear behavior of curved prestressed box girder bridges.** International Association of Bridges and Structural Engineering, IABSE, 132: 13-28.

55. Mari, A. R., Carrascon, S., and Lopez, A. 1988. **Beam models for nonlinear and time-dependant analysis of curved prestressed box girder bridges.** Transportation Research Record, 1180: 59-71.

56. Mcdonald, R. E., Chen, Y., Yilmaz, C., and Yen B. T. 1976. **Open steel box sections with top lateral bracing.** Journal of Structural Division, ASCE, 102(ST1): 35-49.

57. Ministry of Transportation and communications. 1985. **Geometric design standards for Ontario Highways.** Downsview, Ontario, Canada.

58. Mirza, M. S., Ferdjani, A., Hadj-arab, A., Joucdar, K., and Khaled, A. 1990. **An experimental study of static and dynamic responses of prestressed concrete box girder bridges.** Canadian Journal of Civil Engineering, 17(3): 481-493.

59. Mirza, M. S., Manatakos, C. K., Murali, R. D., Igwemezie, J. O., and Wyzykowski, J. 1985. **An analytical-experimental study of the behaviour of a composite concrete deck-steel box girder bridge.** Report for Public Works Canada, Department of Civil Engineering and Applied Mechanics, McGill University, Montreal, Quebec, Canada.

60. Mukherjee, D. and Trikha, D. N. 1980. **Design coefficient for curved box girder concrete bridges.** Indian Concrete Journal, 54(11): 301-306.

61. Ng. S. F., Cheung, M. S., and Hachem, H. M. 1993. **Study of a curved continuous composite box girder bridge.** Canadian Journal of Civil Engineering, 20(1): 107-119.

62. Ng. S. F., Cheung, M. S., and Zhao, J. Q. 1993. **A materially non-linear finite-element model for the analysis of curved reinforced concrete box-girder bridges.** Canadian Journal of Civil Engineering, 20(5): 754-759.

63. Normandin, P., and Massicotte, B. 1994. **Load distribution in composite steel box girder bridges. Proceedings of the 4th International Conference on Short and**

Medium Span Bridges. Halifax, N.S., Canada, 165-176.

64. Nour S. I. 2000. **Load Distribution in Curved Composite Concrete Deck-Steel Multiple-spine Box Girder Bridges**. M.A.Sc. Thesis, University of Windsor, Canada, 31-71.

65. Nutt., R. V., Schamber, R. A., and Zokaie, T. 1988. **Distribution of wheel loads on highway bridges**. Transportation Research Board, National Cooperative Highway Research Council, Imbsen & Associates Inc., Sacramento, Calif.

66. Ontario Ministry of Transportation and Communications. 2000. **Canadian highway bridge design code, CHBDC**. Downsview, Ontario

67. Ontario Ministry of Transportation and Communications. 1983. **Ontario highway bridge design code, OHBDC.** Second edition, Downsview, Ontario.

68. Ontario Ministry of Transportation and Communications. 1992. **Ontario highway bridge design code, OHBDC**. Third edition, Downsview, Ontario.

69. Owens, G. W. et al. 1982. **Experimental behaviour of a composite bifurcated box girder bridge.** Proceedings of International Conference on Short and Medium Span Bridges, Toronto, Ontario, Canada, 1: 357-374.

70. Perry, S. H., Waldron, P., and Pinkney, M. W. 1985. **Design and construction of a model prestressed concrete bifurcated box girder bridges.** Proceedings of the Institute of Civil Engineers, ICE, 2(79): 439-454.

71. Pinkney, M. W., Perry, S. H., and Waldron, P. 1985. **Elastic analysis and experimental behaviour to collapse of a 1:12 scale prestressed concrete bifurcated bridges**. Proceedings of the Institute of Civil Engineers, ICE, 2(79): 454-481.

72. Rabizadeh, R. O., and Shore, S. 1975. **Dynamic analysis of curved box-girder bridges**. ASCE Journal of the Structural Division, 101(9): 1899-1912.

73. Razaqpur, A. G., and Nofal, M. 1989. **Nonlinear analysis of prestressed concrete box girder bridges under flexure**. Canadian Journal of Civil Engineering, 16(6): 845-853.

74. Richardson, James A., and Douglas, Bruce, N. 1993. **Results from field testing a curved box girder bridge using simulated earthquake loads**. Earthquake Engineering & Structural Dynamics, 22(10): 905-922.

75. Schelling, D. R., Galdos, N. H., and Sahin, M. A. 1992. **Evaluation of impact factors for horizontally curved steel box bridges**. ASCE Journal of Structural Engineering ,118(11): 3203-3221.

76. Schelling, D., Namini, A. H., and Fu, C. C. 1989. **Construction effects on bracing on curved I-girders.** ASCE Journal of Structural Engineering, 115(9): 2145-2165.

77. Scordelis, A. C. 1975. **Analytical and experimental studies of multi-cell concrete box girder bridges.** Bulletin of the International Association of Shell and Spatial Structures, Madrid, 58: 9-22.

78. Scordelis, A. C. 1982. **Berkeley computer programs for the analysis of concrete box girder bridges.** Proceedings of the NATO Advanced Study Institute on Analysis and Design of Bridges, Izmir, Turkey, 119-189.

79. Scordelis, A. C., and Larsen, P. K. 1977. **Structural response of curved RC box-girder bridge.** ASCE Journal of the Structural Division, 103(ST8): 1057-1524.

80. Scordelis, A. C., Bouwkaup, J. C., and Larsen, P. K. 1974. **Structural behaviour of a curved two-span reinforced concrete box girder bridge model; Volumes I, II, and III.** Reports No. US/SESM 74-5, US/SESM 74-6, and US/SESM 74-7, University of California, Berkeley, CA.

81. Seible, F., and Scordelis, A. C. 1984. **Nonlinear behaviour and failure analysis of multi-cell reinforced concrete box girder bridges**. Canadian Journal of Civil Engineering, 11(3): 411-422.

82. Senthilvasan, J., Brameld, G. H., and Thambiratnam, D. P. 1997. **Bridge-vehicle interaction in curved box girder bridges**. Microcomputers in Civil Engineering, 12(3): 171-181.

83. Sennah K. 1998. **Load Distribution and Dynamic Characteristics of Curved Composite Concrete Deck-Steel Multiple-spine Cellular Bridges**. Ph.D. Thesis, University of Windsor, Canada.

84. Shore, S., and Chaudhuri, S. 1972. **Free-vibration of horizontally curved beams.** ASCE Journal of the Structural Division, 98(3): 793-796.

85. Siddiqui, A. H., and Ng, S. F. 1988. **Effect of diaphragms on stress reduction in box girder bridge sections**. Canadian Journal of Civil Engineering, 15(1):127-135.

86. Soliman, M. I., and Ghali, M. K. 1994. **Effect of diaphragms on the behaviour of R.C. box girder bridges.** Proceeding of the 4th International Conference on Short and Medium Span Bridges, Halifax, N.S., Canada, 211-222.

87. Soliman, M. I., and Elmekawy, S. M. 1994. **Torsional behaviour of reinforced concrete girder type bridges**. Proceeding of the 4th International Conference on Short and Medium Span Bridges, Halifax, N.S., Canada, 223-234.

88. Tabba, M. M. 1972. **Free-vibration of curved box girder bridges**. M.Eng. thesis, Department of Civil Engineering and Applied Mechanics, McGill University, Montreal, Quebec, Canada.

89. Tan, C. P., and Shore. 1968-a. **Dynamic response of a horizontally curved bridge**. ASCE Journal of the Structural Division, 94(3): 761-781.

90. Tan, C. P., and Shore, S. 1968-b. **Response of horizontally curved bridge to moving load.** ASCE Journal of the Structural Division, 94(9): 2135-2151.

91. United States Steel. 1978. **Steel/concrete composite box girder bridges - A construction manual.** Pittsburgh.

92. Wang, T., Huang, D., and Shahawy, M. 1996. **Dynamic behaviour of continuous and cantilever thin-walled box girder bridges**. ASCE Journal of Bridge Engineering, 1(2): 67-75.

93. Wasti, T. S., and Scordelis, A. C. 1982. **Comparative structural behaviour of straight, curved, and skew reinforced concrete box girder models**. Proceedings of the NATO Advanced Study Institute on Analysis and Design of Bridges, Izmir, Turkey, 191-211.

94. Xi-Jiu, Lin, and De-Rong, Chen. 1987. **Prespex model tests of three span continuous curved box girders**. Research Institute of Highway, China, 1-10.

95. Yabuki, T., Arizumi, Y. and Vinnakota, S. 1995. **Strength of thin-walled box girder bridges curved in plan**. ASCE Journal of Structural Engineering, 121(5): 907-914.

96. Yoo, C., Buchanan, J., Heins, C. P., and Armstrong, W. L. 1976. **Analysis of a continuous curved box girder bridge**. Transportation Research Record, 79: 61-71.

97. Yoo, C. H., and Littrell, P. C. 1985. **Cross-bracing effects in curved stringer bridges.** ASCE Journal of Structural Engineering, 112(9)2127-2140.

98. Zokaie, T., Imbsen, R.A., and Osterkamp, T.A. 1991. **Distribution of wheel loads on highway bridges.** Transportation Research Record, Transportation Research Board, 1290: 119-126.

Table 3.1 Average Concrete Compressive Strength of Model Bridges

Bridge Model	M1	M2	M3
Tested Compressive Concrete Strength (MPa)	33	34	27

Table 5.1 Natural Frequency of the bridge models

Bridge Model		First Mode		Second Mode		Third Mode	
		Frequency (Hz)	Mode Shape	Frequency (Hz)	Mode Shape	Frequency (Hz)	Mode Shape
M1	Experimental	20	LF-TS	58	LF-TS	88	TS
	Finite element	24.4		55.7		103.3	
M2	Experimental	20	LF-TS	61	LF-TS	82	TS
	Finite element	24.4		55.7		97.4	
M3	Experimental	30	LF	-	TS	-	TS
	Finite element	34.9		85.2		94.5	

Table 5.2 Ultimate Loads of bridge models

Bridge Model	Ultimate Load Capacity (kN)
M1	89.4
M2	82.1
M3	114.8

Table 6.1 Geometries of the basic prototype bridges used in the parametric study

Bridge Type	Span L (m)	No. of Lanes	No. of Boxes	Cross section dimensions (mm)								
				A	B	C	D	F	T1	T2	T3	T4
2L-2b-ss-20	20	2	2	9300	2325	300	800	1025	16	10	15	225
3L-3b-ss-20		3	3	13050	2175	300	800	1025	16	10	17	225
4L-4b-ss-20		4	4	16800	2100	300	800	1025	16	10	18	225
2L-2b-ss-40	40	2	2	9300	2325	375	1600	1825	28	14	18	225
3L-3b-ss-40		3	3	13050	2175	375	1600	1825	28	14	20	225
4L-4b-ss-40		4	4	16800	2100	375	1600	1825	28	14	21	225
2L-2b-ss-60	60	2	2	9300	2325	450	2400	2625	40	18	23	225
3L-3b-ss-60		3	3	13050	2175	450	2400	2625	40	18	25	225
4L-4b-ss-60		4	4	16800	2100	450	2400	2625	40	18	26	225
2L-2b-ss-80	80	2	2	9300	2325	530	3200	3425	52	22	26	225
3L-3b-ss-80		3	3	13050	2175	530	3200	3425	52	22	28	225
4L-4b-ss-80		4	4	16800	2100	530	3200	3425	52	22	30	225
2L-2b-ss-100	100	2	2	9300	2325	600	4000	4225	64	26	30	225
3L-3b-ss-100		3	3	13050	2175	600	4000	4225	64	26	33	225
4L-4b-ss-100		4	4	16800	2100	600	4000	4225	64	26	35	225

Table 6.2 Material Properties for Concrete and Steel in the parametric Study

Material Properties	Concrete	Reinforcing Steel	Steel
Modulus of Elasticity, E (MPa)	27,000	200,000	200000
Poisson's ratio, ν	0.20	-	0.30
Density, ρ (Kg/m^3)	2400	-	7800

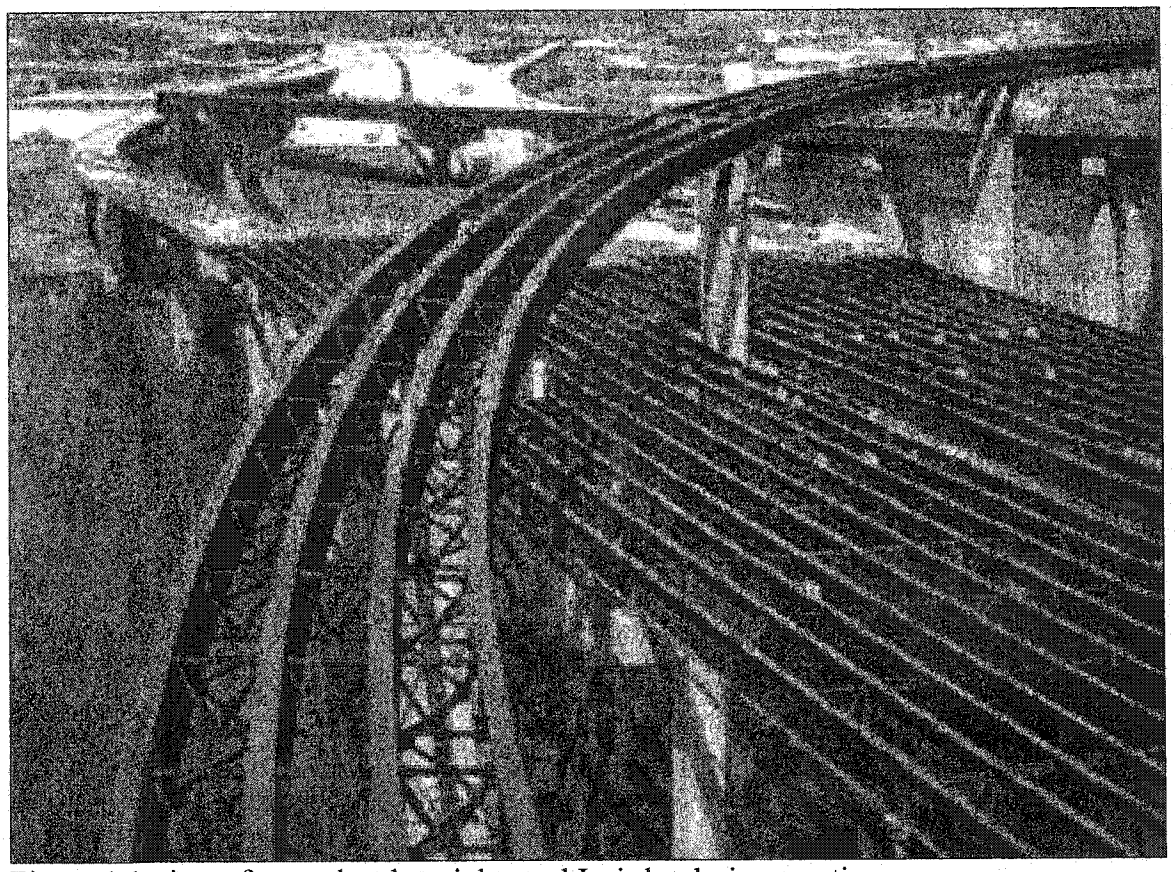

Figure 1.1 view of curved and straight steel I-girder during erection

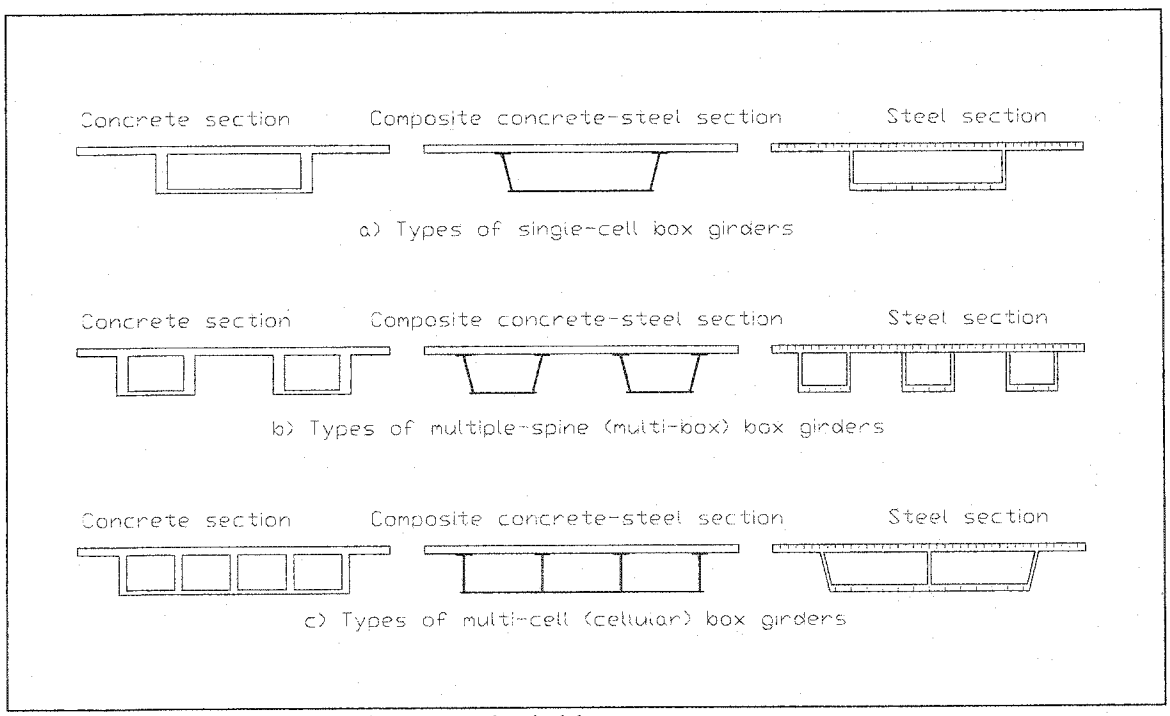

Figure 1.2 Different types of Composite bridges

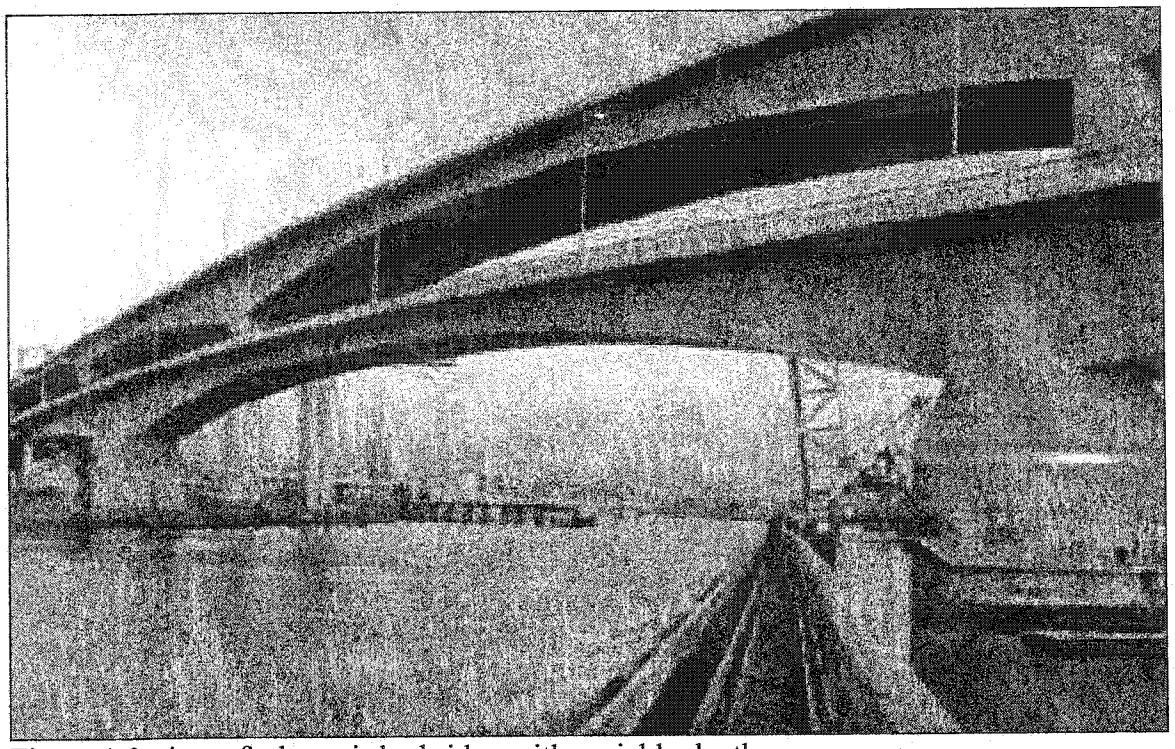

Figure 1.3 view of a box girder bridge with variable depth

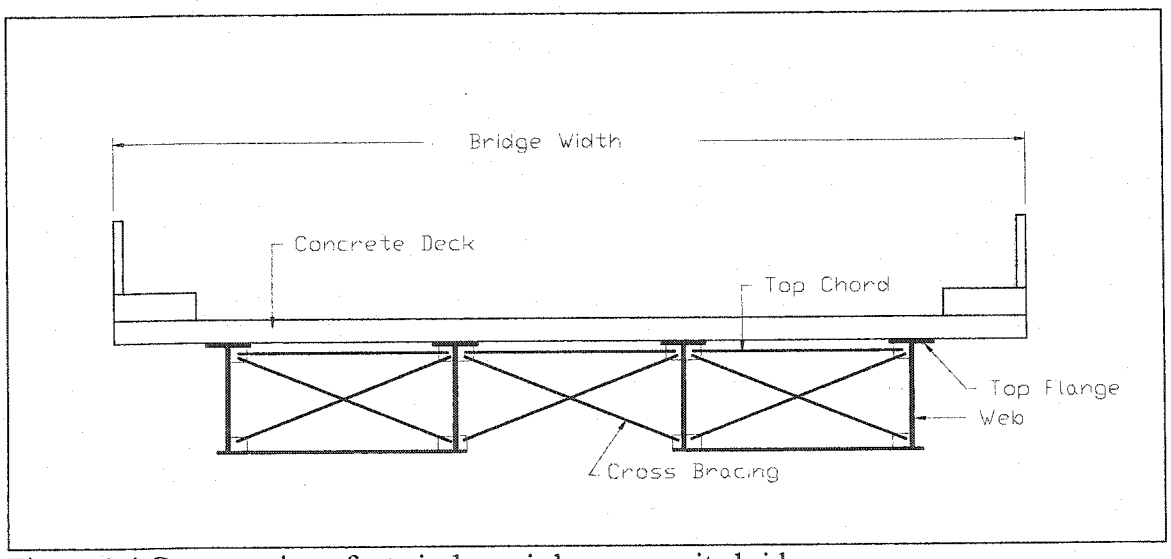

Figure 1.4 Cross section of a twin-box girder composite bridge

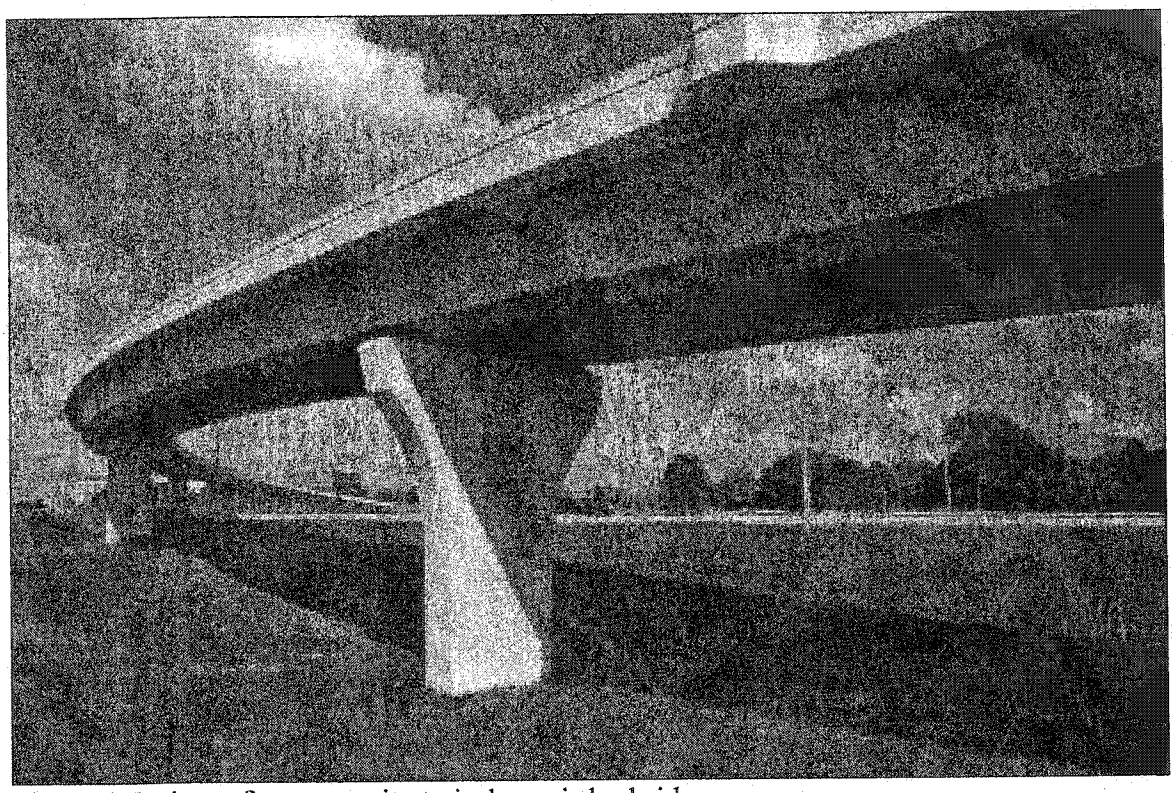

Figure 1.5 view of a composite twin-box girder bridge

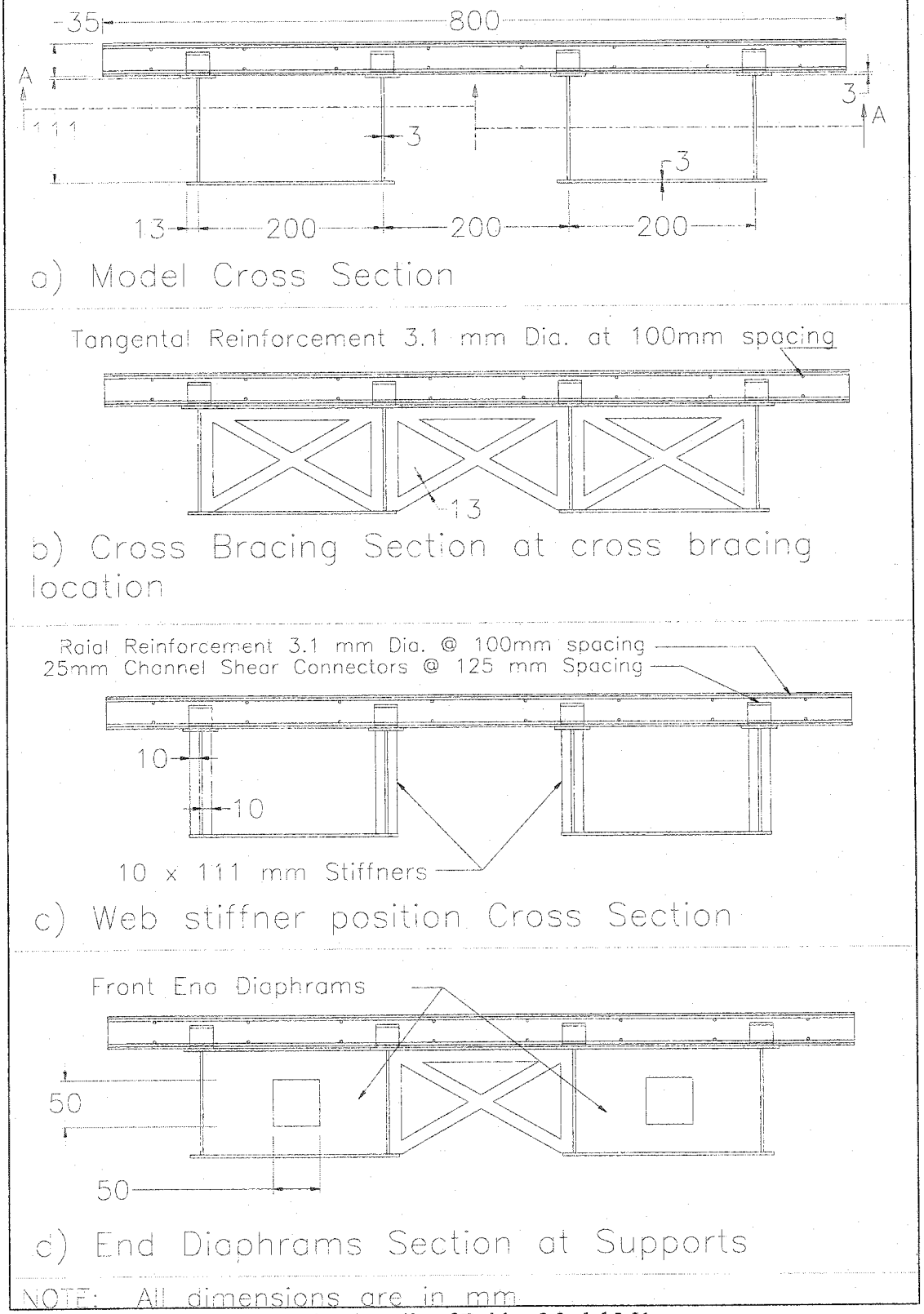

Figure 3.1 Cross Center Section Details of Bridge Model M1

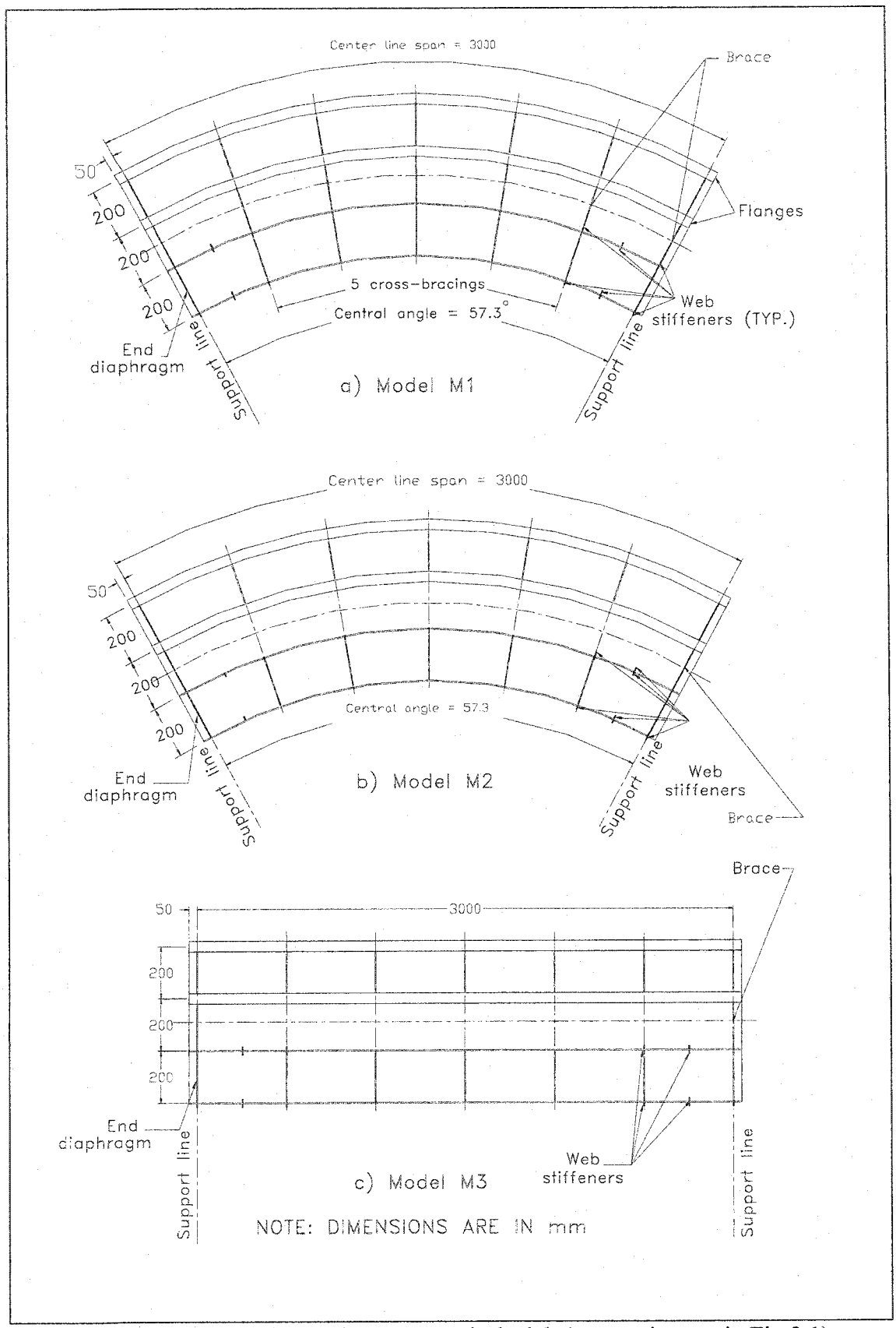

Figure 3.2 Plan view of without the concrete deck slab (see section a-a in Fig.3.1)

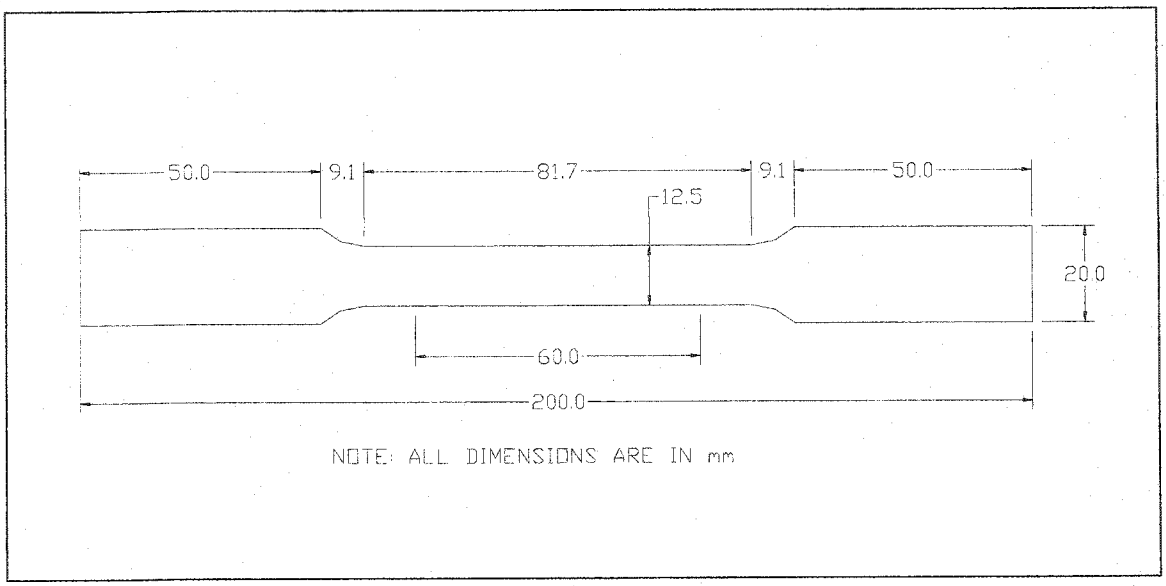

Figure 3.3 Dimensions of steel tension specimen.

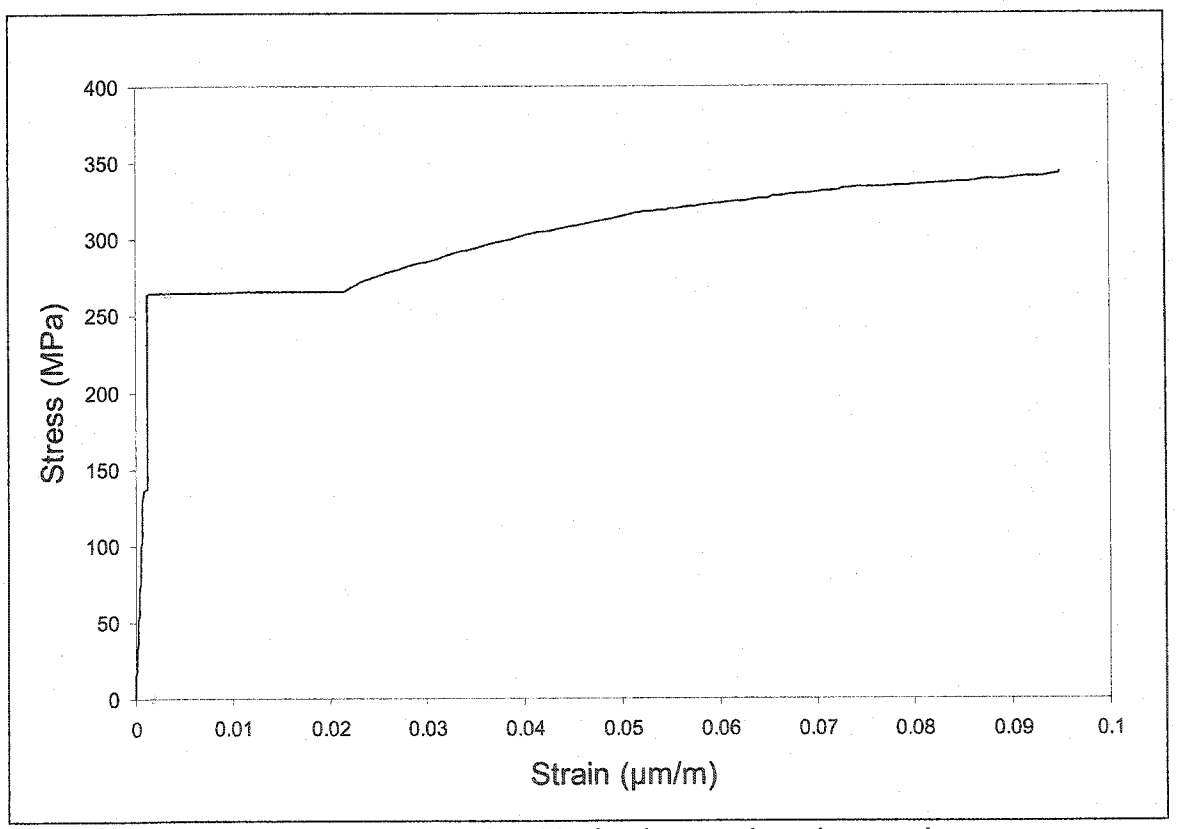

Figure 3.4 Average stress-strain relationship for the tested tension specimen

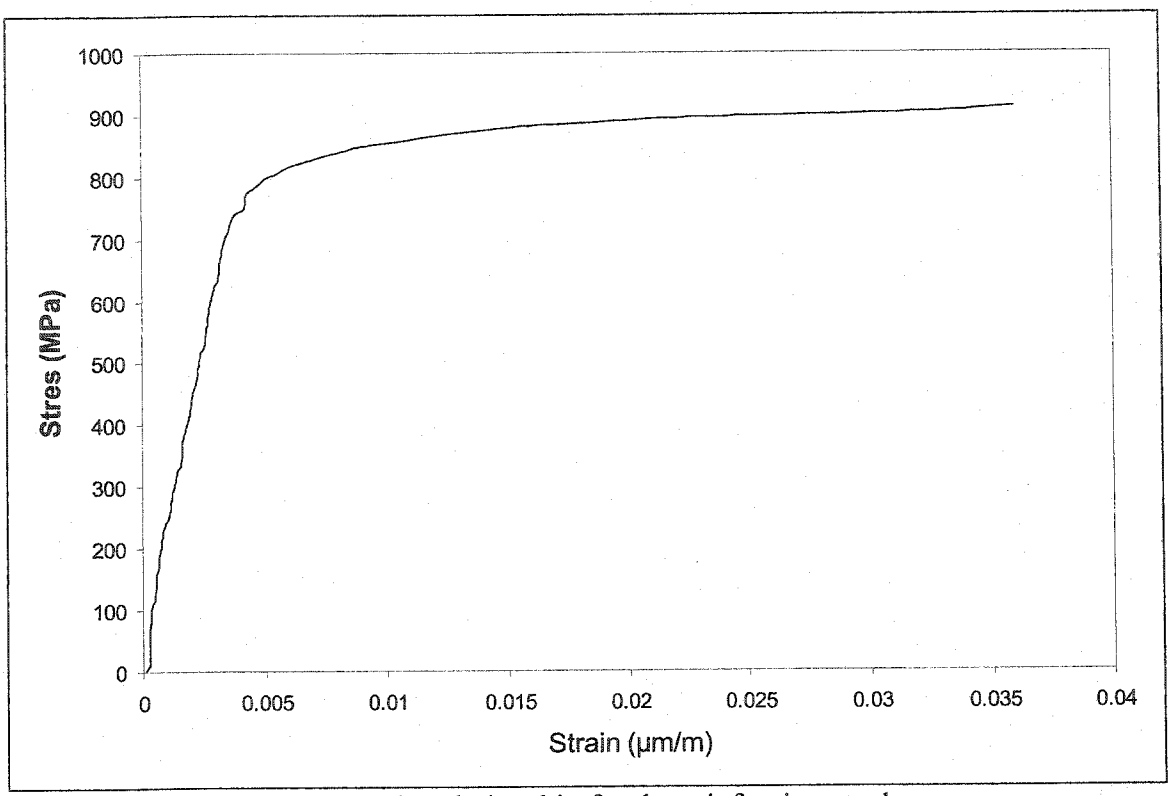

Figure 3.5 Average stress-strain relationship for the reinforcing steel


Figure 3.6 Channel stud welded to top of the steel flange

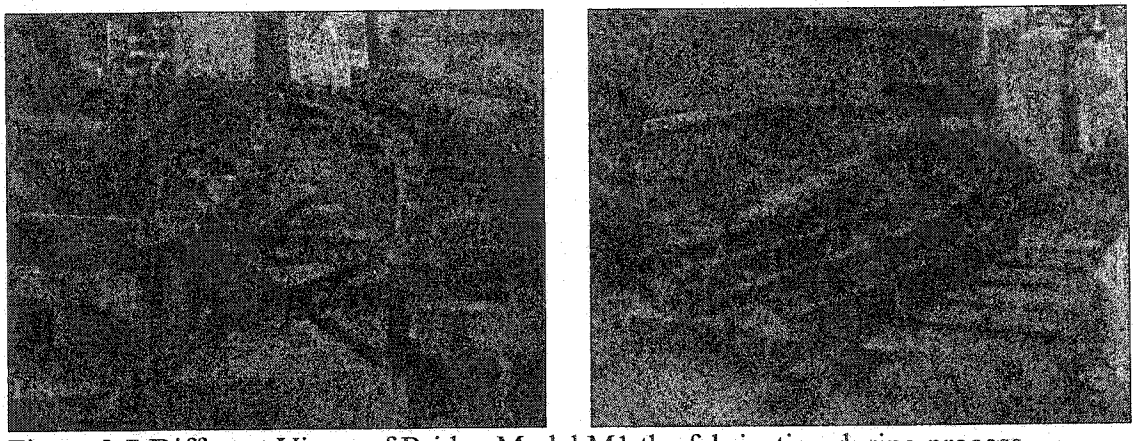

Figure 3.7 Different Views of Bridge Model M1 the fabrication during process

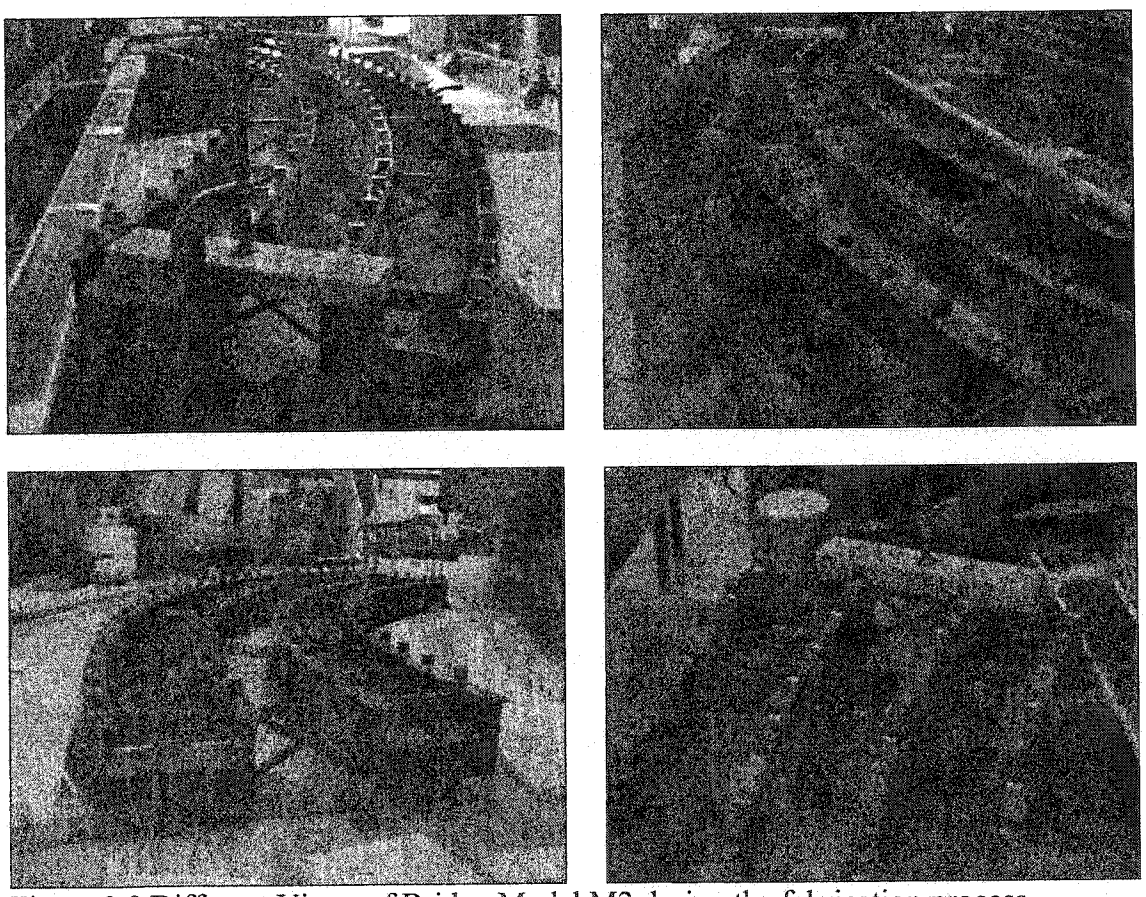

Figure 3.8 Different Views of Bridge Model M2 during the fabrication process

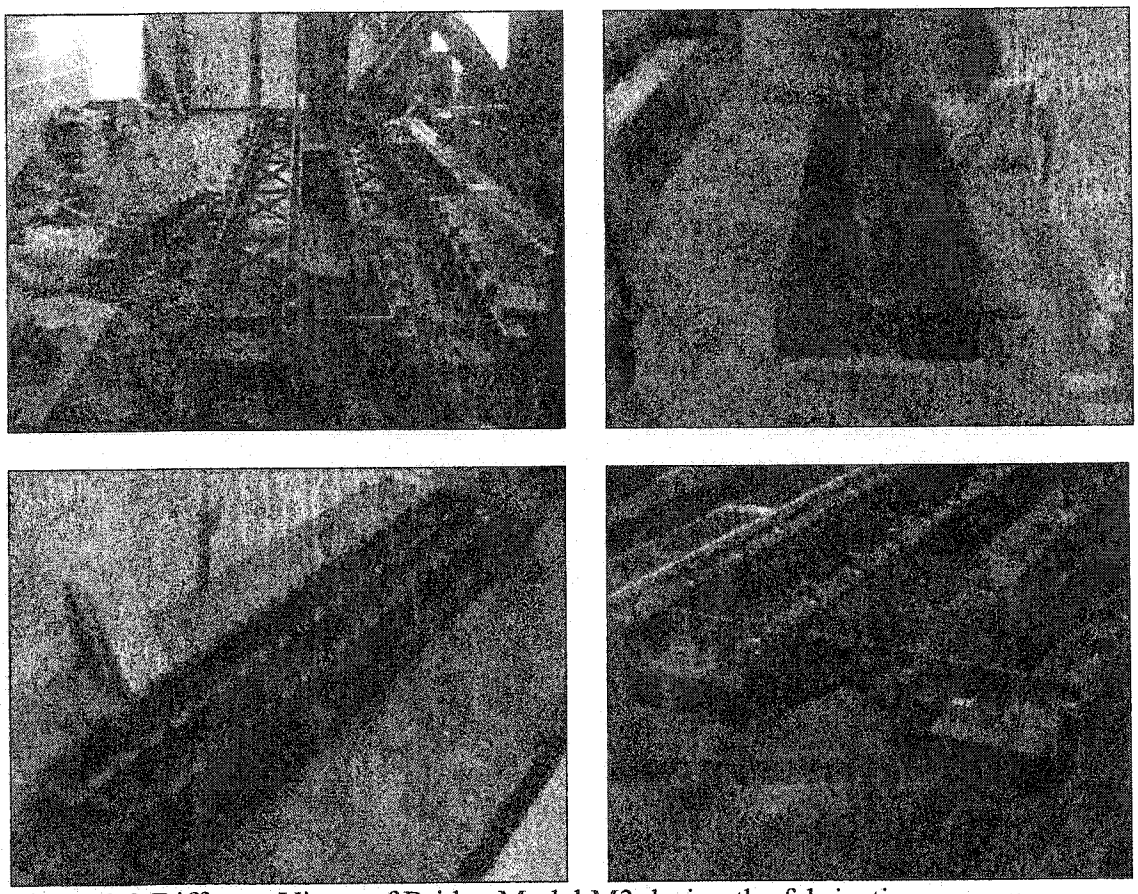

Figure 3.9 Different Views of Bridge Model M3 during the fabrication process

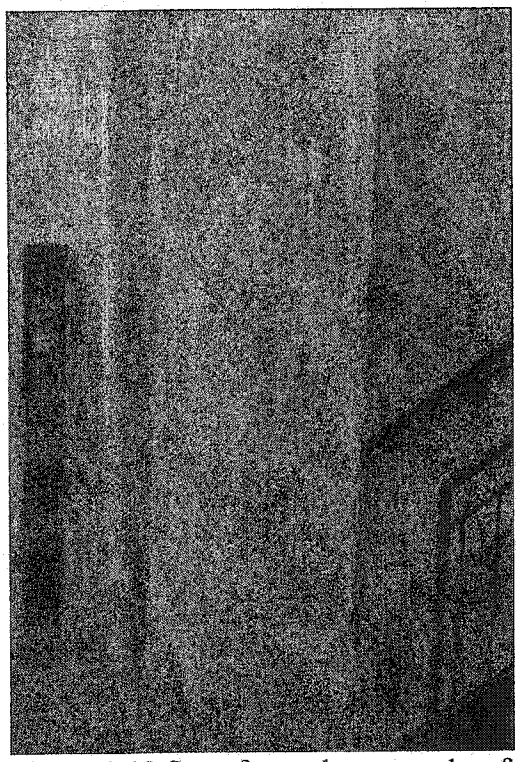

Figure 3.10 Styrofoam sheets used as form work

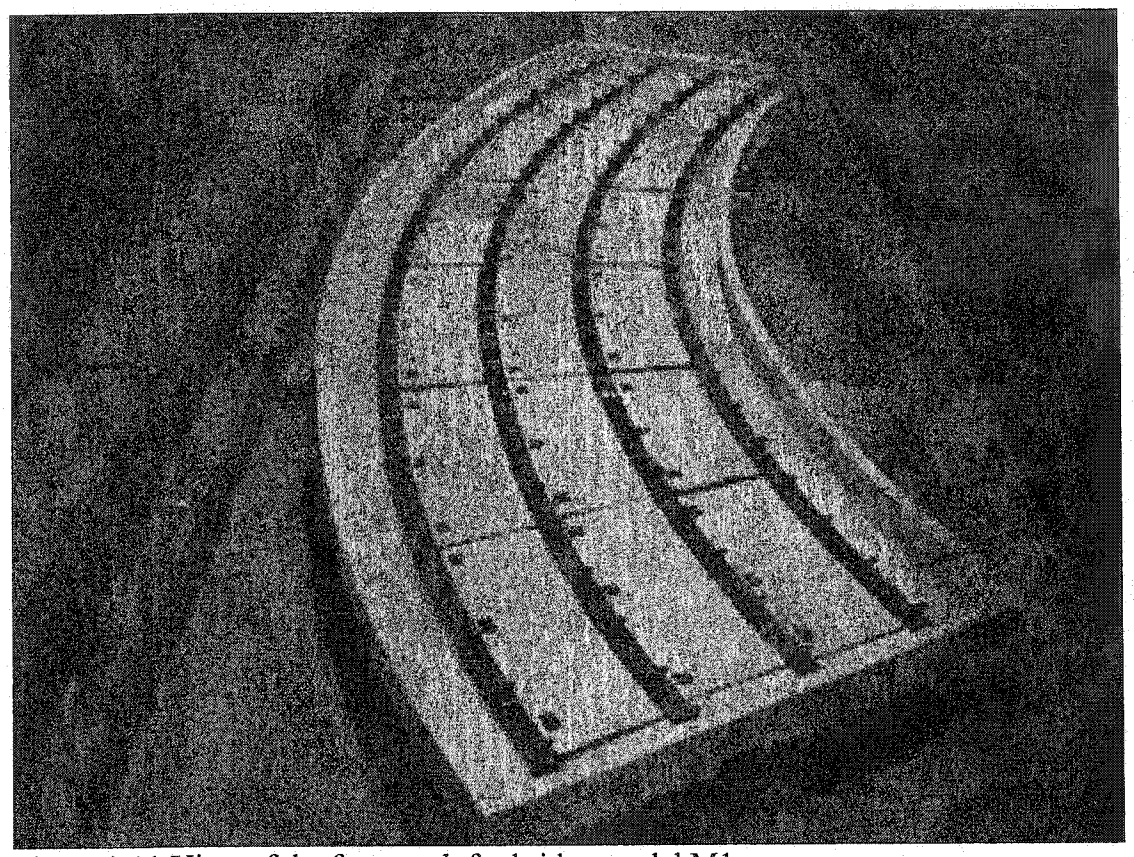

Figure 3.11 View of the formwork for bridge model M1

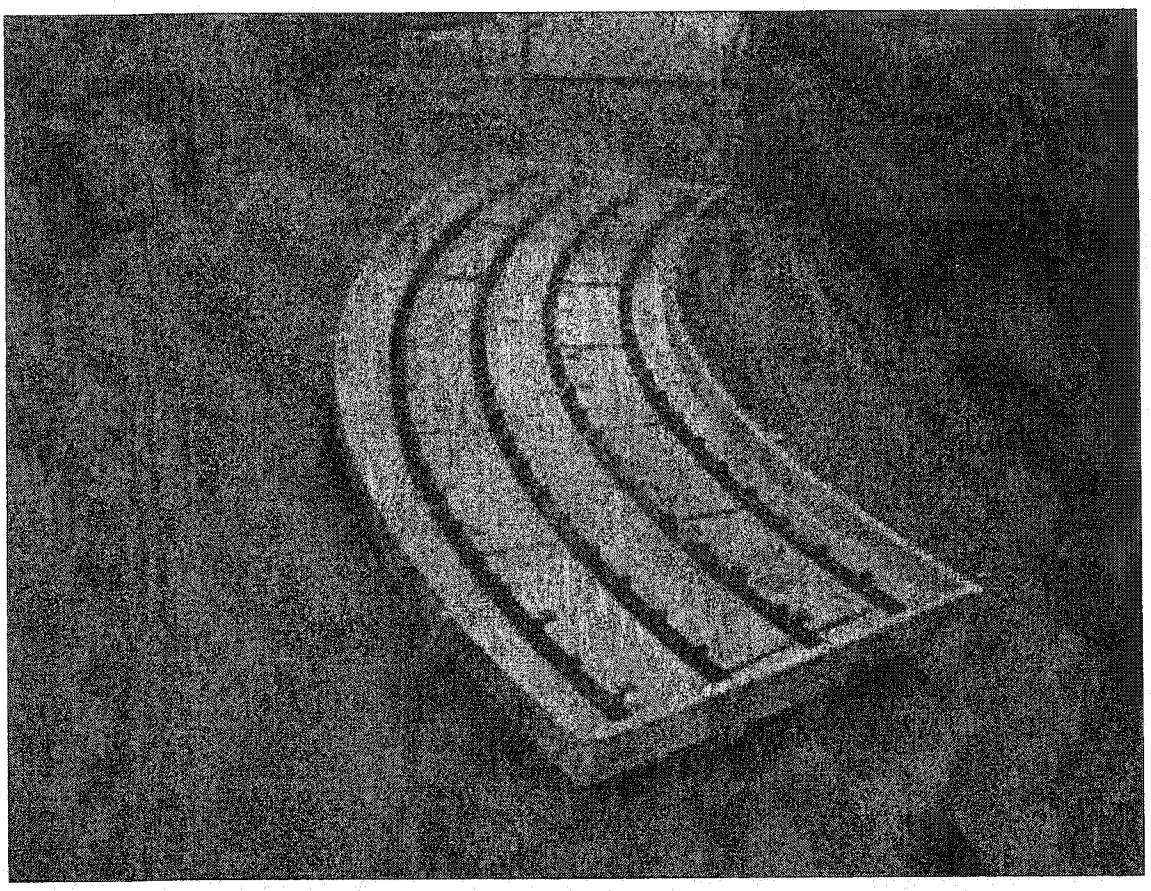

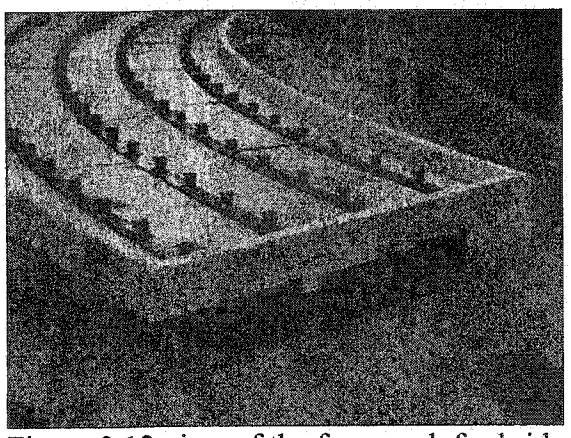

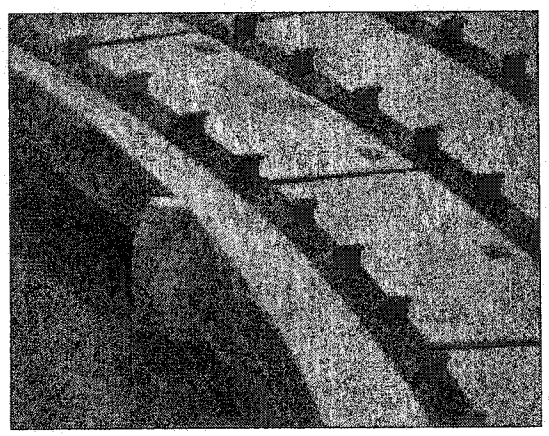

Figure 3.12 view of the formwork for bridge model M2

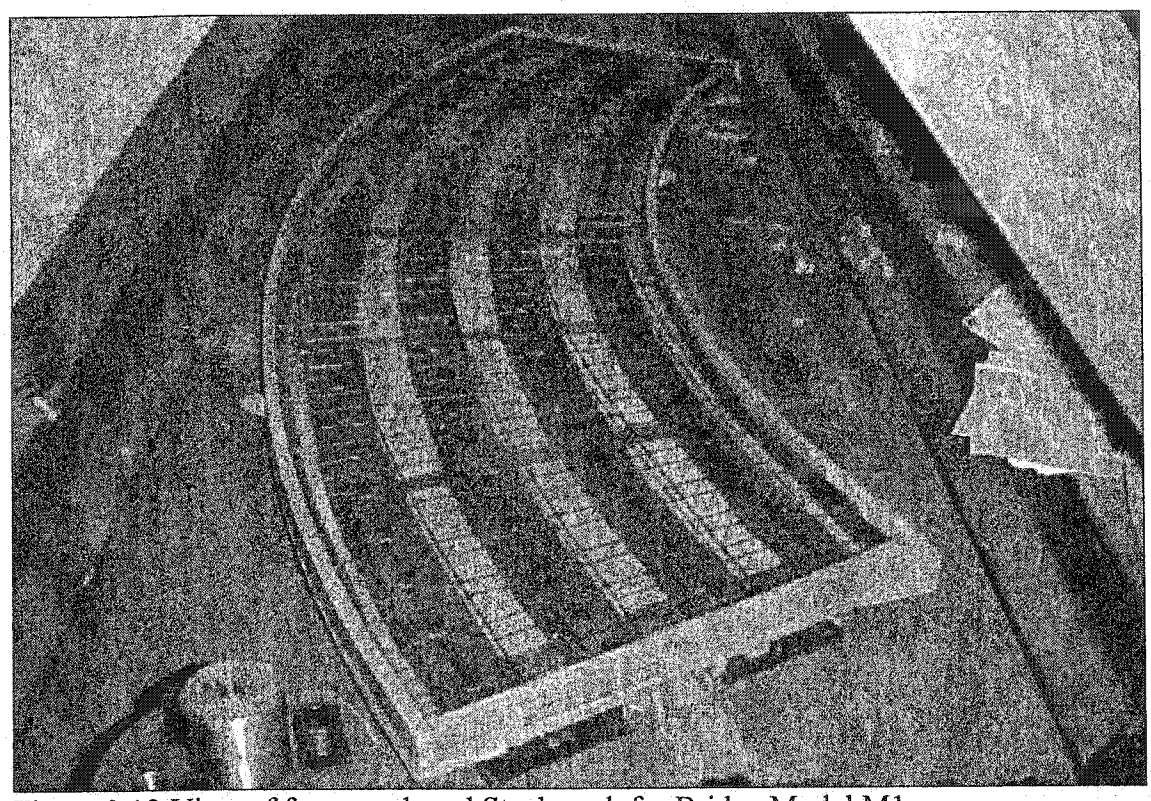

Figure 3.13 View of form work and Steel mesh for Bridge Model M1

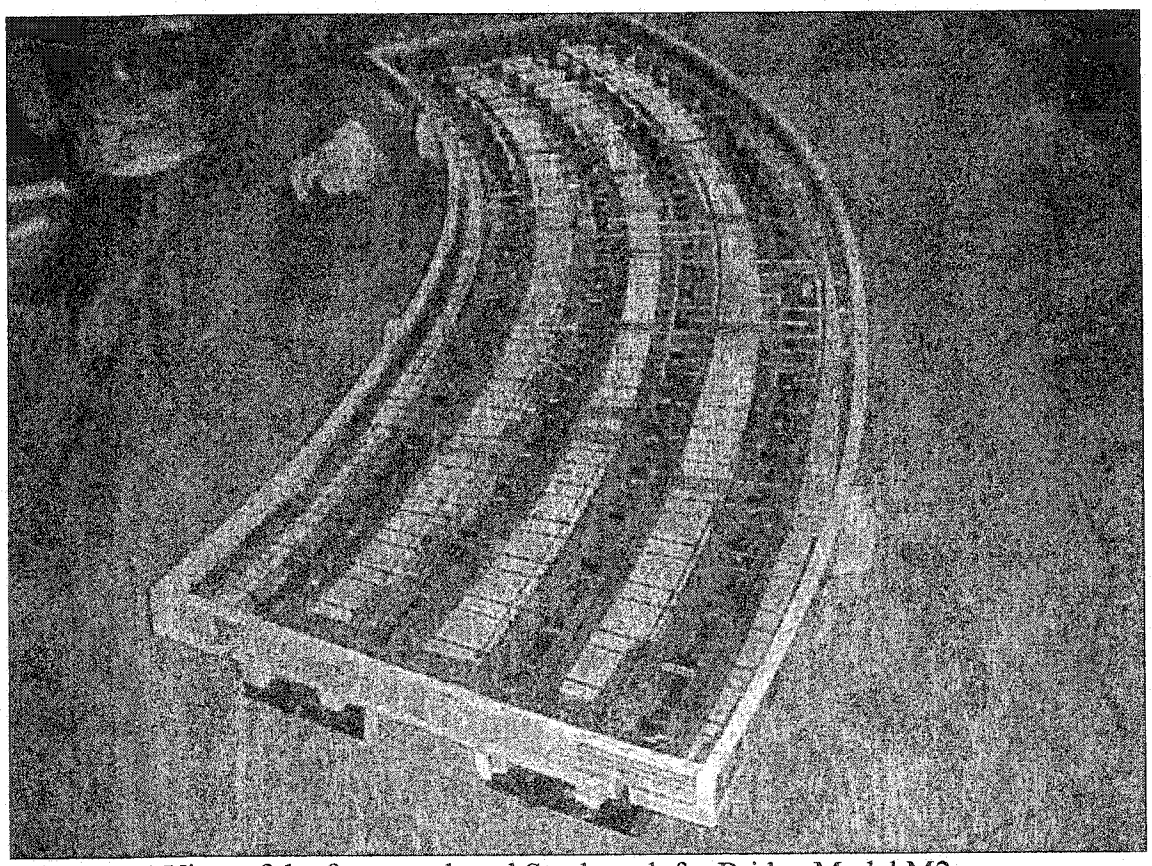

Figure 3.14 View of the form work and Steel mesh for Bridge Model M2

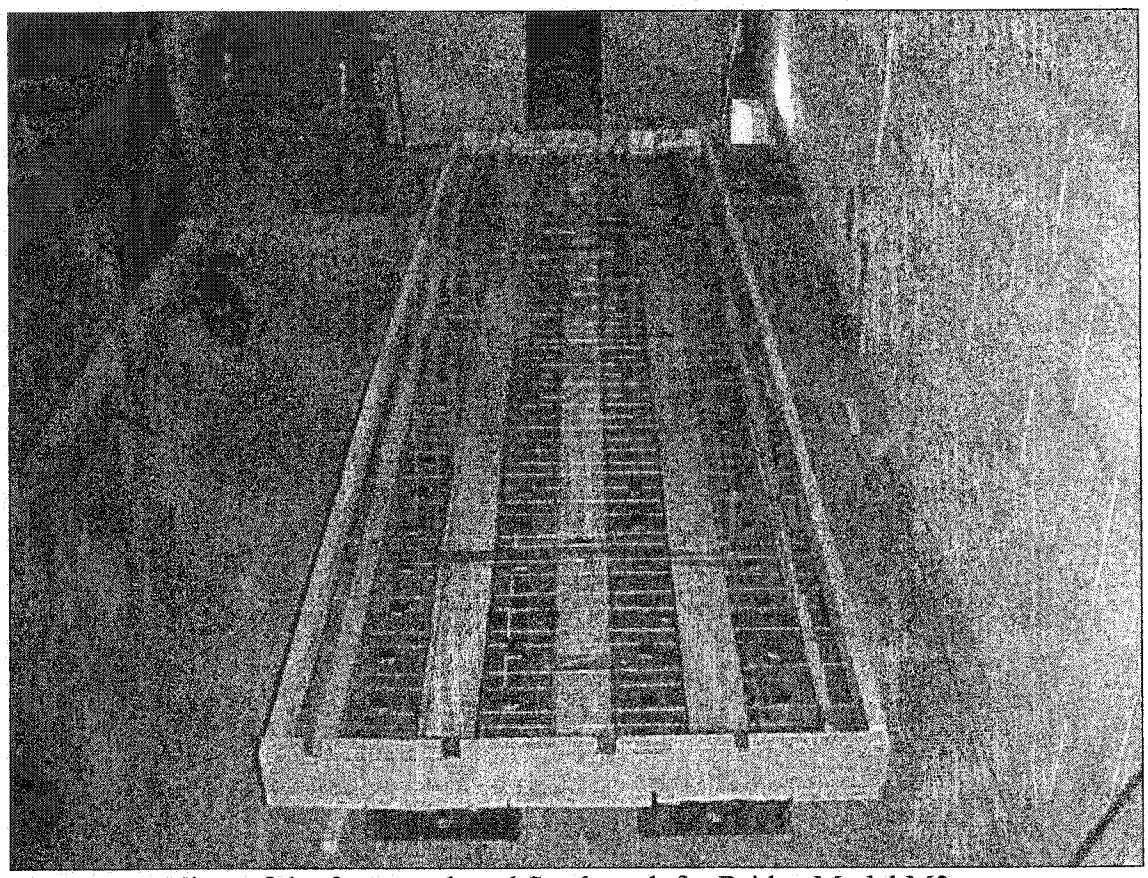

Figure 3.15 View of the form work and Steel mesh for Bridge Model M3

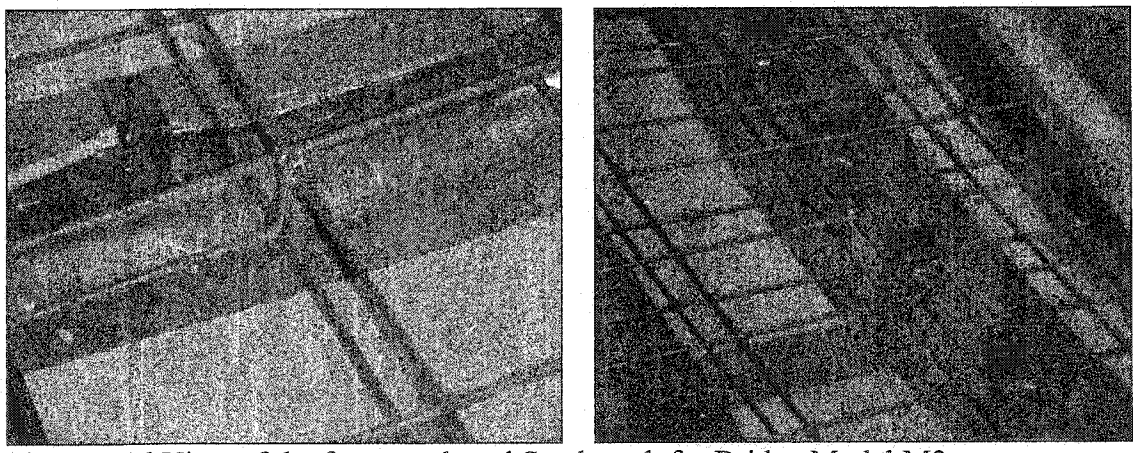

Figure 3.16 View of the form work and Steel mesh for Bridge Model M3

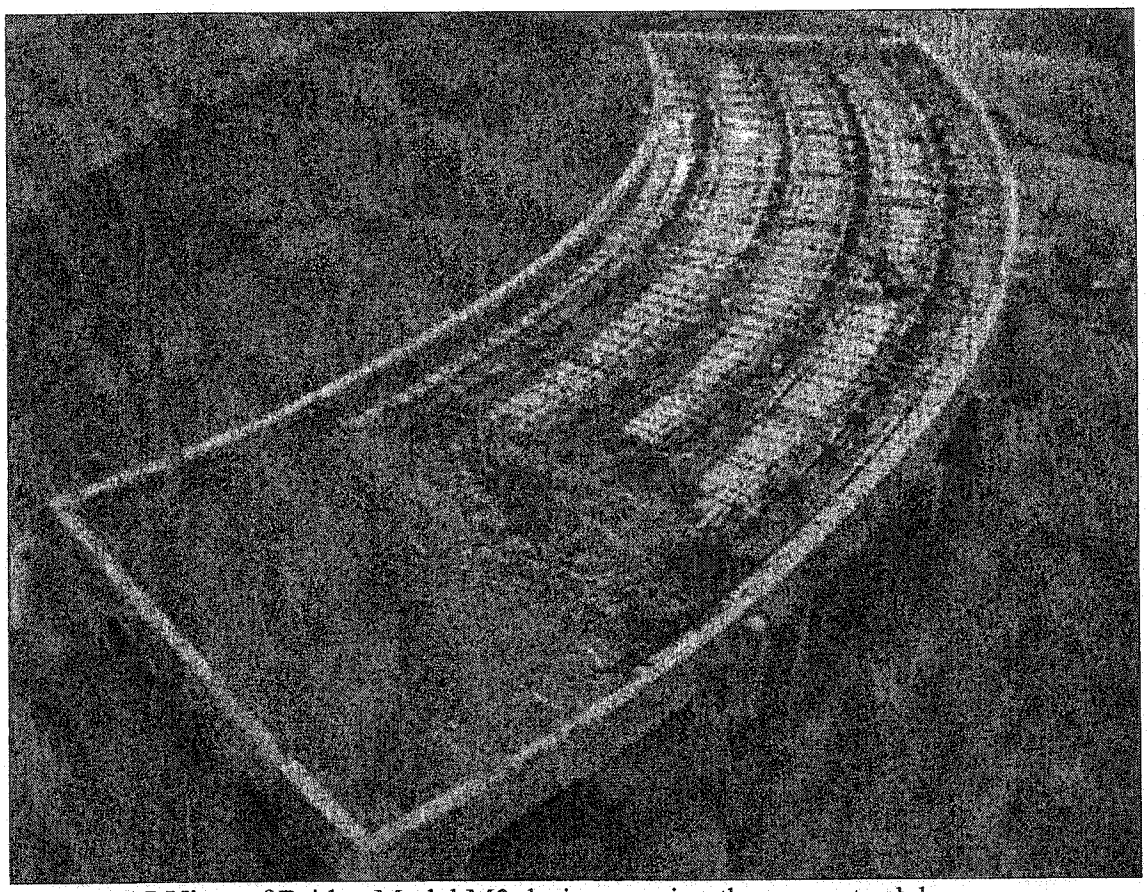

Figure 3.17 View of Bridge Model M2 during pouring the concrete slab

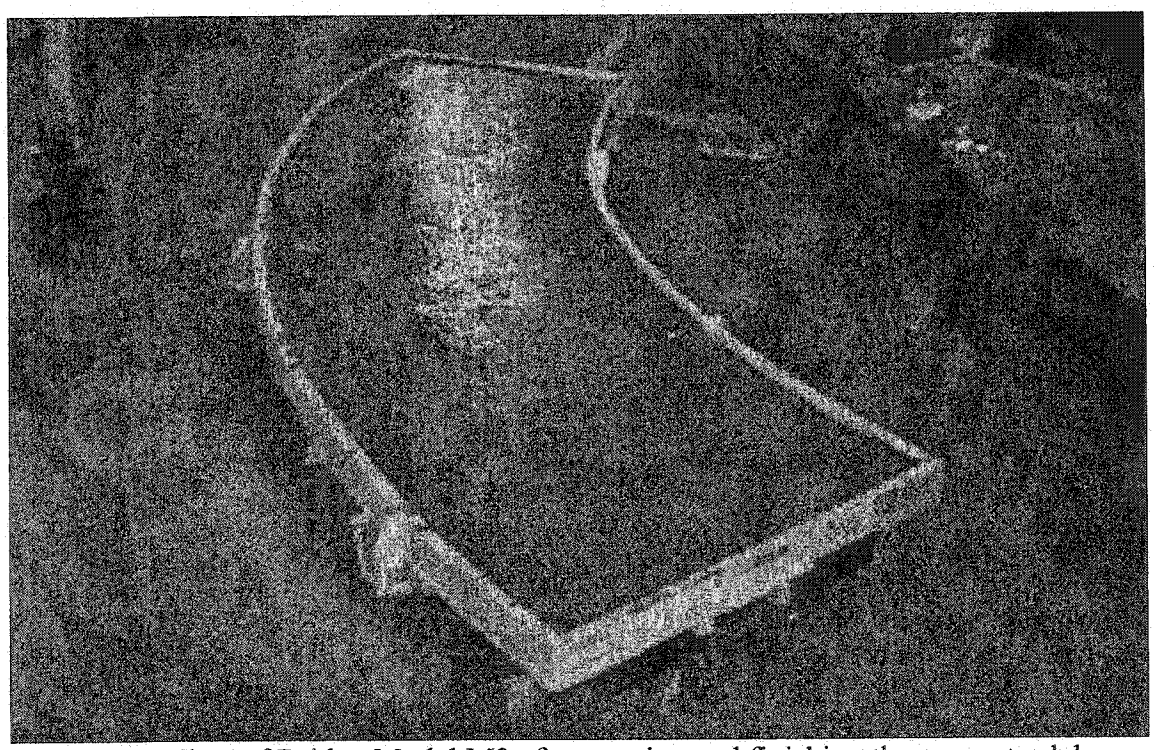

Figure 3.18 View of Bridge Model M2 after pouring and finishing the concrete slab

Figure 3.19 View of bridge model M3 during pouring the concrete slab

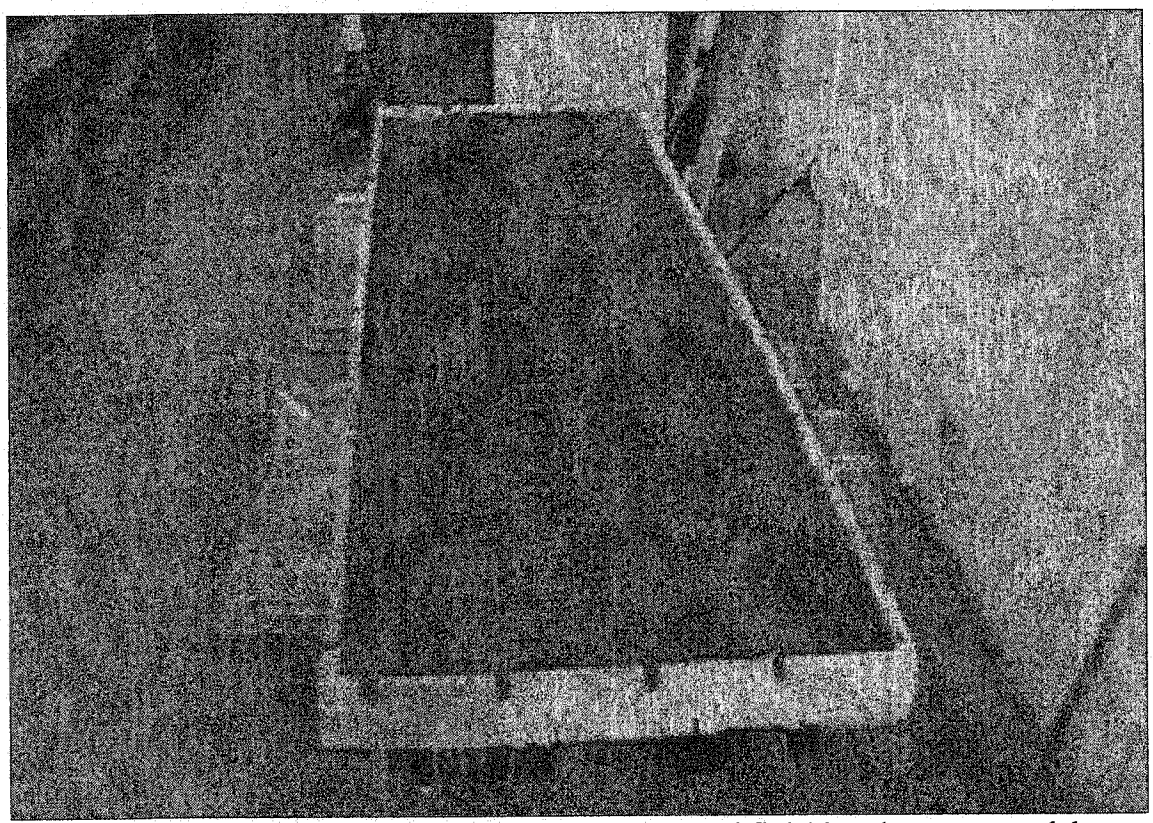

Figure 3.20 View of Bridge Model M3 after pouring and finishing the concrete slab

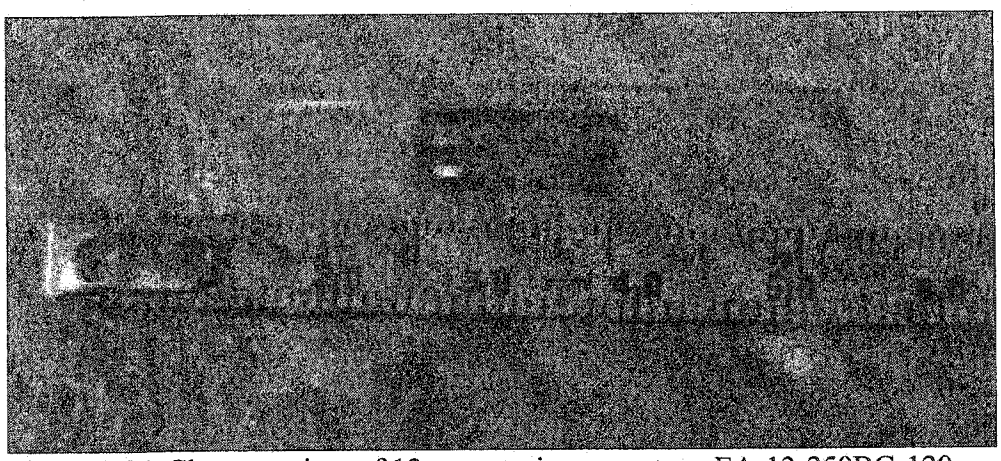

Figure 3.21 Close up view of 13 mm strain gauge type EA-13-250BG-120

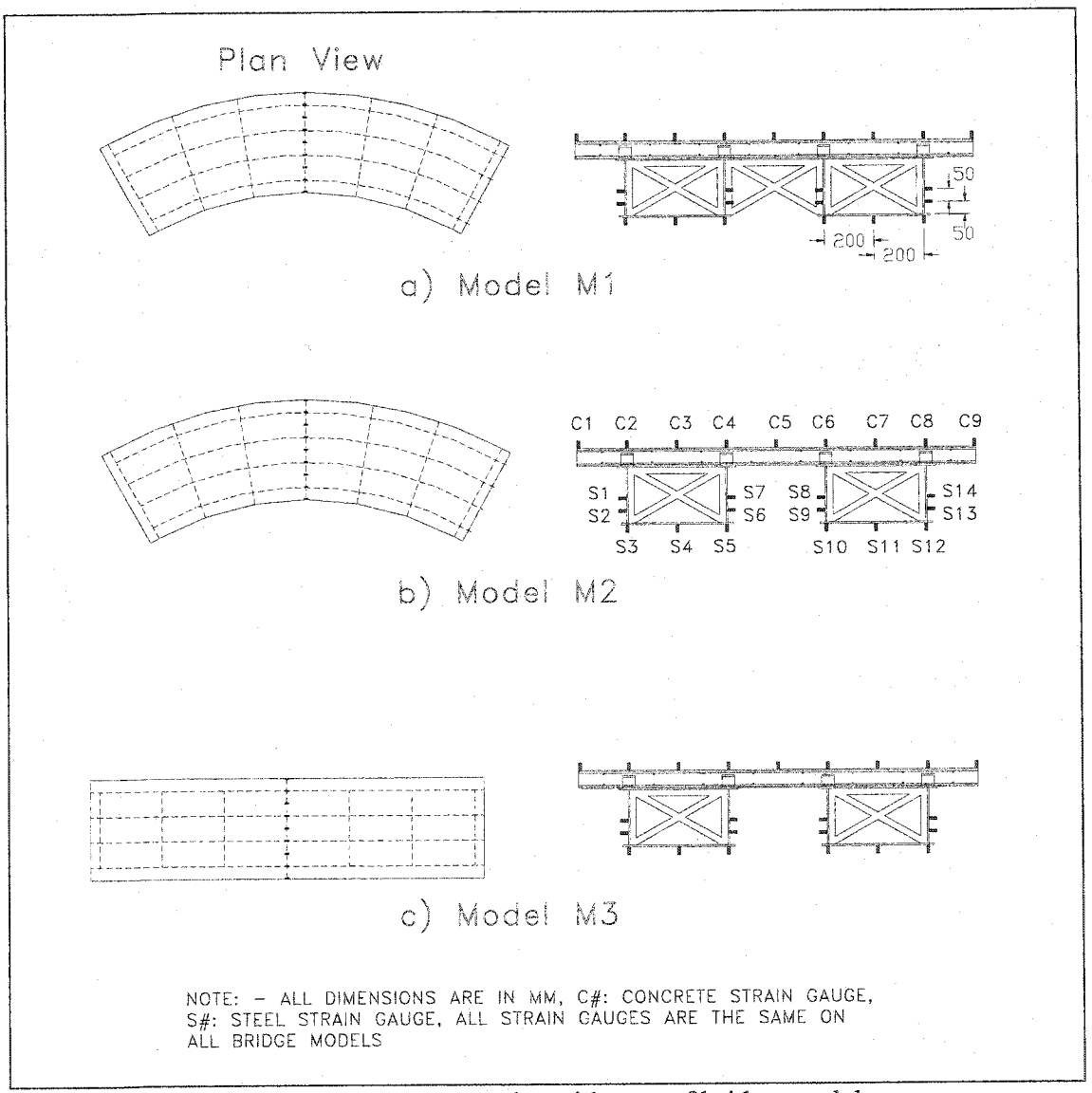

Figure 3.22 Location of strain gauges at the mid span of bridge models

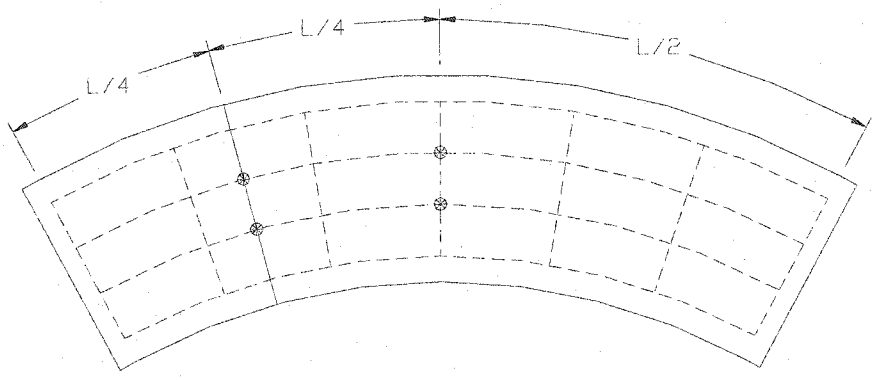

a) Setup type I of LVDT's on model M1 for the natural frequency test

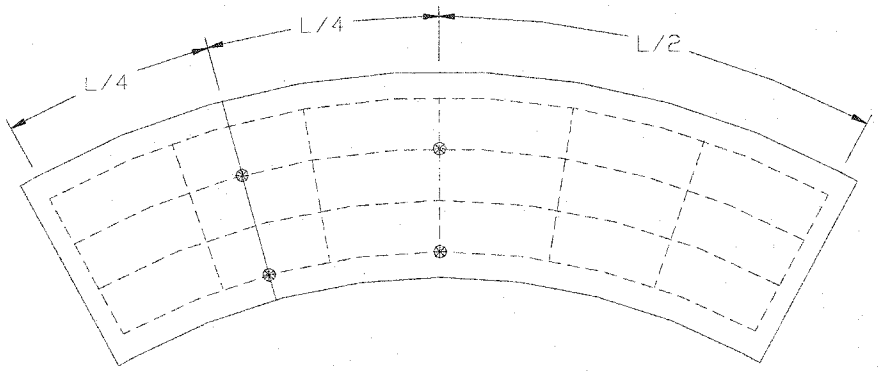

b) Setup type II of LVDT's on model M1 for the natural frequency test

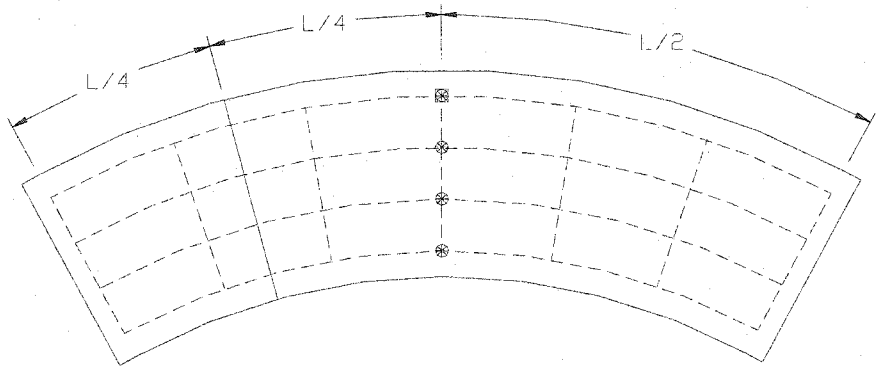

c) Setup of LVDT's on model M1 for all Loading stages

Note: LVDT Location, ⊛ Mechanical Dial Location ⊠

Figure 3.23 Different setups of LVDT's and Mechanical dials for Bridge Model M1

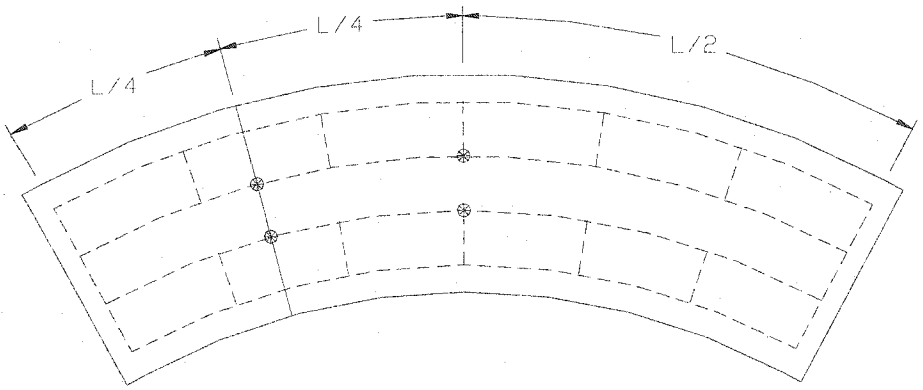

a) Setup type I of LVDT's on model M2 for the natural frequency test

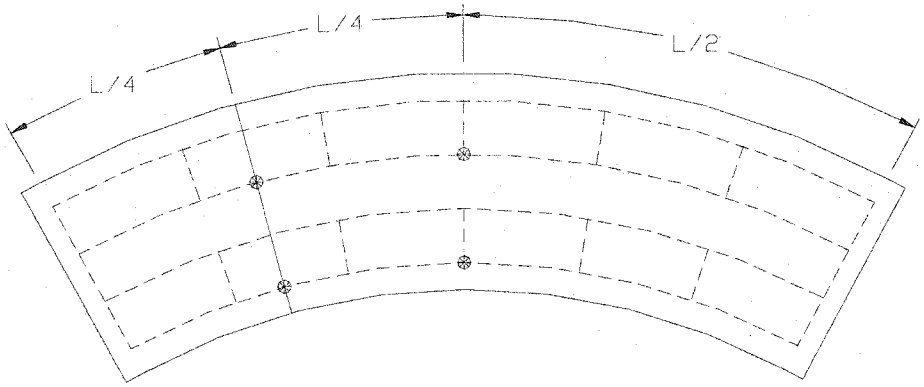

b) Setup type II of LVDT's on model M2 for the natural frequency test

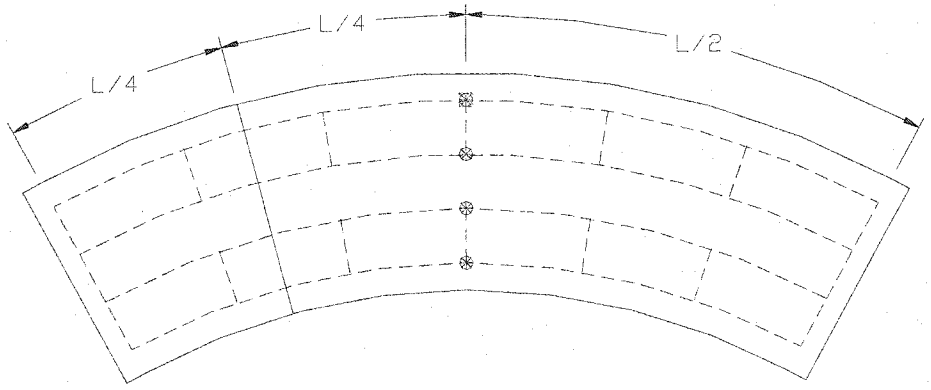

c) Setup of LVDT's on model M2 for all Loading stages

Note: ⊛ LVDT Location, ⊠ Mechanical Dial Location

Figure 3.24 Different setups of LVDT's and Mechanical dials for Bridge Model M2

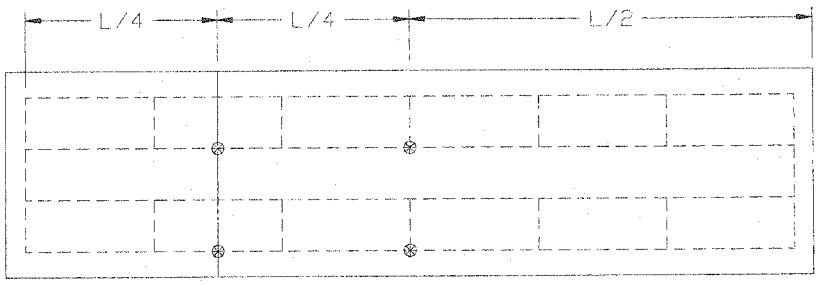

a) Setup type I of LVDT's on model M3 for the natural frequency test

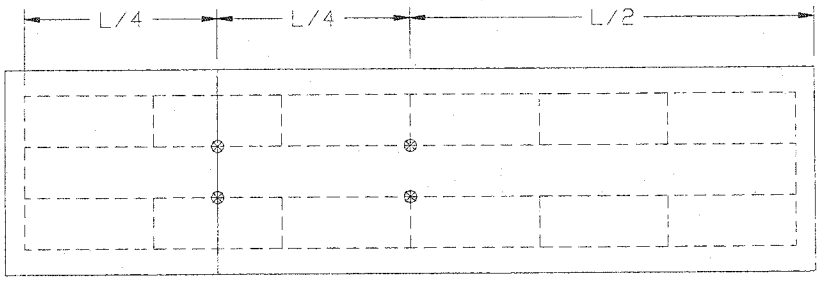

b) Setup type II of LVDT's on model M3 for the natural frequency test

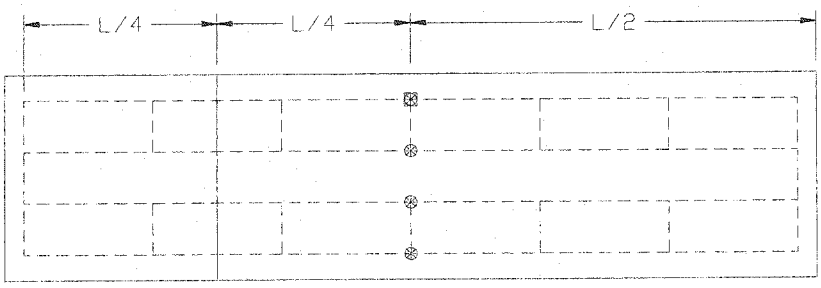

c) Setup of LVDT's on model M3 for all Loading stages

Note: ⊛ LVDT Location, ⊠ Mechanical Dial Location

Figure 3.25 Different setups of LVDT's and Mechanical dials for Bridge Model M3

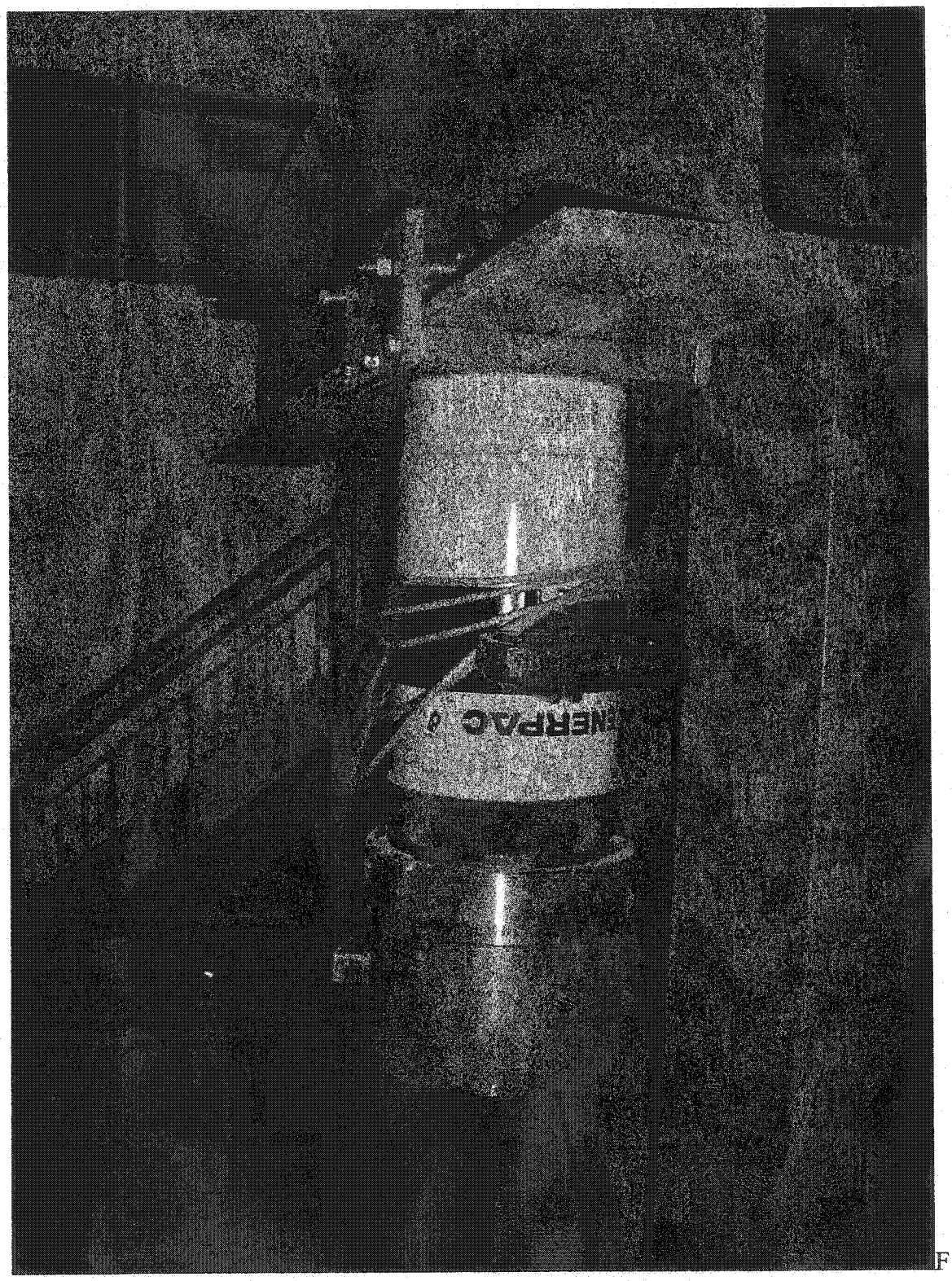

Figure 3.26 The hydraulic jack and load cell used to load bridge models

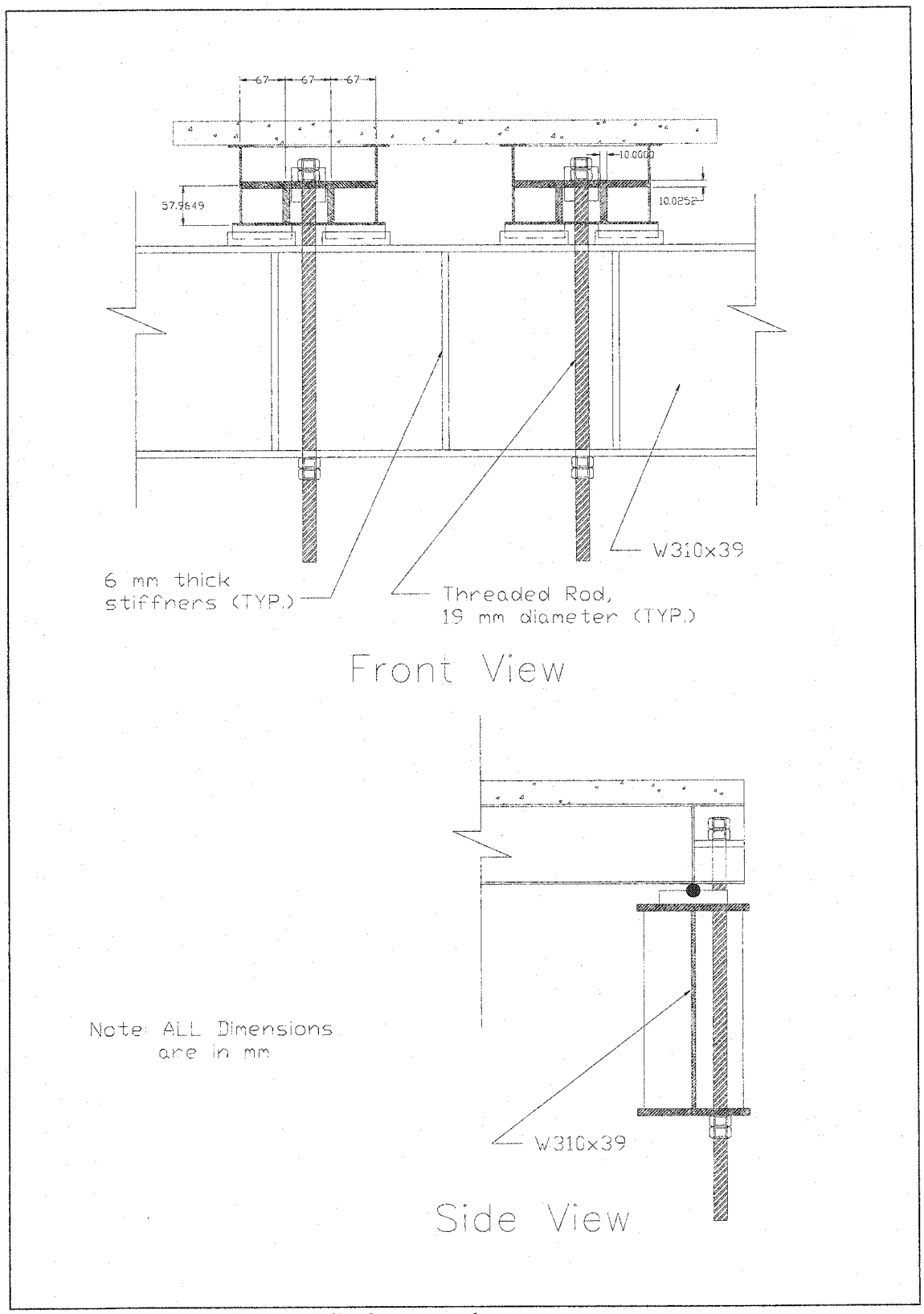

Figure 3.27 Details of the end diaphragm and supports

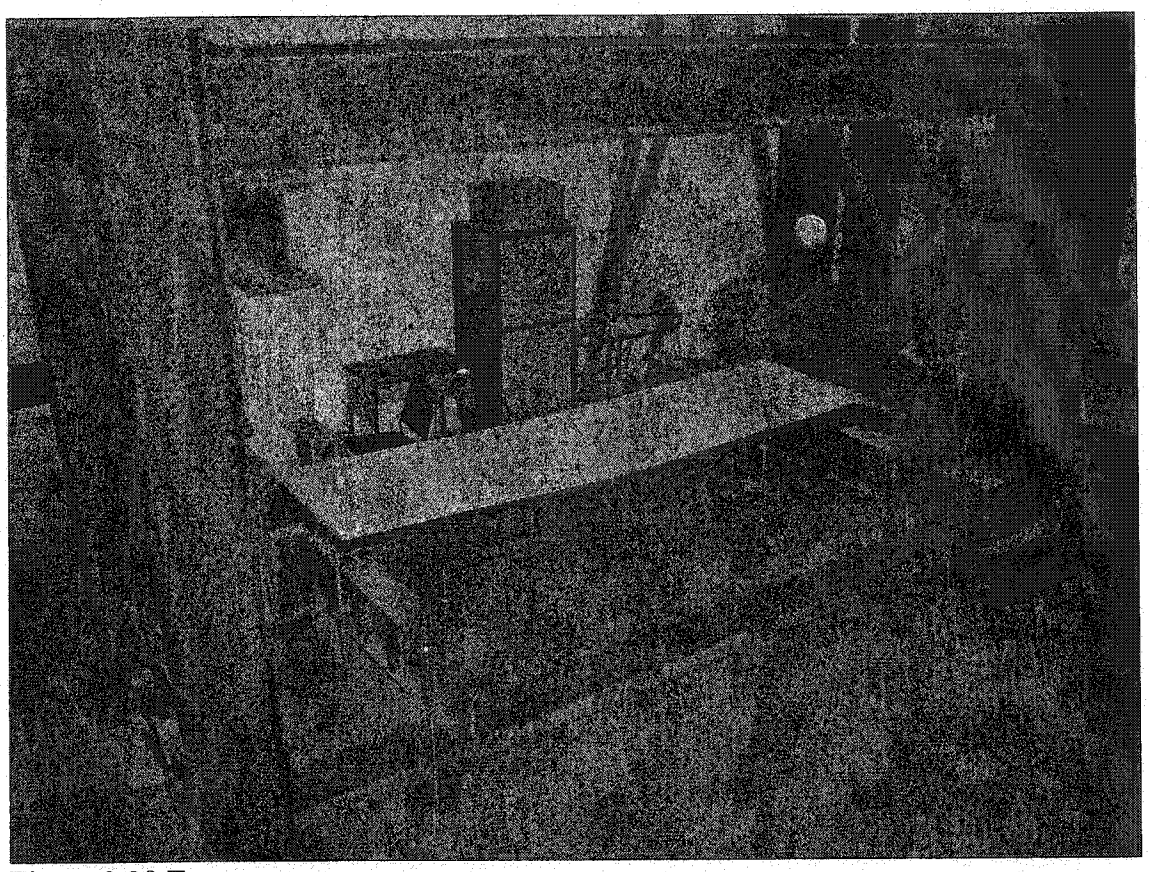

Figure 3.28 Test set up arrangement

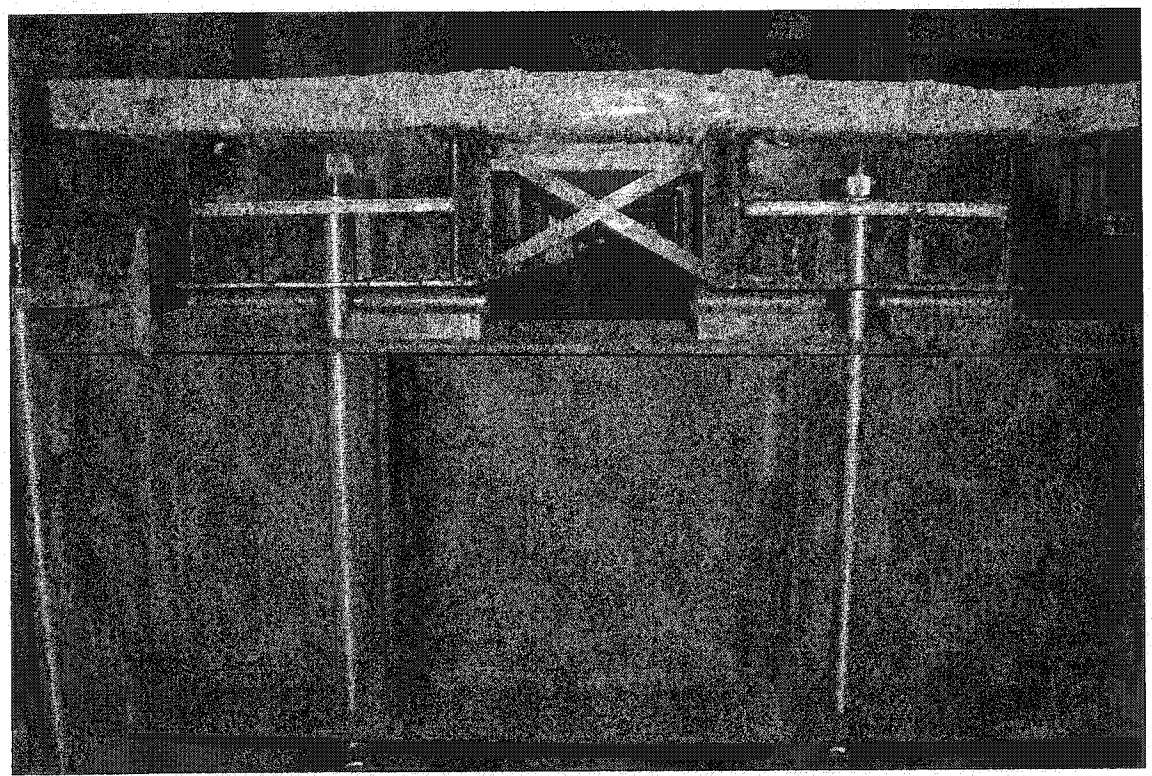

Figure 3.29 View of the tie down system of the bridge support line

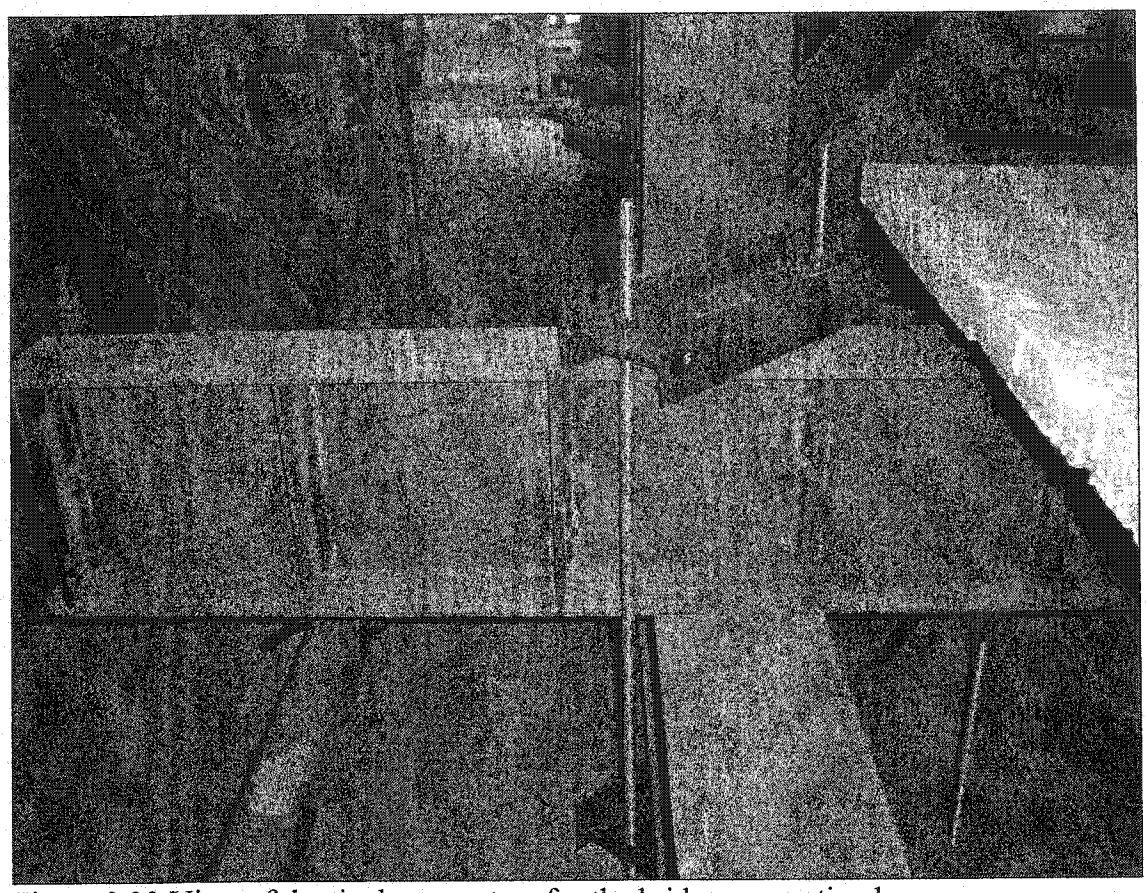

Figure 3.30 View of the tie down system for the bridge supporting beam

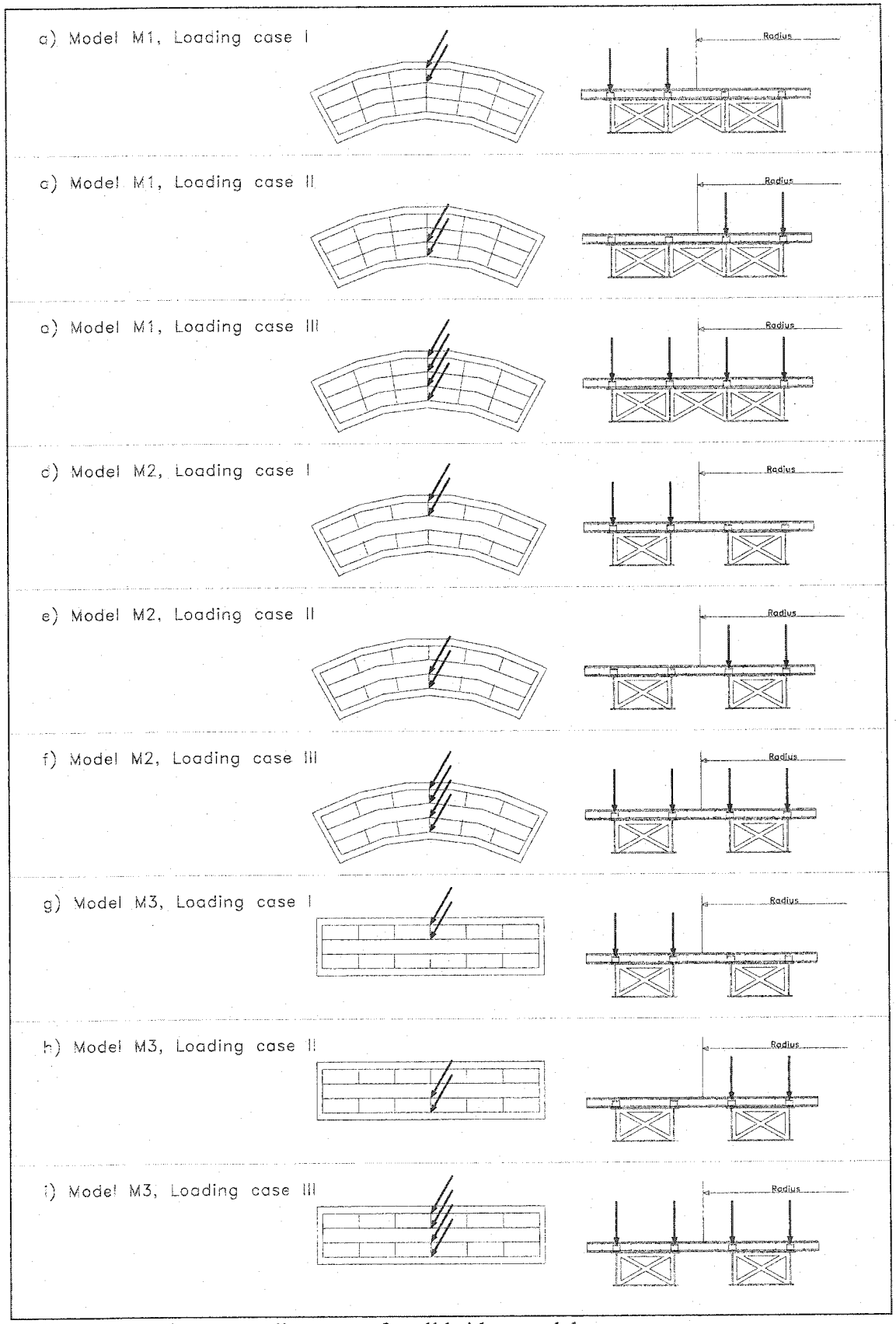

Figure 3.31 Different Loading cases for all bridge models

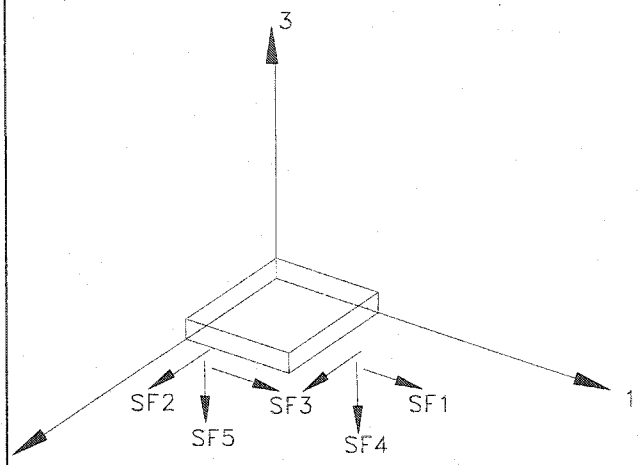

a) Output forces

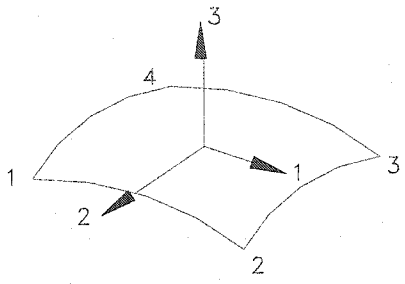

c) Shell element "S4R" (in ABAQUS)

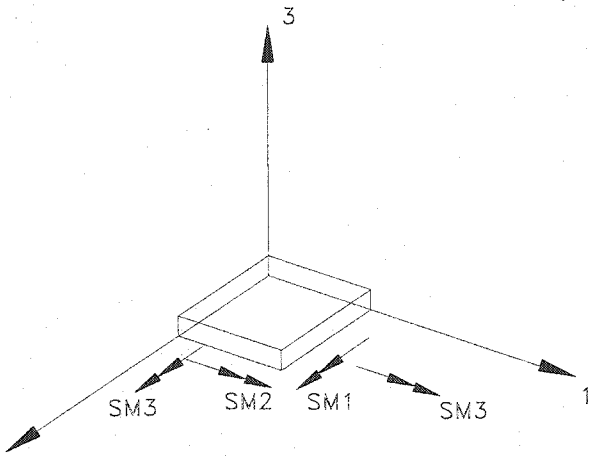

b) Output moments

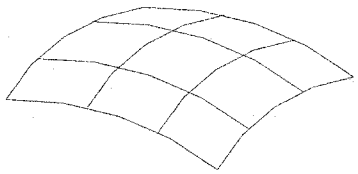

d) Rebar in a shell

Note: - Four-node element1
- Degrees of freedom : U1, U2, U3, F 1, F 2, F 3.
- Output forces :SF1, SF2, SF3, SF4, SF5, SF6
- Output moments :SM1, SM2, SM3
- Stress Components :S11, S22, S12
- Strain Components :E11, S22, S12
- Rebar Option available in two directions

Figure 4.1 Shell Element S4R used for model plates in ABAQUS Software

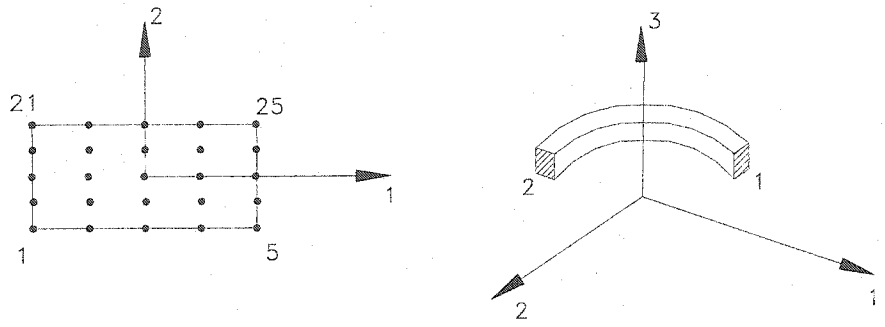

(a) Integration Points in beam element B31H for output results

(b) Element B31H in ABAQUS

Note: - two-node element
- Degrees of freedom : U1, U2, U3, F 1, F 2, F 3.
- Output forces :SF1, SF2, SF3, SF4, SF5, SF6
- Output moments :SM1, SM2, SM3
- Stress Components :S11, S22, S12

Figure 4.2 Beam element "B31H" in space

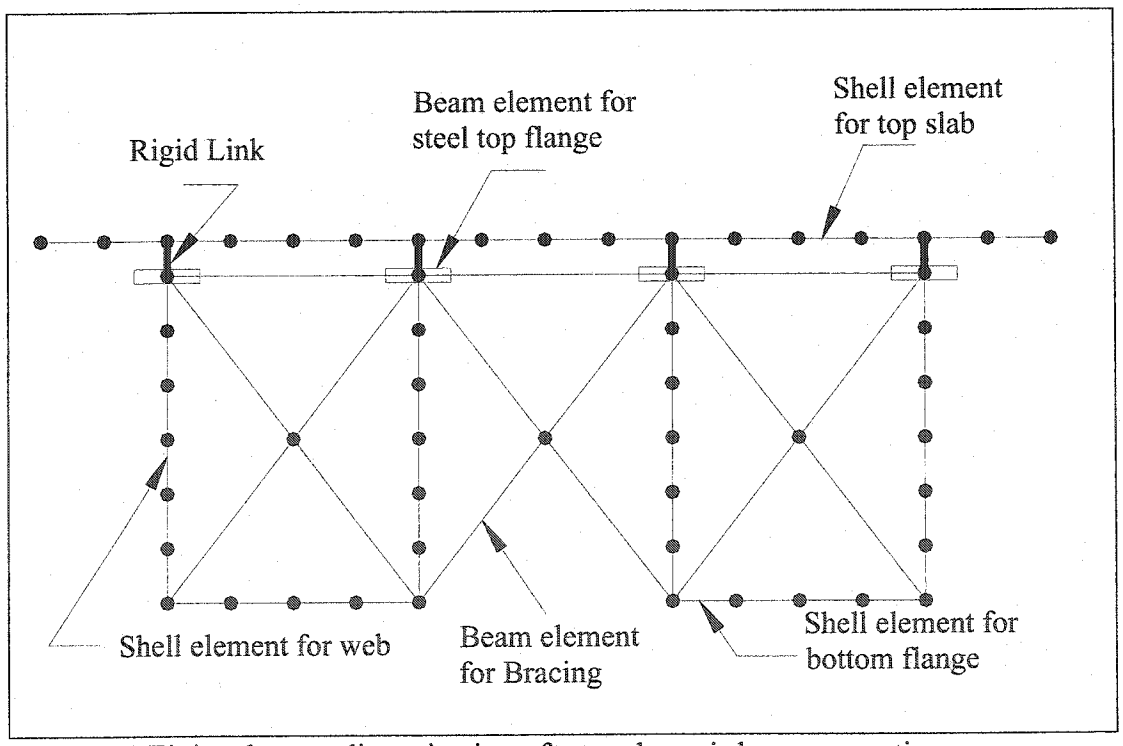

Figure 4.3 Finite element discretization of a two box girder cross section

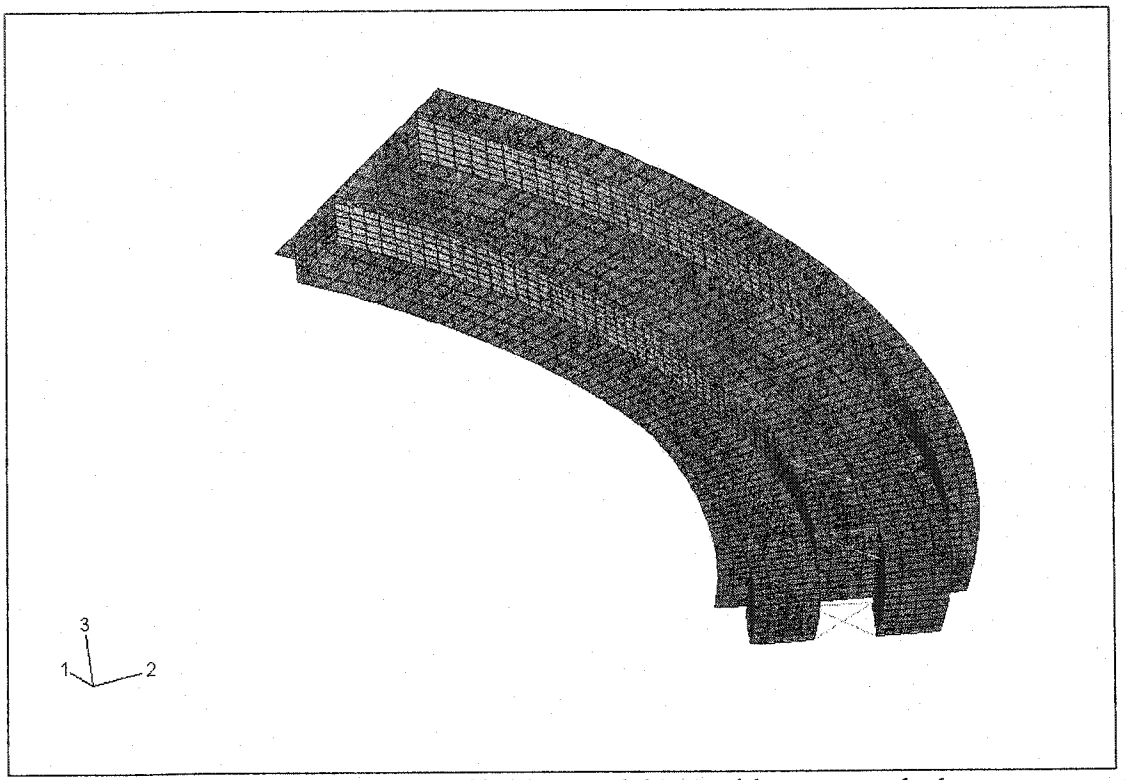

Figure 4.4 ABAQUS model view of bridge model M1 with concrete deck

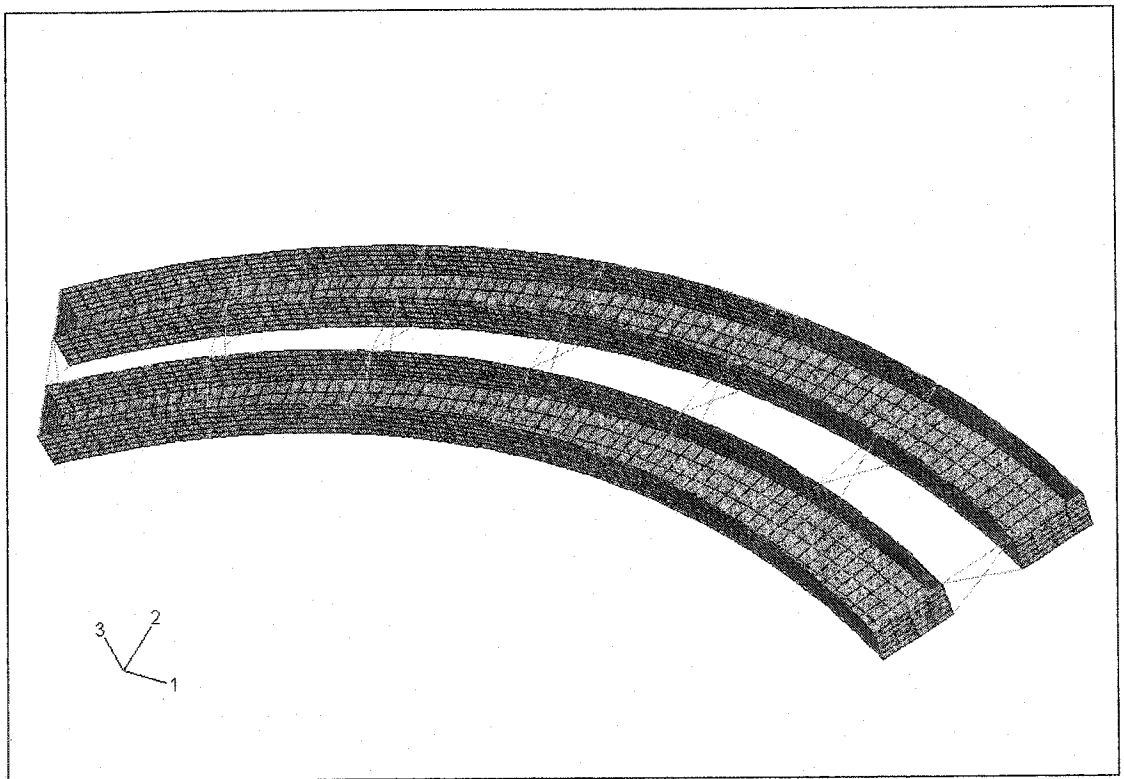

Figure 4.5 ABAQUS model view of bridge model M1 without concrete deck

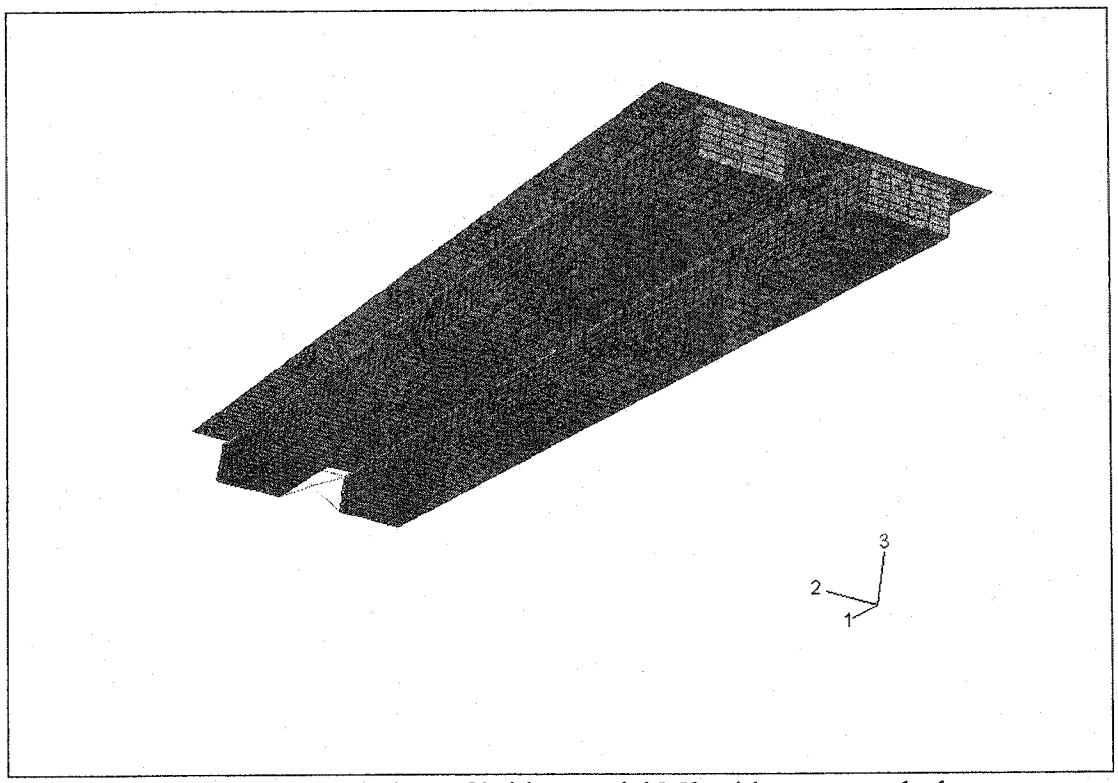

Figure 4.6 ABAQUS model view of bridge model M3 with concrete deck

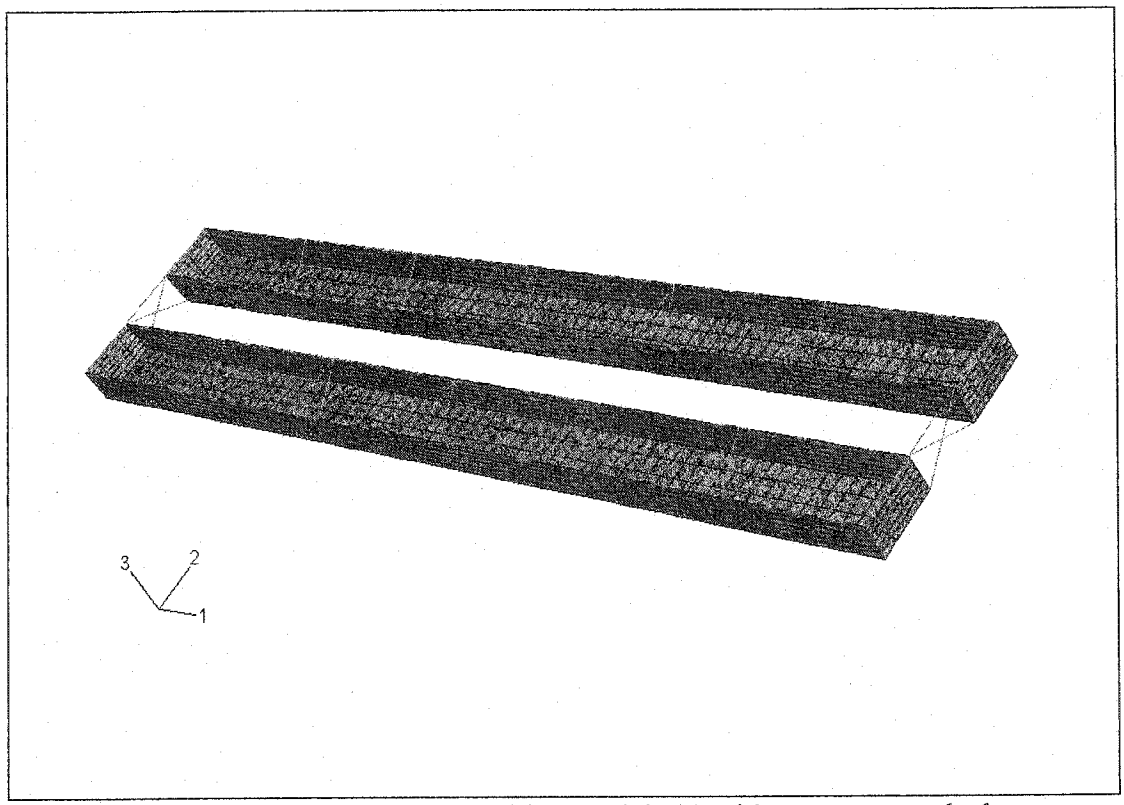

Figure 4.7 ABAQUS model view of bridge model M3 without concrete deck

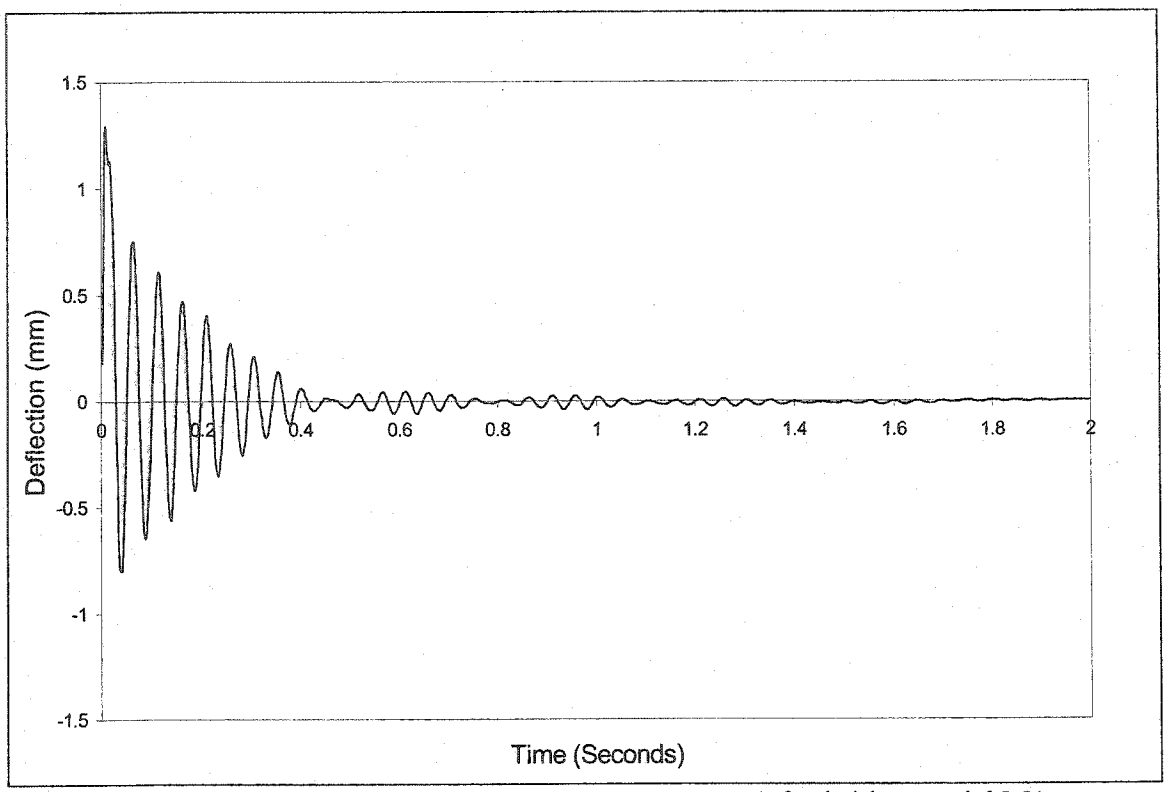

Figure 5.1 Deflection-time curve of LVDT#1 (setup type I) for bridge model M1

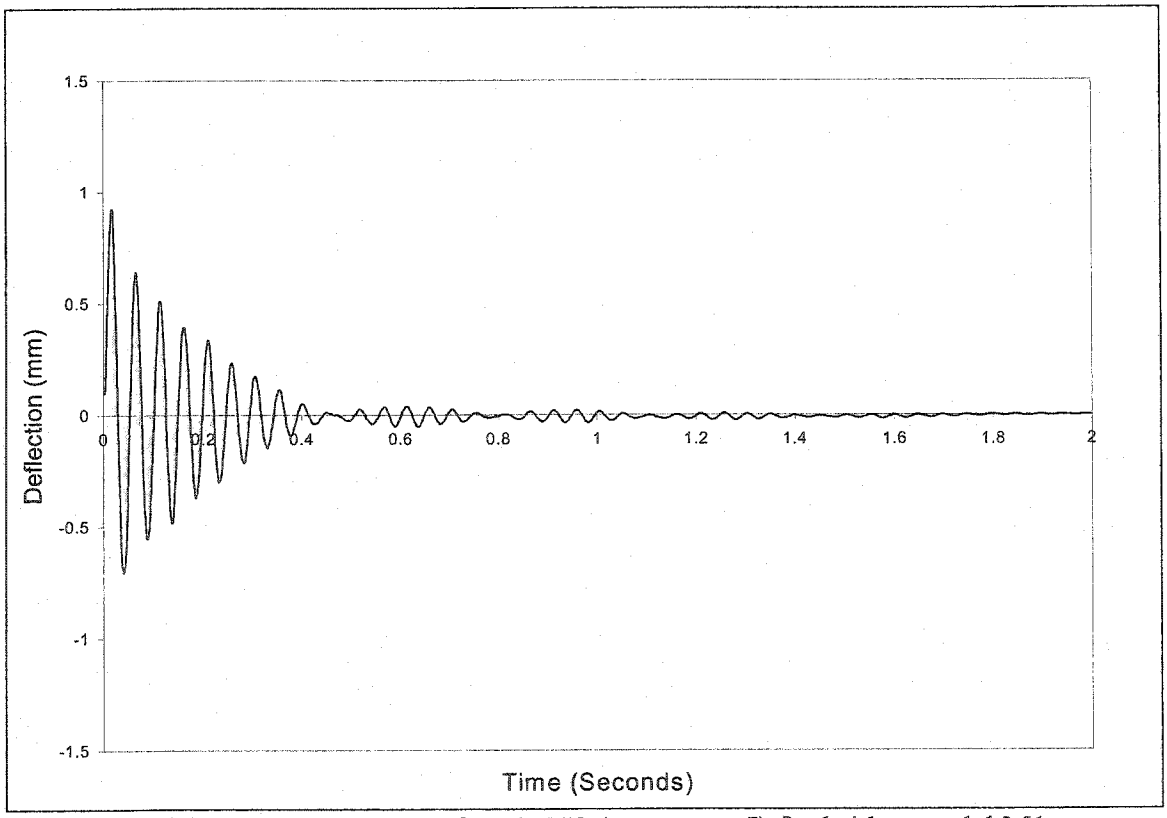

Figure 5.2 Deflection-time curve of LVDT#2 (setup type I) for bridge model M1

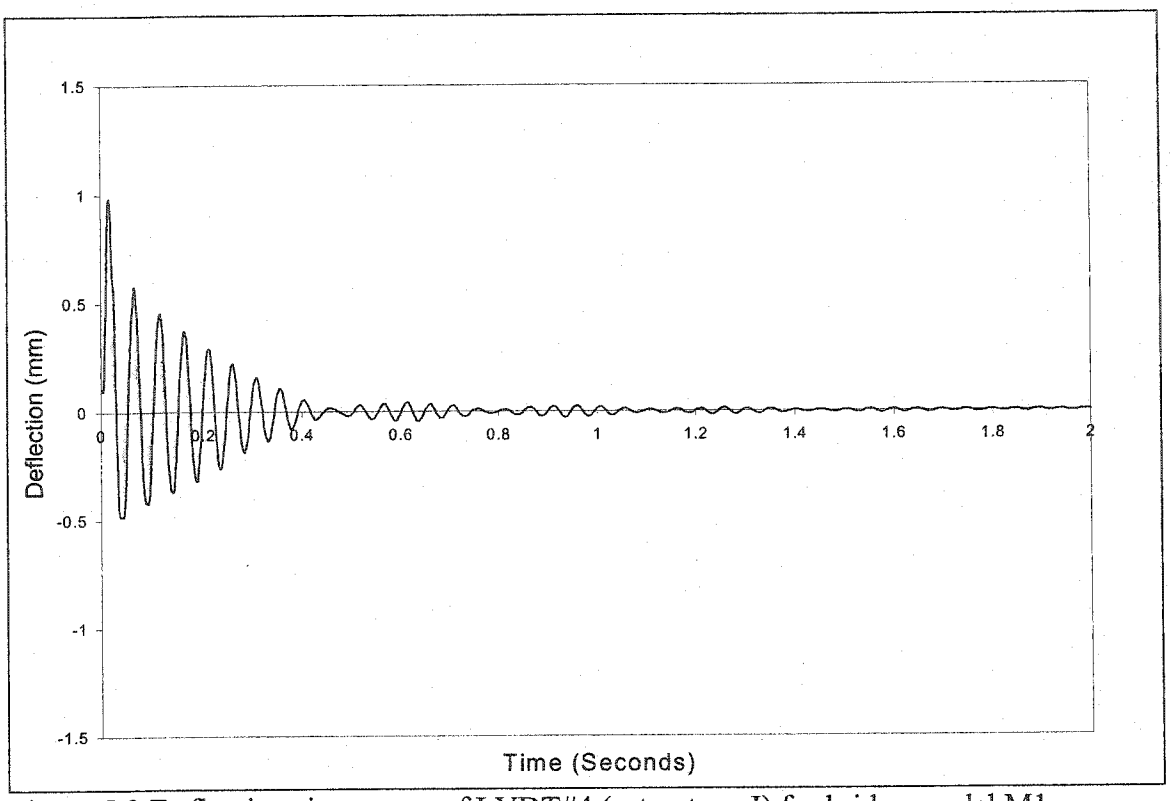

Figure 5.3 Deflection-time curve of LVDT#4 (setup type I) for bridge model M1

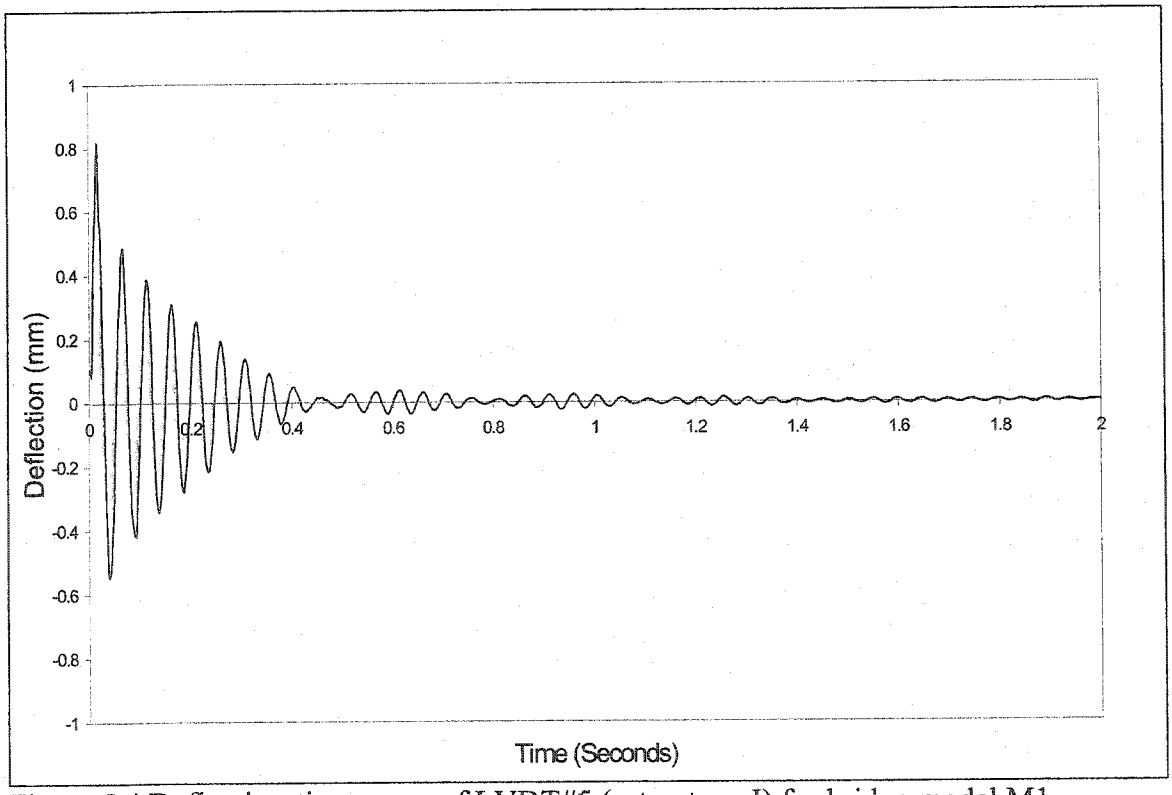

Figure 5.4 Deflection-time curve of LVDT#5 (setup type I) for bridge model M1

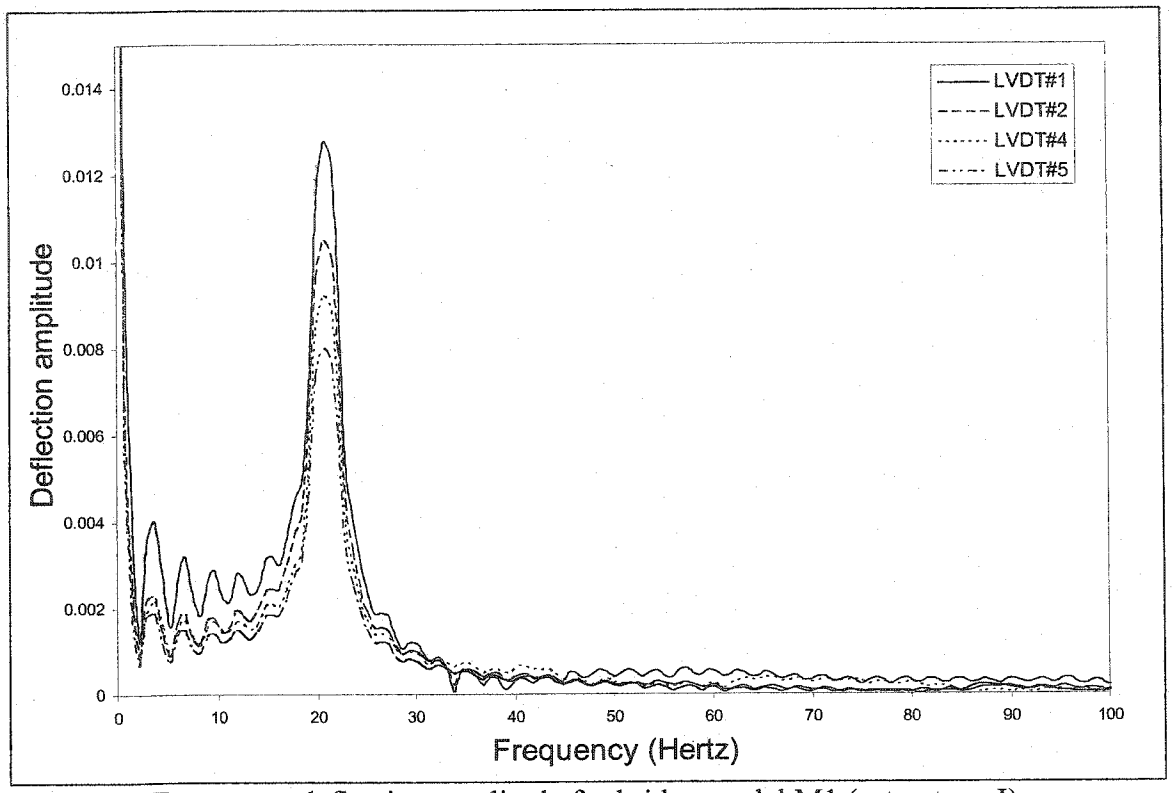

Figure 5.5 Frequency-deflection amplitude for bridge model M1 (setup type I)

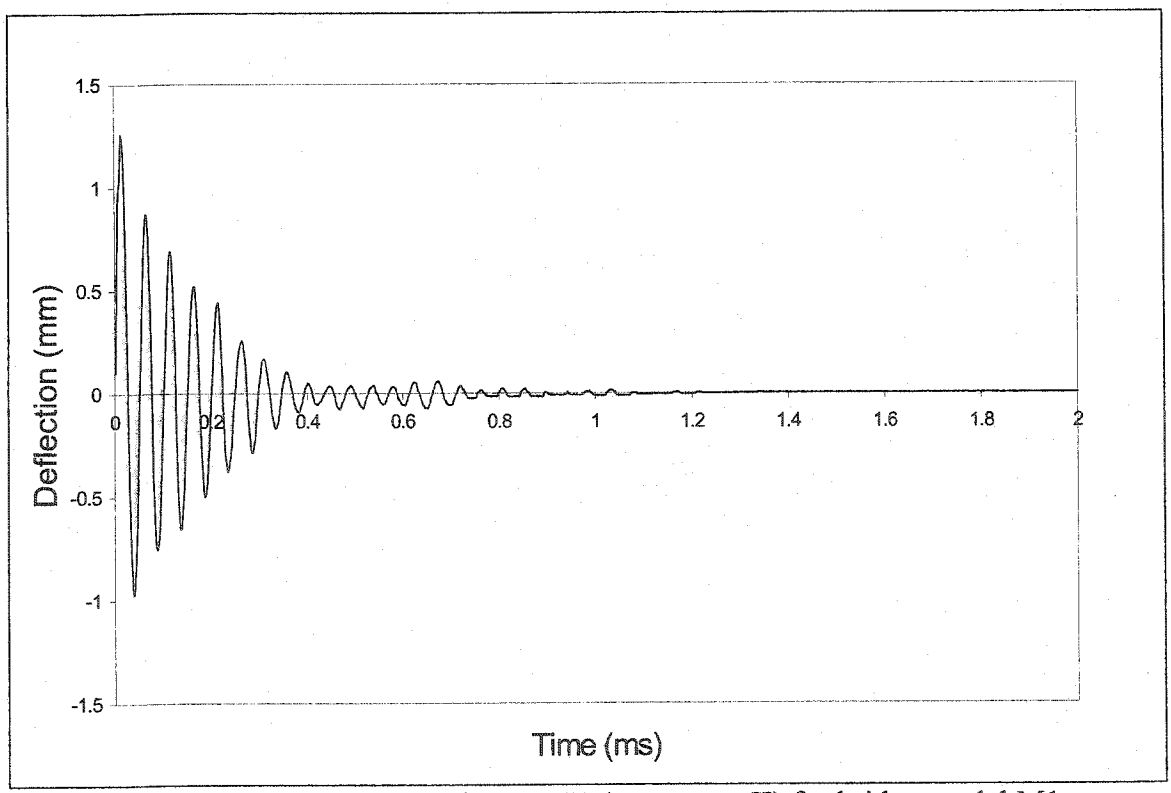

Figure 5.6 Deflection-time curve of LVDT#1 (setup type II) for bridge model M1

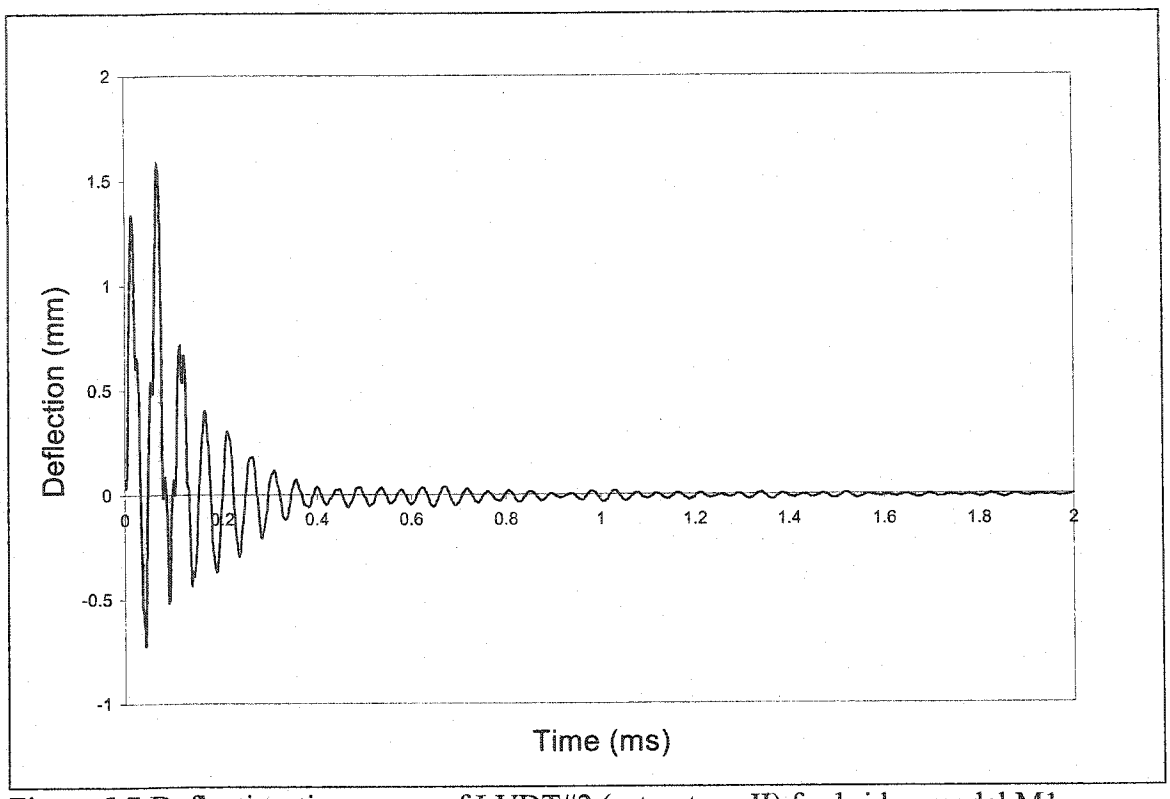

Figure 5.7 Deflection-time curve of LVDT#2 (setup type II) for bridge model M1

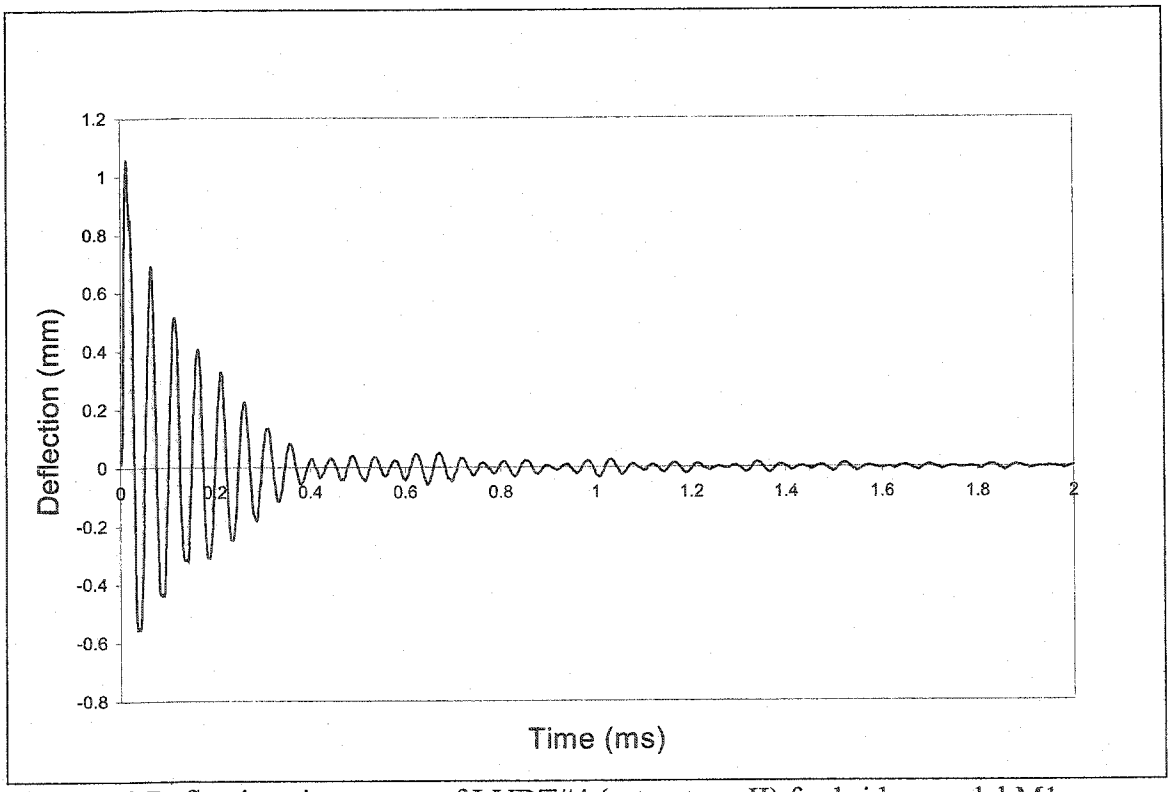

Figure 5.8 Deflection-time curve of LVDT#4 (setup type II) for bridge model M1

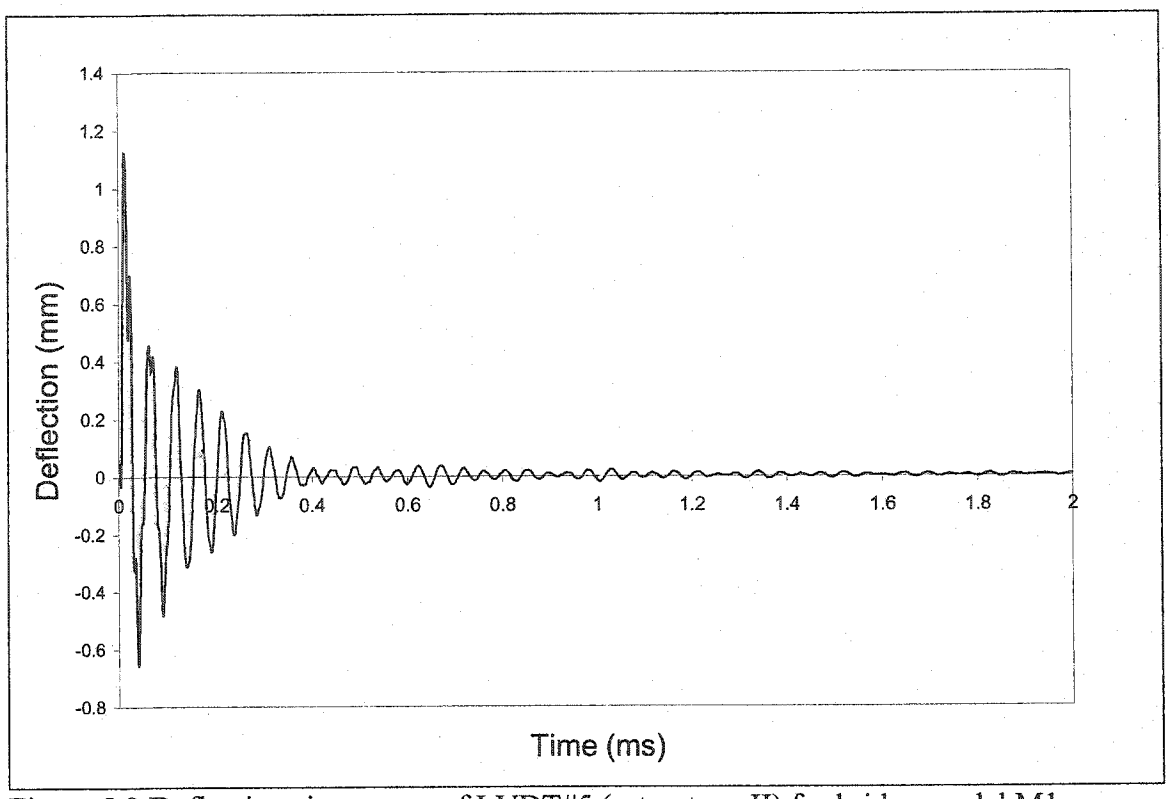

Figure 5.9 Deflection-time curve of LVDT#5 (setup type II) for bridge model M1

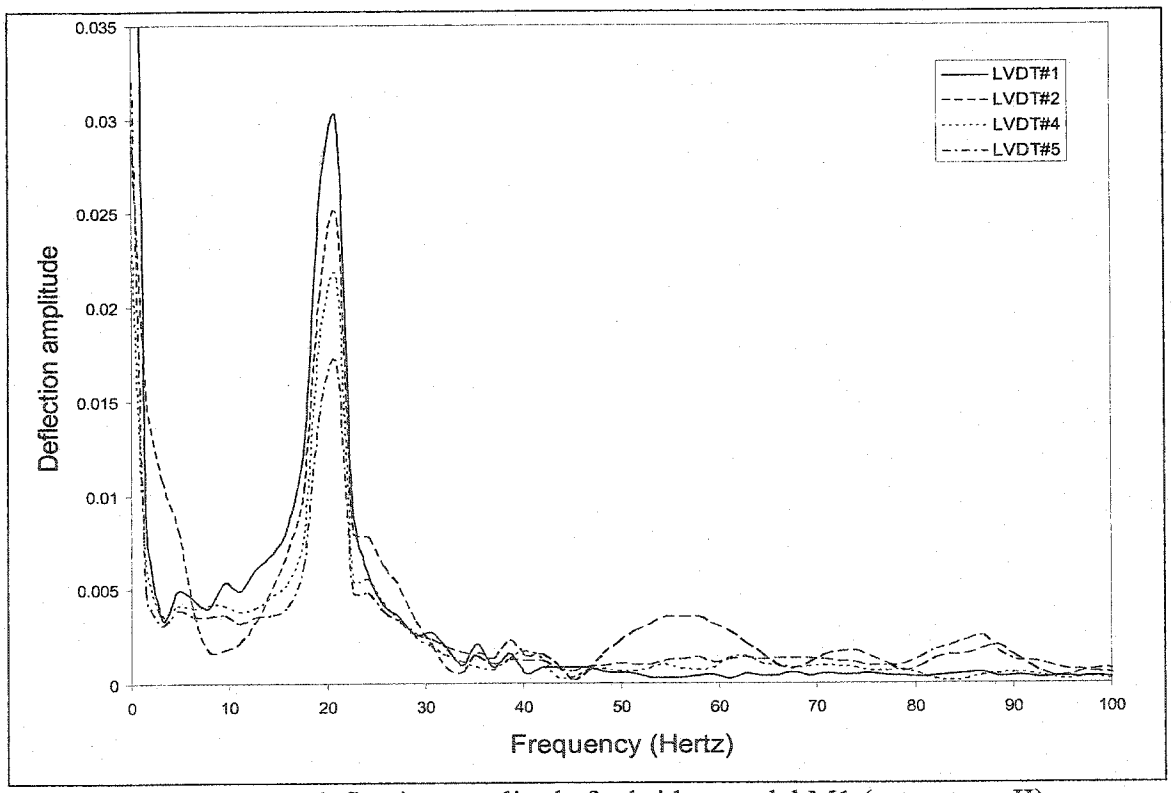

Figure 5.10 Frequency-deflection amplitude for bridge model M1 (setup type II)

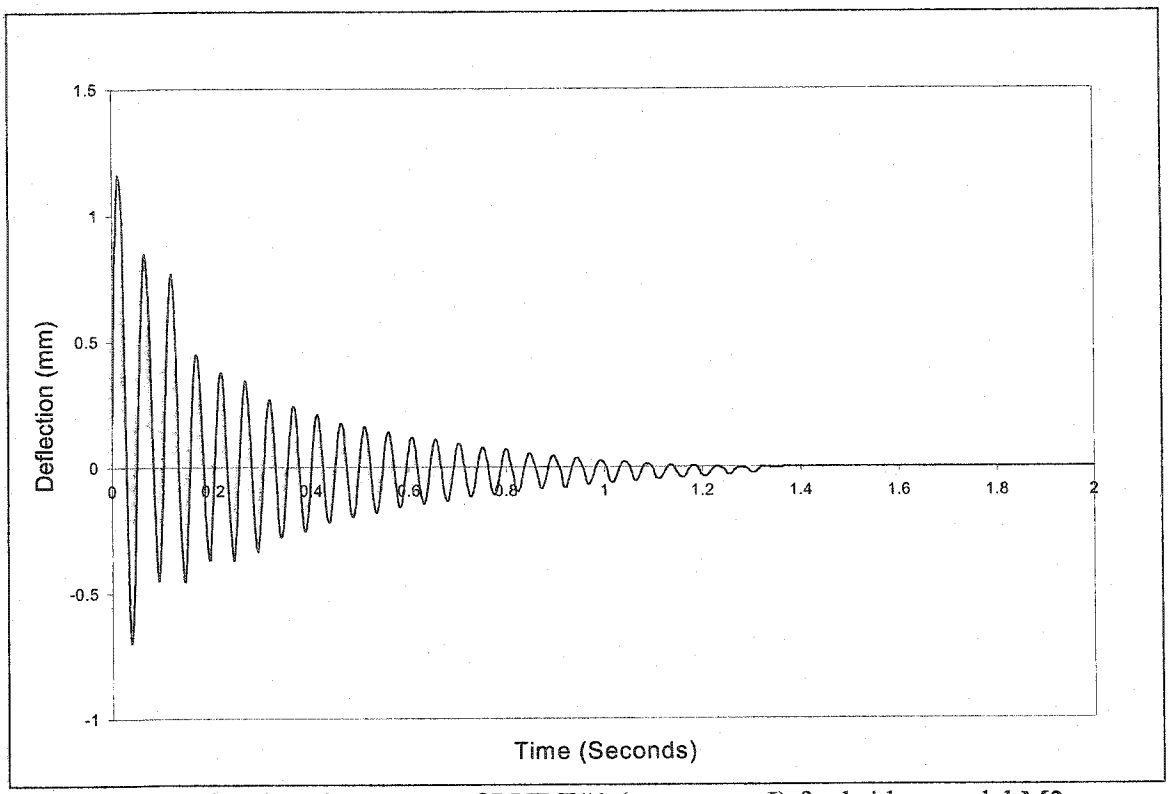

Figure 5.11 Deflection-time curve of LVDT#1 (setup type I) for bridge model M2

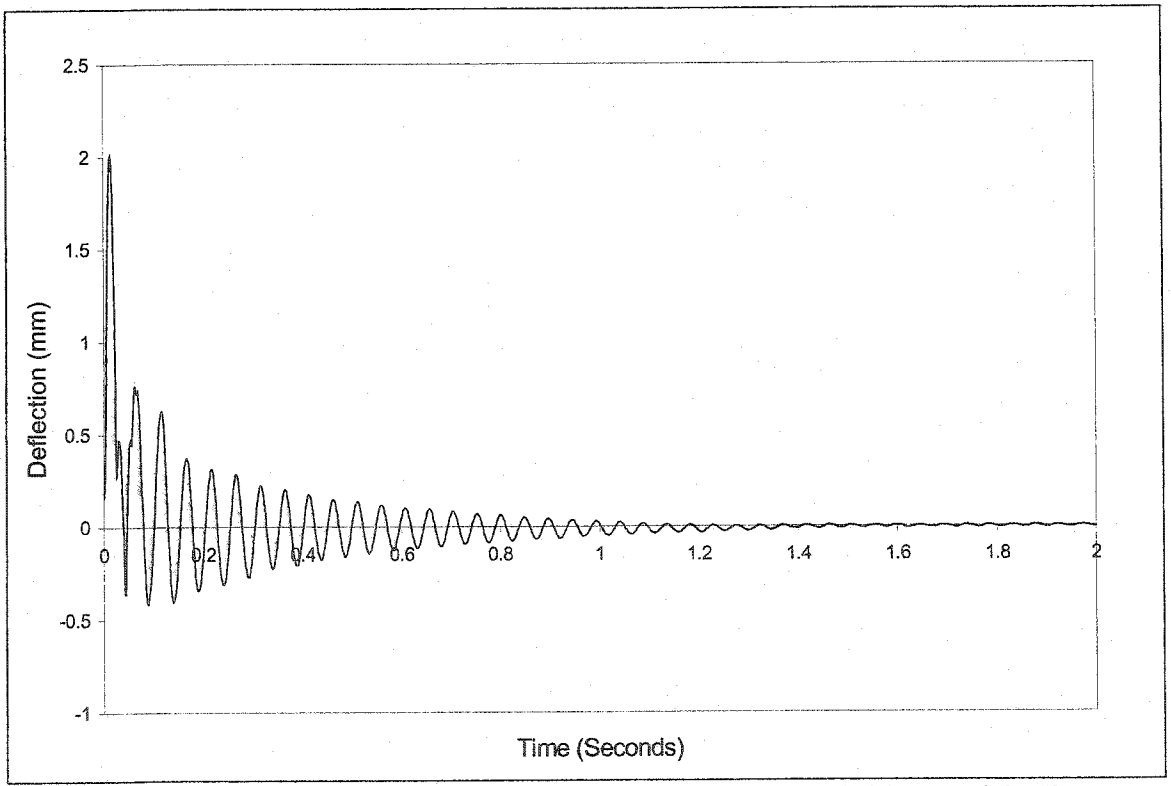

Figure 5.12 Deflection-time curve of LVDT#2 (setup type I) for bridge model M2

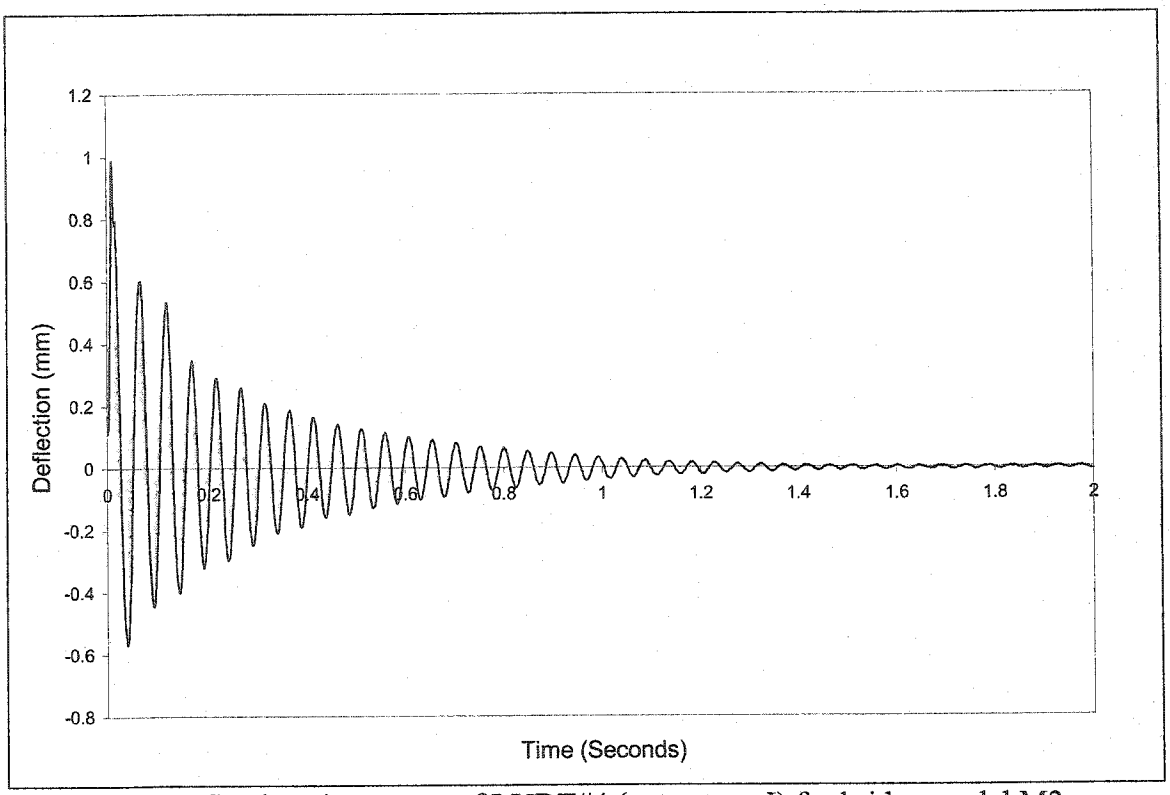

Figure 5.13 Deflection-time curve of LVDT#4 (setup type I) for bridge model M2

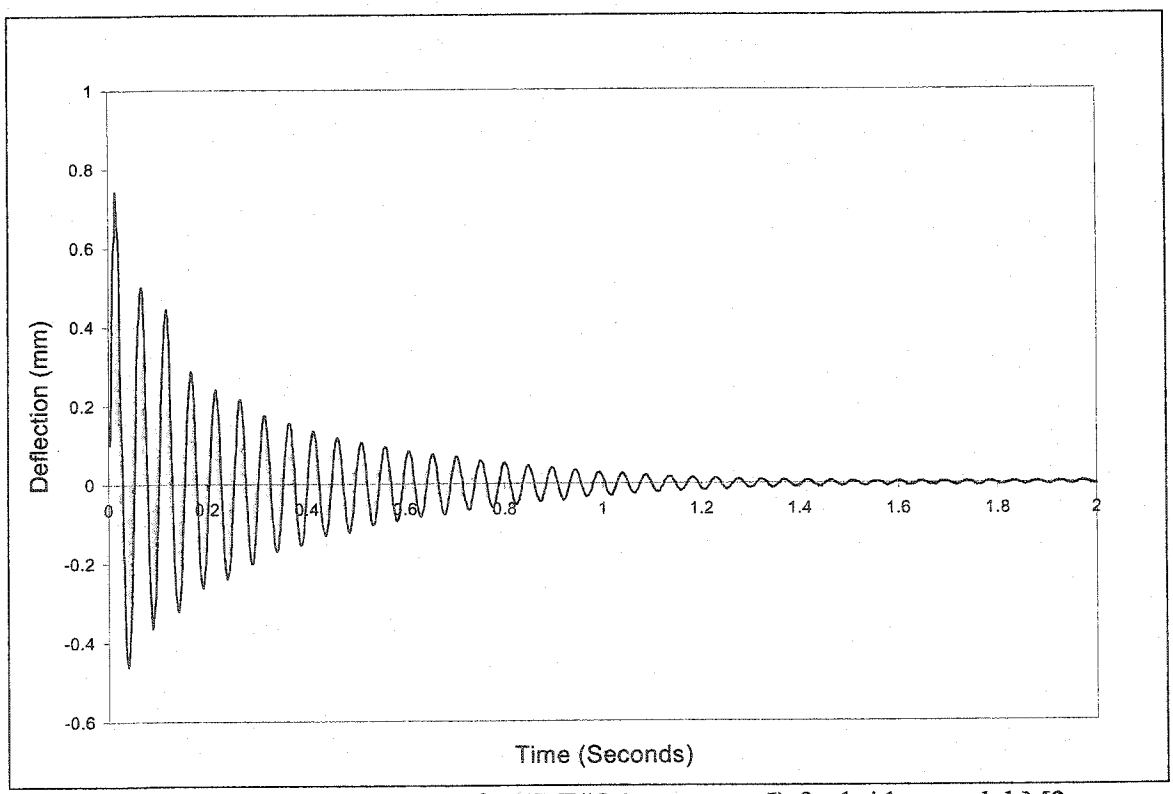

Figure 5.14 Deflection-time curve of LVDT#5 (setup type I) for bridge model M2

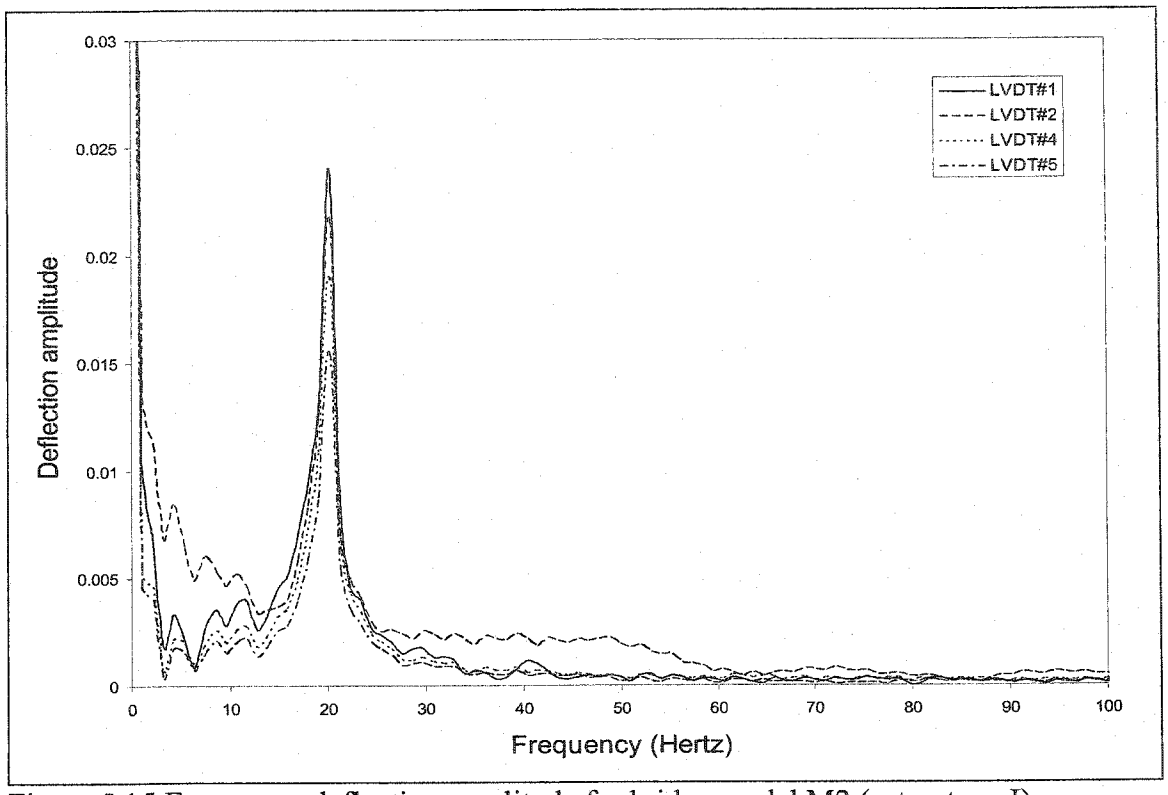

Figure 5.15 Frequency-deflection amplitude for bridge model M2 (setup type I)

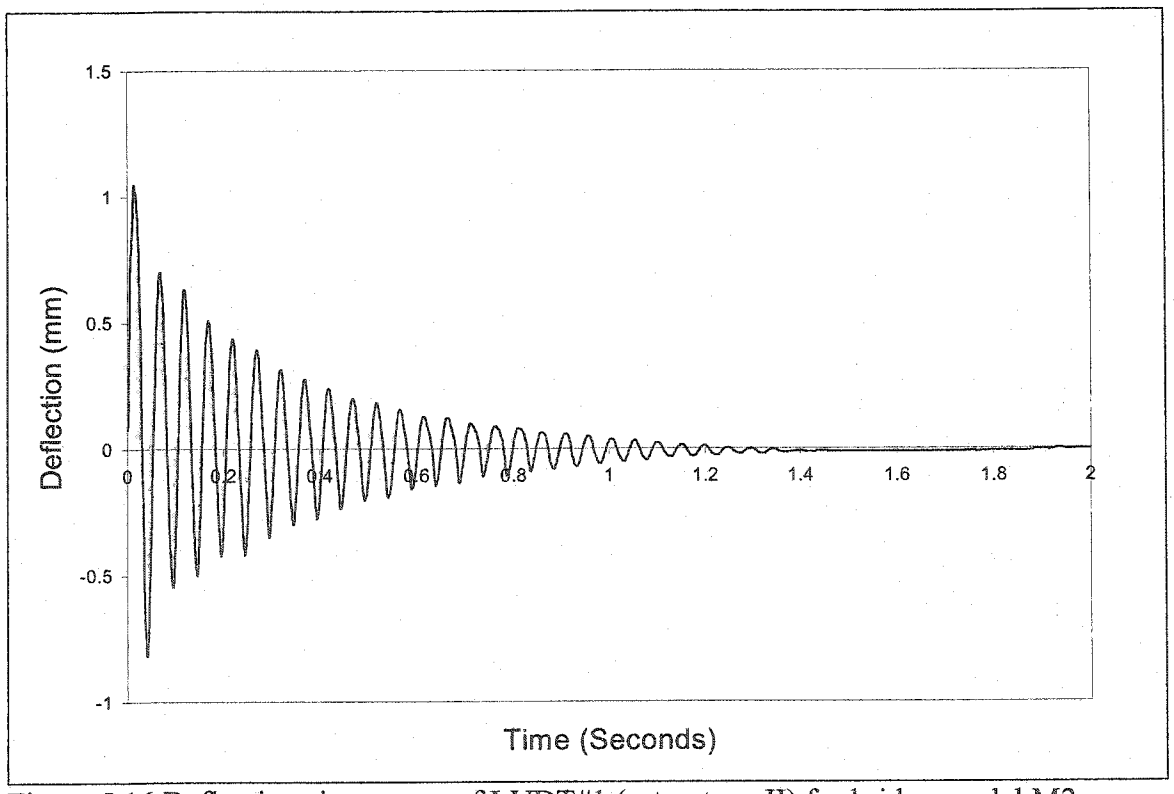

Figure 5.16 Deflection-time curve of LVDT#1 (setup type II) for bridge model M2

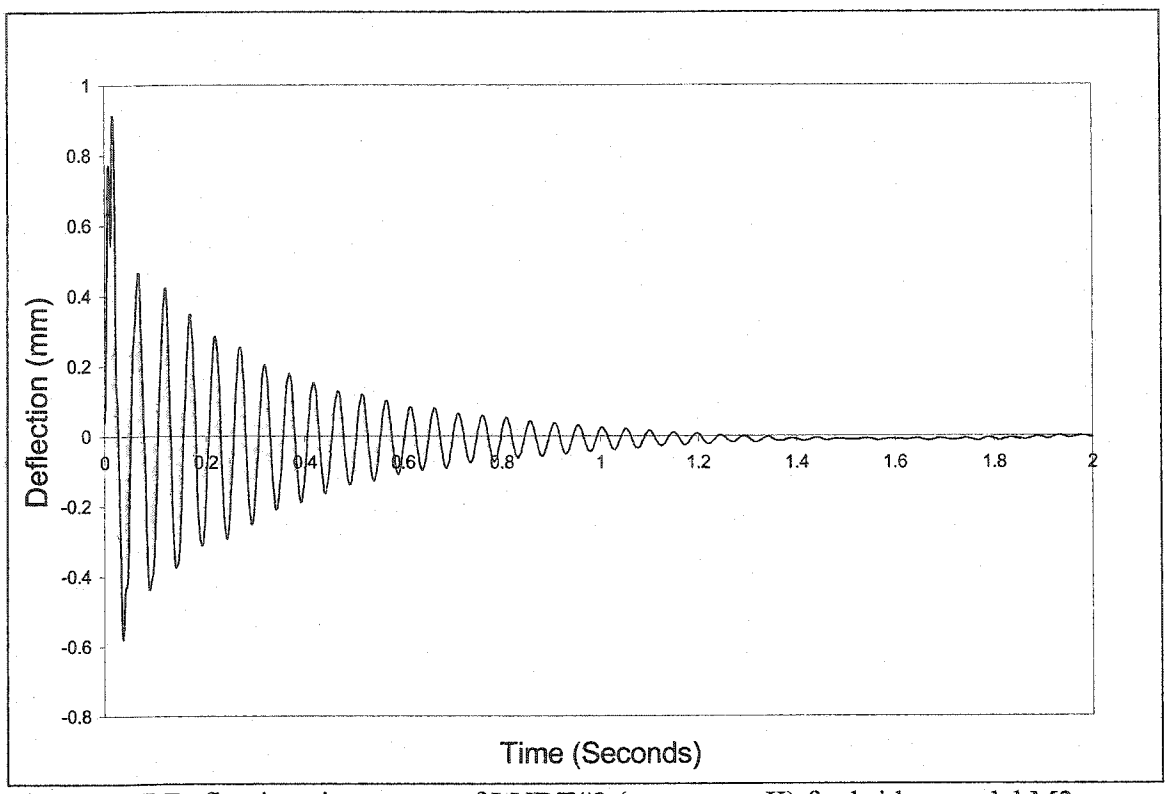

Figure 5.17 Deflection-time curve of LVDT#2 (setup type II) for bridge model M2

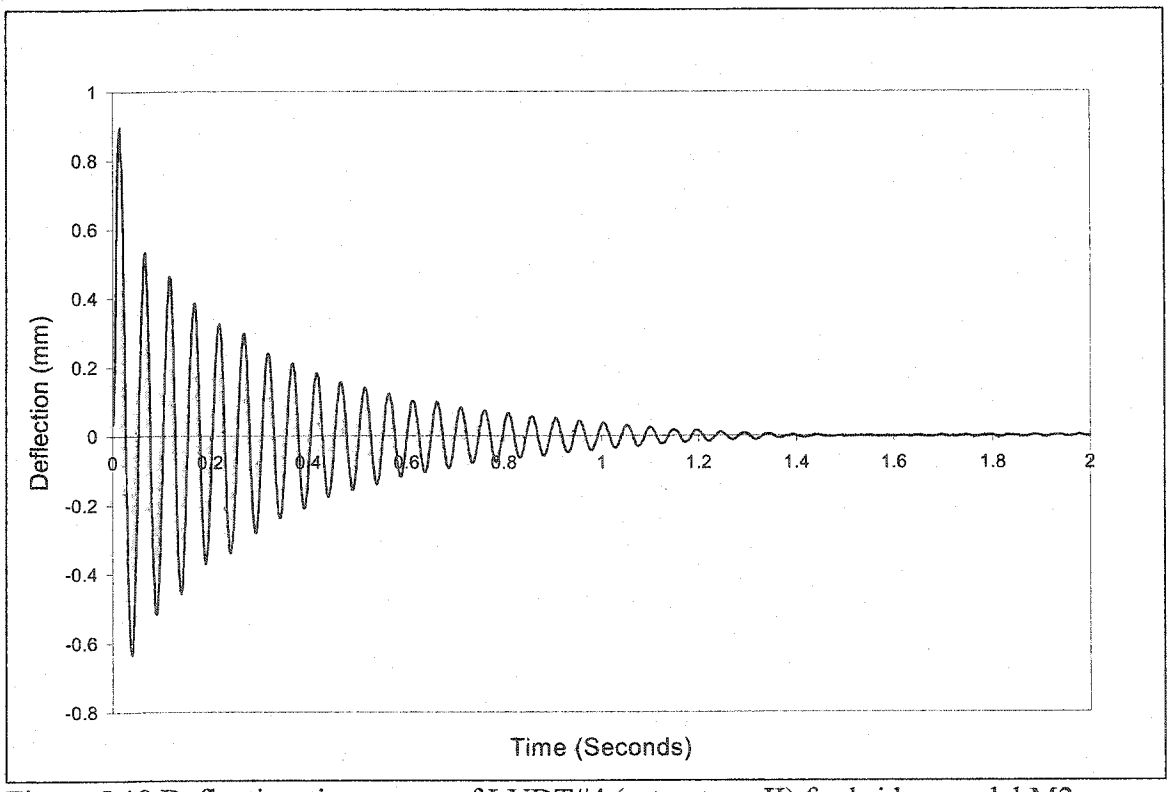

Figure 5.18 Deflection-time curve of LVDT#4 (setup type II) for bridge model M2

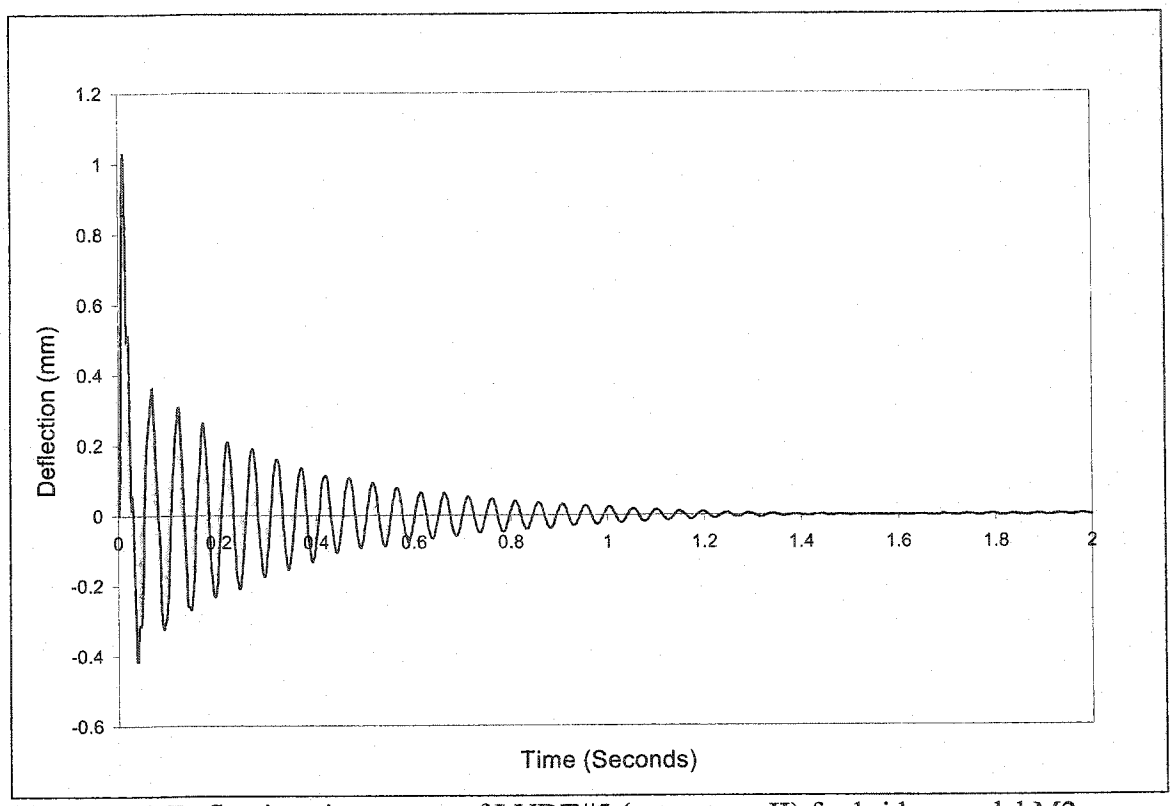

Figure 5.19 Deflection-time curve of LVDT#5 (setup type II) for bridge model M2

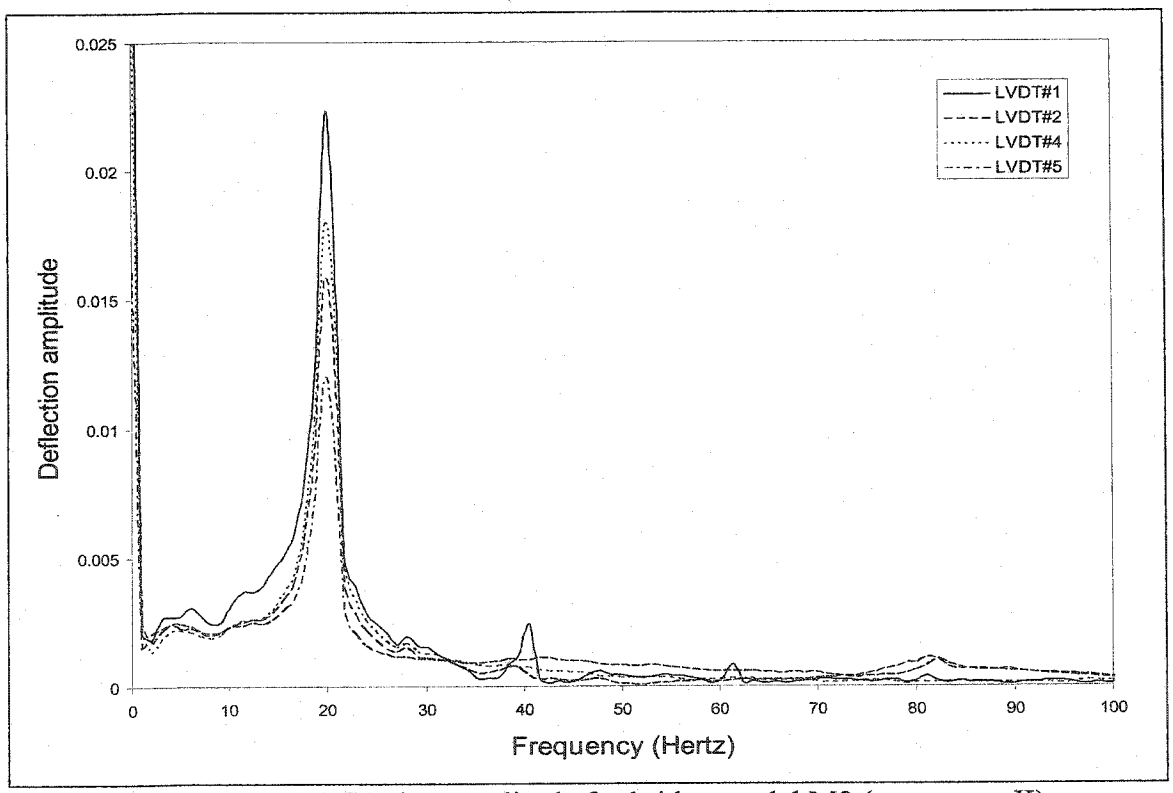

Figure 5.20 Frequency-deflection amplitude for bridge model M2 (setup type II)

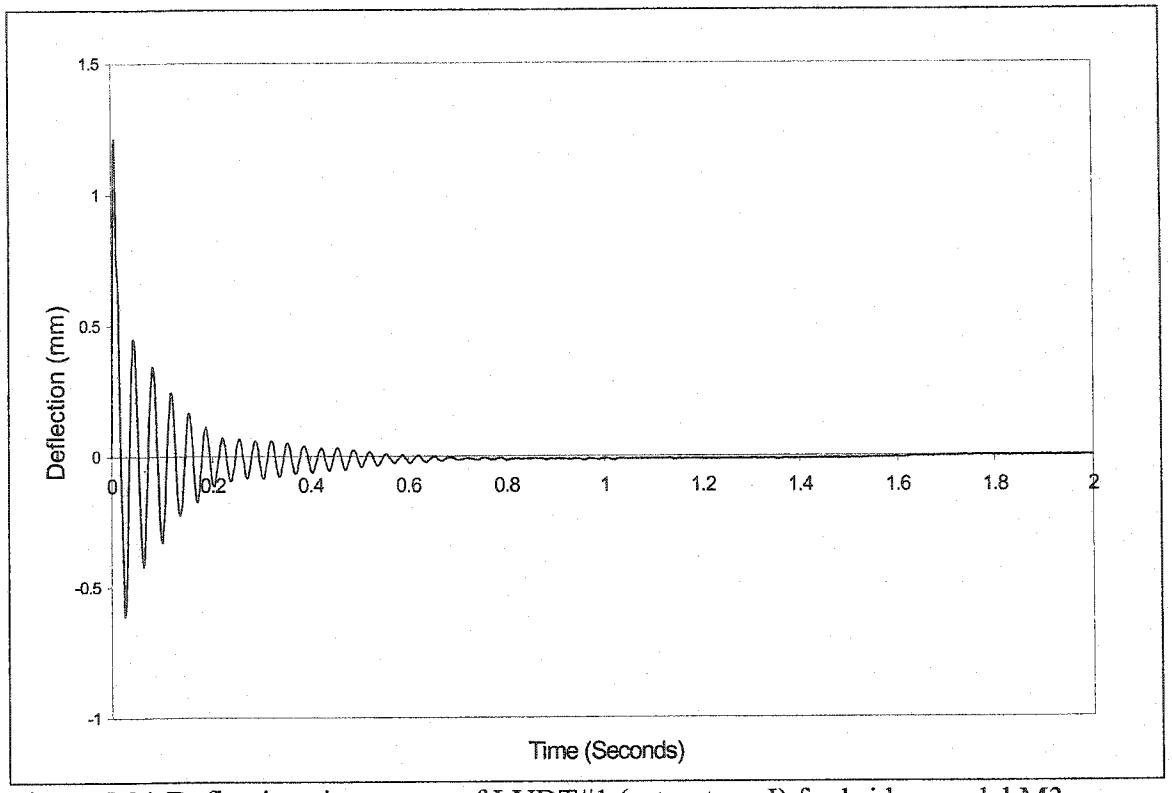

Figure 5.21 Deflection-time curve of LVDT#1 (setup type I) for bridge model M3

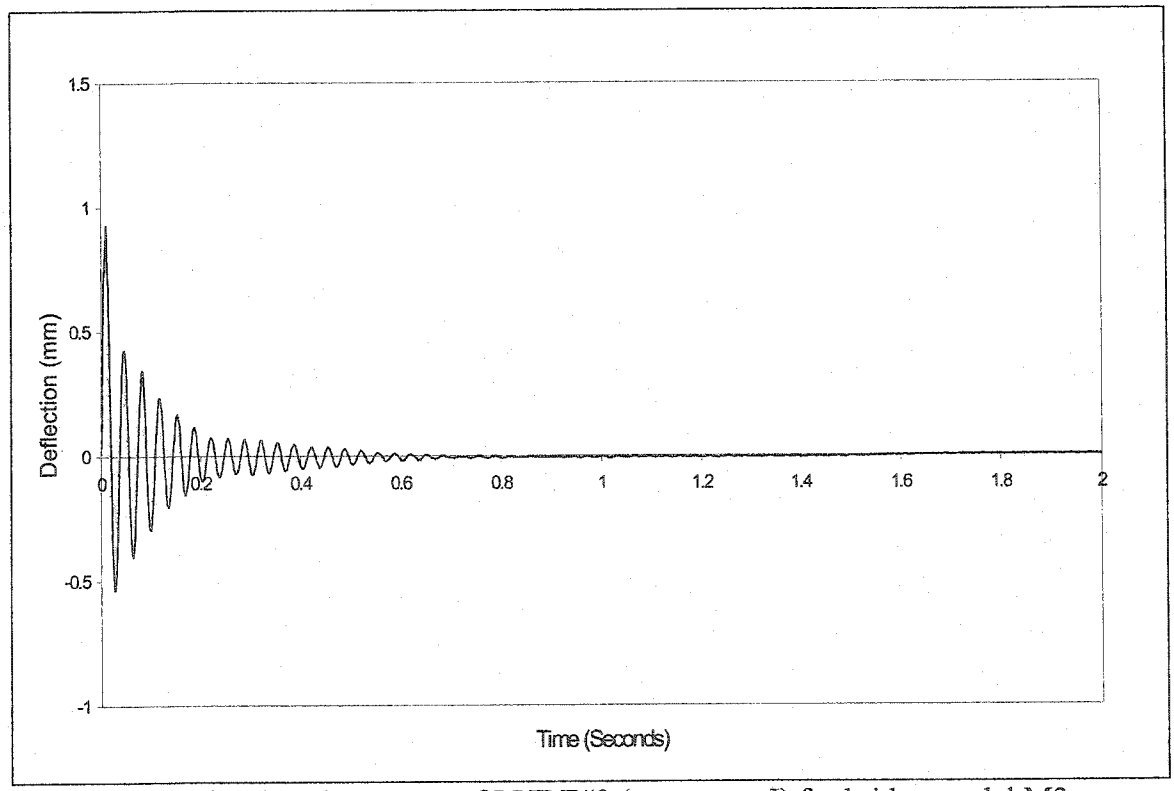

Figure 5.22 Deflection-time curve of LVDT#2 (setup type I) for bridge model M3

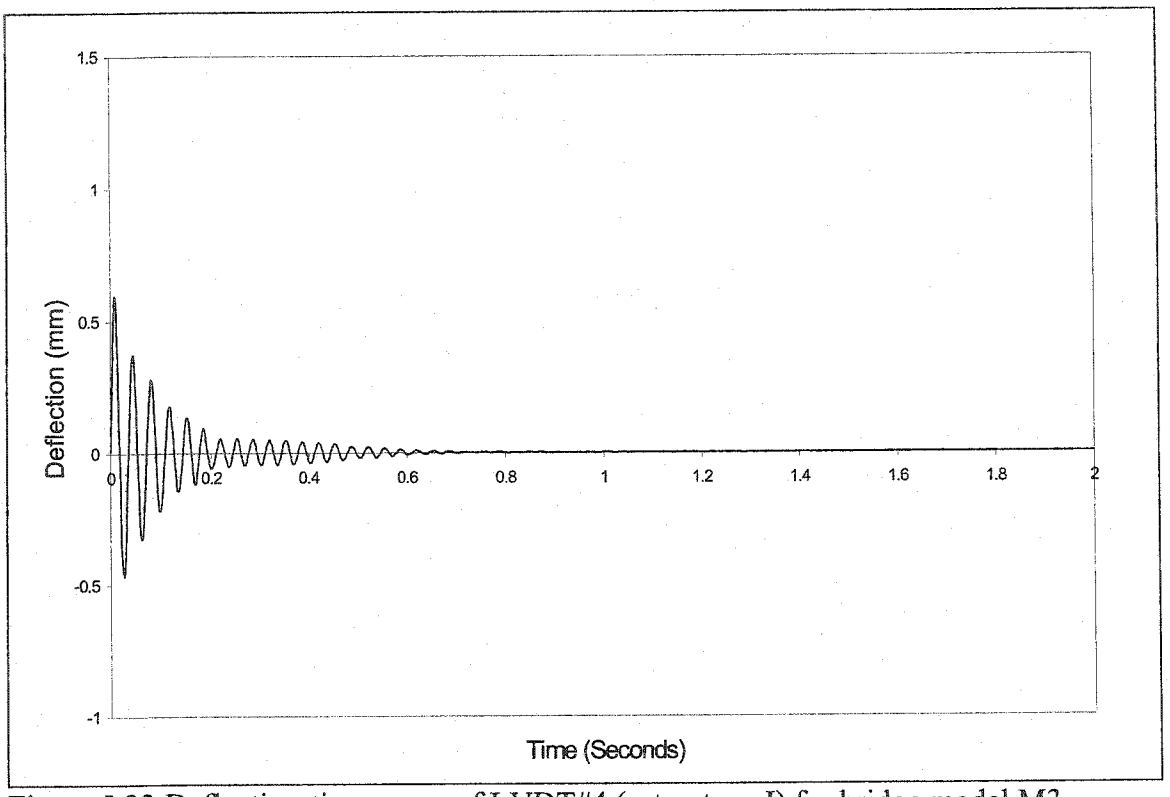

Figure 5.23 Deflection-time curve of LVDT#4 (setup type I) for bridge model M3

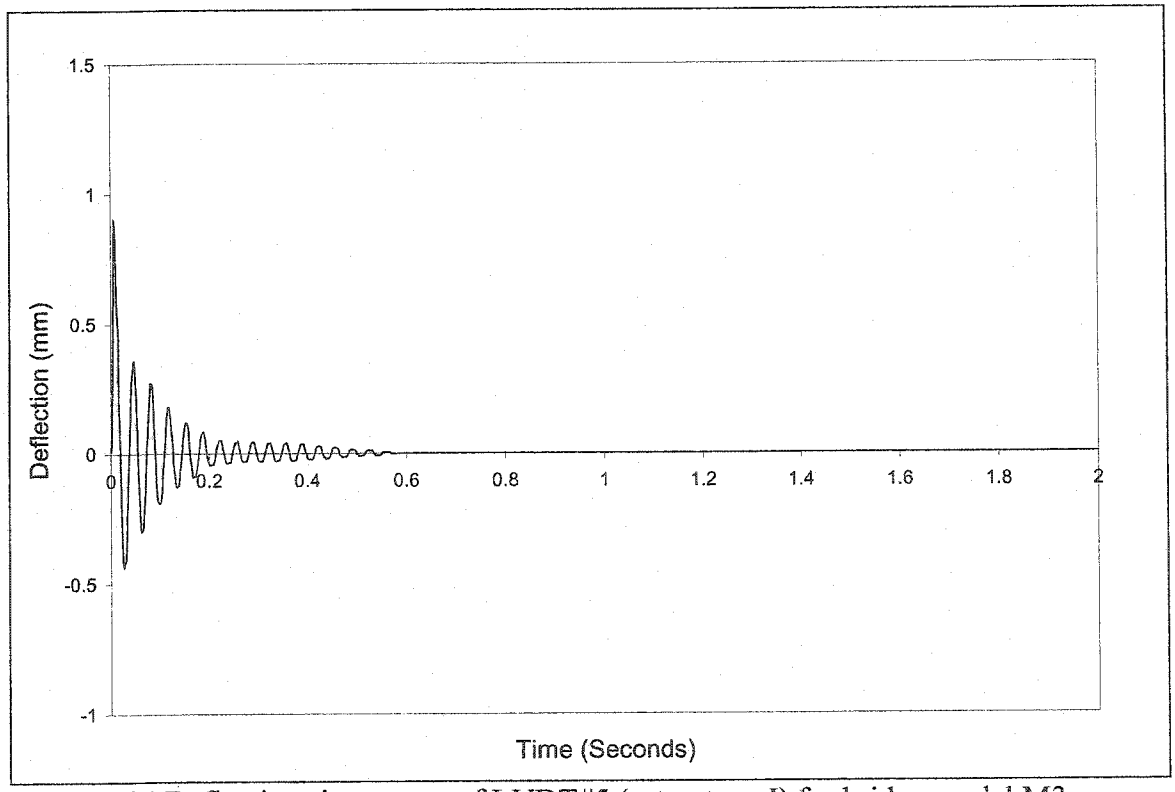

Figure 5.24 Deflection-time curve of LVDT#5 (setup type I) for bridge model M3

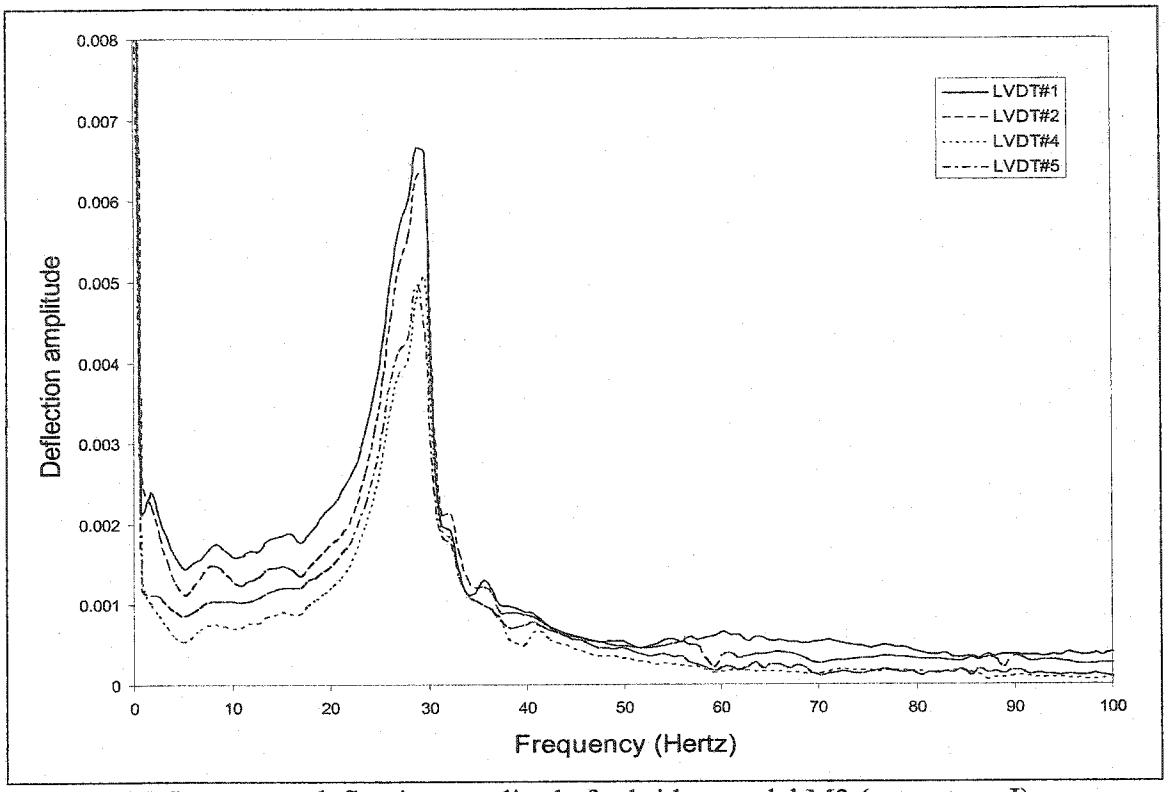

Figure 5.25 Frequency-deflection amplitude for bridge model M3 (setup type I)

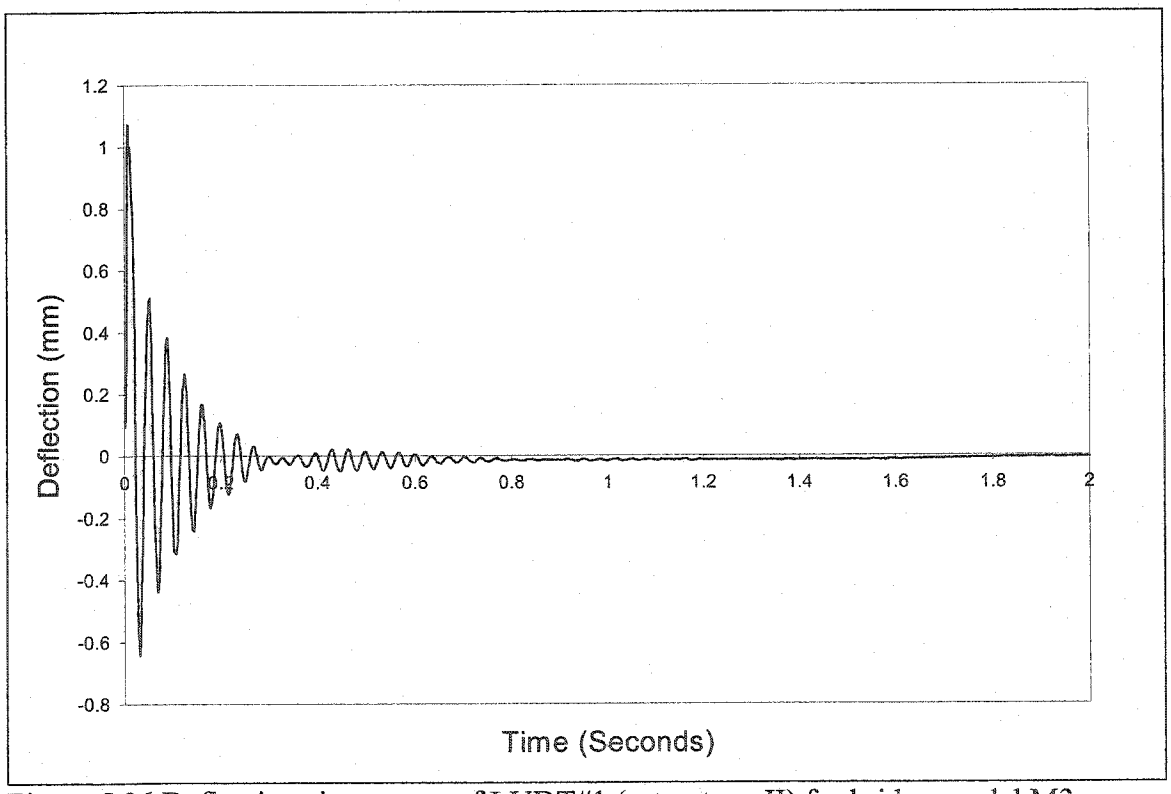

Figure 5.26 Deflection-time curve of LVDT#1 (setup type II) for bridge model M3

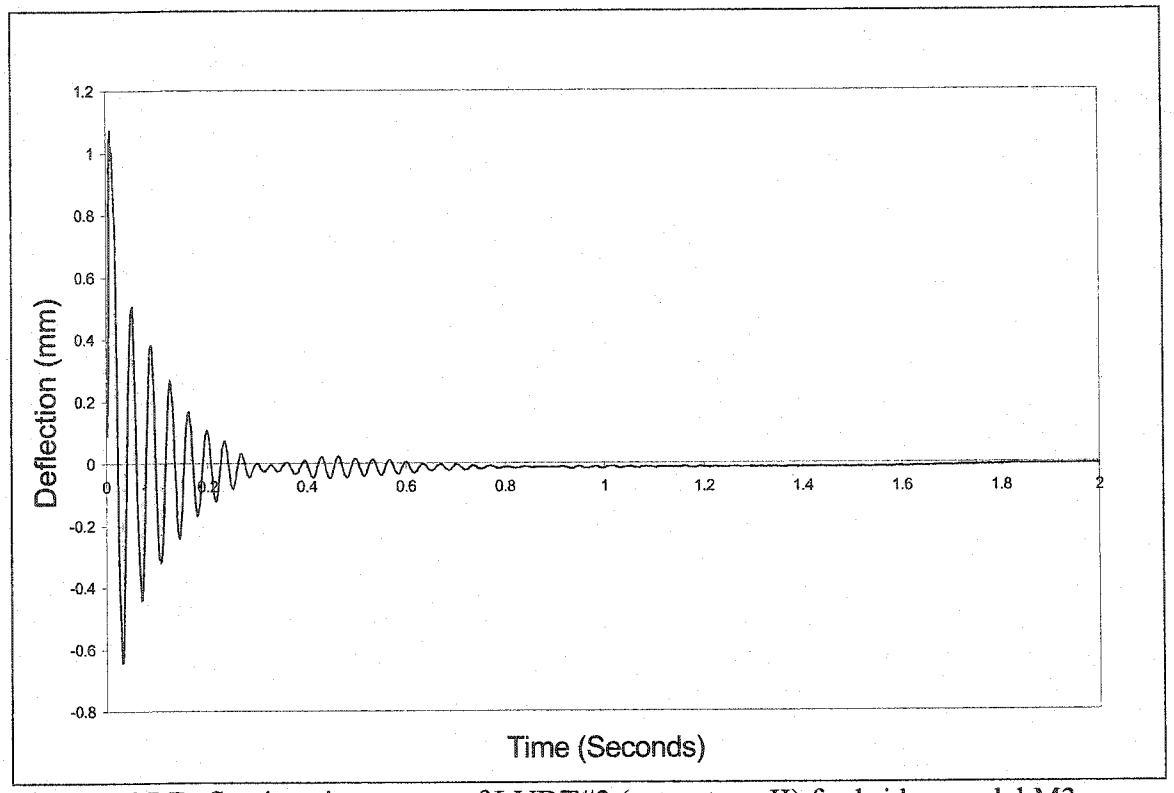

Figure 5.27 Deflection-time curve of LVDT#2 (setup type II) for bridge model M3

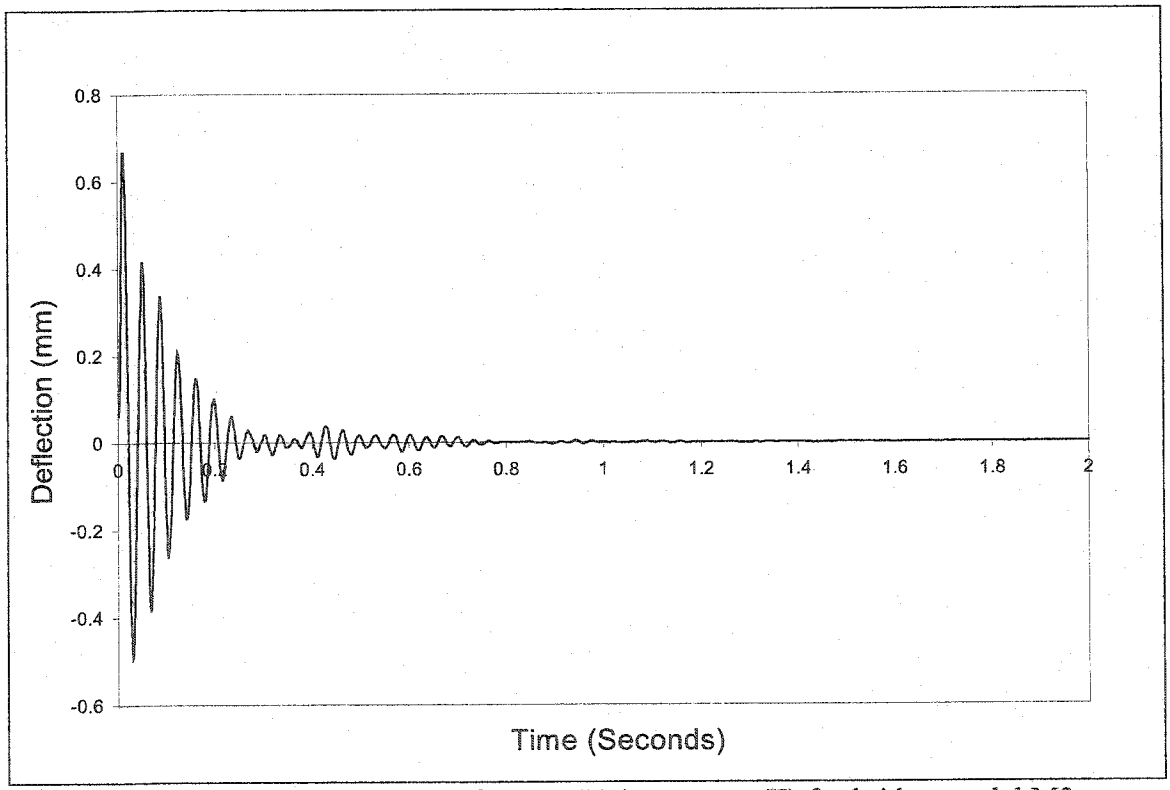

Figure 5.28 Deflection-time curve of LVDT#4 (setup type II) for bridge model M3

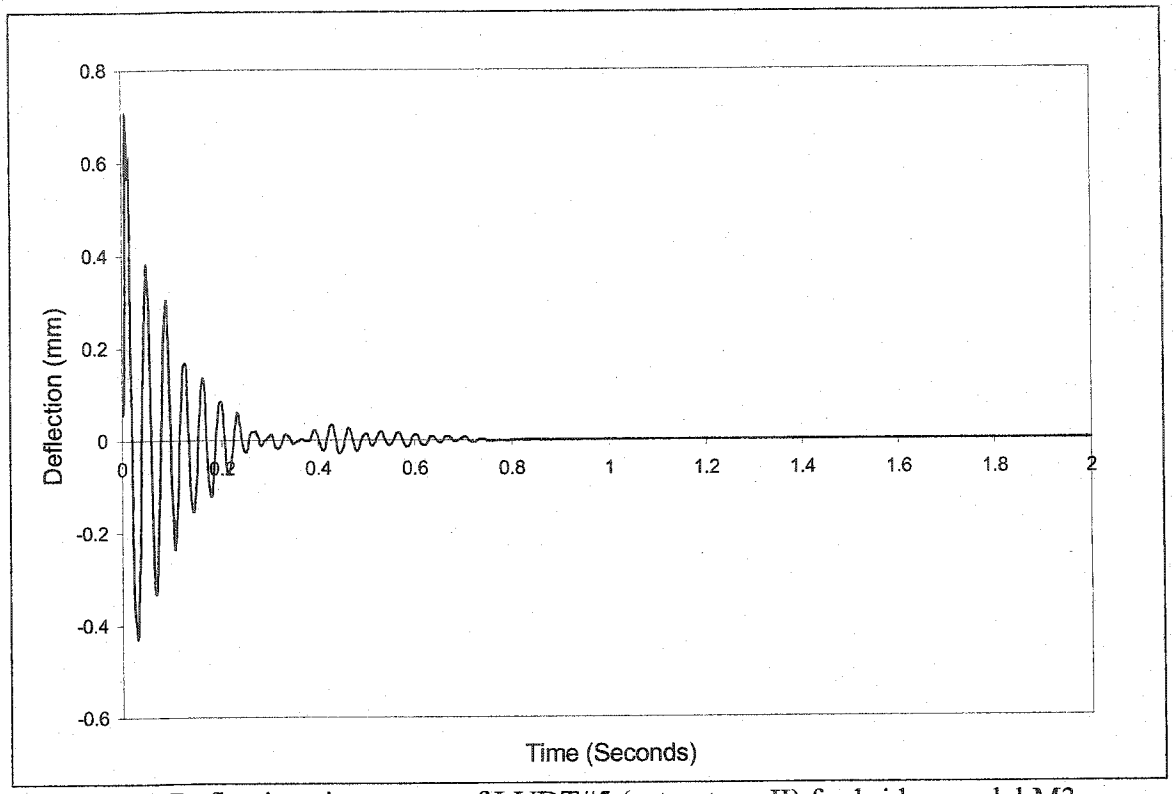

Figure 5.29 Deflection-time curve of LVDT#5 (setup type II) for bridge model M3

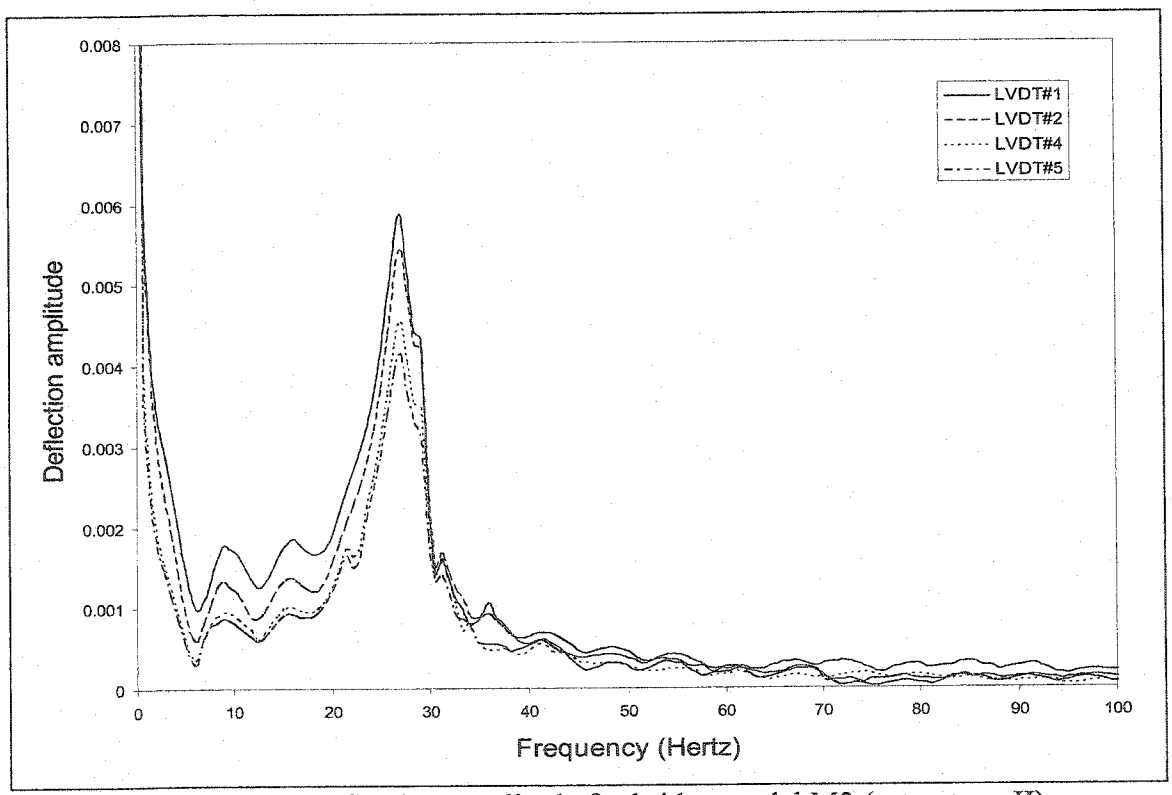

Figure 5.30 Frequency-deflection amplitude for bridge model M3 (setup type II)

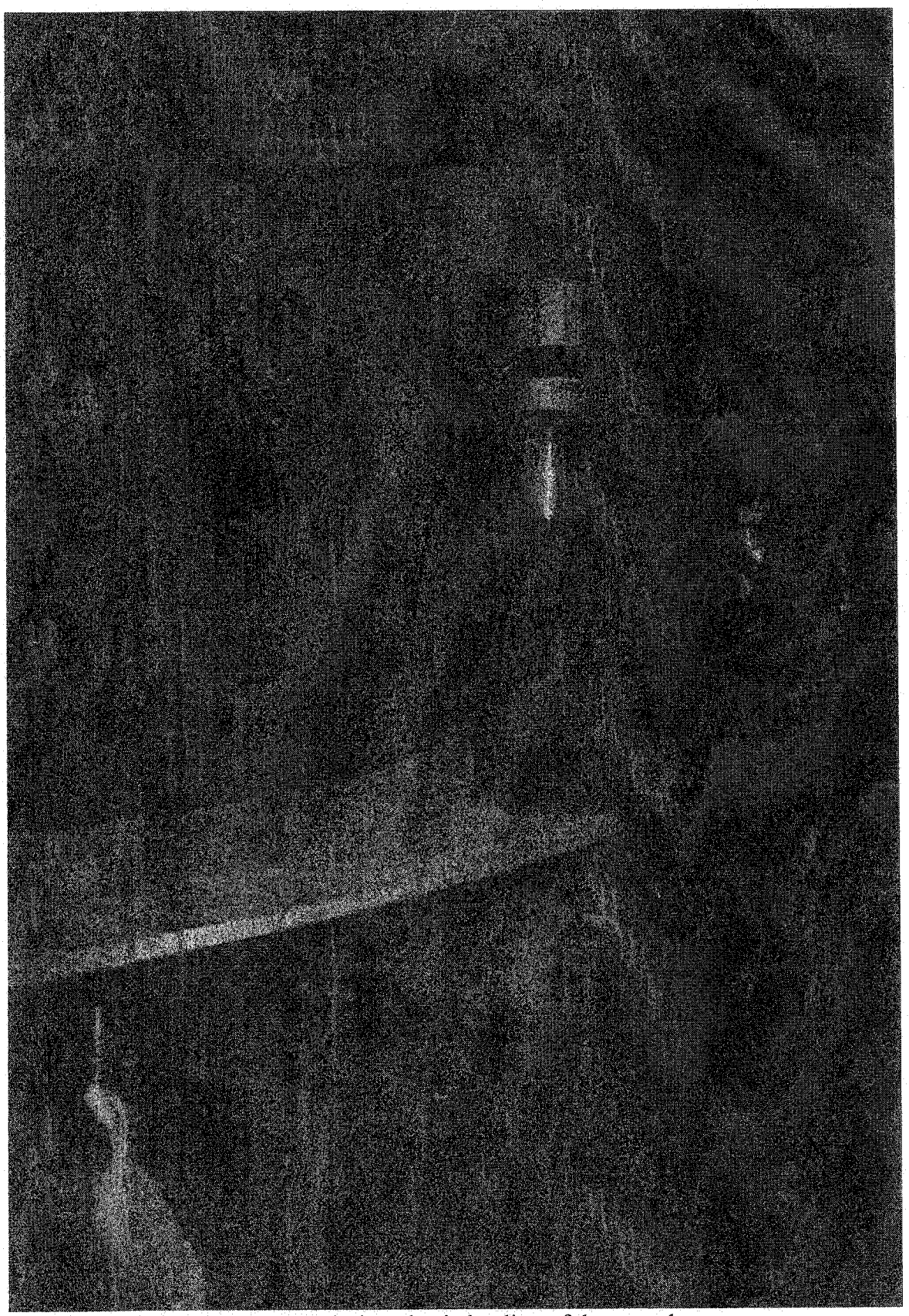

Figure 5.31 View of bridge M1 during elastic loading of the outer lane

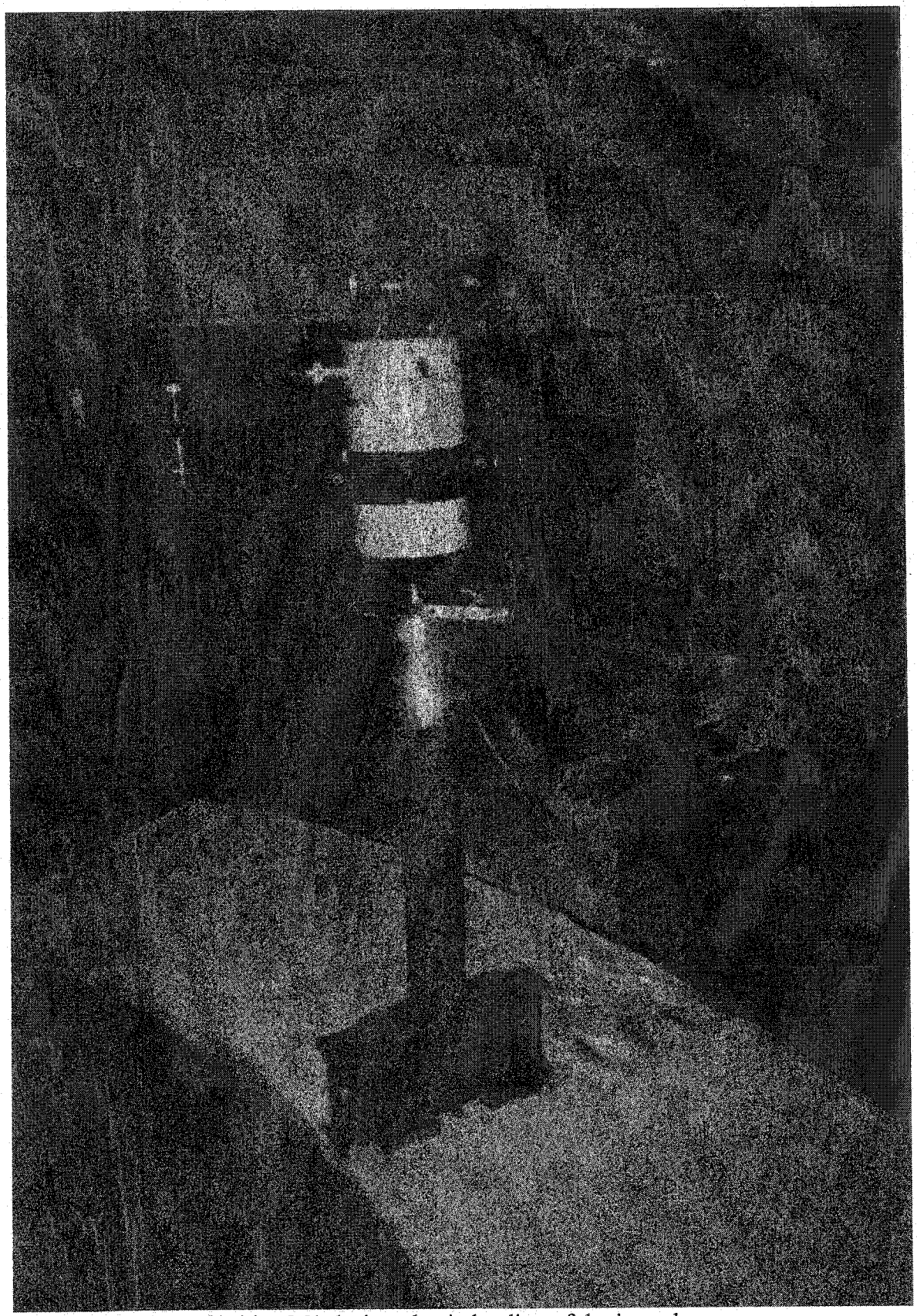

Figure 5.32 View of bridge M1 during elastic loading of the inner lane

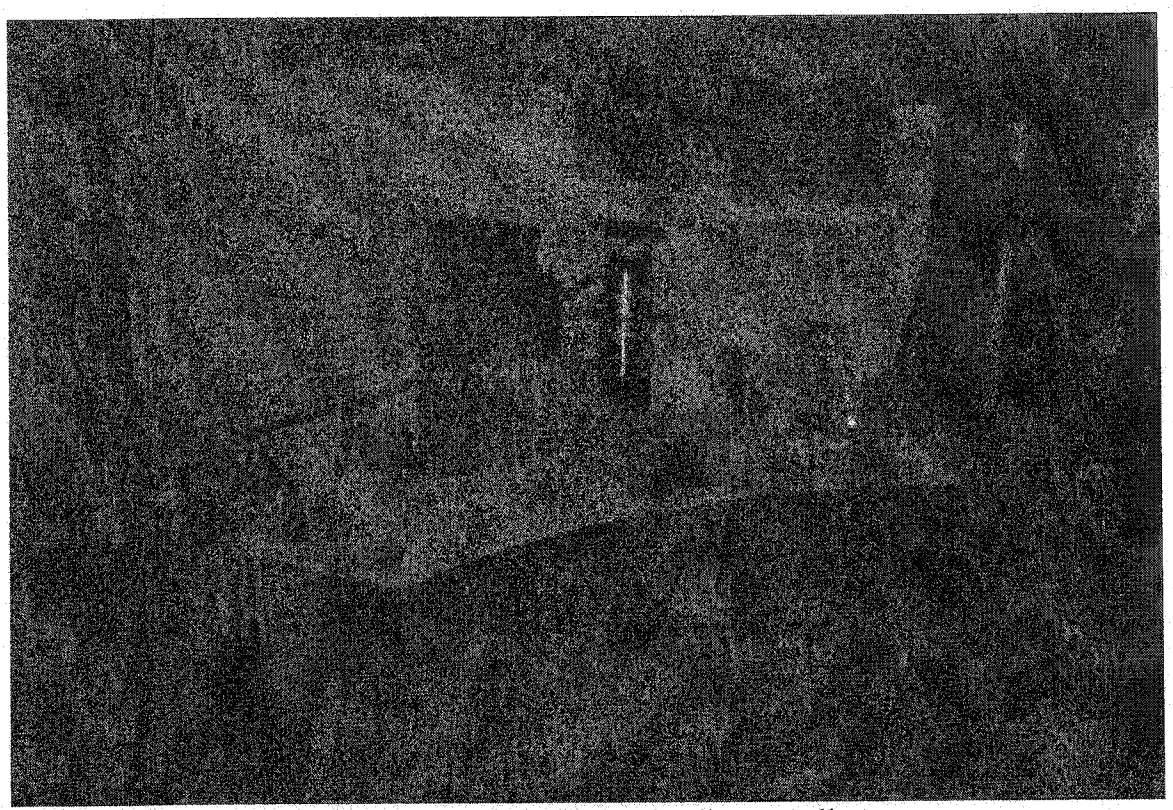

Figure 5.33 View of the bridge model M1 during loading to collapse

Figure 5.34 View of deflected shape of bridge M1 after failure

Figure 5.35 Crack pattern of bridge model M1

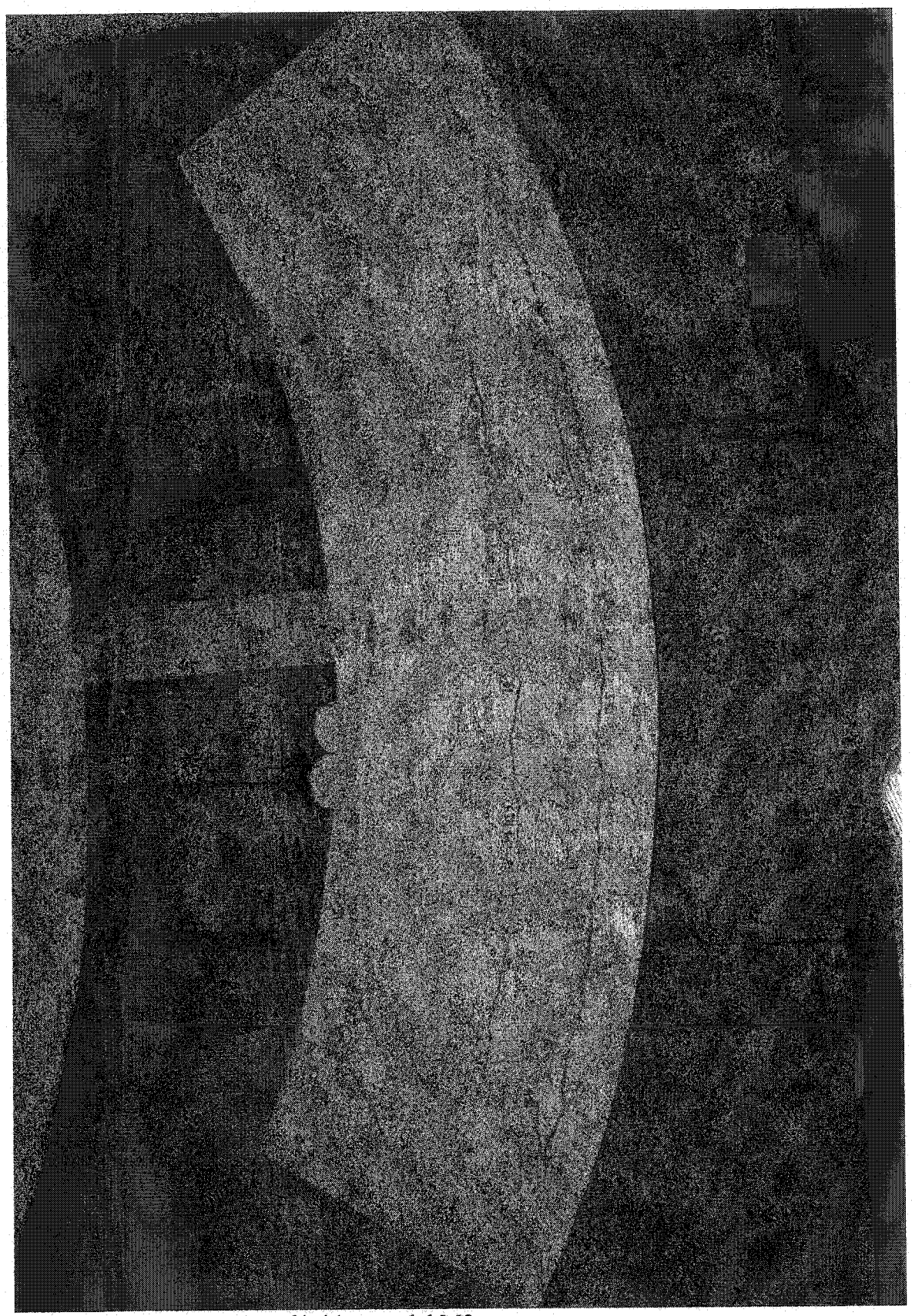

Figure 5.36 Crack pattern of bridge model M2

Figure 5.37 View of bridge M3 during elastic loading of the outer lane

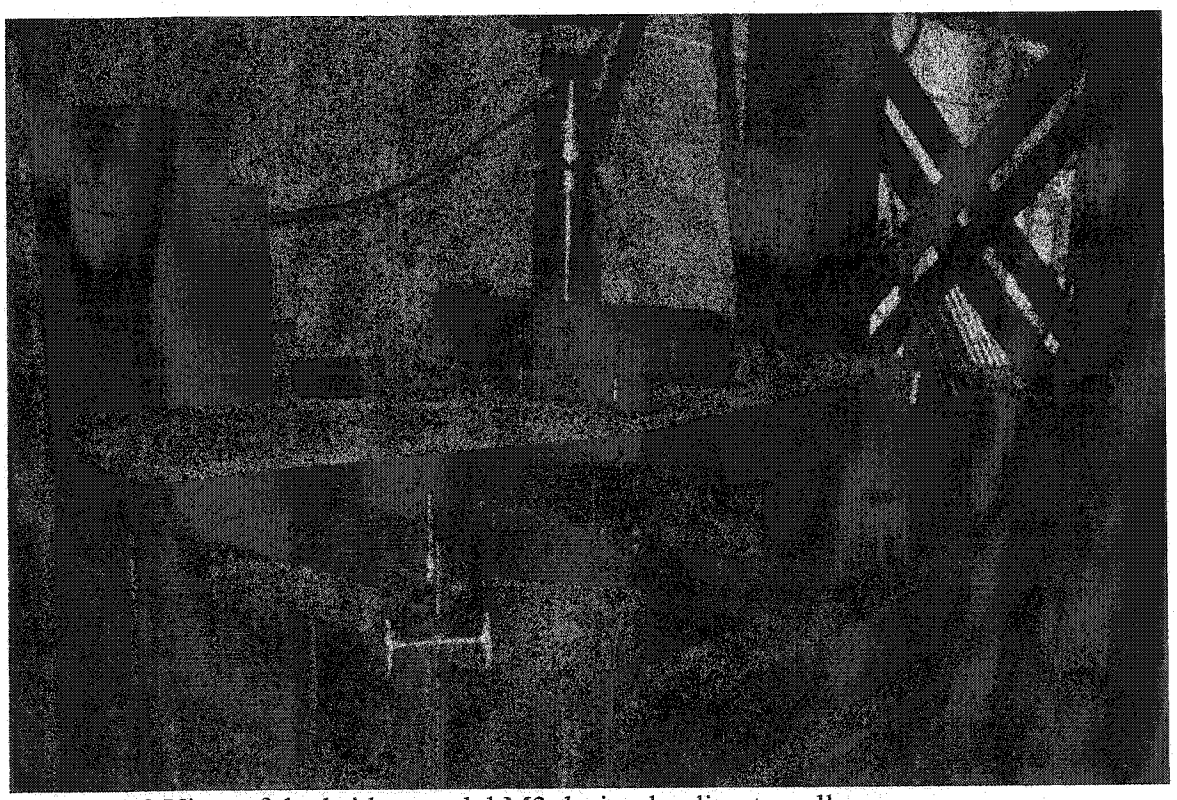

Figure 5.38 View of the bridge model M3 during loading to collapse

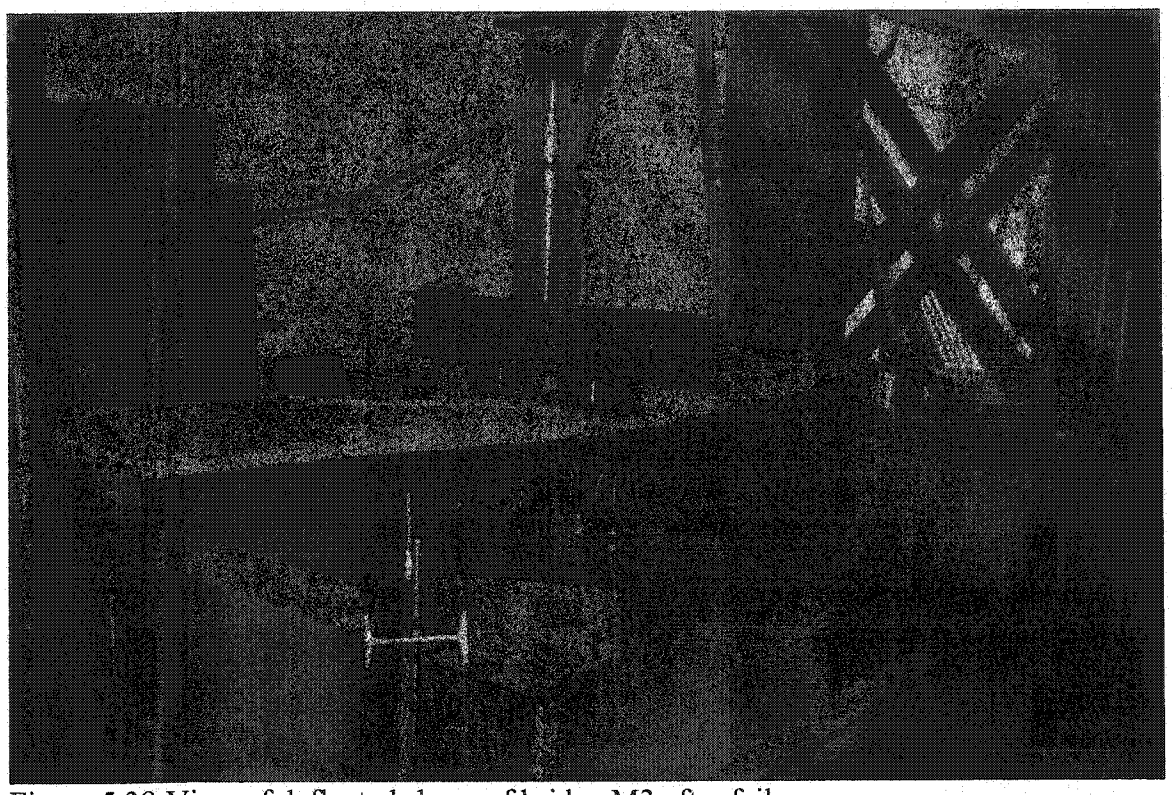

Figure 5.39 View of deflected shape of bridge M3 after failure

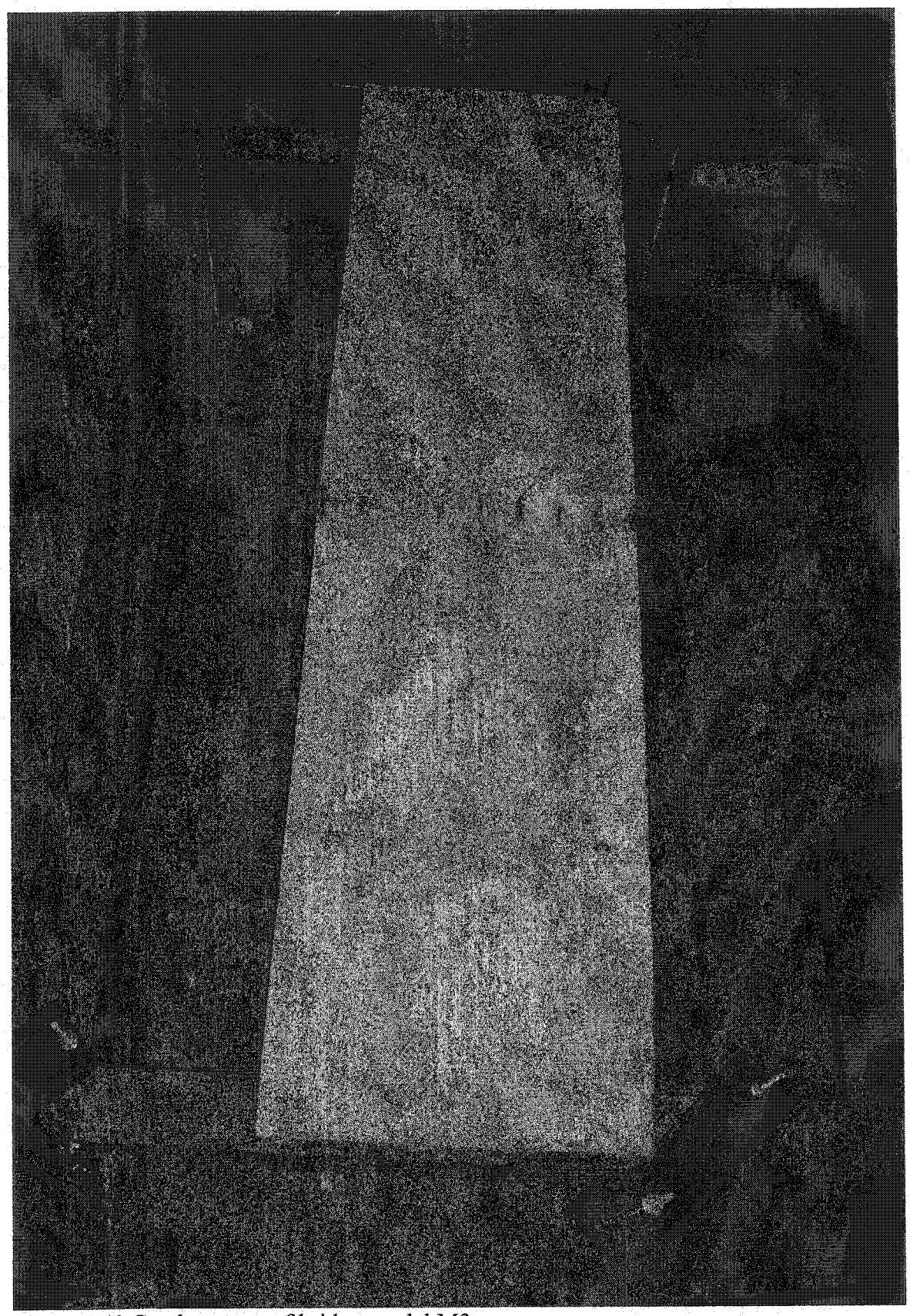

Figure 5.40 Crack pattern of bridge model M3

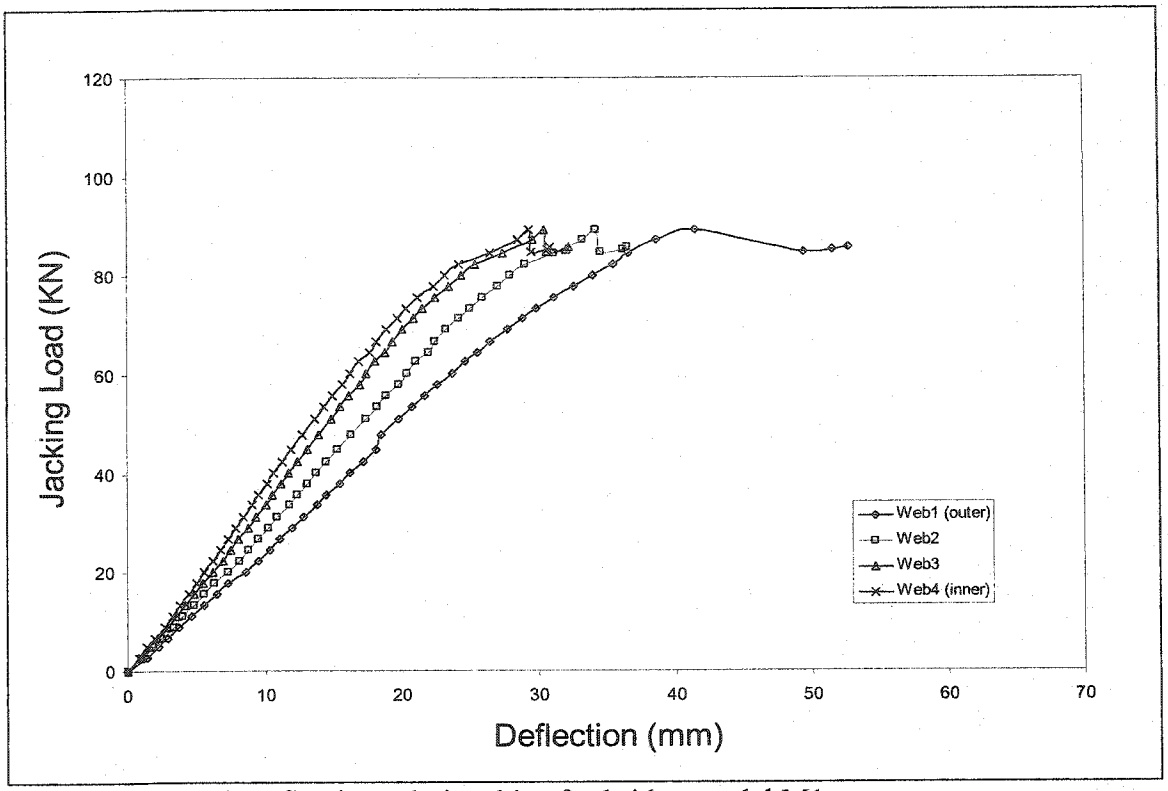

Figure 5.41 Load-Deflection relationships for bridge model M1

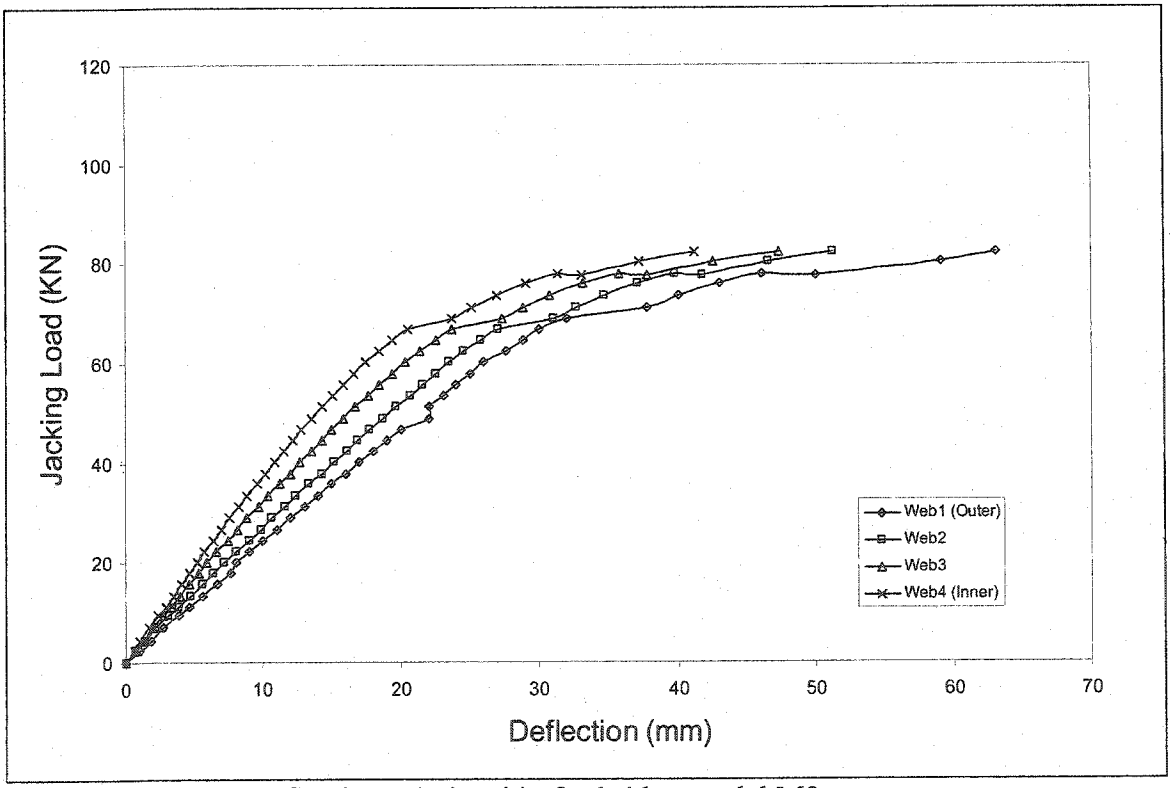

Figure 5.42 Load-Deflection relationship for bridge model M2

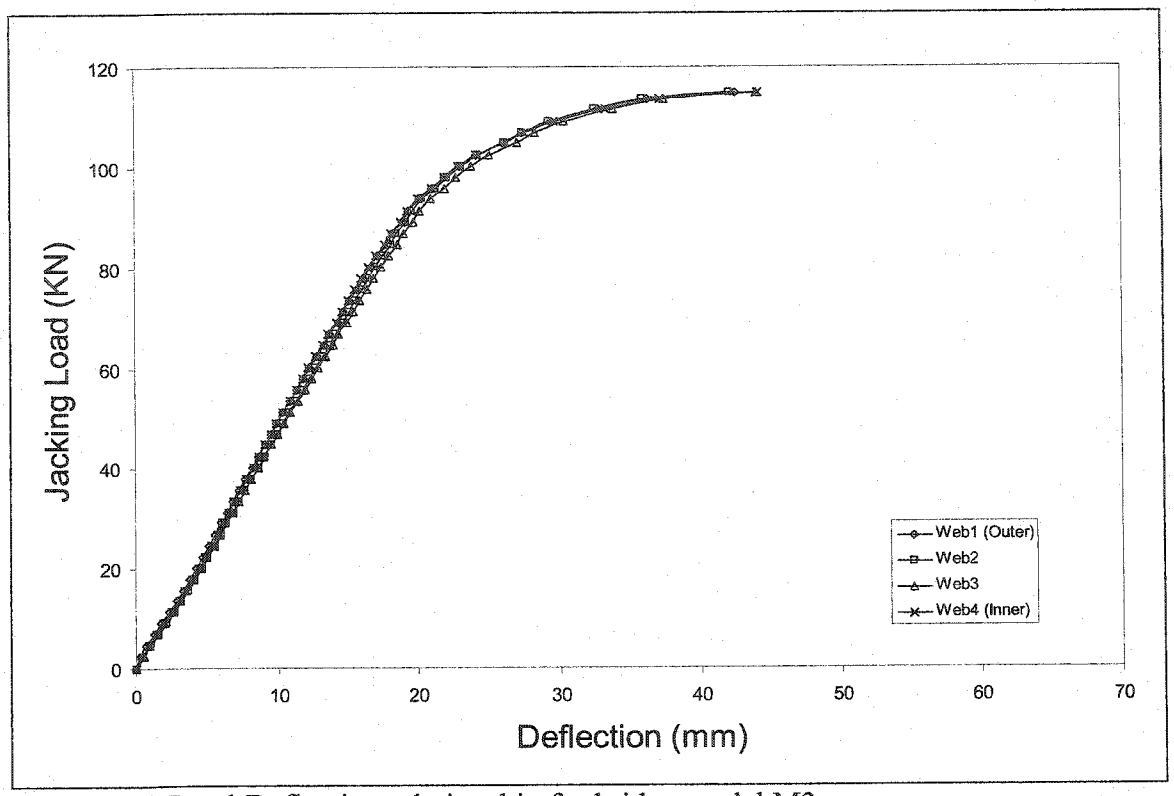

Figure 5.43 Load-Deflection relationship for bridge model M3

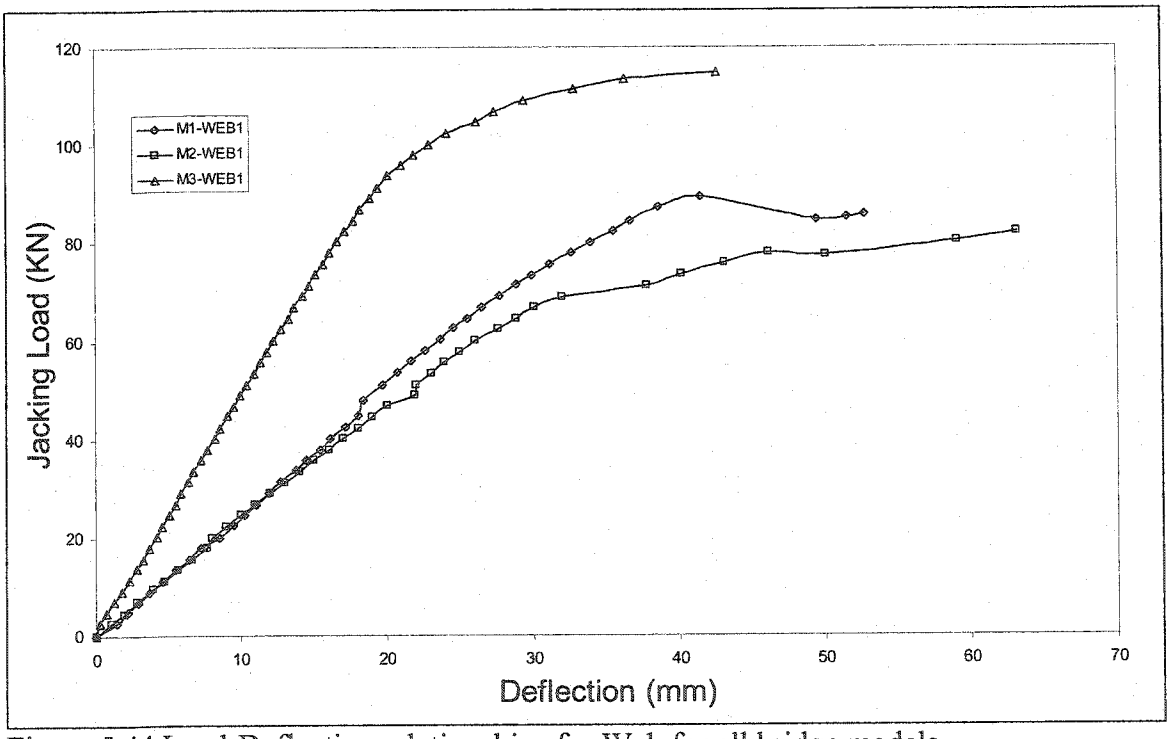

Figure 5.44 Load-Deflection relationships for Web for all bridge models

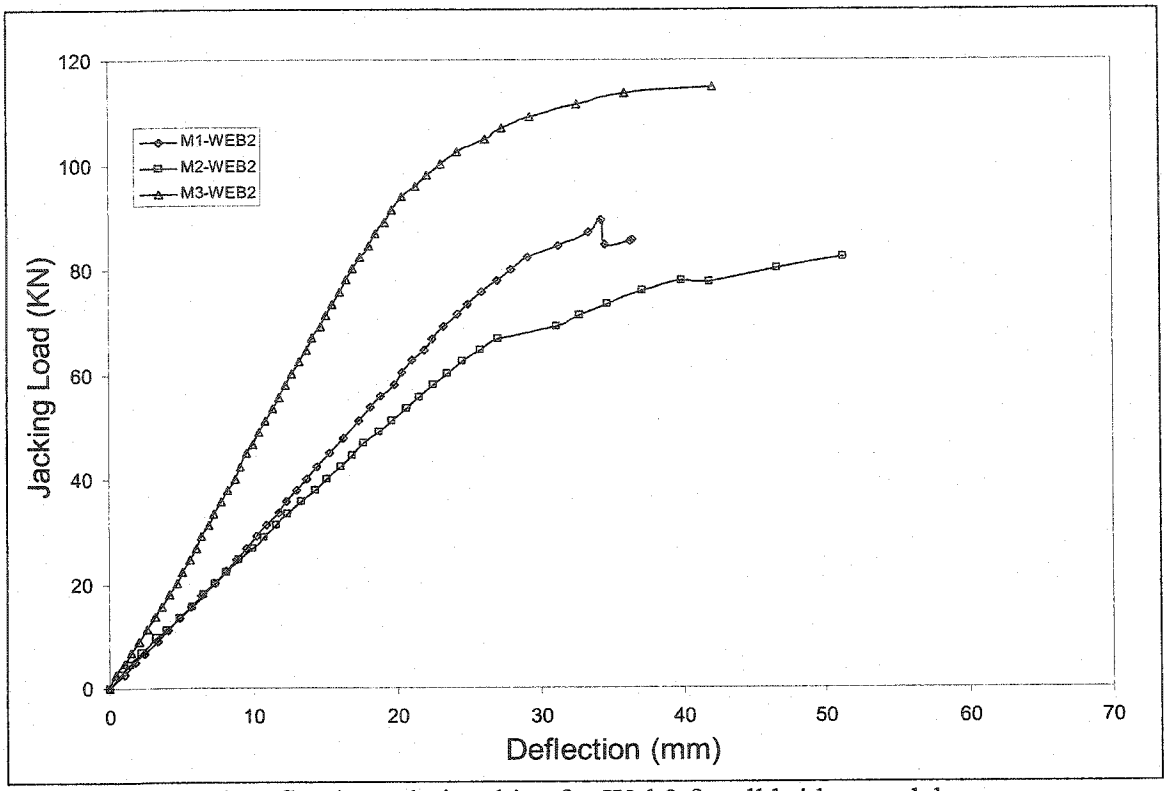

Figure 5.45 Load-Deflection relationships for Web2 for all bridge models

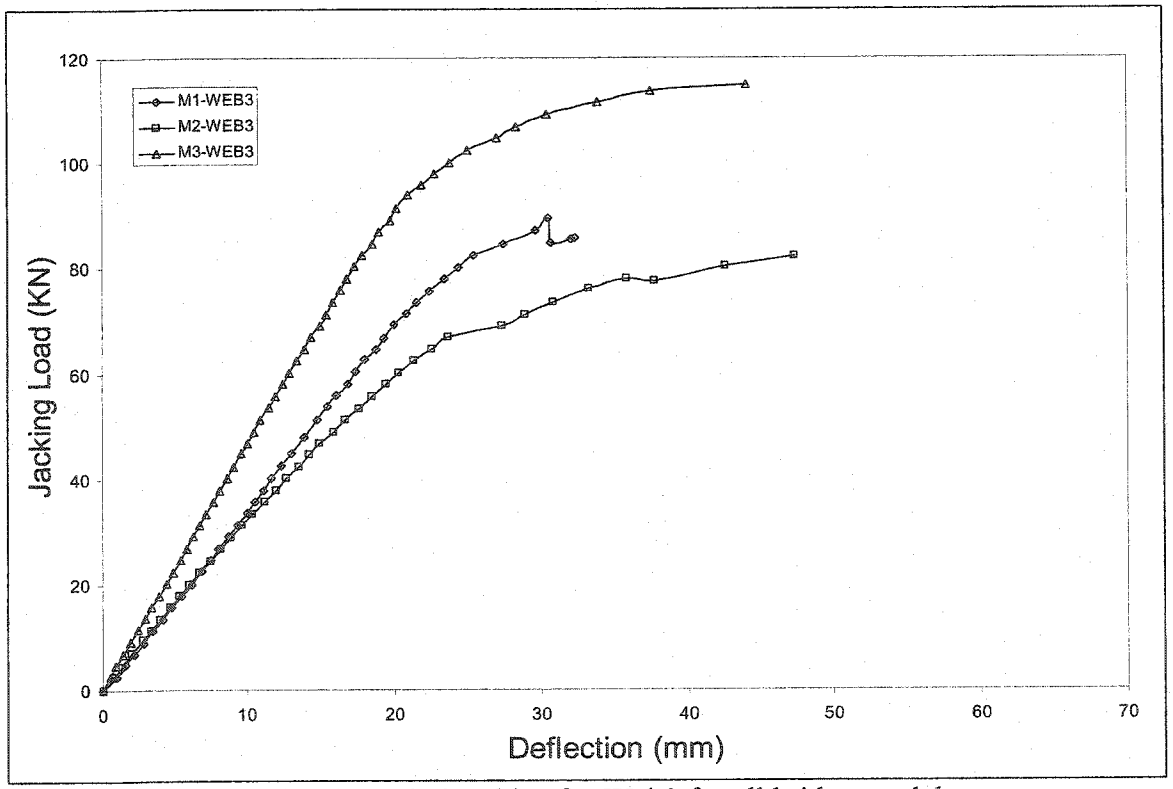

Figure 5.46 Load-Deflection relationships for Web3 for all bridge models

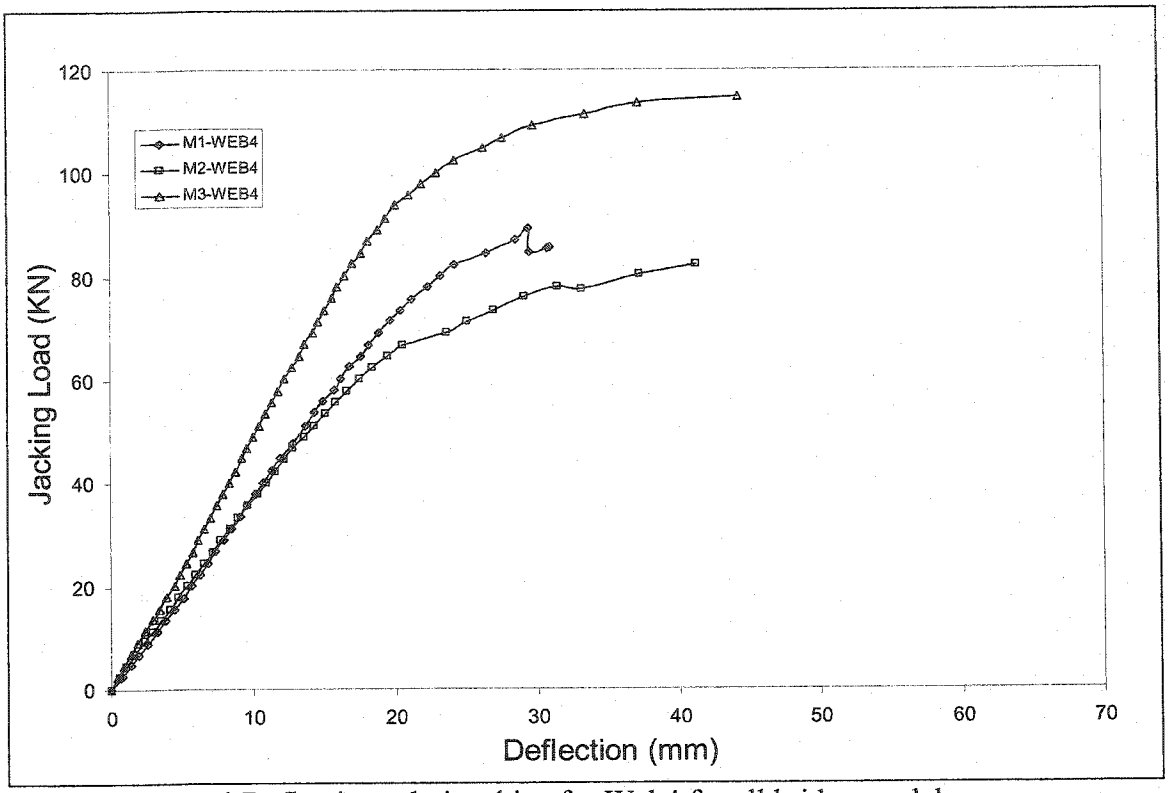

Figure 5.47 Load-Deflection relationships for Web4 for all bridge models

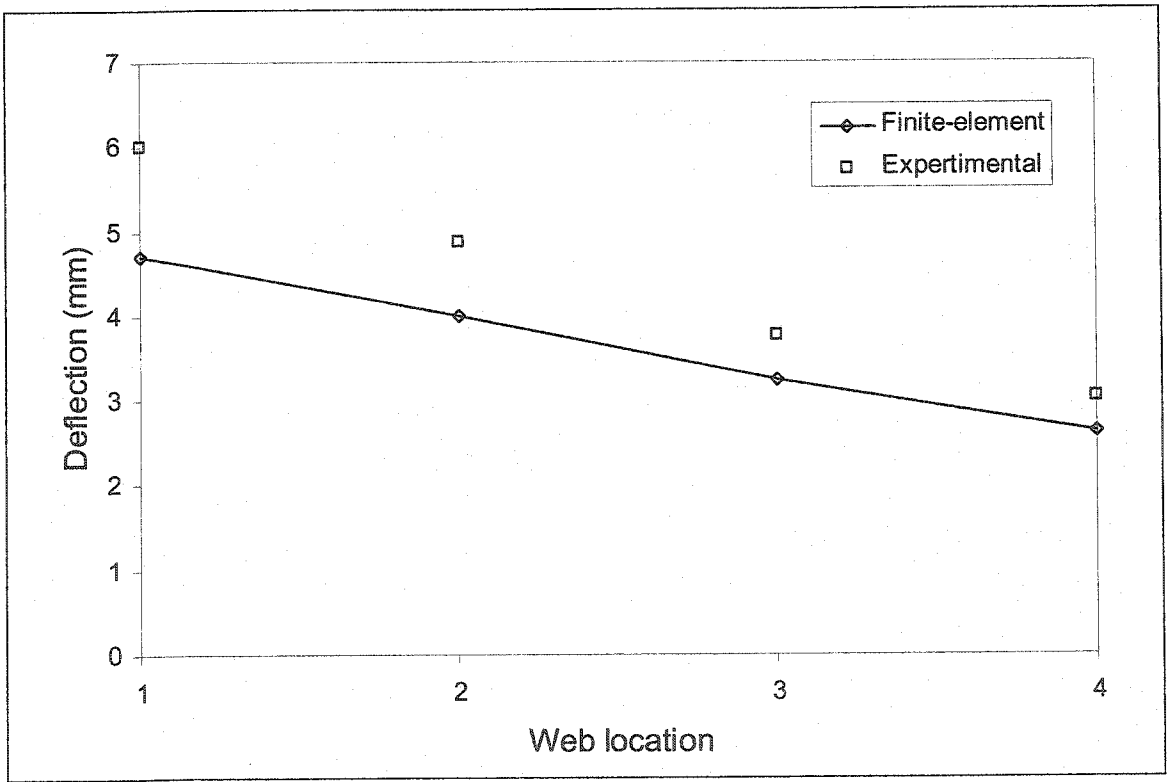

Figure 5.48 Deflection Distribution at mid-span section of bridge model M1 due to loading the outer lane

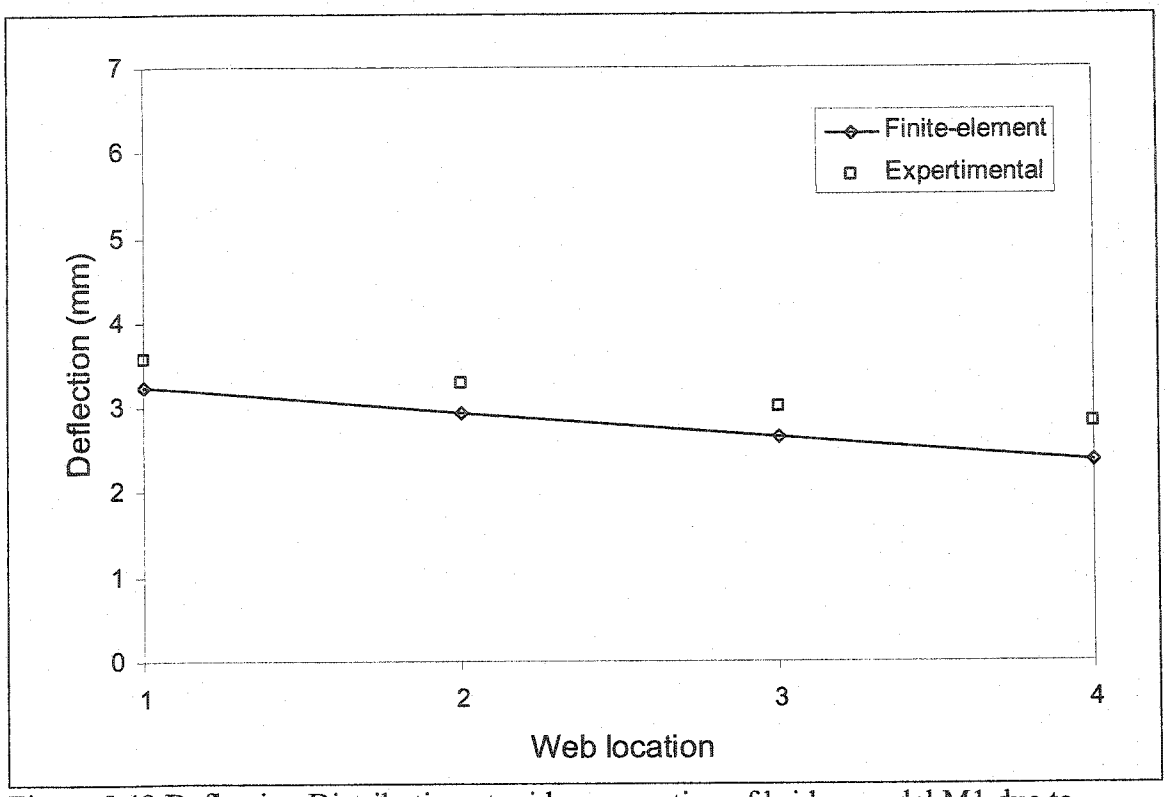

Figure 5.49 Deflection Distribution at mid-span section of bridge model M1 due to loading the inner lane

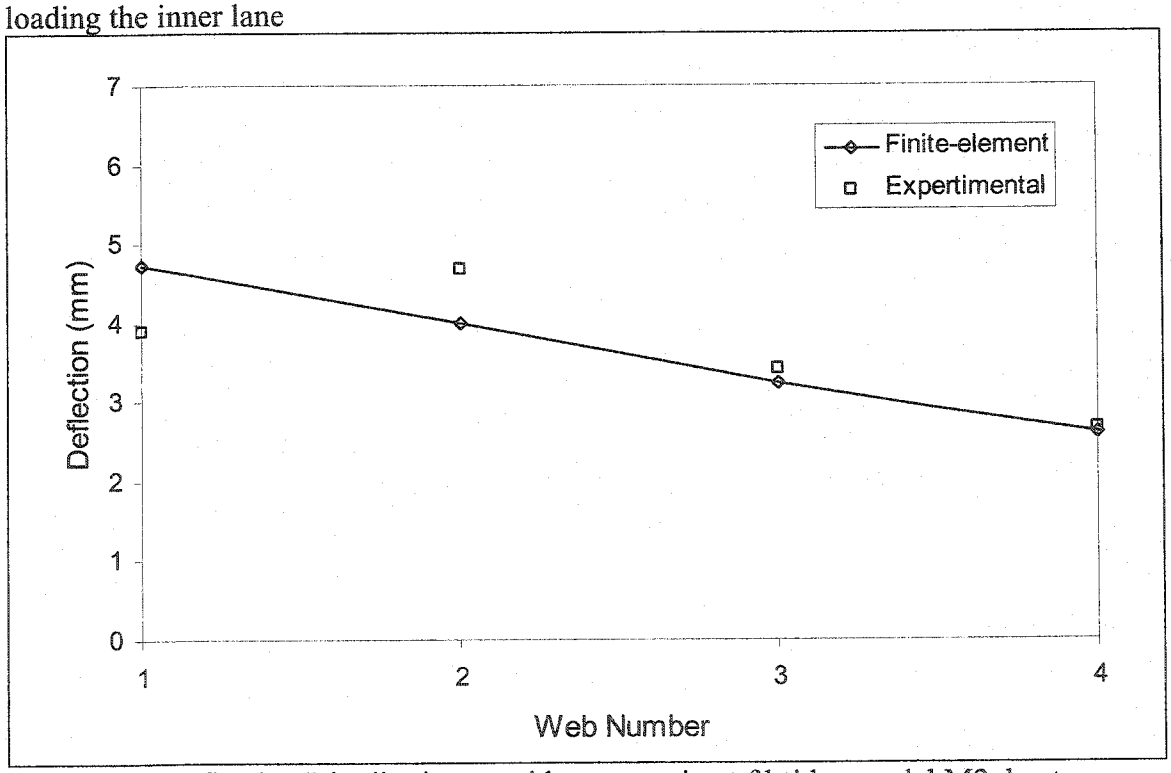

Figure 5.50 Deflection Distribution at mid-span section of bridge model M2 due to loading the outer lane

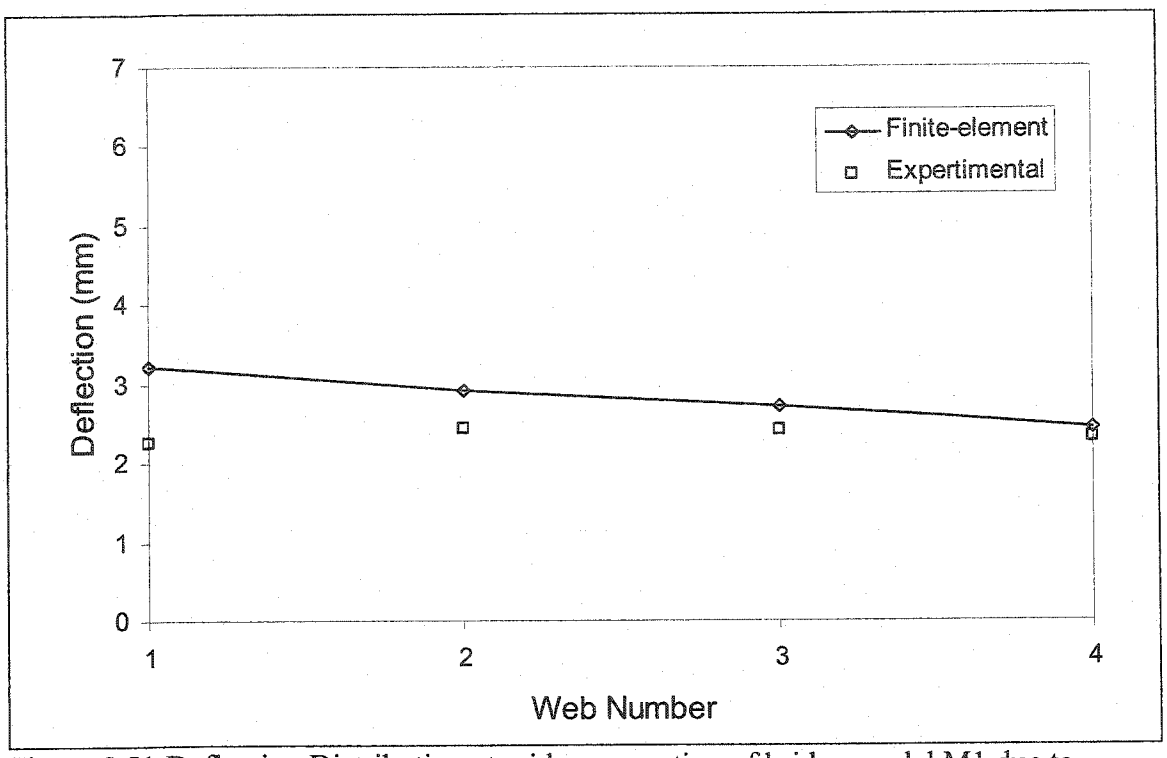

Figure 5.51 Deflection Distribution at mid-span section of bridge model M1 due to loading the inner lane

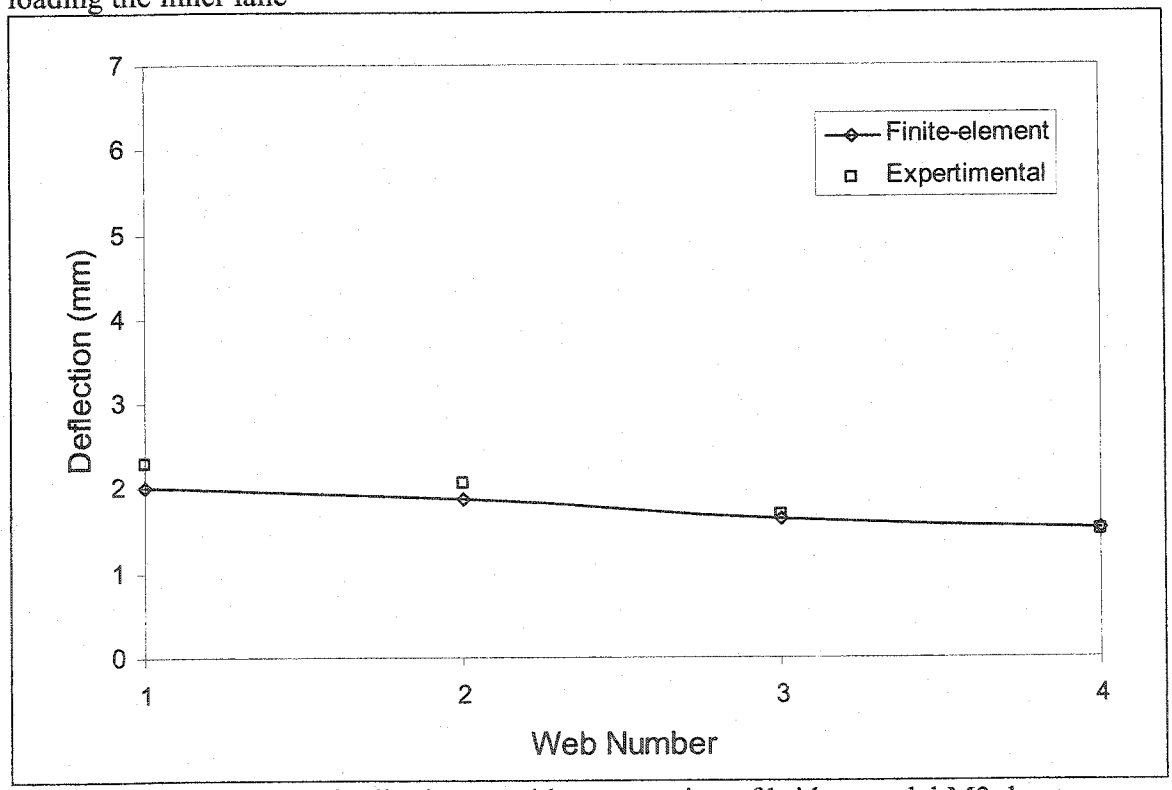

Figure 5.52 Deflection Distribution at mid-span section of bridge model M3 due to loading the outer lane

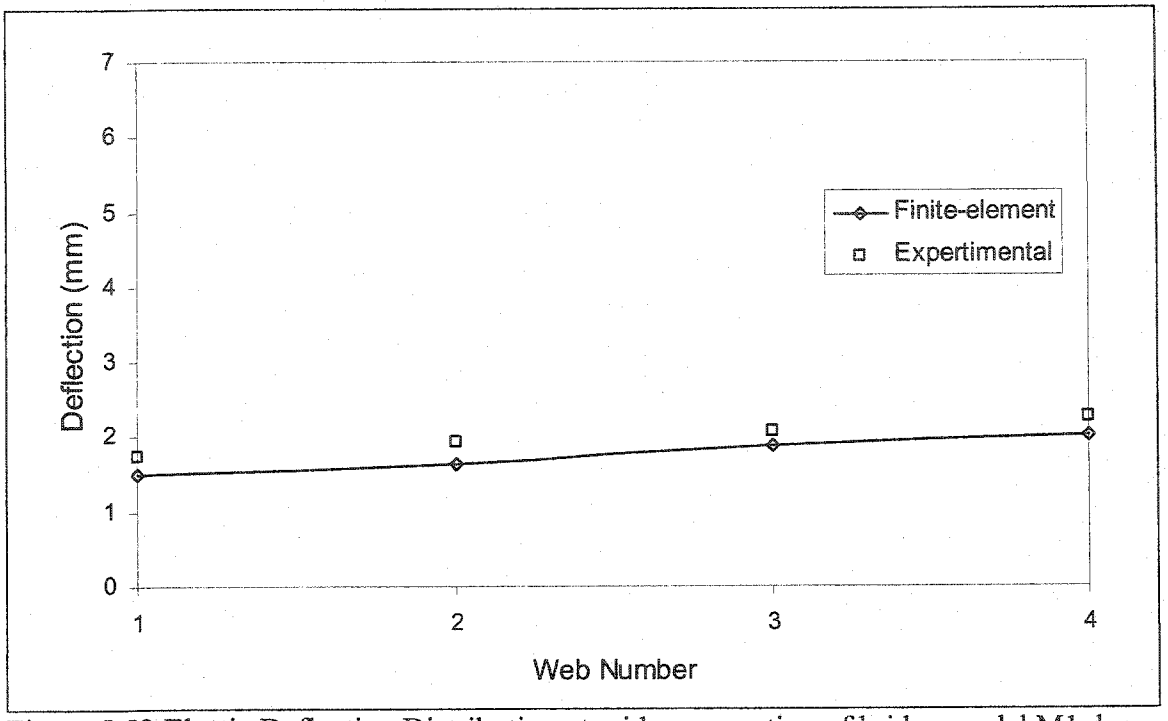

Figure 5.53 Elastic Deflection Distribution at mid-span section of bridge model M1 due to loading the inner lane

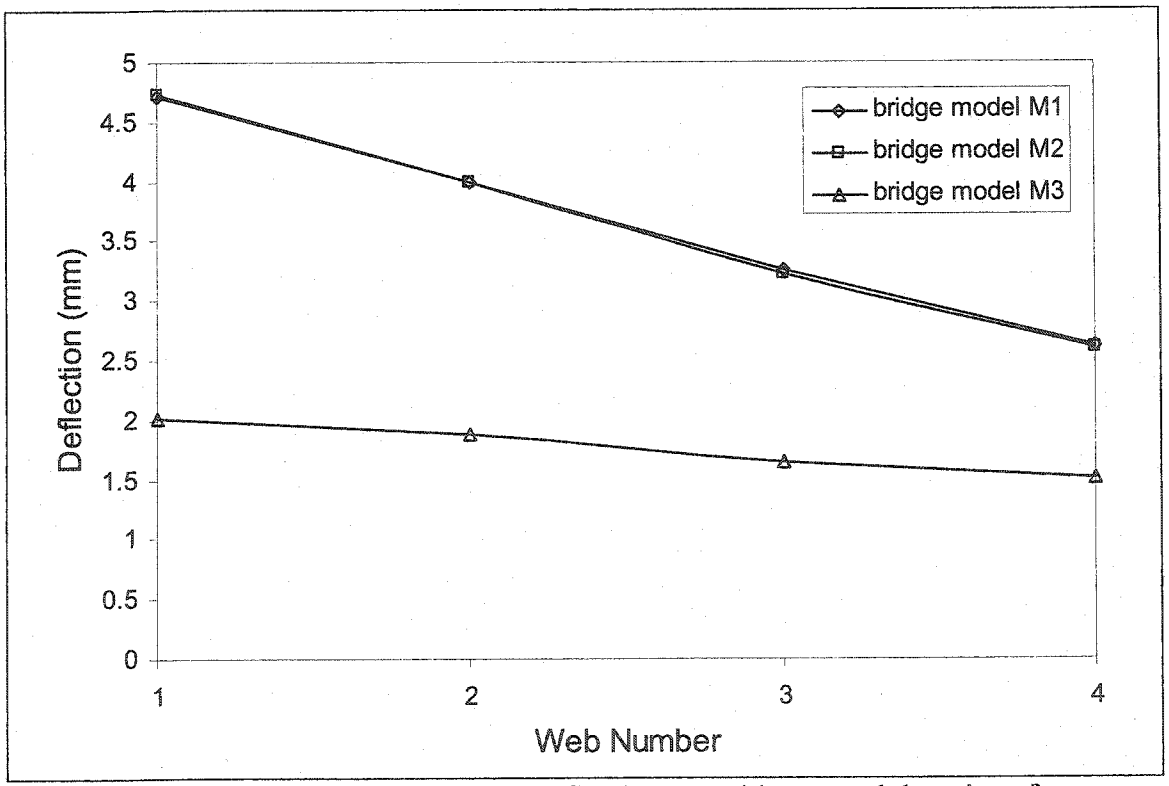

Figure 5.54 Bridge model bottom flange deflections at mid span web locations for outer loading case of 10 kN

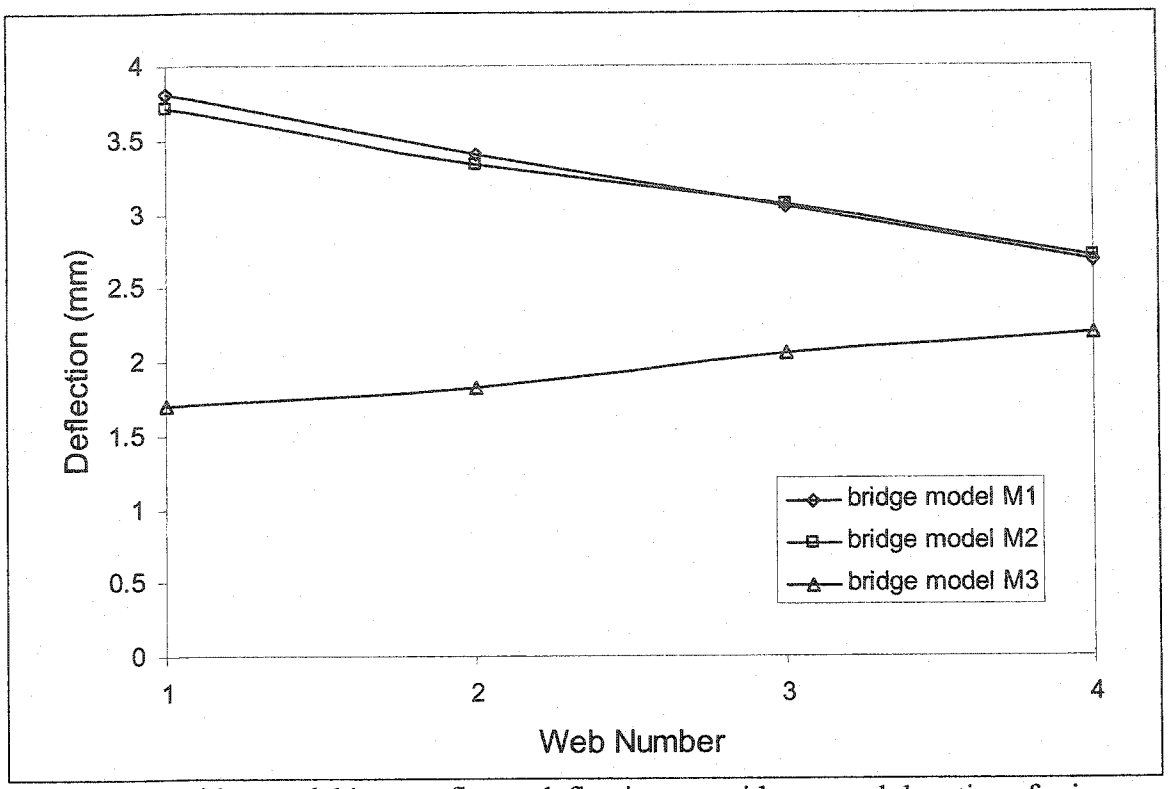

Figure 5.55 Bridge model bottom flange deflections at mid span web locations for inner loading case of 10 kN

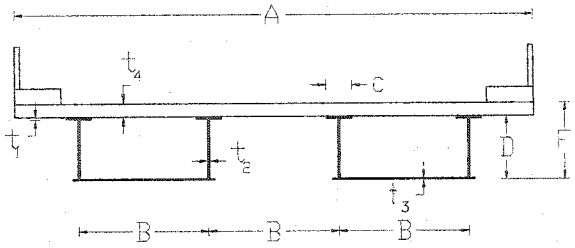

(a) Two-lane two box cross-section

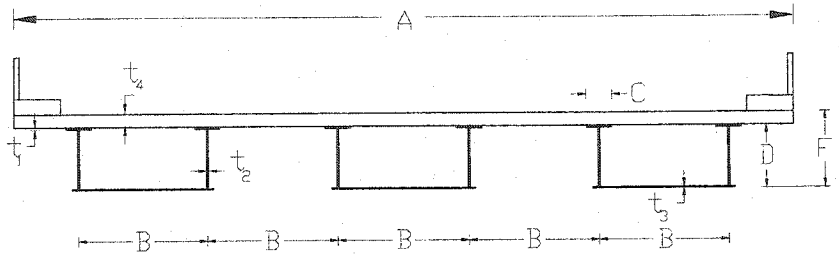

(b) Three-lane three box cross-section

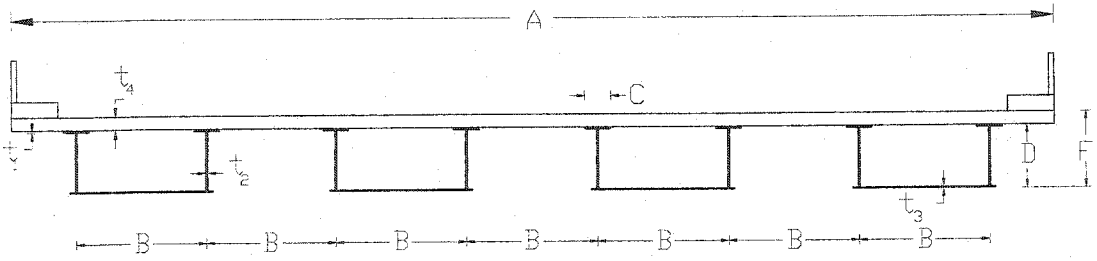

(c) Four-lane four box cross-section

Figure 6.1 Basic cross section configurations and symbols

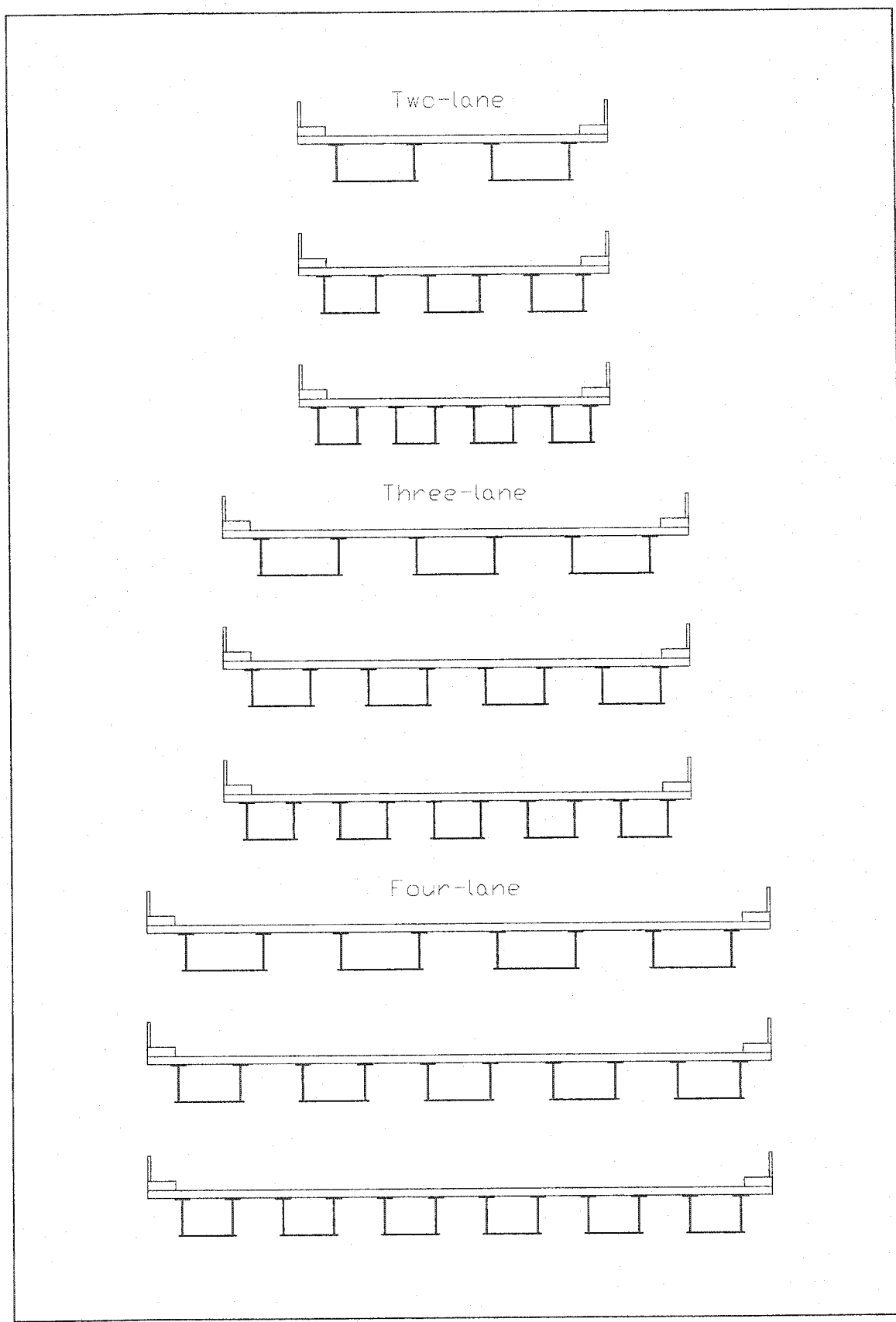

Figure 6.2 Cross section configuration in the parametric study

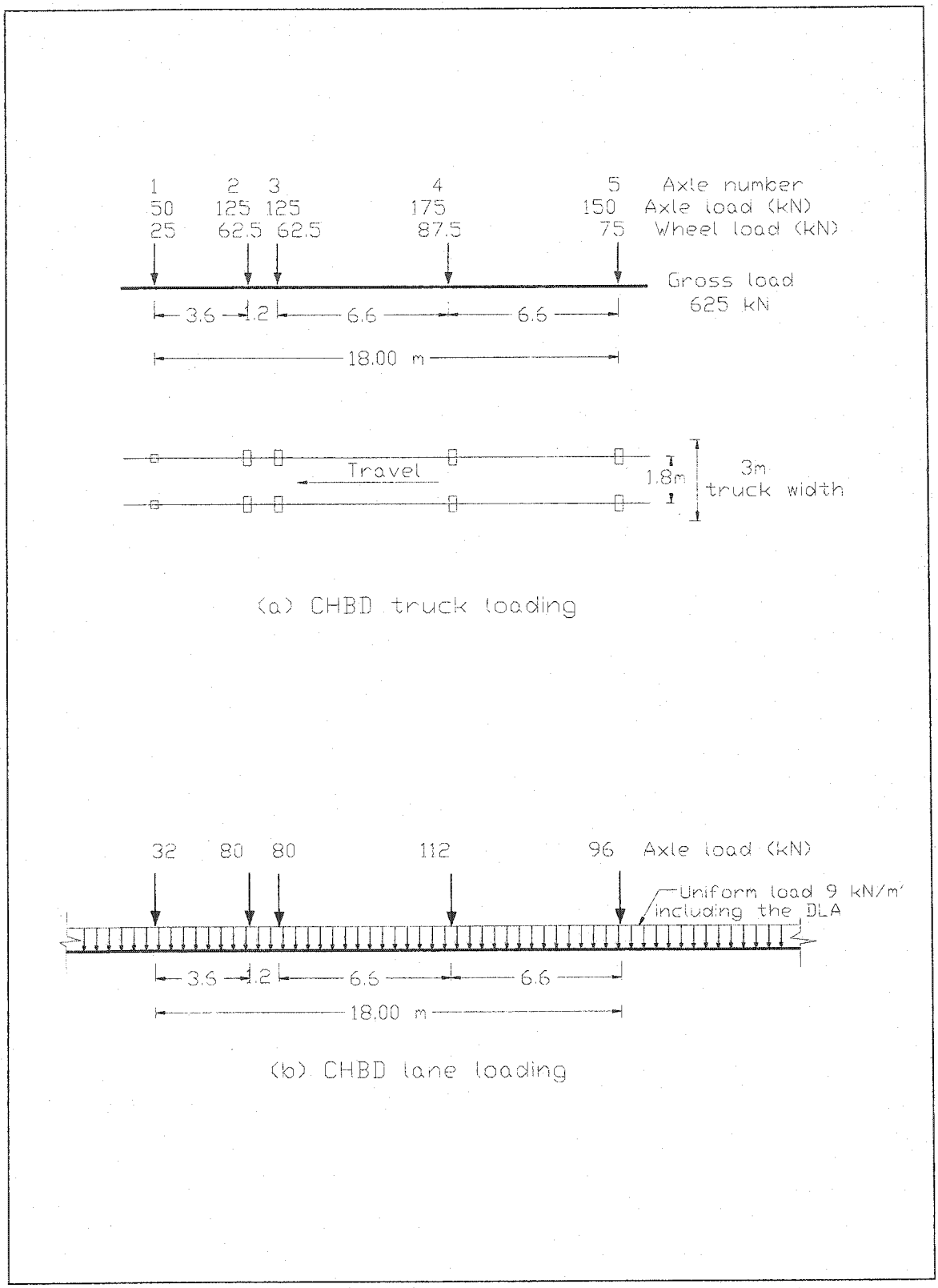

Figure 6.3 CHBDC loading Configuration

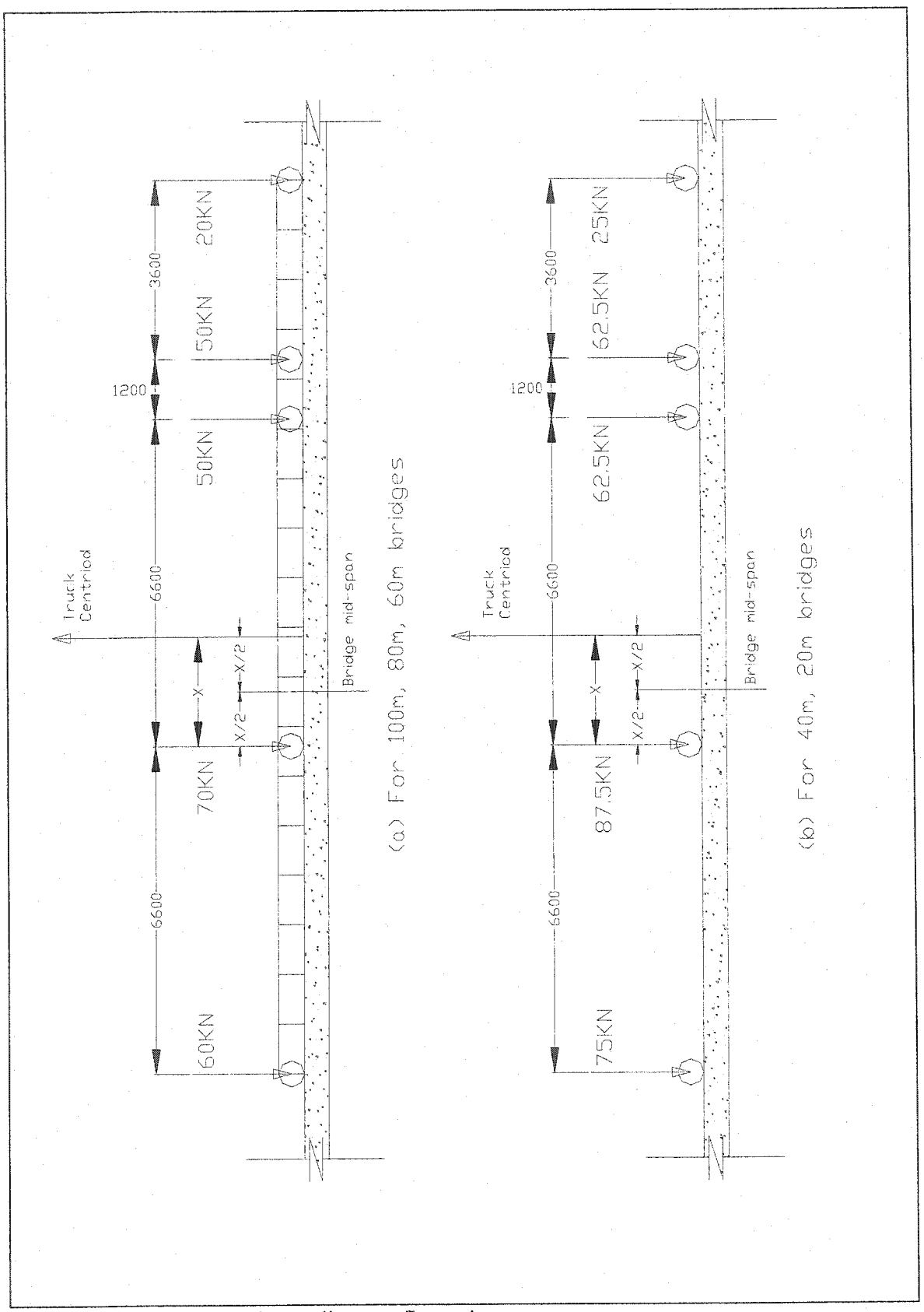

Figure 6.4 CHBDC Truck Loading configurations

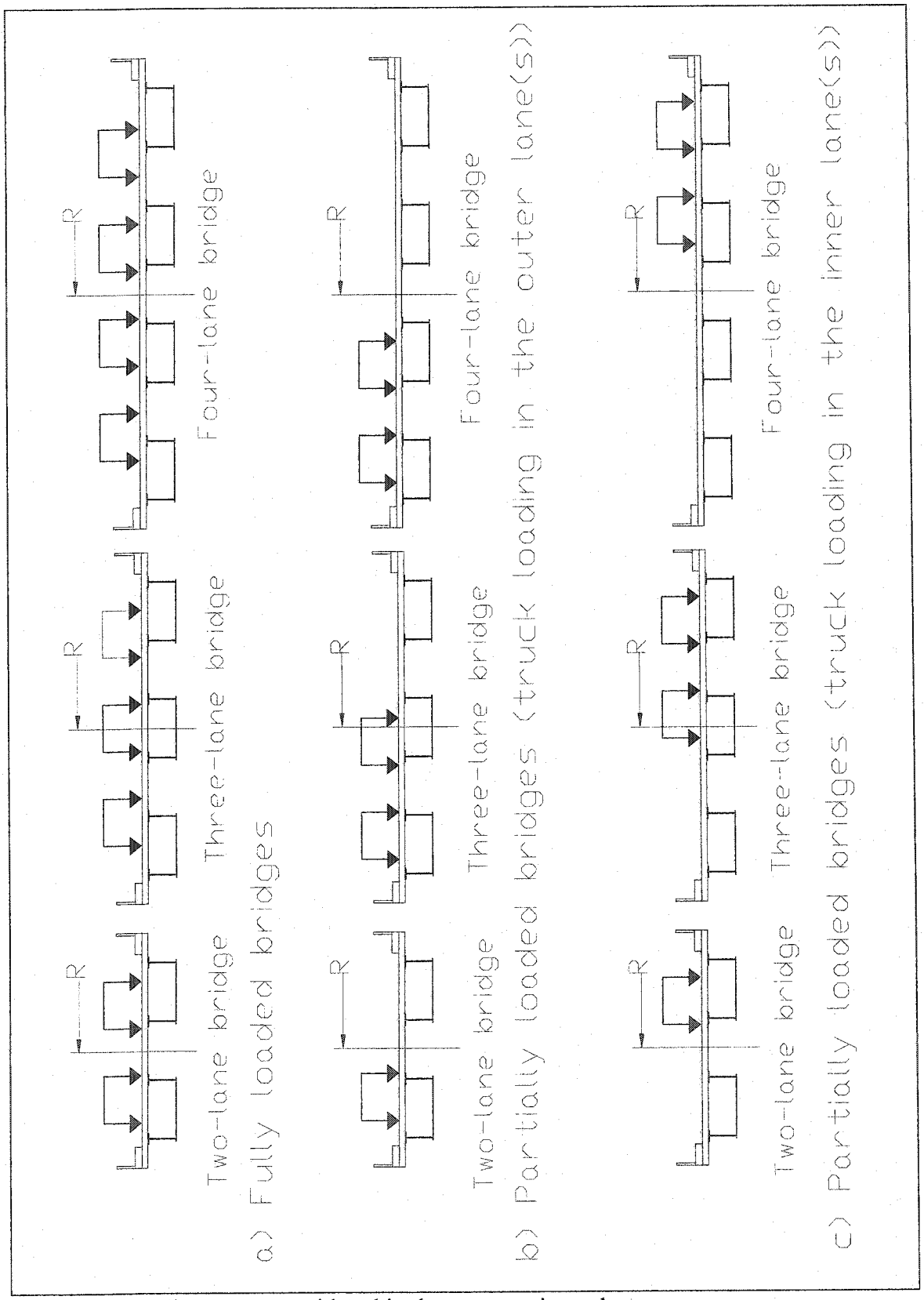

Figure 6.5 Loading cases considered in the parametric study

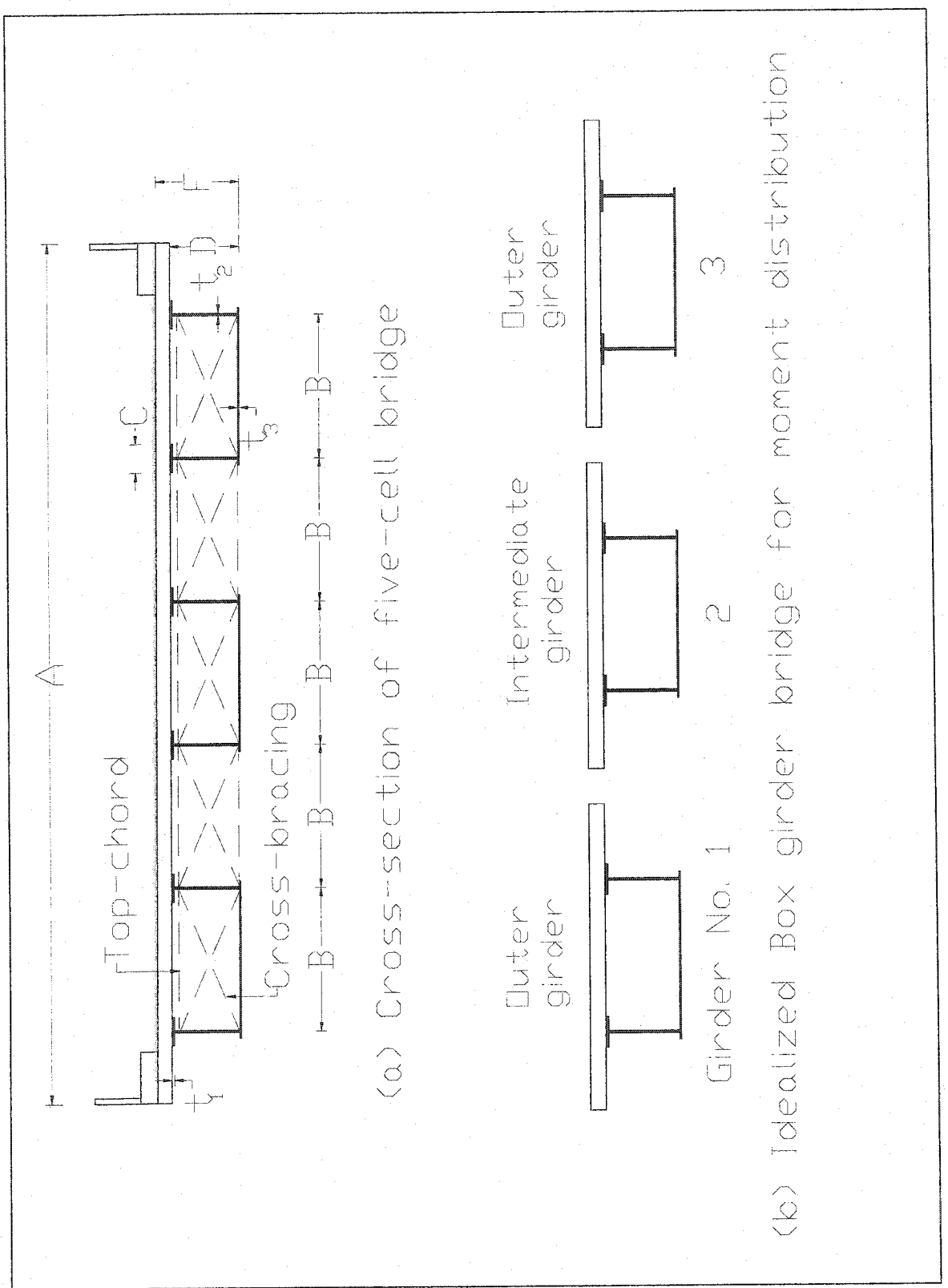

Figure 6.6 Idealized Cross section for moment distribution

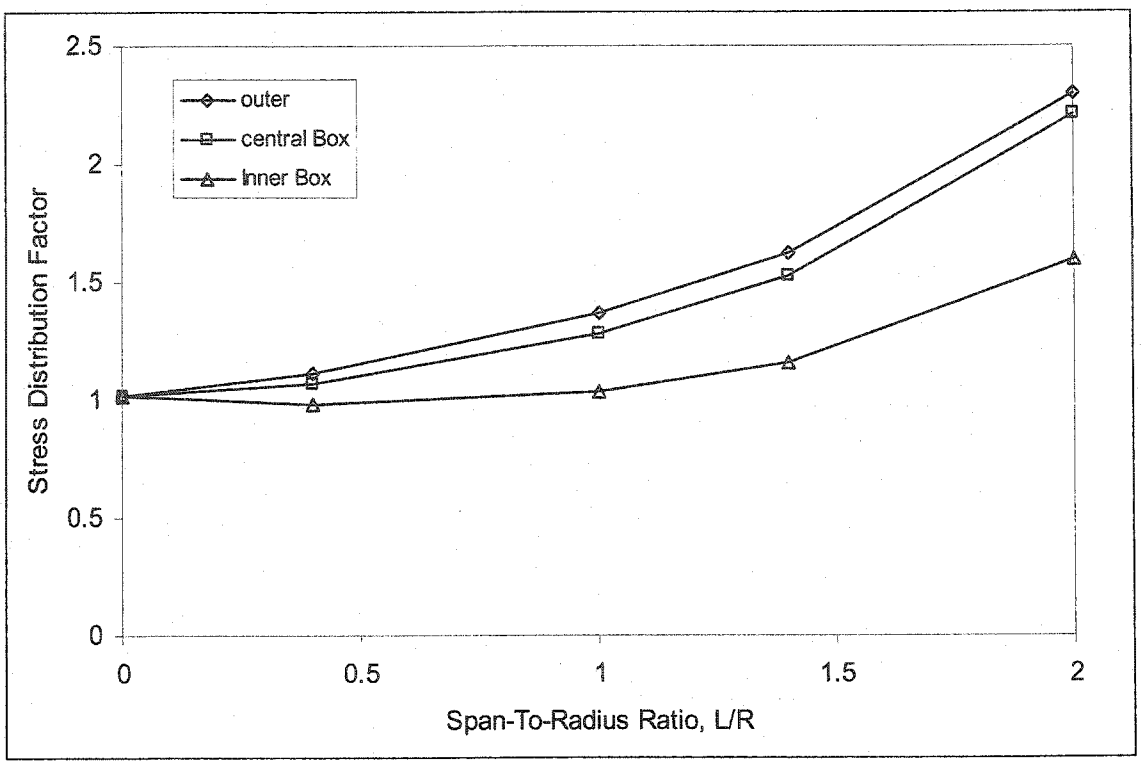

Figure 7.1 Effect of curvature on the stress distribution factor of four lanes, four box girder 100 meter bridges under dead load

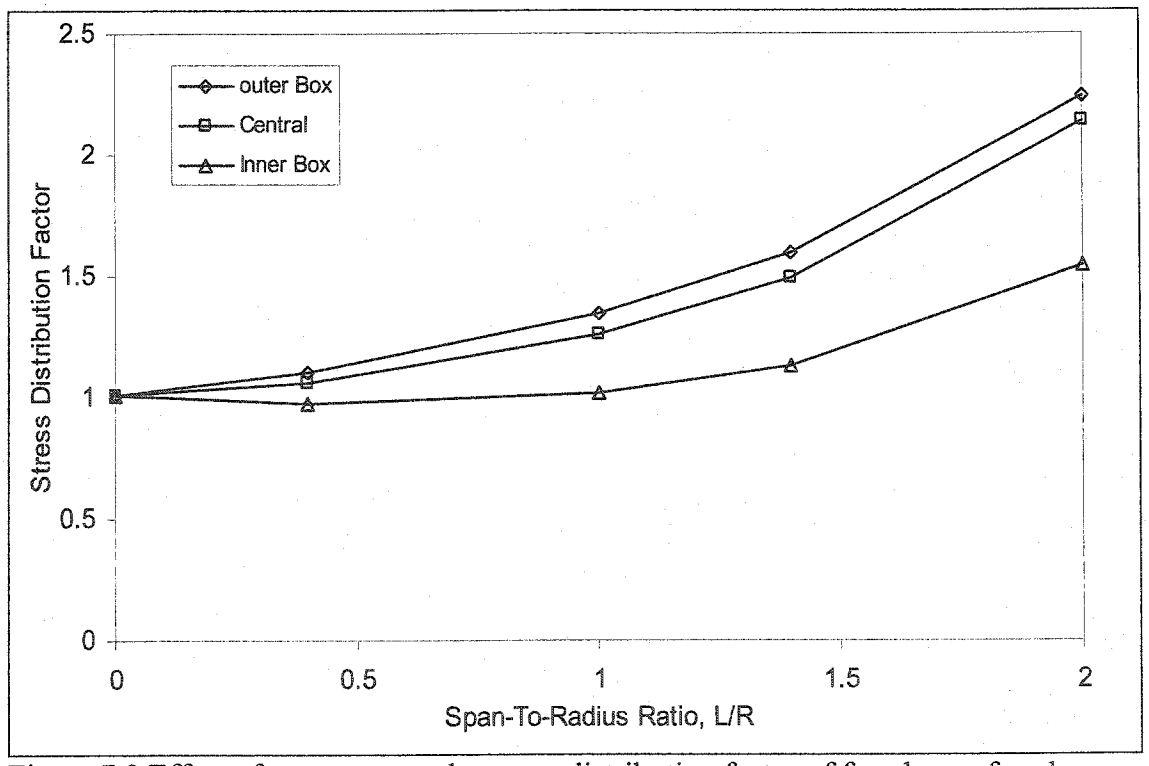

Figure 7.2 Effect of curvature on the stress distribution factor of four lanes, four box girder 100 meter bridges under CHBDC full truck loading

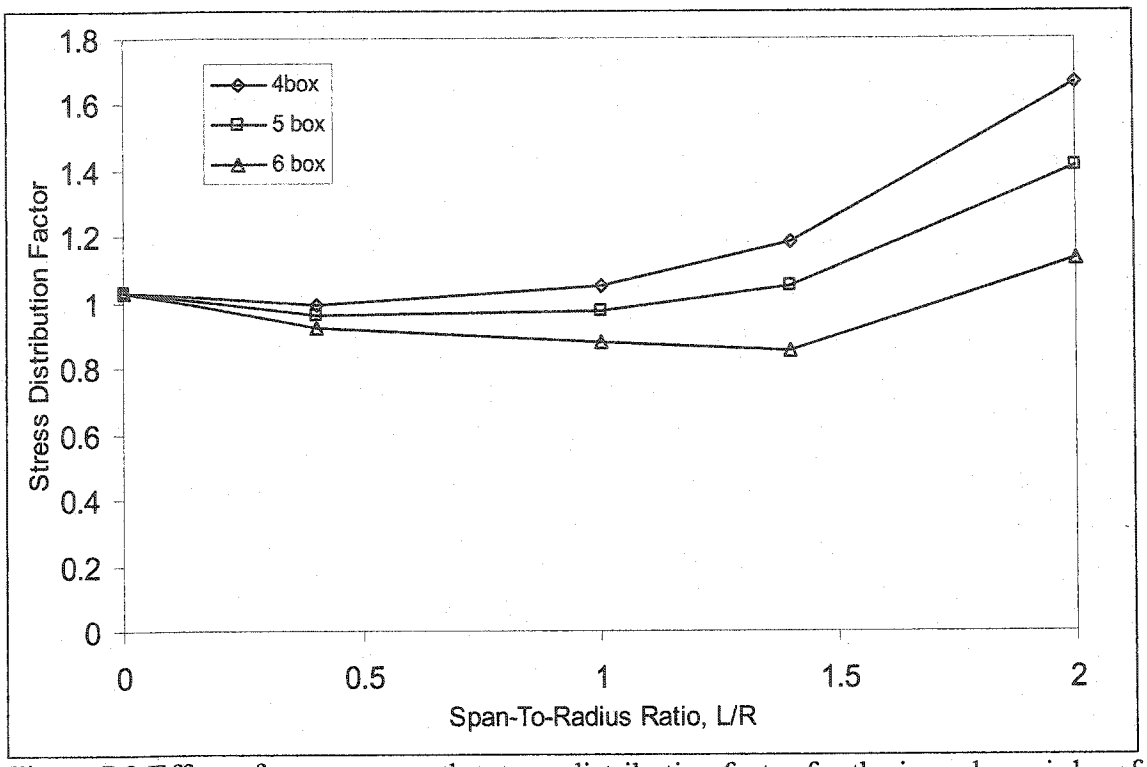

Figure 7.3 Effect of curvature on the stress distribution factor for the inner box girder of four lanes, 80 meter bridges under dead loading

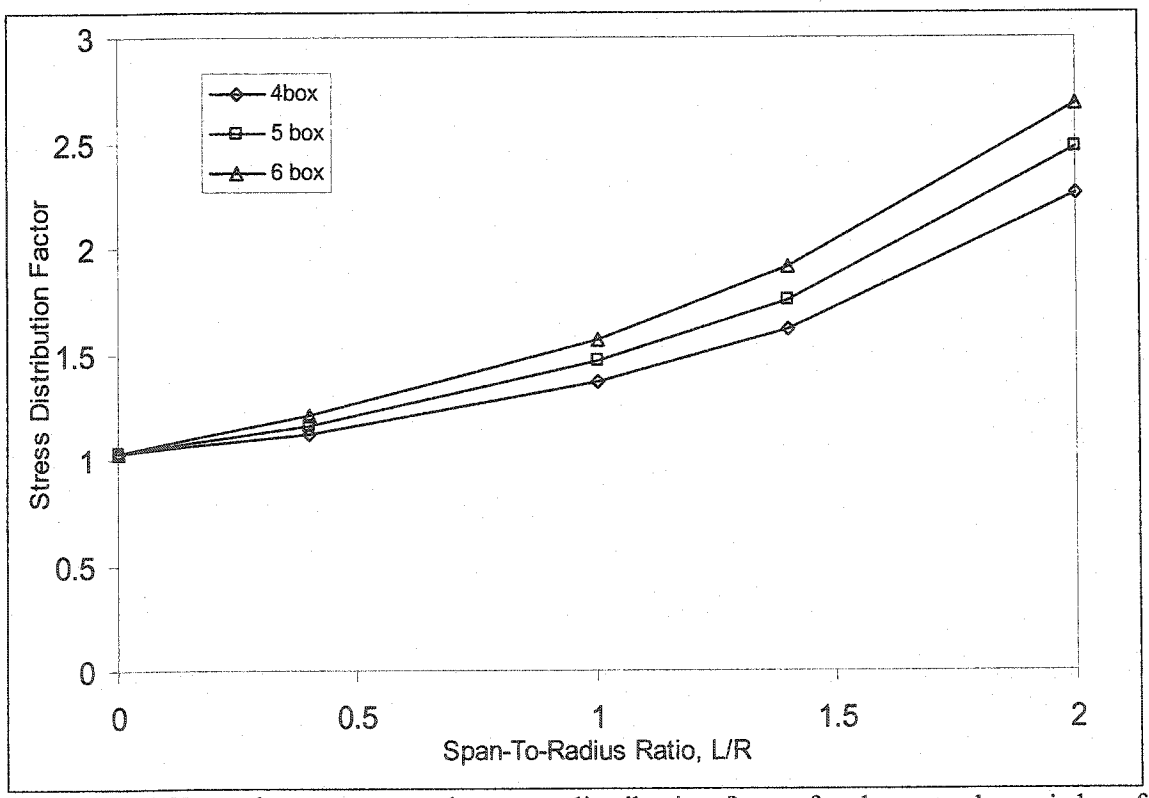

Figure 7.4 Effect of curvature on the stress distribution factor for the outer box girder of four lanes, 80 meter bridges under dead loading

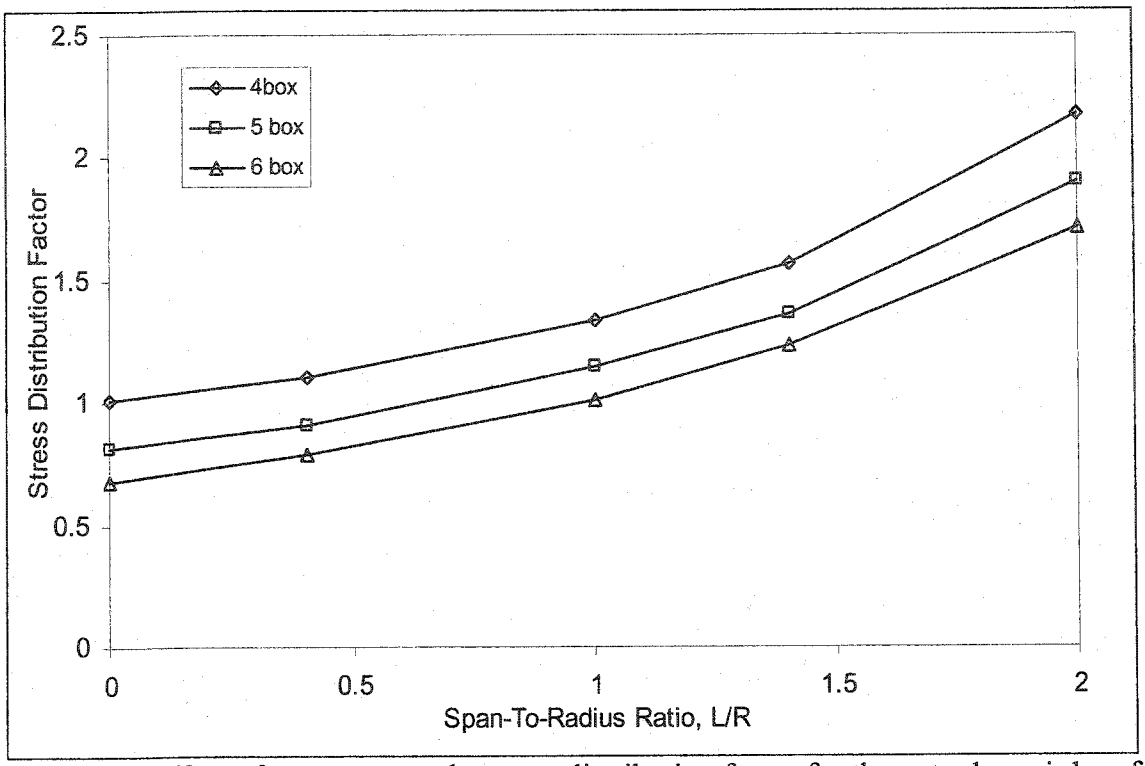

Figure 7.5 Effect of curvature on the stress distribution factor for the outer box girder of four lanes, 80 meter bridges under full CHBDC truck loading

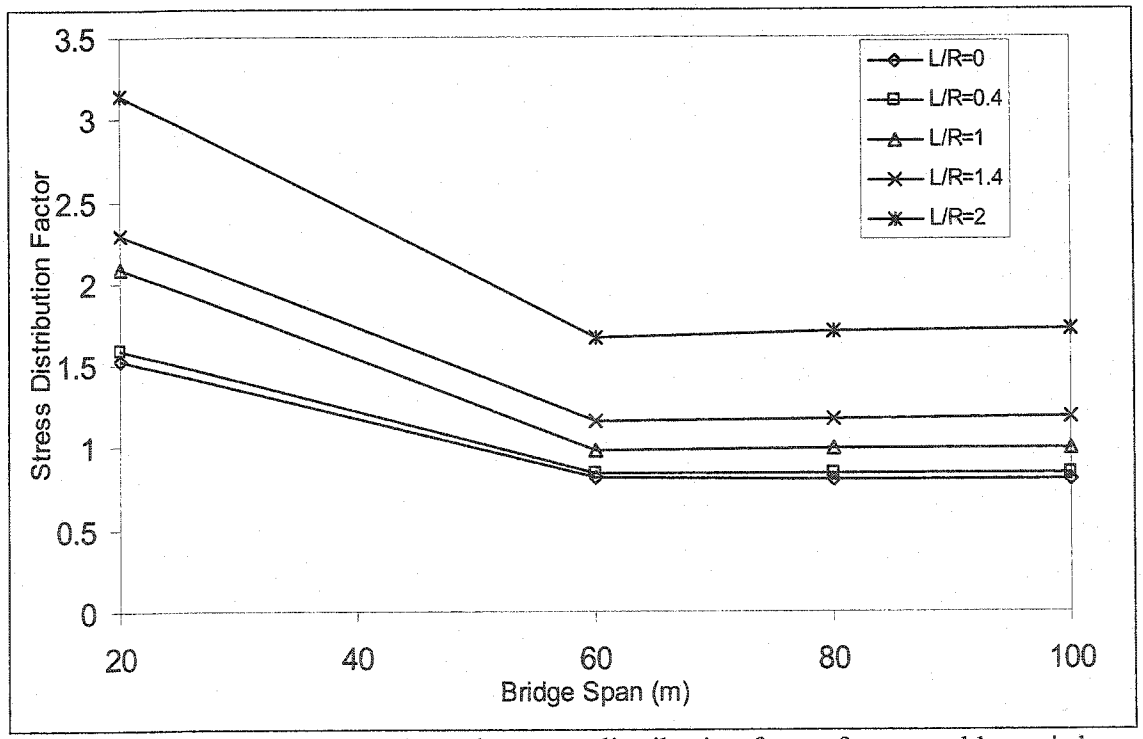

Figure 7.6 Effect of span length on the stress distribution factor for central box girders of four-lane, five-box girder bridges under full CHBDC truck loading

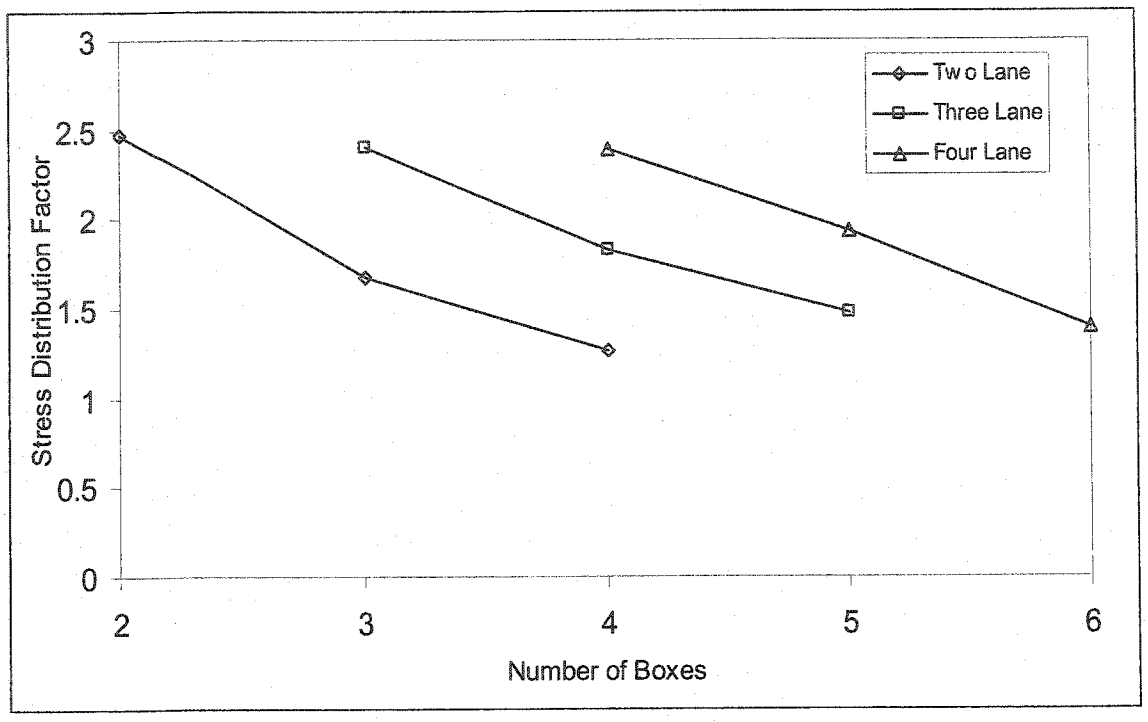

Figure 7.7 Effect of number of box girders on the stress distribution factor for the outer box girders of straight bridges of 40 m span under full CHBDC truck loading

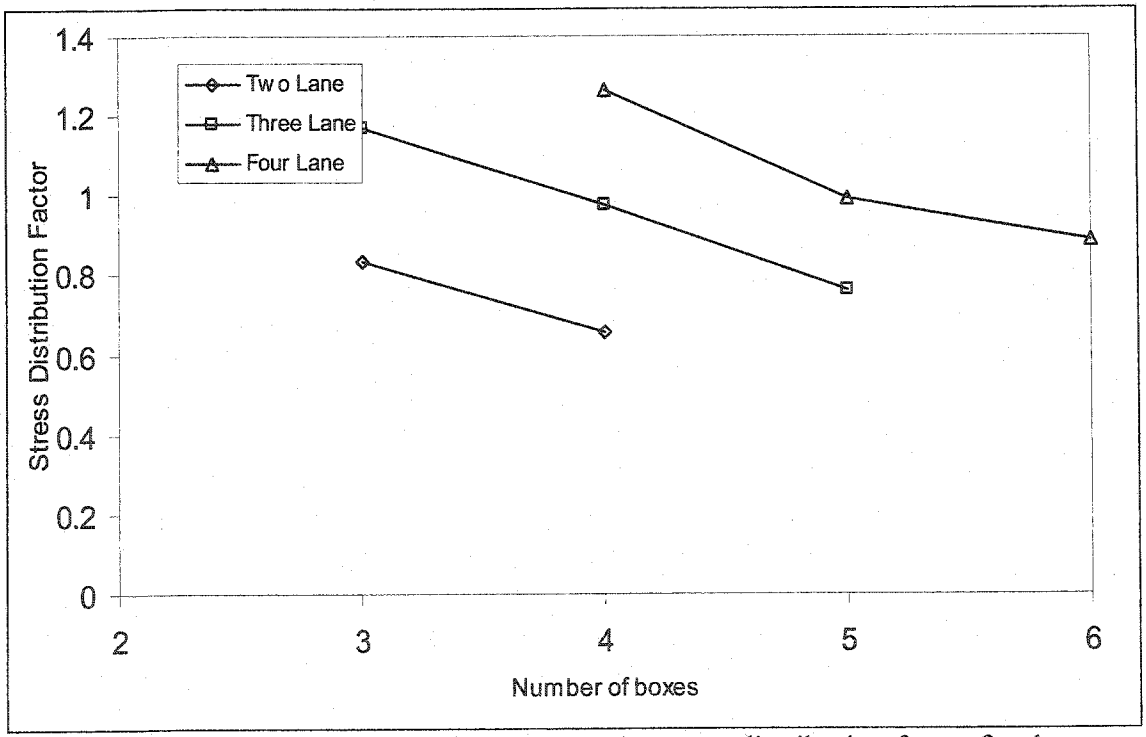

Figure 7.8 Effect of number of traffic lanes on the stress distribution factor for the central box girders of bridges of 100 m span and L/R=1 under full CHBDC truck loading

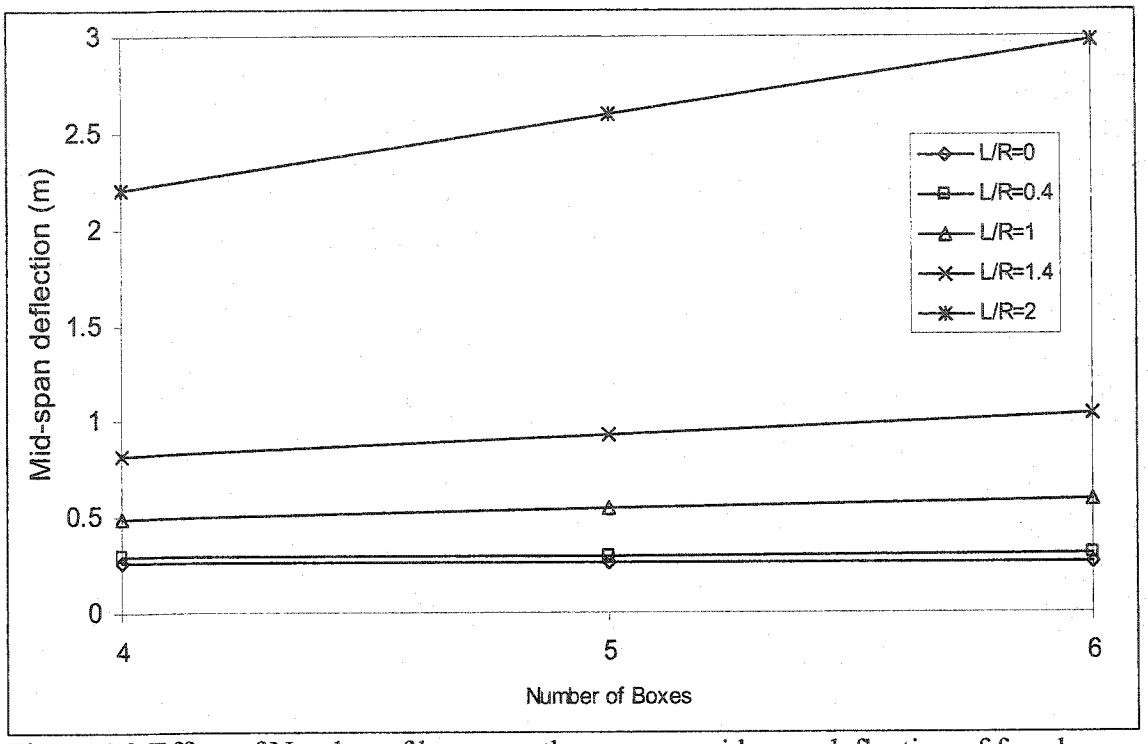

Figure 7.9 Effect of Number of boxes on the average mid-span deflection of four lane bridges of 100 m span under dead load

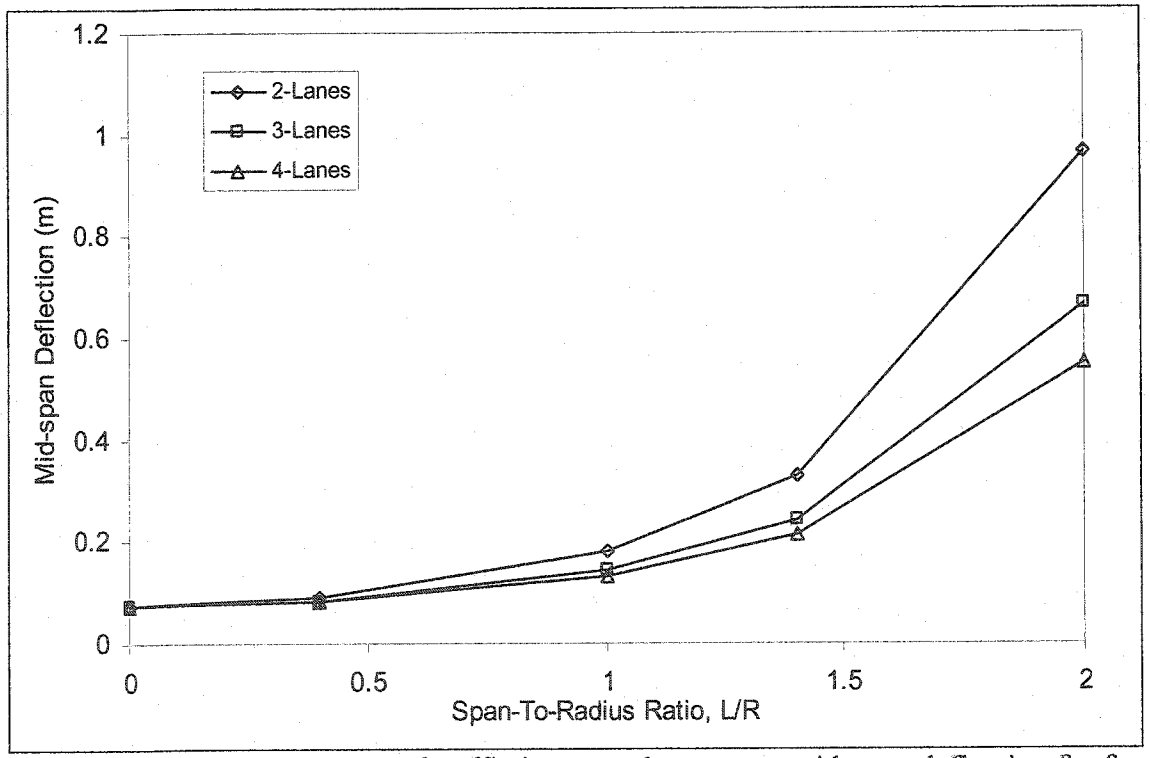

Figure 7.10 Effect of Number of traffic lanes on the average mid-span deflection for four-box girder bridges lane bridges of 80 m span under full CHBDC truck load

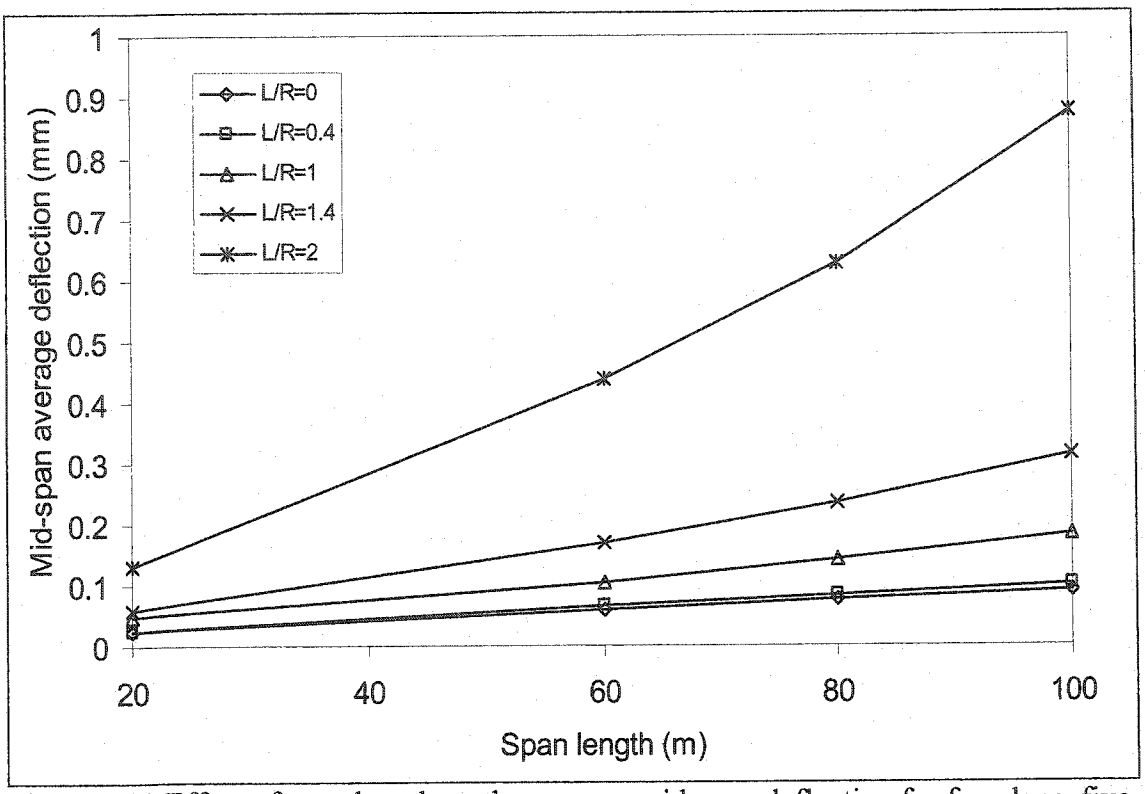

Figure 7.11 Effect of span length on the average mid-span deflection for four-lane, five box girder bridges under full CHBDC truck load

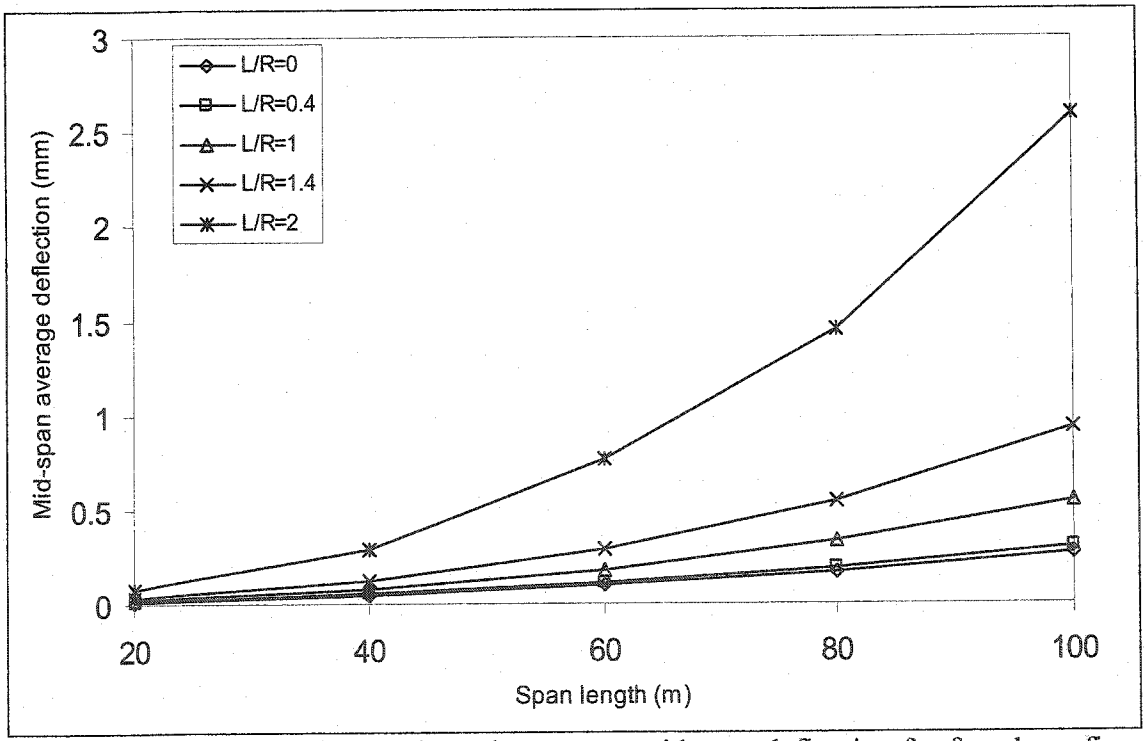

Figure 7.12 Effect of span length on the average mid-span deflection for four-lane, five box girder bridges dead load

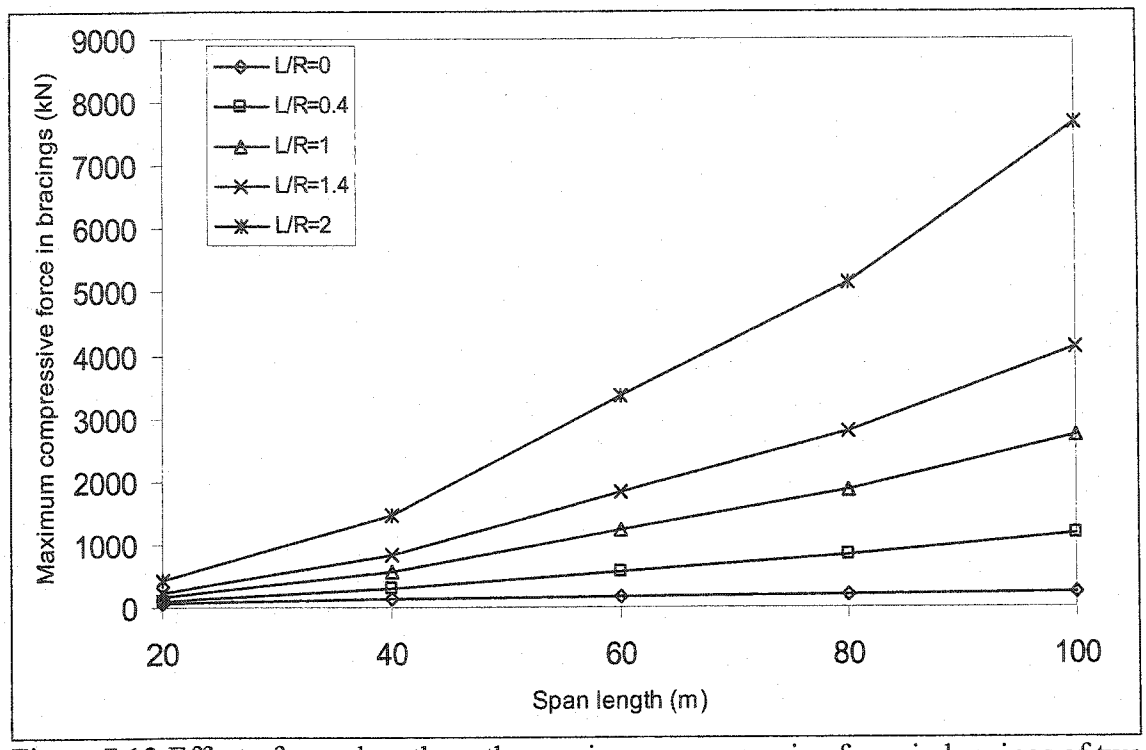

Figure 7.13 Effect of span length on the maximum compressive force in bracings of two-lane, two box girder bridges dead load

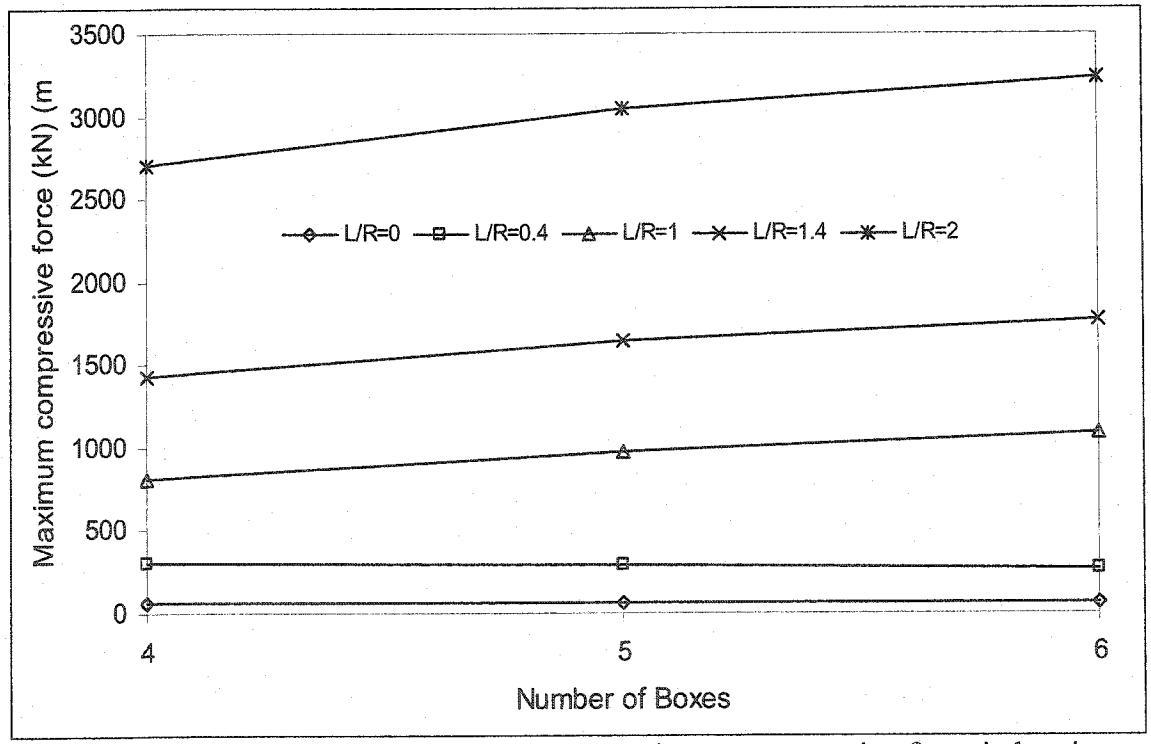

Figure 7.14 Effect of number of boxes on the maximum compressive force in bracings of four-lane bridges of 100 m span under CHBDC truck load

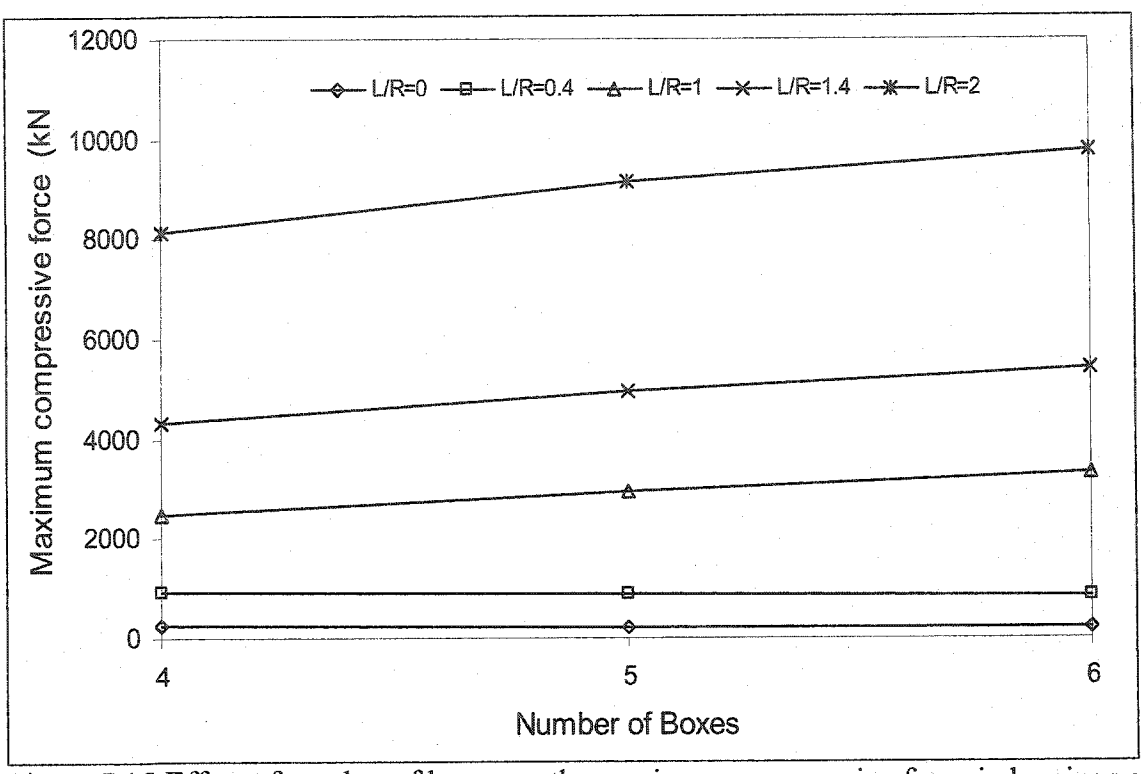

Figure 7.15 Effect of number of boxes on the maximum compressive force in bracings of four-lane bridges of 100 m span under dead load

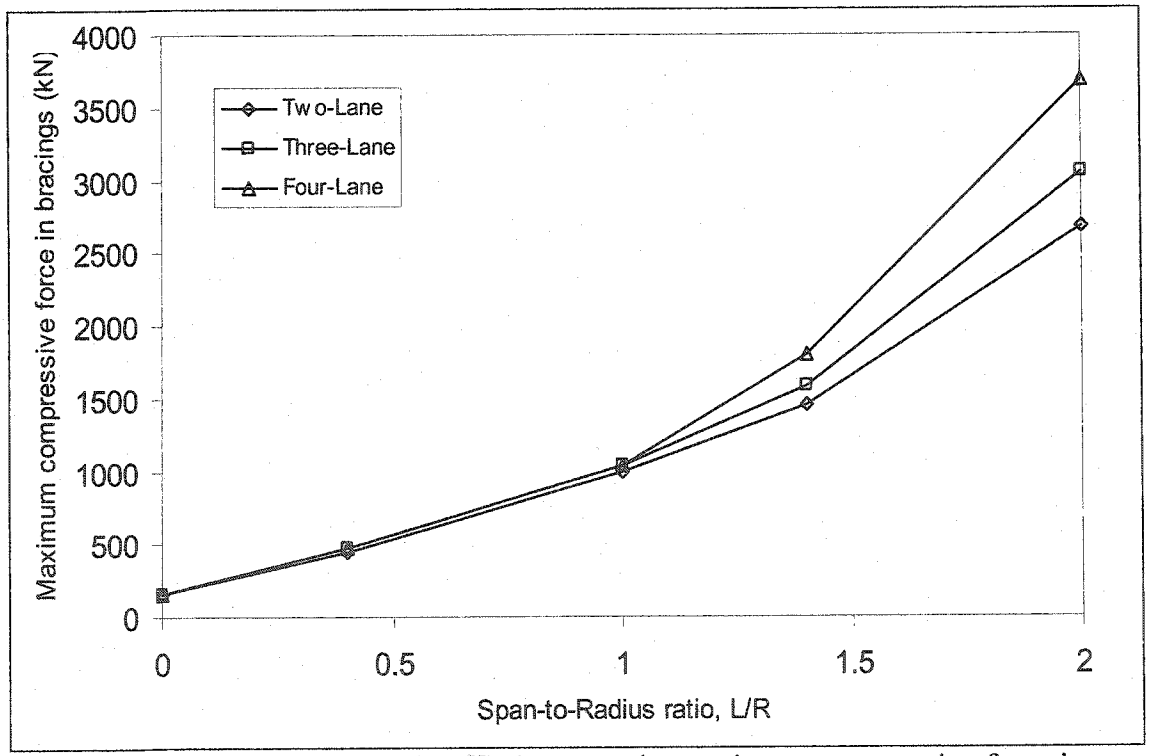

Figure 7.16 Effect of number of traffic lanes on the maximum compressive force in bracings of four-box girder bridges of 60 m span under dead load

APPENDIX

APPENDIX A.1

Stresses and Deflections for all Modeled Bridges Under Dead Load

Table A.1.1 Stresses and deflections under dead load for 2-lane straight bridges

Bridge	Span (m)	Curvature	Boxes	Lanes		Average Stress and Deflections Due to Dead Load						Max Axial Force in Bracing (N)
	L	L/R	Nb	NL		B1 (inner)	B2	B3	B4	B5	B6 (outer)	
2L2b100m	100	0	2	2	σ_{Finite}	133.796	133.796	0.000	0.000	0.000	0.000	247350
					Δ_{Finite}	-0.268	-0.268	0	0.000	0.000	0.000	
2L2b80m	80	0	2	2	σ_{Finite}	114.610	114.610	0.000	0.000	0.000	0.000	213210
					Δ_{Finite}	-0.176	-0.176	0.000	0.000	0.000	0.000	
2L2b60m	60	0	2	2	σ_{Finite}	92.315	92.291	0.000	0.000	0.000	0.000	174810
					Δ_{Finite}	-0.103	-0.103	0.000	0.000	0.000	0.000	
2L2b40m	40	0	2	2	σ_{Finite}	71.779	71.779	0.000	0.000	0.000	0.000	124860
					Δ_{Finite}	-0.050	-0.050	0.000	0.000	0.000	0.000	
2L2b20m	20	0	2	2	σ_{Finite}	37.656	37.656	0.000	0.000	0.000	0.000	58110
					Δ_{Finite}	-0.013	-0.013	0.000	0.000	0.000	0.000	
2L3b100m	100	0	3	2	σ_{Finite}	133.890	133.818	133.890	0.000	0.000	0.000	239610
					Δ_{Finite}	-0.268	-0.268	-0.268	0.000	0.000	0.000	
2L3b80m	80	0	3	2	σ_{Finite}	117.134	117.000	117.134	0.000	0.000	0.000	205570
					Δ_{Finite}	-0.178	-0.178	-0.178	0.000	0.000	0.000	
2L3b60m	60	0	3	2	σ_{Finite}	0.000	0.000	0.000	0.000	0.000	0.000	0
					Δ_{Finite}	0	0.000	0.000	0.000	0.000	0.000	
2L3b40m	40	0	3	2	σ_{Finite}	72.539	72.200	72.539	0.000	0.000	0.000	120990
					Δ_{Finite}	-0.049	-0.049	-0.049	0.000	0.000	0.000	
2L3b20m	20	0	3	2	σ_{Finite}	38.913	38.517	38.913	0.000	0.000	0.000	60159
					Δ_{Finite}	-0.013	-0.013	-0.013	0.000	0.000	0.000	
2L4b100m	100	0	4	2	σ_{Finite}	134.140	134.070	134.070	134.140	0.000	0.000	230150
					Δ_{Finite}	-0.267	-0.267	-0.267	-0.267	0.000	0.000	
2L4b80m	80	0	4	2	σ_{Finite}	117.502	117.370	117.370	117.502	0.000	0.000	193480
					Δ_{Finite}	-0.178	-0.178	-0.178	-0.178	0.000	0.000	
2L4b60m	60	0	4	2	σ_{Finite}	96.623	96.213	96.278	96.193	0.000	0.000	152050
					Δ_{Finite}	-0.105	-0.105	-0.105	-0.105	0.000	0.000	
2L4b40m	40	0	4	2	σ_{Finite}	72.472	72.052	72.052	72.472	0.000	0.000	109690
					Δ_{Finite}	-0.049	-0.049	-0.049	-0.049	0.000	0.000	
2L4b20m	20	0	4	2	σ_{Finite}	40.746	40.192	40.192	40.746	0.000	0.000	52694
					Δ_{Finite}	-0.013	-0.012	-0.012	-0.013	0.000	0.000	
Note: All stresses are in MPa, all deflections are in meters												

Table A.1.2 Stresses and deflections under dead load for 3-lane straight bridges

Bridge	Span (m)	Curvature	Boxes	Lanes		Average Stress and Deflections Due to Dead Load						Max Axial Force in Bracing (N)
	L	L/R	Nb	NL		B1 (inner)	B2	B3	B4	B5	B6 (outer)	
3L3b100m	100	0	3	3	σ_{Finite}	129.176	128.876	129.176	0.000	0.000	0.000	235570
					Δ_{Finite}	-0.263	-0.262	-0.263	0.000	0.000	0.000	
3L3b80m	80	0	3	3	σ_{Finite}	111.052	110.664	111.052	0.000	0.000	0.000	199930
					Δ_{Finite}	-0.173	-0.172	-0.173	0.000	0.000	0.000	
3L3b60m	60	0	3	3	σ_{Finite}	88.557	88.016	88.540	0.000	0.000	0.000	160750
					Δ_{Finite}	-0.099	-0.099	-0.100	0.000	0.000	0.000	
3L3b40m	40	0	3	3	σ_{Finite}	67.496	66.897	67.496	0.000	0.000	0.000	112780
					Δ_{Finite}	-0.048	-0.047	-0.048	0.000	0.000	0.000	
3L3b20m	20	0	3	3	σ_{Finite}	34.738	34.157	34.738	0.000	0.000	0.000	52587
					Δ_{Finite}	-0.012	-0.012	-0.012	0.000	0.000	0.000	
3L4b100m	100	0	4	3	σ_{Finite}	129.236	128.928	128.928	129.236	0.000	0.000	234200
					Δ_{Finite}	-0.262	-0.262	-0.262	-0.262	0.000	0.000	
3L4b80m	80	0	4	3	σ_{Finite}	111.472	111.062	111.062	111.472	0.000	0.000	198010
					Δ_{Finite}	-0.173	-0.172	-0.172	-0.173	0.000	0.000	
3L4b60m	60	0	4	3	σ_{Finite}	89.027	87.981	88.070	88.485	0.000	0.000	158150
					Δ_{Finite}	-0.099	-0.099	-0.099	-0.099	0.000	0.000	
3L4b40m	40	0	4	3	σ_{Finite}	70.212	69.481	69.481	70.212	0.000	0.000	112520
					Δ_{Finite}	-0.048	-0.048	-0.048	-0.048	0.000	0.000	
3L4b20m	20	0	4	3	σ_{Finite}	37.426	36.658	36.658	37.426	0.000	0.000	56653
					Δ_{Finite}	-0.012	-0.012	-0.012	-0.012	0.000	0.000	
3L5b100m	100	0	5	3	σ_{Finite}	127.612	127.332	127.196	127.332	127.612	0.000	229170
					Δ_{Finite}	-0.260	-0.260	-0.260	-0.260	-0.260	0.000	
3L5b80m	80	0	5	3	σ_{Finite}	109.982	109.602	109.442	109.602	109.982	0.000	194910
					Δ_{Finite}	-0.171	-0.170	-0.170	-0.170	-0.171	0.000	
3L5b60m	60	0	5	3	σ_{Finite}	90.187	89.625	89.390	89.627	90.152	0.000	160350
					Δ_{Finite}	-0.100	-0.099	-0.099	-0.099	-0.100	0.000	
3L5b40m	40	0	5	3	σ_{Finite}	71.912	71.144	70.887	71.144	71.912	0.000	103610
					Δ_{Finite}	-0.049	-0.049	-0.048	-0.049	-0.049	0.000	
3L5b20m	20	0	5	3	σ_{Finite}	37.656	36.817	36.543	36.817	37.656	0.000	54691
					Δ_{Finite}	-0.012	-0.012	-0.012	-0.012	-0.012	0.000	
Note: All stresses are in Mpa, all deflections are in meters												

Table A.1.3 Stresses and deflections under dead load for 4-lane straight bridges

Bridge	Span (m)	Curvature	Boxes	Lanes		Average Stress and Deflections Due to Dead Load						Max Axial Force in Bracing (N)
	L	L/R	Nb	NL		B1 (inner)	B2	B3	B4	B5	B6 (outer)	
4L4b100m	100	0	4	4	σ_{Finite}	126.552	125.968	125.968	126.552	0.000	0.000	231590
					Δ_{Finite}	-0.259	-0.259	-0.259	-0.259	0.000	0.000	
4L4b80m	80	0	4	4	σ_{Finite}	107.962	107.252	107.252	107.962	0.000	0.000	197680
					Δ_{Finite}	-0.170	-0.169	-0.169	-0.170	0.000	0.000	
4L4b60m	60	0	4	4	σ_{Finite}	87.515	85.918	86.001	86.845	0.000	0.000	160750
					Δ_{Finite}	-0.098	-0.098	-0.098	-0.098	0.000	0.000	
4L4b40m	40	0	4	4	σ_{Finite}	65.842	64.823	64.823	65.842	0.000	0.000	111430
					Δ_{Finite}	-0.047	-0.046	-0.046	-0.047	0.000	0.000	
4L4b20m	20	0	4	4	σ_{Finite}	33.682	32.820	32.820	33.682	0.000	0.000	48869
					Δ_{Finite}	-0.012	-0.012	-0.012	-0.012	0.000	0.000	
4L5b100m	100	0	5	4	σ_{Finite}	128.120	127.578	127.372	127.578	128.120	0.000	229750
					Δ_{Finite}	-0.261	-0.260	-0.260	-0.260	-0.261	0.000	
4L5b80m	80	0	5	4	σ_{Finite}	110.012	109.232	108.924	109.232	110.012	0.000	189870
					Δ_{Finite}	-0.171	-0.171	-0.170	-0.171	-0.171	0.000	
4L5b60m	60	0	5	4	σ_{Finite}	86.115	85.178	84.886	85.181	86.095	0.000	157350
					Δ_{Finite}	-0.097	-0.096	-0.096	-0.096	-0.097	0.000	
4L5b40m	40	0	5	4	σ_{Finite}	64.812	63.768	63.444	63.768	64.812	0.000	115230
					Δ_{Finite}	-0.046	-0.045	-0.045	-0.045	-0.046	0.000	
4L5b20m	20	0	5	4	σ_{Finite}	34.325	33.369	33.104	33.369	34.325	0.000	52515
					Δ_{Finite}	-0.012	-0.011	-0.011	-0.011	-0.012	0.000	
4L6b100m	100	0	6	4	σ_{Finite}	127.904	127.410	127.108	127.108	127.410	127.904	225790
					Δ_{Finite}	-0.261	-0.261	-0.260	-0.260	-0.261	-0.261	
4L6b80m	80	0	6	4	σ_{Finite}	110.356	109.724	109.368	109.368	109.724	110.356	186920
					Δ_{Finite}	-0.171	-0.171	-0.170	-0.170	-0.171	-0.171	
4L6b60m	60	0	6	4	σ_{Finite}	87.191	86.302	85.864	85.865	86.305	87.168	153530
					Δ_{Finite}	-0.097	-0.097	-0.097	-0.097	-0.097	-0.097	
4L6b40m	40	0	6	4	σ_{Finite}	58.938	57.969	57.529	57.529	57.969	58.938	108600
					Δ_{Finite}	-0.042	-0.042	-0.042	-0.042	-0.042	-0.042	
4L5620m	20	0	6	4	σ_{Finite}	34.487	33.523	33.133	33.133	33.523	34.487	53488
					Δ_{Finite}	-0.011	-0.011	-0.011	-0.011	-0.011	-0.011	
Note: All stresses are in Mpa, all deflections are in meters												

Table A.1.4 Stresses and deflections under dead load for 2-lane bridges having curvatures of L/R=0.4

Bridge	Span (m)	Curvature	Boxes	Lanes		Average Stress and Deflections Due to Dead Load						Max Axial Force in Bracing (N)
	L	L/R	Nb	NL		B1 (inner)	B2	B3	B4	B5	B6 (outer)	
2L2b100m	100	0.4	2	2	σ_{Finite}	135.110	141.672	0.000	0.000	0.000	0.000	1153100
					Δ_{Finite}	-0.287	-0.316	0	0.000	0.000	0.000	
2L2b80m	80	0.4	2	2	σ_{Finite}	115.730	121.244	0.000	0.000	0.000	0.000	819700
					Δ_{Finite}	-0.186	-0.206	0.000	0.000	0.000	0.000	
2L2b60m	60	0.4	2	2	σ_{Finite}	91.671	98.664	0.000	0.000	0.000	0.000	564980
					Δ_{Finite}	-0.106	-0.119	0.000	0.000	0.000	0.000	
2L2b40m	40	0.4	2	2	σ_{Finite}	72.145	75.542	0.000	0.000	0.000	0.000	289620
					Δ_{Finite}	-0.050	-0.058	0.000	0.000	0.000	0.000	
2L2b20m	20	0.4	2	2	σ_{Finite}	37.418	39.931	0.000	0.000	0.000	0.000	104190
					Δ_{Finite}	-0.012	-0.016	0.000	0.000	0.000	0.000	
2L3b100m	100	0.4	3	2	σ_{Finite}	131.664	139.894	147.658	0.000	0.000	0.000	1118100
					Δ_{Finite}	-0.287	-0.316	-0.345	0.000	0.000	0.000	
2L3b80m	80	0.4	3	2	σ_{Finite}	115.154	122.380	129.262	0.000	0.000	0.000	773190
					Δ_{Finite}	-0.185	-0.205	-0.225	0.000	0.000	0.000	
2L3b60m	60	0.4	3	2	σ_{Finite}	0.000	0.000	0.000	0.000	0.000	0.000	0
					Δ_{Finite}	0	0.000	0.000	0.000	0.000	0.000	
2L3b40m	40	0.4	3	2	σ_{Finite}	70.533	74.765	79.061	0.000	0.000	0.000	262430
					Δ_{Finite}	-0.048	-0.054	-0.061	0.000	0.000	0.000	
2L3b20m	20	0.4	3	2	σ_{Finite}	37.483	39.799	42.233	0.000	0.000	0.000	104720
					Δ_{Finite}	-0.011	-0.014	-0.016	0.000	0.000	0.000	
2L4b100m	100	0.4	4	2	σ_{Finite}	126.886	137.570	147.470	157.236	0.000	0.000	1221600
					Δ_{Finite}	-0.287	-0.318	-0.350	-0.382	0.000	0.000	
2L4b80m	80	0.4	4	2	σ_{Finite}	110.930	120.366	128.780	137.418	0.000	0.000	806380
					Δ_{Finite}	-0.184	-0.204	-0.225	-0.246	0.000	0.000	
2L4b60m	60	0.4	4	2	σ_{Finite}	87.271	99.005	104.939	116.058	0.000	0.000	480860
					Δ_{Finite}	-0.105	-0.116	-0.128	-0.140	0.000	0.000	
2L4b40m	40	0.4	4	2	σ_{Finite}	67.713	72.850	77.143	82.204	0.000	0.000	227550
					Δ_{Finite}	-0.046	-0.052	-0.058	-0.064	0.000	0.000	
2L4b20m	20	0.4	4	2	σ_{Finite}	38.410	40.539	42.496	44.910	0.000	0.000	90971
					Δ_{Finite}	-0.011	-0.013	-0.015	-0.017	0.000	0.000	
Note: All stresses are in Mpa, all deflections are in meters												

Table A.1.5 Stresses and deflections under dead load for 3-lane bridges having curvatures of L/R=0.4

Bridge	Span (m)	Curvature	Boxes	Lanes		Average Stress and Deflections Due to Dead Load						Max Axial Force in Bracing (N)
	L	L/R	Nb	NL		B1 (inner)	B2	B3	B4	B5	B6 (outer)	
3L3b100m	100	0.4	3	3	σ_{Finite}	127.442	133.264	138.988	0.000	0.000	0.000	1035400
					Δ_{Finite}	-0.269	-0.295	-0.322	0.000	0.000	0.000	
3L3b80m	80	0.4	3	3	σ_{Finite}	0.000	0.000	0.000	0.000	0.000	0.000	0
					Δ_{Finite}	0	0.000	0.000	0.000	0.000	0.000	
3L3b60m	60	0.4	3	3	σ_{Finite}	85.760	90.846	96.498	0.000	0.000	0.000	505670
					Δ_{Finite}	-0.098	-0.109	-0.122	0.000	0.000	0.000	
3L3b40m	40	0.4	3	3	σ_{Finite}	66.169	69.053	72.425	0.000	0.000	0.000	261950
					Δ_{Finite}	-0.045	-0.051	-0.059	0.000	0.000	0.000	
3L3b20m	20	0.4	3	3	σ_{Finite}	32.940	35.532	38.330	0.000	0.000	0.000	101930
					Δ_{Finite}	-0.010	-0.013	-0.016	0.000	0.000	0.000	
3L4b100m	100	0.4	4	3	σ_{Finite}	123.412	130.724	137.550	144.340	0.000	0.000	979880
					Δ_{Finite}	-0.264	-0.291	-0.317	-0.345	0.000	0.000	
3L4b80m	80	0.4	4	3	σ_{Finite}	106.498	112.662	118.444	124.330	0.000	0.000	686790
					Δ_{Finite}	-0.169	-0.187	-0.205	-0.223	0.000	0.000	
3L4b60m	60	0.4	4	3	σ_{Finite}	82.482	89.696	94.221	101.790	0.000	0.000	474900
					Δ_{Finite}	-0.095	-0.106	-0.116	-0.128	0.000	0.000	
3L4b40m	40	0.4	4	3	σ_{Finite}	66.827	70.218	73.675	77.498	0.000	0.000	247270
					Δ_{Finite}	-0.044	-0.050	-0.056	-0.062	0.000	0.000	
3L4b20m	20	0.4	4	3	σ_{Finite}	34.574	36.876	39.377	41.994	0.000	0.000	104340
					Δ_{Finite}	-0.010	-0.012	-0.015	-0.017	0.000	0.000	
3L5b100m	100	0.4	5	3	σ_{Finite}	116.774	125.452	133.540	141.376	149.132	0.000	921460
					Δ_{Finite}	-0.258	-0.285	-0.312	-0.339	-0.367	0.000	
3L5b80m	80	0.4	5	3	σ_{Finite}	100.498	108.064	114.976	121.702	128.586	0.000	627700
					Δ_{Finite}	-0.164	-0.181	-0.199	-0.217	-0.236	0.000	
3L5b60m	60	0.4	5	3	σ_{Finite}	78.926	88.124	93.665	99.222	108.346	0.000	434620
					Δ_{Finite}	-0.093	-0.103	-0.114	-0.125	-0.136	0.000	
3L5b40m	40	0.4	5	3	σ_{Finite}	66.676	70.356	73.748	77.226	81.315	0.000	222810
					Δ_{Finite}	-0.043	-0.048	-0.054	-0.059	-0.065	0.000	
3L5b20m	20	0.4	5	3	σ_{Finite}	34.178	36.110	38.113	40.216	42.680	0.000	99969
					Δ_{Finite}	-0.009	-0.011	-0.013	-0.015	-0.017	0.000	
Note: All stresses are in Mpa, all deflections are in meters												

Table A.1.6 Stresses and deflections under dead load for 4-lane bridges having curvatures of L/R=0.4

Bridge	Span (m)	Curvature	Boxes	Lanes		Average Stress and Deflections Due to Dead Load						Max Axial Force in Bracing (N)
	L	L/R	Nb	NL		B1 (inner)	B2	B3	B4	B5	B6 (outer)	
4L4b100m	100	0.4	4	4	σ_{Finite}	121.834	127.496	132.946	138.544	0.000	0.000	941010
					Δ_{Finite}	-0.253	-0.278	-0.304	-0.330	0.000	0.000	
4L4b80m	80	0.4	4	4	σ_{Finite}	104.046	108.614	113.236	118.080	0.000	0.000	673780
					Δ_{Finite}	-0.162	-0.179	-0.196	-0.215	0.000	0.000	
4L4b60m	60	0.4	4	4	σ_{Finite}	82.505	87.453	91.453	97.205	0.000	0.000	479800
					Δ_{Finite}	-0.092	-0.102	-0.114	-0.125	0.000	0.000	
4L4b40m	40	0.4	4	4	σ_{Finite}	62.968	65.492	68.580	71.960	0.000	0.000	253310
					Δ_{Finite}	-0.041	-0.047	-0.054	-0.061	0.000	0.000	
4L4b20m	20	0.4	4	4	σ_{Finite}	30.203	32.875	35.861	38.792	0.000	0.000	103620
					Δ_{Finite}	-0.009	-0.011	-0.014	-0.018	0.000	0.000	
4L5b100m	100	0.4	5	4	σ_{Finite}	119.326	126.148	132.568	138.880	145.206	0.000	895590
					Δ_{Finite}	-0.250	-0.274	-0.299	-0.324	-0.350	0.000	
4L5b80m	80	0.4	5	4	σ_{Finite}	102.646	108.142	113.410	118.674	124.088	0.000	636670
					Δ_{Finite}	-0.160	-0.176	-0.192	-0.209	-0.227	0.000	
4L5b60m	60	0.4	5	4	σ_{Finite}	77.975	83.887	88.134	92.469	99.146	0.000	458730
					Δ_{Finite}	-0.088	-0.098	-0.108	-0.118	-0.129	0.000	
4L5b40m	40	0.4	5	4	σ_{Finite}	59.908	62.787	65.873	69.127	72.779	0.000	250790
					Δ_{Finite}	-0.039	-0.044	-0.050	-0.056	-0.062	0.000	
4L5b20m	20	0.4	5	4	σ_{Finite}	30.440	32.447	34.748	37.129	39.662	0.000	105730
					Δ_{Finite}	-0.008	-0.010	-0.012	-0.015	-0.018	0.000	
4L6b100m	100	0.4	6	4	σ_{Finite}	114.750	122.390	129.542	136.530	143.358	150.180	835510
					Δ_{Finite}	-0.245	-0.269	-0.293	-0.318	-0.343	-0.369	
4L6b80m	80	0.4	6	4	σ_{Finite}	98.708	104.906	111.236	117.620	123.718	129.290	565830
					Δ_{Finite}	-0.156	-0.172	-0.188	-0.205	-0.223	-0.241	
4L6b60m	60	0.4	6	4	σ_{Finite}	75.622	82.768	87.172	91.893	96.379	104.077	430400
					Δ_{Finite}	-0.086	-0.095	-0.105	-0.114	-0.125	-0.135	
4L6b40m	40	0.4	6	4	σ_{Finite}	52.813	55.536	58.214	61.021	63.908	67.367	240540
					Δ_{Finite}	-0.035	-0.039	-0.044	-0.048	-0.054	-0.059	
4L5620m	20	0.4	6	4	σ_{Finite}	30.232	31.898	33.755	35.709	37.721	40.095	103670
					Δ_{Finite}	-0.008	-0.009	-0.011	-0.013	-0.015	-0.018	
Note: All stresses are in Mpa, all deflections are in meters												

Table A.1.7 Stresses and deflections under dead load for 2-lane bridges having curvatures of L/R=1.0

Bridge	Span (m) L	Curvature L/R	Boxes Nb	Lanes NL		Average Stress and Deflections Due to Dead Load						Max Axial Force in Bracing (N)
						B1 (inner)	B2	B3	B4	B5	B6 (outer)	
2L2b100m	100	1.0	2	2	σ_{Finite}	153.680	169.392	0.000	0.000	0.000	0.000	2724200
					Δ_{Finite}	-0.467	-0.555	0	0.000	0.000	0.000	
2L2b80m	80	1.0	2	2	σ_{Finite}	131.458	144.470	0.000	0.000	0.000	0.000	1869600
					Δ_{Finite}	-0.286	-0.347	0.000	0.000	0.000	0.000	
2L2b60m	60	1.0	2	2	σ_{Finite}	100.879	118.646	0.000	0.000	0.000	0.000	1238800
					Δ_{Finite}	-0.158	-0.197	0.000	0.000	0.000	0.000	
2L2b40m	40	1.0	2	2	σ_{Finite}	81.062	88.282	0.000	0.000	0.000	0.000	573670
					Δ_{Finite}	-0.068	-0.091	0.000	0.000	0.000	0.000	
2L2b20m	20	1.0	2	2	σ_{Finite}	42.180	46.444	0.000	0.000	0.000	0.000	181240
					Δ_{Finite}	-0.015	-0.025	0.000	0.000	0.000	0.000	
2L3b100m	100	1.0	3	2	σ_{Finite}	144.824	167.030	185.372	0.000	0.000	0.000	3573600
					Δ_{Finite}	-0.525	-0.612	-0.700	0.000	0.000	0.000	
2L3b80m	80	1.0	3	2	σ_{Finite}	126.500	146.170	162.068	0.000	0.000	0.000	2295800
					Δ_{Finite}	-0.312	-0.370	-0.430	0.000	0.000	0.000	
2L3b60m	60	1.0	3	2	σ_{Finite}	93.164	117.318	138.360	0.000	0.000	0.000	1406000
					Δ_{Finite}	-0.166	-0.202	-0.239	0.000	0.000	0.000	
2L3b40m	40	1.0	3	2	σ_{Finite}	75.863	87.468	95.820	0.000	0.000	0.000	637350
					Δ_{Finite}	-0.066	-0.084	-0.104	0.000	0.000	0.000	
2L3b20m	20	1.0	3	2	σ_{Finite}	40.625	46.661	49.647	0.000	0.000	0.000	201750
					Δ_{Finite}	-0.013	-0.020	-0.027	0.000	0.000	0.000	
2L4b100m	100	1.0	4	2	σ_{Finite}	130.734	158.192	180.460	199.458	0.000	0.000	3423100
					Δ_{Finite}	-0.470	-0.560	-0.651	-0.742	0.000	0.000	
2L4b80m	80	1.0	4	2	σ_{Finite}	112.966	140.160	161.782	182.042	0.000	0.000	2797900
					Δ_{Finite}	-0.342	-0.403	-0.465	-0.527	0.000	0.000	
2L4b60m	60	1.0	4	2	σ_{Finite}	82.663	116.284	130.788	159.260	0.000	0.000	1567500
					Δ_{Finite}	-0.176	-0.210	-0.245	-0.280	0.000	0.000	
2L4b40m	40	1.0	4	2	σ_{Finite}	68.327	83.591	93.430	103.583	0.000	0.000	701730
					Δ_{Finite}	-0.064	-0.081	-0.099	-0.117	0.000	0.000	
2L4b20m	20	1.0	4	2	σ_{Finite}	40.384	47.034	50.237	53.270	0.000	0.000	204860
					Δ_{Finite}	-0.012	-0.017	-0.023	-0.029	0.000	0.000	
Note: All stresses are in Mpa, all deflections are in meters												

Table A.1.8 Stresses and deflections under dead load for 3-lane bridges having curvatures of L/R=1.0

Bridge	Span (m) L	Curvature L/R	Boxes Nb	Lanes NL		Average Stress and Deflections Due to Dead Load						Max Axial Force in Bracing (N)
						B1 (inner)	B2	B3	B4	B5	B6 (outer)	
3L3b100m	100	1.0	3	3	σ_{Finite}	139.804	155.924	168.154	0.000	0.000	0.000	2518500
					Δ_{Finite}	-0.420	-0.500	-0.581	0.000	0.000	0.000	
3L3b80m	80	1.0	3	3	σ_{Finite}	120.636	134.136	144.120	0.000	0.000	0.000	1653800
					Δ_{Finite}	-0.254	-0.309	-0.366	0.000	0.000	0.000	
3L3b60m	60	1.0	3	3	σ_{Finite}	91.235	105.585	117.675	0.000	0.000	0.000	1100000
					Δ_{Finite}	-0.137	-0.172	-0.208	0.000	0.000	0.000	
3L3b40m	40	1.0	3	3	σ_{Finite}	72.495	80.520	85.437	0.000	0.000	0.000	519150
					Δ_{Finite}	-0.056	-0.076	-0.098	0.000	0.000	0.000	
3L3b20m	20	1.0	3	3	σ_{Finite}	36.389	42.830	45.381	0.000	0.000	0.000	189550
					Δ_{Finite}	-0.011	-0.019	-0.029	0.000	0.000	0.000	
3L4b100m	100	1.0	4	3	σ_{Finite}	128.930	150.538	167.652	182.308	0.000	0.000	3163300
					Δ_{Finite}	-0.445	-0.525	-0.604	-0.685	0.000	0.000	
3L4b80m	80	1.0	4	3	σ_{Finite}	111.520	130.000	144.146	156.238	0.000	0.000	2071500
					Δ_{Finite}	-0.262	-0.314	-0.368	-0.422	0.000	0.000	
3L4b60m	60	1.0	4	3	σ_{Finite}	82.414	103.872	114.210	131.510	0.000	0.000	1290200
					Δ_{Finite}	-0.138	-0.170	-0.202	-0.235	0.000	0.000	
3L4b40m	40	1.0	4	3	σ_{Finite}	70.304	81.031	88.097	93.925	0.000	0.000	606600
					Δ_{Finite}	-0.055	-0.072	-0.090	-0.109	0.000	0.000	
3L4b20m	20	1.0	4	3	σ_{Finite}	36.860	44.103	47.716	49.929	0.000	0.000	213180
					Δ_{Finite}	-0.010	-0.016	-0.024	-0.032	0.000	0.000	
3L5b100m	100	1.0	5	3	σ_{Finite}	112.666	139.096	161.100	179.982	197.024	0.000	3792400
					Δ_{Finite}	-0.472	-0.552	-0.633	-0.714	-0.797	0.000	
3L5b80m	80	1.0	5	3	σ_{Finite}	96.574	120.006	138.654	154.332	168.930	0.000	2443500
					Δ_{Finite}	-0.269	-0.322	-0.375	-0.429	-0.484	0.000	
3L5b60m	60	1.0	5	3	σ_{Finite}	69.080	97.365	111.981	124.142	145.442	0.000	1490700
					Δ_{Finite}	-0.140	-0.171	-0.203	-0.236	-0.270	0.000	
3L5b40m	40	1.0	5	3	σ_{Finite}	67.485	79.745	87.994	94.184	100.901	0.000	638360
					Δ_{Finite}	-0.054	-0.069	-0.085	-0.101	-0.118	0.000	
3L5b20m	20	1.0	5	3	σ_{Finite}	35.472	42.505	46.298	48.406	50.833	0.000	212320
					Δ_{Finite}	-0.009	-0.014	-0.020	-0.026	-0.033	0.000	
Note: All stresses are in Mpa, all deflections are in meters												

Table A.1.9 Stresses and deflections under dead load for 4-lane bridges having curvatures of L/R=1.0

Bridge	Span (m)	Curvature	Boxes	Lanes		Average Stress and Deflections Due to Dead Load						Max Axial Force in Bracing (N)
	L	L/R	Nb	NL		B1 (inner)	B2	B3	B4	B5	B6 (outer)	
4L4b100m	100	1.0	4	4	σ_{Finite}	128.408	145.900	159.022	169.764	0.000	0.000	2464800
					Δ_{Finite}	-0.380	-0.455	-0.531	-0.608	0.000	0.000	
4L4b80m	80	1.0	4	4	σ_{Finite}	110.280	124.730	135.388	143.916	0.000	0.000	1643600
					Δ_{Finite}	-0.226	-0.277	-0.330	-0.383	0.000	0.000	
4L4b60m	60	1.0	4	4	σ_{Finite}	85.210	101.190	109.694	120.895	0.000	0.000	1087400
					Δ_{Finite}	-0.123	-0.155	-0.188	-0.223	0.000	0.000	
4L4b40m	40	1.0	4	4	σ_{Finite}	73.209	78.974	82.946	69.925	0.000	0.000	551770
					Δ_{Finite}	-0.066	-0.080	-0.100	-0.117	0.000	0.000	
4L4b20m	20	1.0	4	4	σ_{Finite}	37.397	42.603	46.770	40.540	0.000	0.000	226200
					Δ_{Finite}	-0.010	-0.017	-0.027	-0.037	0.000	0.000	
4L5b100m	100	1.0	5	4	σ_{Finite}	119.198	140.946	158.214	172.512	184.974	0.000	2935800
					Δ_{Finite}	-0.393	-0.466	-0.541	-0.616	-0.693	0.000	
4L5b80m	80	1.0	5	4	σ_{Finite}	103.512	121.524	135.414	146.680	156.602	0.000	1938800
					Δ_{Finite}	-0.229	-0.278	-0.327	-0.378	-0.430	0.000	
4L5b60m	60	1.0	5	4	σ_{Finite}	74.298	93.423	104.362	112.765	126.531	0.000	1252600
					Δ_{Finite}	-0.118	-0.147	-0.178	-0.209	-0.242	0.000	
4L5b40m	40	1.0	5	4	σ_{Finite}	60.796	71.355	78.441	83.446	88.146	0.000	602770
					Δ_{Finite}	-0.044	-0.060	-0.076	-0.094	-0.113	0.000	
4L5b20m	20	1.0	5	4	σ_{Finite}	35.485	43.077	47.040	49.308	51.343	0.000	248000
					Δ_{Finite}	-0.009	-0.015	-0.023	-0.032	-0.043	0.000	
4L6b100m	100	1.0	6	4	σ_{Finite}	106.572	131.410	151.868	169.334	184.404	198.170	3325200
					Δ_{Finite}	-0.404	-0.476	-0.549	-0.623	-0.698	-0.774	
4L6b80m	80	1.0	6	4	σ_{Finite}	94.220	114.824	131.100	144.768	156.360	167.410	2158900
					Δ_{Finite}	-0.231	-0.278	-0.325	-0.373	-0.422	-0.472	
4L6b60m	60	1.0	6	4	σ_{Finite}	65.854	89.095	101.531	112.282	120.559	137.402	1375500
					Δ_{Finite}	-0.118	-0.145	-0.174	-0.203	-0.233	-0.264	
4L6b40m	40	1.0	6	4	σ_{Finite}	50.599	61.028	68.097	73.367	77.453	82.374	632030
					Δ_{Finite}	-0.039	-0.052	-0.065	-0.080	-0.095	-0.111	
4L5620m	20	1.0	6	4	σ_{Finite}	36.068	42.806	46.325	48.460	49.758	51.980	237620
					Δ_{Finite}	-0.008	-0.013	-0.019	-0.026	-0.034	-0.043	
Note: All stresses are in Mpa, all deflections are in meters												

Table A.1.10 Stresses and deflections under dead load for 2-lane bridges having curvatures of L/R=1.4

Bridge	Span (m)	Curvature	Boxes	Lanes		Average Stress and Deflections Due to Dead Load						Max Axial Force in Bracing (N)
	L	L/R	Nb	NL		B1 (inner)	B2	B3	B4	B5	B6 (outer)	
2L2b100m	100	1.4	2	2	σ_{Finite}	178.590	200.308	0.000	0.000	0.000	0.000	4126300
					Δ_{Finite}	-0.772	-0.926	0	0.000	0.000	0.000	
2L2b80m	80	1.4	2	2	σ_{Finite}	152.602	170.342	0.000	0.000	0.000	0.000	2804300
					Δ_{Finite}	-0.456	-0.563	0.000	0.000	0.000	0.000	
2L2b60m	60	1.4	2	2	σ_{Finite}	114.648	140.726	0.000	0.000	0.000	0.000	1838100
					Δ_{Finite}	-0.247	-0.316	0.000	0.000	0.000	0.000	
2L2b40m	40	1.4	2	2	σ_{Finite}	93.977	102.540	0.000	0.000	0.000	0.000	825820
					Δ_{Finite}	-0.099	-0.140	0.000	0.000	0.000	0.000	
2L2b20m	20	1.4	2	2	σ_{Finite}	50.079	53.271	0.000	0.000	0.000	0.000	249020
					Δ_{Finite}	-0.021	-0.038	0.000	0.000	0.000	0.000	
2L3b100m	100	1.4	3	2	σ_{Finite}	163.824	197.600	222.970	0.000	0.000	0.000	5489400
					Δ_{Finite}	-0.937	-1.090	-1.245	0.000	0.000	0.000	
2L3b80m	80	1.4	3	2	σ_{Finite}	142.862	172.862	194.534	0.000	0.000	0.000	3470700
					Δ_{Finite}	-0.532	-0.635	-0.739	0.000	0.000	0.000	
2L3b60m	60	1.4	3	2	σ_{Finite}	100.323	137.973	168.426	0.000	0.000	0.000	2068200
					Δ_{Finite}	-0.273	-0.337	0.000	0.000	0.000	0.000	
2L3b40m	40	1.4	3	2	σ_{Finite}	85.705	102.818	112.559	0.000	0.000	0.000	929110
					Δ_{Finite}	-0.099	-0.132	-0.166	0.000	0.000	0.000	
2L3b20m	20	1.4	3	2	σ_{Finite}	47.669	55.258	56.673	0.000	0.000	0.000	283730
					Δ_{Finite}	-0.018	-0.030	-0.043	0.000	0.000	0.000	
2L4b100m	100	1.4	4	2	σ_{Finite}	138.060	186.118	224.156	256.860	0.000	0.000	6511800
					Δ_{Finite}	-1.152	-1.316	-1.481	-1.647	0.000	0.000	
2L4b80m	80	1.4	4	2	σ_{Finite}	119.666	162.904	194.490	222.472	0.000	0.000	3942400
					Δ_{Finite}	-0.625	-0.732	-0.840	-0.948	0.000	0.000	
2L4b60m	60	1.4	4	2	σ_{Finite}	82.910	136.365	156.960	198.832	0.000	0.000	2228900
					Δ_{Finite}	-0.305	-0.365	-0.426	-0.488	0.000	0.000	
2L4b40m	40	1.4	4	2	σ_{Finite}	73.803	97.868	110.661	123.183	0.000	0.000	998070
					Δ_{Finite}	-0.100	-0.130	-0.161	-0.192	0.000	0.000	
2L4b20m	20	1.4	4	2	σ_{Finite}	46.872	56.485	58.712	60.752	0.000	0.000	292850
					Δ_{Finite}	-0.017	-0.026	-0.035	-0.046	0.000	0.000	
Note: All stresses are in Mpa, all deflections are in meters												

Table A.1.11 Stresses and deflections under dead load for 3-lane bridges having curvatures of L/R=1.4

Bridge	Span (m)	Curvature	Boxes	Lanes		Average Stress and Deflections Due to Dead Load						Max Axial Force in Bracing (N)
	L	L/R	Nb	NL		B1 (inner)	B2	B3	B4	B5	B6 (outer)	
3L3b100m	100	1.4	3	3	σ_{Finite}	159.670	183.876	199.320	0.000	0.000	0.000	4298000
					Δ_{Finite}	-0.690	-0.831	-0.974	0.000	0.000	0.000	
3L3b80m	80	1.4	3	3	σ_{Finite}	138.206	158.270	170.240	0.000	0.000	0.000	2780400
					Δ_{Finite}	-0.401	-0.498	-0.597	0.000	0.000	0.000	
3L3b60m	60	1.4	3	3	σ_{Finite}	102.377	123.954	139.739	0.000	0.000	0.000	1755700
					Δ_{Finite}	-0.211	-0.273	-0.337	0.000	0.000	0.000	
3L3b40m	40	1.4	3	3	σ_{Finite}	84.130	94.989	98.693	0.000	0.000	0.000	832480
					Δ_{Finite}	-0.080	-0.115	-0.153	0.000	0.000	0.000	
3L3b20m	20	1.4	3	3	σ_{Finite}	45.160	51.754	51.292	0.000	0.000	0.000	313090
					Δ_{Finite}	-0.014	-0.029	-0.046	0.000	0.000	0.000	
3L4b100m	100	1.4	4	3	σ_{Finite}	141.902	176.276	200.634	219.558	0.000	0.000	5151700
					Δ_{Finite}	-0.775	-0.914	-1.055	-1.197	0.000	0.000	
3L4b80m	80	1.4	4	3	σ_{Finite}	123.204	152.626	172.224	187.256	0.000	0.000	3339800
					Δ_{Finite}	-0.433	-0.526	-0.620	-0.715	0.000	0.000	
3L4b60m	60	1.4	4	3	σ_{Finite}	88.670	122.432	135.986	159.876	0.000	0.000	2026300
					Δ_{Finite}	-0.221	-0.277	-0.334	-0.393	0.000	0.000	
3L4b40m	40	1.4	4	3	σ_{Finite}	79.726	96.202	103.989	109.288	0.000	0.000	940930
					Δ_{Finite}	-0.079	-0.109	-0.141	-0.174	0.000	0.000	
3L4b20m	20	1.4	4	3	σ_{Finite}	45.366	54.772	56.202	56.095	0.000	0.000	347330
					Δ_{Finite}	-0.013	-0.024	-0.037	-0.052	0.000	0.000	
3L5b100m	100	1.4	5	3	σ_{Finite}	115.828	159.028	192.210	218.500	240.926	0.000	5907300
					Δ_{Finite}	-0.868	-1.010	-1.152	-1.294	-1.438	0.000	
3L5b80m	80	1.4	5	3	σ_{Finite}	99.139	137.612	165.342	186.530	205.280	0.000	3704300
					Δ_{Finite}	-0.471	-0.563	-0.657	-0.751	-0.847	0.000	
3L5b60m	60	1.4	5	3	σ_{Finite}	65.343	111.574	132.850	148.520	178.450	0.000	2244200
					Δ_{Finite}	-0.233	-0.289	-0.345	-0.403	-0.463	0.000	
3L5b40m	40	1.4	5	3	σ_{Finite}	74.753	94.577	105.131	111.228	118.254	0.000	977160
					Δ_{Finite}	-0.079	-0.105	-0.133	-0.162	-0.192	0.000	
3L5b20m	20	1.4	5	3	σ_{Finite}	43.435	53.606	56.139	55.829	56.848	0.000	347730
					Δ_{Finite}	-0.011	-0.020	-0.030	-0.041	-0.053	0.000	
Note: All stresses are in Mpa, all deflections are in meters												

Table A.1.12 Stresses and deflections under dead load for 4-lane bridges having curvatures of L/R=1.4

Bridge	Span (m)	Curvature	Boxes	Lanes		Average Stress and Deflections Due to Dead Load						Max Axial Force in Bracing (N)
	L	L/R	Nb	NL		B1 (inner)	B2	B3	B4	B5	B6 (outer)	
4L4b100m	100	1.4	4	4	σ_{Finite}	143.522	171.342	189.086	201.548	0.000	0.000	4328400
					Δ_{Finite}	-0.619	-0.750	-0.884	-1.020	0.000	0.000	
4L4b80m	80	1.4	4	4	σ_{Finite}	124.190	147.028	160.710	169.814	0.000	0.000	2857100
					Δ_{Finite}	-0.353	-0.442	-0.534	-0.628	0.000	0.000	
4L4b60m	60	1.4	4	4	σ_{Finite}	95.251	120.109	130.134	143.942	0.000	0.000	1863000
					Δ_{Finite}	-0.187	-0.243	-0.303	-0.365	0.000	0.000	
4L4b40m	40	1.4	4	4	σ_{Finite}	78.902	91.492	96.038	97.612	0.000	0.000	947210
					Δ_{Finite}	-0.065	-0.097	-0.132	-0.169	0.000	0.000	
4L4b20m	20	1.4	4	4	σ_{Finite}	43.216	52.145	52.994	52.141	0.000	0.000	408120
					Δ_{Finite}	-0.009	-0.022	-0.038	-0.058	0.000	0.000	
4L5b100m	100	1.4	5	4	σ_{Finite}	127.668	163.558	188.964	207.742	222.748	0.000	4957800
					Δ_{Finite}	-0.669	-0.798	-0.929	-1.061	-1.195	0.000	
4L5b80m	80	1.4	5	4	σ_{Finite}	112.296	142.024	161.848	175.800	187.066	0.000	3255900
					Δ_{Finite}	-0.370	-0.456	-0.542	-0.631	-0.721	0.000	
4L5b60m	60	1.4	5	4	σ_{Finite}	77.714	109.001	124.120	133.506	151.586	0.000	2049500
					Δ_{Finite}	-0.184	-0.235	-0.289	-0.345	-0.402	0.000	
4L5b40m	40	1.4	5	4	σ_{Finite}	68.983	85.907	93.919	97.651	101.180	0.000	996890
					Δ_{Finite}	-0.062	-0.089	-0.118	-0.149	-0.183	0.000	
4L5b20m	20	1.4	5	4	σ_{Finite}	42.930	52.127	53.264	52.605	52.388	0.000	417850
					Δ_{Finite}	-0.008	-0.017	-0.029	-0.043	-0.060	0.000	
4L6b100m	100	1.4	6	4	σ_{Finite}	107.029	148.854	180.344	204.940	224.510	241.532	5396200
					Δ_{Finite}	-0.717	-0.845	-0.973	-1.103	-1.234	-1.366	
4L6b80m	80	1.4	6	4	σ_{Finite}	90.852	128.084	156.474	177.738	192.762	203.906	3653400
					Δ_{Finite}	-0.397	-0.483	-0.570	-0.658	-0.748	-0.839	
4L6b60m	60	1.4	6	4	σ_{Finite}	63.528	102.216	120.613	134.381	143.418	166.484	2199500
					Δ_{Finite}	-0.188	-0.237	-0.287	-0.338	-0.392	-0.447	
4L6b40m	40	1.4	6	4	σ_{Finite}	55.779	73.225	82.234	87.208	90.029	94.561	1049400
					Δ_{Finite}	-0.055	-0.078	-0.101	-0.126	-0.153	-0.182	
4L5620m	20	1.4	6	4	σ_{Finite}	42.127	51.627	53.129	52.812	51.761	52.645	411450
					Δ_{Finite}	-0.007	-0.014	-0.023	-0.034	-0.047	-0.061	
Note: All stresses are in Mpa, all deflections are in meters												

Table A.1.13 Stresses and deflections under dead load for 2-lane bridges having curvatures of L/R=2.0

Bridge	Span (m)	Curvature	Boxes	Lanes		Average Stress and Deflections Due to Dead Load						Max Axial Force in Bracing (N)
	L	L/R	Nb	NL		B1 (inner)	B2	B3	B4	B5	B6 (outer)	
2L2b100m	100	2.0	2	2	σ_{Finite}	254.142	287.172	0.000	0.000	0.000	0.000	7667500
					Δ_{Finite}	-2.109	-2.511	0	0.000	0.000	0.000	
2L2b80m	80	2.0	2	2	σ_{Finite}	216.990	242.884	0.000	0.000	0.000	0.000	5162900
					Δ_{Finite}	-1.199	-1.479	0.000	0.000	0.000	0.000	
2L2b60m	60	2.0	2	2	σ_{Finite}	158.311	202.278	0.000	0.000	0.000	0.000	3348900
					Δ_{Finite}	-0.634	-0.820	0.000	0.000	0.000	0.000	
2L2b40m	40	2.0	2	2	σ_{Finite}	134.564	142.024	0.000	0.000	0.000	0.000	1461300
					Δ_{Finite}	-0.236	-0.342	0.000	0.000	0.000	0.000	
2L2b20m	20	2.0	2	2	σ_{Finite}	75.539	71.050	0.000	0.000	0.000	0.000	448320
					Δ_{Finite}	-0.046	-0.090	0.000	0.000	0.000	0.000	
2L3b100m	100	2.0	3	2	σ_{Finite}	183.038	288.522	364.992	0.000	0.000	0.000	8504000
					Δ_{Finite}	-3.027	-3.466	-3.907	0.000	0.000	0.000	
2L3b80m	80	2.0	3	2	σ_{Finite}	196.172	249.484	281.048	0.000	0.000	0.000	5501100
					Δ_{Finite}	-1.511	-1.777	-2.047	0.000	0.000	0.000	
2L3b60m	60	2.0	3	2	σ_{Finite}	128.426	197.582	247.838	0.000	0.000	0.000	3354000
					Δ_{Finite}	-0.748	-0.916	-1.087	0.000	0.000	0.000	
2L3b40m	40	2.0	3	2	σ_{Finite}	120.096	147.328	156.514	0.000	0.000	0.000	1539700
					Δ_{Finite}	-0.246	-0.331	-0.420	0.000	0.000	0.000	
2L3b20m	20	2.0	3	2	σ_{Finite}	72.757	78.922	74.080	0.000	0.000	0.000	496560
					Δ_{Finite}	-0.039	-0.070	-0.103	0.000	0.000	0.000	
2L4b100m	100	2.0	4	2	σ_{Finite}	173.342	264.432	328.574	378.990	0.000	0.000	9683700
					Δ_{Finite}	-3.642	-4.064	-4.489	-4.914	0.000	0.000	
2L4b80m	80	2.0	4	2	σ_{Finite}	150.124	232.294	284.018	325.992	0.000	0.000	6077500
					Δ_{Finite}	-1.899	-2.174	-2.451	-2.730	0.000	0.000	
2L4b60m	60	2.0	4	2	σ_{Finite}	94.403	196.258	228.572	299.158	0.000	0.000	3495100
					Δ_{Finite}	-0.879	-1.038	-1.199	-1.362	0.000	0.000	
2L4b40m	40	2.0	4	2	σ_{Finite}	98.299	142.090	157.672	172.382	0.000	0.000	1593600
					Δ_{Finite}	-0.263	-0.339	-0.417	-0.497	0.000	0.000	
2L4b20m	20	2.0	4	2	σ_{Finite}	71.697	84.305	80.567	78.721	0.000	0.000	529710
					Δ_{Finite}	-0.036	-0.059	-0.084	-0.111	0.000	0.000	
Note: All stresses are in Mpa, all deflections are in meters												

Table A.1.14 Stresses and deflections under dead load for 3-lane bridges having curvatures of L/R=2.0

Bridge	Span (m)	Curvature	Boxes	Lanes		Average Stress and Deflections Due to Dead Load						Max Axial Force in Bracing (N)
	L	L/R	Nb	NL		B1 (inner)	B2	B3	B4	B5	B6 (outer)	
3L3b100m	100	2.0	3	3	σ_{Finite}	224.806	266.004	284.448	0.000	0.000	0.000	7610700
					Δ_{Finite}	-1.889	-2.254	-2.623	0.000	0.000	0.000	
3L3b80m	80	2.0	3	3	σ_{Finite}	195.910	228.952	241.106	0.000	0.000	0.000	5148000
					Δ_{Finite}	-1.051	-1.303	-1.559	0.000	0.000	0.000	
3L3b60m	60	2.0	3	3	σ_{Finite}	141.578	177.940	199.244	0.000	0.000	0.000	3397300
					Δ_{Finite}	-0.536	-0.701	-0.870	0.000	0.000	0.000	
3L3b40m	40	2.0	3	3	σ_{Finite}	124.320	137.036	133.700	0.000	0.000	0.000	1587700
					Δ_{Finite}	-0.185	-0.277	-0.374	0.000	0.000	0.000	
3L3b20m	20	2.0	3	3	σ_{Finite}	78.172	75.033	64.721	0.000	0.000	0.000	584810
					Δ_{Finite}	-0.029	-0.067	-0.112	0.000	0.000	0.000	
3L4b100m	100	2.0	4	3	σ_{Finite}	190.188	255.038	292.570	316.838	0.000	0.000	8978400
					Δ_{Finite}	-2.259	-2.618	-2.979	-3.343	0.000	0.000	
3L4b80m	80	2.0	4	3	σ_{Finite}	166.848	221.930	250.176	267.738	0.000	0.000	5816900
					Δ_{Finite}	-1.205	-1.443	-1.685	-1.929	0.000	0.000	
3L4b60m	60	2.0	4	3	σ_{Finite}	116.279	179.228	196.368	232.962	0.000	0.000	3546000
					Δ_{Finite}	-0.591	-0.739	-0.890	-1.045	0.000	0.000	
3L4b40m	40	2.0	4	3	σ_{Finite}	115.804	142.914	147.298	148.078	0.000	0.000	1743700
					Δ_{Finite}	-0.189	-0.266	-0.348	-0.433	0.000	0.000	
3L4b20m	20	2.0	4	3	σ_{Finite}	80.332	85.334	76.386	69.597	0.000	0.000	673650
					Δ_{Finite}	-0.025	-0.054	-0.087	-0.124	0.000	0.000	
3L5b100m	100	2.0	5	3	σ_{Finite}	139.898	225.258	282.206	321.280	351.582	0.000	9861600
					Δ_{Finite}	-2.671	-3.033	-3.398	-3.765	-4.134	0.000	
3L5b80m	80	2.0	5	3	σ_{Finite}	120.505	196.658	242.660	272.000	296.166	0.000	6301100
					Δ_{Finite}	-1.387	-1.625	-1.865	-2.107	-2.353	0.000	
3L5b60m	60	2.0	5	3	σ_{Finite}	68.870	159.714	193.648	213.334	260.692	0.000	3788700
					Δ_{Finite}	-0.657	-0.803	-0.951	-1.102	-1.256	0.000	
3L5b40m	40	2.0	5	3	σ_{Finite}	106.267	142.768	154.010	155.514	160.634	0.000	1812600
					Δ_{Finite}	-0.193	-0.261	-0.331	-0.405	-0.481	0.000	
3L5b20m	20	2.0	5	3	σ_{Finite}	78.353	88.010	81.355	72.616	69.726	0.000	698530
					Δ_{Finite}	-0.022	-0.044	-0.069	-0.097	-0.127	0.000	
Note: All stresses are in Mpa, all deflections are in meters												

Table A.1.15 Stresses and deflections under dead load for 4-lane bridges having curvatures of L/R=2.0

Bridge	Span (m)	Curvature	Boxes	Lanes		Average Stress and Deflections Due to Dead Load						Max Axial Force in Bracing (N)
	L	L/R	Nb	NL		B1 (inner)	B2	B3	B4	B5	B6 (outer)	
4L4b100m	100	2.0	4	4	σ_{Finite}	198.748	250.278	274.094	285.610	0.000	0.000	8132700
					Δ_{Finite}	-1.691	-2.031	-2.376	-2.725	0.000	0.000	
4L4b80m	80	2.0	4	4	σ_{Finite}	174.908	216.118	231.832	237.752	0.000	0.000	5402500
					Δ_{Finite}	-0.918	-1.150	-1.387	-1.628	0.000	0.000	
4L4b60m	60	2.0	4	4	σ_{Finite}	134.141	178.602	186.964	203.996	0.000	0.000	3693800
					Δ_{Finite}	-0.472	-0.623	-0.780	-0.943	0.000	0.000	
4L4b40m	40	2.0	4	4	σ_{Finite}	122.362	138.780	134.960	128.410	0.000	0.000	1853700
					Δ_{Finite}	-0.147	-0.230	-0.318	-0.412	0.000	0.000	
4L4b20m	20	2.0	4	4	σ_{Finite}	91.827	84.126	70.576	61.791	0.000	0.000	826680
					Δ_{Finite}	-0.016	-0.049	-0.091	-0.139	0.000	0.000	
4L5b100m	100	2.0	5	4	σ_{Finite}	166.552	237.638	278.564	302.606	318.692	0.000	9134500
					Δ_{Finite}	-1.923	-2.254	-2.590	-2.929	-3.272	0.000	
4L5b80m	80	2.0	5	4	σ_{Finite}	150.738	209.070	238.626	253.684	263.842	0.000	5999600
					Δ_{Finite}	-1.009	-1.228	-1.451	-1.678	-1.909	0.000	
4L5b60m	60	2.0	5	4	σ_{Finite}	100.210	160.957	181.767	188.782	214.656	0.000	3870300
					Δ_{Finite}	-0.480	-0.616	-0.757	-0.902	-1.051	0.000	
4L5b40m	40	2.0	5	4	σ_{Finite}	104.975	133.862	137.952	134.158	132.600	0.000	2016200
					Δ_{Finite}	-0.143	-0.213	-0.287	-0.366	-0.450	0.000	
4L5b20m	20	2.0	5	4	σ_{Finite}	94.984	90.546	76.448	66.027	60.866	0.000	876460
					Δ_{Finite}	-0.013	-0.037	-0.067	-0.103	-0.142	0.000	
4L6b100m	100	2.0	6	4	σ_{Finite}	125.952	211.864	267.108	303.724	328.466	348.406	9769900
					Δ_{Finite}	-2.151	-2.478	-2.807	-3.139	-3.474	-3.813	
4L6b80m	80	2.0	6	4	σ_{Finite}	121.064	192.312	233.272	257.968	273.086	287.128	6458800
					Δ_{Finite}	-1.095	-1.305	-1.518	-1.733	-1.953	-2.175	
4L6b60m	60	2.0	6	4	σ_{Finite}	72.187	149.952	179.388	195.451	202.084	237.620	3980700
					Δ_{Finite}	-0.510	-0.639	-0.770	-0.905	-1.043	-1.186	
4L6b40m	40	2.0	6	4	σ_{Finite}	83.669	116.652	125.098	124.834	121.458	123.314	2182600
					Δ_{Finite}	-0.132	-0.189	-0.249	-0.313	-0.381	-0.452	
4L5620m	20	2.0	6	4	σ_{Finite}	96.751	95.414	81.409	70.679	62.301	60.339	890810
					Δ_{Finite}	-0.011	-0.030	-0.053	-0.080	-0.111	-0.144	
Note: All stresses are in Mpa, all deflections are in meters												

APPENDIX A.2

Stresses and Deflections for all Modeled Bridges Under Full CHBDC Truck Load

Table A.2.1 Stresses and deflections under CHBDC full truck load for 2-lane straight bridges

Bridge	Span (m)	Curvature	Boxes	Lanes		Average Stress and Deflections Due to CHBDC full Truck Load						Max Axial Force in Bracing (N)
	L	L/R	Nb	NL		B1 (inner)	B2	B3	B4	B5	B6 (outer)	
2L2b100m	100	0	2	2	σ_{Finite}	46.298	46.298	0.000	0.000	0.000	0.000	68825
					Δ_{Finite}	-0.088	-0.088	0.000	0.000	0.000	0.000	
2L2b80m	80	0	2	2	σ_{Finite}	50.857	50.857	0.000	0.000	0.000	0.000	75225
					Δ_{Finite}	-0.074	-0.074	0.000	0.000	0.000	0.000	
2L2b60m	60	0	2	2	σ_{Finite}	54.656	54.653	0.000	0.000	0.000	0.000	82391
					Δ_{Finite}	-0.057	-0.057	0.000	0.000	0.000	0.000	
2L2b40m	40	0	2	2	σ_{Finite}	120.984	120.984	0.000	0.000	0.000	0.000	186570
					Δ_{Finite}	-0.082	-0.082	0.000	0.000	0.000	0.000	
2L2b20m	20	0	2	2	σ_{Finite}	75.528	75.528	0.000	0.000	0.000	0.000	123340
					Δ_{Finite}	-0.026	-0.026	0.000	0.000	0.000	0.000	
2L3b100m	100	0	3	2	σ_{Finite}	45.669	45.677	45.669	0.000	0.000	0.000	64830
					Δ_{Finite}	-0.086	-0.086	-0.086	0.000	0.000	0.000	
2L3b80m	80	0	3	2	σ_{Finite}	51.731	51.626	51.731	0.000	0.000	0.000	71142
					Δ_{Finite}	-0.074	0.000	-0.074	0.000	0.000	0.000	
2L3b60m	60	0	3	2	σ_{Finite}	0.000	0.000	0.000	0.000	0.000	0.000	0
					Δ_{Finite}	0	0.000	0.000	0.000	0.000	0.000	
2L3b40m	40	0	3	2	σ_{Finite}	121.806	120.808	121.624	0.000	0.000	0.000	180690
					Δ_{Finite}	-0.081	-0.081	-0.081	0.000	0.000	0.000	
2L3b20m	20	0	3	2	σ_{Finite}	76.335	74.638	76.335	0.000	0.000	0.000	128360
					Δ_{Finite}	-0.025	-0.025	-0.025	0.000	0.000	0.000	
2L4b100m	100	0	4	2	σ_{Finite}	46.347	46.329	46.329	46.347	0.000	0.000	62396
					Δ_{Finite}	-0.087	-0.087	-0.087	-0.087	0.000	0.000	
2L4b80m	80	0	4	2	σ_{Finite}	52.222	52.102	52.102	52.222	0.000	0.000	66601
					Δ_{Finite}	-0.075	-0.075	-0.075	-0.075	0.000	0.000	
2L4b60m	60	0	4	2	σ_{Finite}	56.445	55.519	55.637	56.958	0.000	0.000	67944
					Δ_{Finite}	-0.058	-0.058	-0.058	-0.058	0.000	0.000	
2L4b40m	40	0	4	2	σ_{Finite}	120.812	119.912	119.912	120.812	0.000	0.000	162880
					Δ_{Finite}	-0.080	-0.080	-0.080	-0.080	0.000	0.000	
2L4b20m	20	0	4	2	σ_{Finite}	78.428	76.930	76.930	78.428	0.000	0.000	112360
					Δ_{Finite}	-0.024	-0.024	-0.024	-0.024	0.000	0.000	
Note: All stresses are in Mpa, all deflections are in meters												

Table A.2.2 Stresses and deflections under CHBDC full truck load for 3-lane straight bridges

Bridge	Span (m)	Curvature	Boxes	Lanes		Average Stress and Deflections Due to CHBDC full Truck Load						Max Axial Force in Bracing (N)
	L	L/R	Nb	NL		B1 (inner)	B2	B3	B4	B5	B6 (outer)	
3L3b100m	100	0	3	3	σ_{Finite}	44.348	44.196	44.237	0.000	0.000	0.000	66796
					Δ_{Finite}	-0.085	-0.085	-0.085	0.000	0.000	0.000	
3L3b80m	80	0	3	3	σ_{Finite}	51.162	50.844	50.840	0.000	0.000	0.000	77961
					Δ_{Finite}	-0.075	-0.075	-0.075	0.000	0.000	0.000	
3L3b60m	60	0	3	3	σ_{Finite}	55.344	53.700	54.056	0.000	0.000	0.000	123810
					Δ_{Finite}	-0.058	-0.058	-0.057	0.000	0.000	0.000	
3L3b40m	40	0	3	3	σ_{Finite}	116.118	114.740	115.302	0.000	0.000	0.000	179870
					Δ_{Finite}	-0.080	-0.079	-0.079	0.000	0.000	0.000	
3L3b20m	20	0	3	3	σ_{Finite}	72.983	70.091	68.891	0.000	0.000	0.000	137460
					Δ_{Finite}	-0.025	-0.025	-0.024	0.000	0.000	0.000	
3L4b100m	100	0	4	3	σ_{Finite}	45.514	45.488	45.488	45.514	0.000	0.000	65494
					Δ_{Finite}	-0.087	-0.087	-0.087	-0.087	0.000	0.000	
3L4b80m	80	0	4	3	σ_{Finite}	50.548	50.422	50.422	50.548	0.000	0.000	70641
					Δ_{Finite}	-0.074	-0.074	-0.074	-0.074	0.000	0.000	
3L4b60m	60	0	4	3	σ_{Finite}	53.992	53.273	53.463	54.570	0.000	0.000	98552
					Δ_{Finite}	-0.057	-0.057	-0.057	-0.057	0.000	0.000	
3L4b40m	40	0	4	3	σ_{Finite}	119.890	118.726	118.726	119.890	0.000	0.000	173150
					Δ_{Finite}	-0.081	-0.081	-0.081	-0.081	0.000	0.000	
3L4b20m	20	0	4	3	σ_{Finite}	75.440	74.144	73.962	75.405	0.000	0.000	129150
					Δ_{Finite}	-0.025	-0.025	-0.025	-0.025	0.000	0.000	
3L5b100m	100	0	5	3	σ_{Finite}	44.818	44.817	44.833	44.817	44.818	0.000	63312
					Δ_{Finite}	-0.086	-0.086	-0.086	-0.086	-0.086	0.000	
3L5b80m	80	0	5	3	σ_{Finite}	50.507	50.395	50.407	50.395	50.507	0.000	69359
					Δ_{Finite}	-0.074	-0.074	-0.074	-0.074	-0.074	0.000	
3L5b60m	60	0	5	3	σ_{Finite}	56.493	55.190	55.328	55.188	56.480	0.000	101280
					Δ_{Finite}	35893499.942	-0.058	-0.058	-0.058	-0.058	0.000	
3L5b40m	40	0	5	3	σ_{Finite}	122.046	120.758	120.546	120.758	122.046	0.000	158730
					Δ_{Finite}	-0.081	-0.081	-0.081	-0.081	-0.081	0.000	
3L5b20m	20	0	5	3	σ_{Finite}	74.705	73.040	72.925	72.855	74.677	0.000	114860
					Δ_{Finite}	-0.024	-0.024	-0.024	-0.024	-0.024	0.000	
Note: All stresses are in Mpa, all deflections are in meters												

Table A.2.3 Stresses and deflections under CHBDC full truck load for 4-lane straight bridges

Bridge	Span (m)	Curvature	Boxes	Lanes		Average Stress and Deflections Due to CHBDC full Truck Load						Max Axial Force in Bracing (N)
	L	L/R	Nb	NL		B1 (inner)	B2	B3	B4	B5	B6 (outer)	
4L4b100m	100	0	4	4	σ_{Finite}	45.532	45.448	45.448	45.532	0.000	0.000	66201
					Δ_{Finite}	-0.088	-0.088	-0.088	-0.088	0.000	0.000	
4L4b80m	80	0	4	4	σ_{Finite}	50.199	50.037	50.037	50.199	0.000	0.000	71727
					Δ_{Finite}	-0.074	-0.074	-0.074	-0.074	0.000	0.000	
4L4b60m	60	0	4	4	σ_{Finite}	54.369	53.862	54.021	54.897	0.000	0.000	129660
					Δ_{Finite}	-0.058	-0.058	-0.058	-0.058	0.000	0.000	
4L4b40m	40	0	4	4	σ_{Finite}	113.648	112.348	112.348	113.648	0.000	0.000	166030
					Δ_{Finite}	-0.079	-0.078	-0.078	-0.079	0.000	0.000	
4L4b20m	20	0	4	4	σ_{Finite}	69.088	68.616	68.616	69.088	0.000	0.000	114450
					Δ_{Finite}	-0.024	-0.024	-0.024	-0.024	0.000	0.000	
4L5b100m	100	0	5	4	σ_{Finite}	46.162	45.994	45.920	45.994	46.162	0.000	65781
					Δ_{Finite}	-0.089	-0.089	-0.088	-0.089	-0.089	0.000	
4L5b80m	80	0	5	4	σ_{Finite}	51.080	50.607	50.482	50.607	51.080	0.000	67470
					Δ_{Finite}	-0.075	-0.075	-0.075	-0.075	-0.075	0.000	
4L5b60m	60	0	5	4	σ_{Finite}	54.119	53.199	53.388	53.197	54.116	0.000	77420
					Δ_{Finite}	-0.057	-0.057	-0.057	-0.057	-0.057	0.000	
4L5b40m	40	0	5	4	σ_{Finite}	111.624	109.986	109.696	109.986	111.624	0.000	172670
					Δ_{Finite}	-0.077	-0.077	-0.077	-0.077	-0.077	0.000	
4L5b20m	20	0	5	4	σ_{Finite}	69.311	67.841	67.965	67.841	69.311	0.000	105920
					Δ_{Finite}	-0.023	-0.023	-0.023	-0.023	-0.023	0.000	
4L6b100m	100	0	6	4	σ_{Finite}	45.670	45.556	45.496	45.496	45.556	45.670	63554
					Δ_{Finite}	-0.088	-0.088	-0.088	-0.088	-0.088	-0.088	
4L6b80m	80	0	6	4	σ_{Finite}	49.776	49.543	49.465	49.465	49.543	49.776	66133
					Δ_{Finite}	-0.073	-0.073	-0.073	-0.073	-0.073	-0.073	
4L6b60m	60	0	6	4	σ_{Finite}	53.901	52.849	52.894	52.894	52.843	53.893	97003
					Δ_{Finite}	-0.056	-0.056	-0.056	-0.056	-0.056	-0.056	
4L6b40m	40	0	6	4	σ_{Finite}	97.012	95.663	95.132	95.132	95.663	97.012	155710
					Δ_{Finite}	-0.068	-0.068	-0.068	-0.068	-0.068	-0.068	
4L5620m	20	0	6	4	σ_{Finite}	68.565	67.141	66.922	66.922	67.141	68.565	103310
					Δ_{Finite}	-0.023	-0.023	-0.023	-0.023	-0.023	-0.023	
Note: All stresses are in Mpa, all deflections are in meters												

Table A.2.3 Stresses and deflections under CHBDC full truck load for 2-lane bridges having curvatures of L/R=0.4

Bridge	Span (m)	Curvature	Boxes	Lanes		Average Stress and Deflections Due to CHBDC full Truck Load						Max Axial Force in Bracing (N)
	L	L/R	Nb	NL		B1 (inner)	B2	B3	B4	B5	B6 (outer)	
2L2b100m	100	0.4	2	2	σ_{Finite}	46.718	48.988	0.000	0.000	0.000	0.000	356900
					Δ_{Finite}	-0.094	-0.103	0.000	0.000	0.000	0.000	
2L2b80m	80	0.4	2	2	σ_{Finite}	51.312	53.742	0.000	0.000	0.000	0.000	321730
					Δ_{Finite}	-0.078	-0.086	0.000	0.000	0.000	0.000	
2L2b60m	60	0.4	2	2	σ_{Finite}	54.256	58.283	0.000	0.000	0.000	0.000	291140
					Δ_{Finite}	-0.059	-0.066	0.000	0.000	0.000	0.000	
2L2b40m	40	0.4	2	2	σ_{Finite}	121.576	127.134	0.000	0.000	0.000	0.000	452400
					Δ_{Finite}	-0.083	-0.095	0.000	0.000	0.000	0.000	
2L2b20m	20	0.4	2	2	σ_{Finite}	75.305	79.451	0.000	0.000	0.000	0.000	211080
					Δ_{Finite}	-0.025	-0.031	0.000	0.000	0.000	0.000	
2L3b100m	100	0.4	3	2	σ_{Finite}	44.876	47.713	50.329	0.000	0.000	0.000	341870
					Δ_{Finite}	-0.092	-0.101	-0.111	0.000	0.000	0.000	
2L3b80m	80	0.4	3	2	σ_{Finite}	50.827	53.950	57.026	0.000	0.000	0.000	302850
					Δ_{Finite}	-0.077	-0.085	-0.094	0.000	0.000	0.000	
2L3b60m	60	0.4	3	2	σ_{Finite}	0.000	0.000	0.000	0.000	0.000	0.000	0
					Δ_{Finite}	0	0.000	0.000	0.000	0.000	0.000	
2L3b40m	40	0.4	3	2	σ_{Finite}	118.424	125.000	132.412	0.000	0.000	0.000	408730
					Δ_{Finite}	-0.079	-0.089	-0.100	0.000	0.000	0.000	
2L3b20m	20	0.4	3	2	σ_{Finite}	73.765	76.975	82.375	0.000	0.000	0.000	214070
					Δ_{Finite}	-0.022	-0.027	-0.031	0.000	0.000	0.000	
2L4b100m	100	0.4	4	2	σ_{Finite}	43.869	47.519	50.888	54.223	0.000	0.000	387000
					Δ_{Finite}	-0.093	-0.104	-0.114	-0.124	0.000	0.000	
2L4b80m	80	0.4	4	2	σ_{Finite}	49.352	53.409	57.077	60.929	0.000	0.000	326740
					Δ_{Finite}	-0.077	-0.085	-0.094	-0.103	0.000	0.000	
2L4b60m	60	0.4	4	2	σ_{Finite}	51.131	57.118	60.548	68.262	0.000	0.000	251390
					Δ_{Finite}	-0.058	-0.064	-0.070	-0.077	0.000	0.000	
2L4b40m	40	0.4	4	2	σ_{Finite}	112.986	121.214	128.252	136.808	0.000	0.000	352550
					Δ_{Finite}	-0.076	-0.085	-0.094	-0.104	0.000	0.000	
2L4b20m	20	0.4	4	2	σ_{Finite}	74.242	77.617	81.071	85.956	0.000	0.000	180180
					Δ_{Finite}	-0.021	-0.025	-0.028	-0.032	0.000	0.000	
Note: All stresses are in Mpa, all deflections are in meters												

Table A.2.4 Stresses and deflections under CHBDC full truck load for 3-lane bridges having curvatures of L/R=0.4

Bridge	Span (m)	Curvature	Boxes	Lanes		Average Stress and Deflections Due to CHBDC full Truck Load						Max Axial Force in Bracing (N)
	L	L/R	Nb	NL		B1 (inner)	B2	B3	B4	B5	B6 (outer)	
3L3b100m	100	0.4	3	3	σ_{Finite}	43.723	45.652	47.550	0.000	0.000	0.000	314180
					Δ_{Finite}	-0.087	-0.095	-0.104	0.000	0.000	0.000	
3L3b80m	80	0.4	3	3	σ_{Finite}	0.000	0.000	0.000	0.000	0.000	0.000	0
					Δ_{Finite}	0	0.000	0.000	0.000	0.000	0.000	
3L3b60m	60	0.4	3	3	σ_{Finite}	53.489	55.145	58.664	0.000	0.000	0.000	243480
					Δ_{Finite}	-0.057	-0.063	-0.069	0.000	0.000	0.000	
3L3b40m	40	0.4	3	3	σ_{Finite}	113.858	118.170	123.302	0.000	0.000	0.000	406710
					Δ_{Finite}	-0.075	-0.086	-0.097	0.000	0.000	0.000	
3L3b20m	20	0.4	3	3	σ_{Finite}	69.634	71.745	74.616	0.000	0.000	0.000	199900
					Δ_{Finite}	-0.021	-0.026	-0.031	0.000	0.000	0.000	
3L4b100m	100	0.4	4	3	σ_{Finite}	43.465	46.095	48.468	50.764	0.000	0.000	307240
					Δ_{Finite}	-0.088	-0.097	-0.105	-0.114	0.000	0.000	
3L4b80m	80	0.4	4	3	σ_{Finite}	48.305	51.114	53.694	56.282	0.000	0.000	273390
					Δ_{Finite}	-0.072	-0.080	-0.088	-0.095	0.000	0.000	
3L4b60m	60	0.4	4	3	σ_{Finite}	50.071	54.294	57.055	62.428	0.000	0.000	259890
					Δ_{Finite}	-0.055	-0.061	-0.067	-0.073	0.000	0.000	
3L4b40m	40	0.4	4	3	σ_{Finite}	114.248	119.930	125.666	132.006	0.000	0.000	385690
					Δ_{Finite}	-0.074	-0.083	-0.093	-0.104	0.000	0.000	
3L4b20m	20	0.4	4	3	σ_{Finite}	70.594	74.681	78.610	83.325	0.000	0.000	220930
					Δ_{Finite}	-0.020	-0.025	-0.029	-0.034	0.000	0.000	
3L5b100m	100	0.4	5	3	σ_{Finite}	41.083	44.173	47.015	49.651	52.243	0.000	295290
					Δ_{Finite}	-0.085	-0.094	-0.103	-0.112	-0.121	0.000	
3L5b80m	80	0.4	5	3	σ_{Finite}	46.254	49.708	52.884	55.818	58.869	0.000	258330
					Δ_{Finite}	-0.071	-0.078	-0.086	-0.094	-0.102	0.000	
3L5b60m	60	0.4	5	3	σ_{Finite}	49.740	54.296	57.871	60.893	67.463	0.000	229390
					Δ_{Finite}	-0.054	-0.061	-0.067	-0.073	-0.079	0.000	
3L5b40m	40	0.4	5	3	σ_{Finite}	113.346	119.430	125.260	130.826	137.660	0.000	344780
					Δ_{Finite}	-0.072	-0.081	-0.089	-0.098	-0.108	0.000	
3L5b20m	20	0.4	5	3	σ_{Finite}	68.628	71.973	75.677	78.702	83.527	0.000	194280
					Δ_{Finite}	-0.019	-0.022	-0.026	-0.030	-0.034	0.000	
Note: All stresses are in Mpa, all deflections are in meters												

Table A.2.5 Stresses and deflections under CHBDC full truck load for 4-lane bridges having curvatures of L/R=0.4

Bridge	Span (m)	Curvature	Boxes	Lanes		Average Stress and Deflections Due to CHBDC full Truck Load						Max Axial Force in Bracing (N)
	L	L/R	Nb	NL		B1 (inner)	B2	B3	B4	B5	B6 (outer)	
4L4b100m	100	0.4	4	4	σ_{Finite}	43.833	45.966	47.899	49.784	0.000	0.000	299410
					Δ_{Finite}	-0.086	-0.095	-0.103	-0.112	0.000	0.000	
4L4b80m	80	0.4	4	4	σ_{Finite}	48.381	50.629	52.735	54.808	0.000	0.000	272170
					Δ_{Finite}	-0.071	-0.079	-0.086	-0.094	0.000	0.000	
4L4b60m	60	0.4	4	4	σ_{Finite}	51.289	54.797	57.235	61.116	0.000	0.000	333530
					Δ_{Finite}	-0.054	-0.061	-0.067	-0.073	0.000	0.000	
4L4b40m	40	0.4	4	4	σ_{Finite}	108.986	113.466	118.454	123.638	0.000	0.000	405070
					Δ_{Finite}	-0.070	-0.080	-0.090	-0.102	0.000	0.000	
4L4b20m	20	0.4	4	4	σ_{Finite}	63.738	69.073	73.404	77.220	0.000	0.000	217390
					Δ_{Finite}	-0.018	-0.023	-0.029	-0.035	0.000	0.000	
4L5b100m	100	0.4	5	4	σ_{Finite}	43.066	45.490	47.737	49.958	52.186	0.000	284640
					Δ_{Finite}	-0.085	-0.093	-0.102	-0.110	-0.119	0.000	
4L5b80m	80	0.4	5	4	σ_{Finite}	47.700	50.200	52.584	54.928	57.374	0.000	255900
					Δ_{Finite}	-0.070	-0.077	-0.084	-0.091	-0.099	0.000	
4L5b60m	60	0.4	5	4	σ_{Finite}	49.243	52.457	55.308	57.481	61.953	0.000	241280
					Δ_{Finite}	-0.052	-0.058	-0.064	-0.070	-0.076	0.000	
4L5b40m	40	0.4	5	4	σ_{Finite}	103.694	108.466	113.672	118.680	124.608	0.000	389780
					Δ_{Finite}	-0.066	-0.075	-0.084	-0.094	-0.104	0.000	
4L5b20m	20	0.4	5	4	σ_{Finite}	63.217	66.772	70.768	73.760	77.823	0.000	202070
					Δ_{Finite}	-0.017	-0.021	-0.025	-0.030	-0.035	0.000	
4L6b100m	100	0.4	6	4	σ_{Finite}	41.109	43.830	46.348	48.765	51.095	53.435	262920
					Δ_{Finite}	-0.083	-0.091	-0.099	-0.107	-0.115	-0.124	
4L6b80m	80	0.4	6	4	σ_{Finite}	44.773	47.435	50.212	52.972	55.587	58.117	221520
					Δ_{Finite}	-0.066	-0.073	-0.080	-0.087	-0.095	-0.102	
4L6b60m	60	0.4	6	4	σ_{Finite}	47.095	50.821	53.672	56.394	58.689	63.900	222450
					Δ_{Finite}	-0.050	-0.055	-0.061	-0.066	-0.072	-0.078	
4L6b40m	40	0.4	6	4	σ_{Finite}	87.369	91.876	96.224	100.612	104.976	110.310	359120
					Δ_{Finite}	-0.057	-0.064	-0.071	-0.078	-0.086	-0.095	
4L5620m	20	0.4	6	4	σ_{Finite}	61.699	64.891	68.179	71.087	73.781	77.679	192620
					Δ_{Finite}	-0.016	-0.019	-0.023	-0.026	-0.030	-0.034	
Note: All stresses are in Mpa, all deflections are in meters												

Table A.2.6 Stresses and deflections under CHBDC full truck load for 2-lane bridges having curvatures of L/R=1.0

Bridge	Span (m)	Curvature	Boxes	Lanes		Average Stress and Deflections Due to CHBDC full Truck Load						Max Axial Force in Bracing (N)
	L	L/R	Nb	NL		B1 (inner)	B2	B3	B4	B5	B6 (outer)	
2L2b100m	100	1	2	2	σ_{Finite}	52.878	58.364	0.000	0.000	0.000	0.000	857700
					Δ_{Finite}	-0.152	-0.180	0.000	0.000	0.000	0.000	
2L2b80m	80	1	2	2	σ_{Finite}	57.965	63.755	0.000	0.000	0.000	0.000	749270
					Δ_{Finite}	-0.119	-0.144	0.000	0.000	0.000	0.000	
2L2b60m	60	1	2	2	σ_{Finite}	59.356	69.617	0.000	0.000	0.000	0.000	652420
					Δ_{Finite}	-0.088	-0.109	0.000	0.000	0.000	0.000	
2L2b40m	40	1	2	2	σ_{Finite}	136.084	147.964	0.000	0.000	0.000	0.000	911030
					Δ_{Finite}	-0.111	-0.149	0.000	0.000	0.000	0.000	
2L2b20m	20	1	2	2	σ_{Finite}	84.291	90.991	0.000	0.000	0.000	0.000	358700
					Δ_{Finite}	-0.030	-0.048	0.000	0.000	0.000	0.000	
2L3b100m	100	1	3	2	σ_{Finite}	49.101	56.712	62.976	0.000	0.000	0.000	1121400
					Δ_{Finite}	-0.168	-0.196	-0.224	0.000	0.000	0.000	
2L3b80m	80	1	3	2	σ_{Finite}	55.537	64.125	71.220	0.000	0.000	0.000	927610
					Δ_{Finite}	-0.129	-0.153	-0.178	0.000	0.000	0.000	
2L3b60m	60	1	3	2	σ_{Finite}	55.306	68.011	81.550	0.000	0.000	0.000	754950
					Δ_{Finite}	-0.092	-0.112	-0.132	0.000	0.000	0.000	
2L3b40m	40	1	3	2	σ_{Finite}	126.954	145.750	160.014	0.000	0.000	0.000	1014300
					Δ_{Finite}	-0.107	-0.138	-0.170	0.000	0.000	0.000	
2L3b20m	20	1	3	2	σ_{Finite}	79.629	89.487	95.869	0.000	0.000	0.000	388290
					Δ_{Finite}	-0.026	-0.038	-0.052	0.000	0.000	0.000	
2L4b100m	100	1	4	2	σ_{Finite}	43.902	53.028	60.431	66.813	0.000	0.000	1071200
					Δ_{Finite}	-0.150	-0.179	-0.208	-0.237	0.000	0.000	
2L4b80m	80	1	4	2	σ_{Finite}	50.084	61.883	71.335	80.337	0.000	0.000	1135800
					Δ_{Finite}	-0.143	-0.168	-0.194	-0.219	0.000	0.000	
2L4b60m	60	1	4	2	σ_{Finite}	48.492	66.790	75.070	92.735	0.000	0.000	835110
					Δ_{Finite}	-0.097	-0.115	-0.134	-0.153	0.000	0.000	
2L4b40m	40	1	4	2	σ_{Finite}	113.848	138.682	154.854	171.888	0.000	0.000	1115000
					Δ_{Finite}	-0.105	-0.133	-0.161	-0.190	0.000	0.000	
2L4b20m	20	1	4	2	σ_{Finite}	77.978	89.519	95.058	101.075	0.000	0.000	390010
					Δ_{Finite}	-0.024	-0.034	-0.044	-0.055	0.000	0.000	
Note: All stresses are in Mpa, all deflections are in meters												

Table A.2.8 Stresses and deflections under CHBDC full truck load for 3-lane bridges having curvatures of L/R=1.0

Bridge	Span (m)	Curvature	Boxes	Lanes		Average Stress and Deflections Due to CHBDC full Truck Load						Max Axial Force in Bracing (N)
	L	L/R	Nb	NL		B1 (inner)	B2	B3	B4	B5	B6 (outer)	
3L3b100m	100	1	3	3	σ_{Finite}	47.710	53.144	57.314	0.000	0.000	0.000	792400
					Δ_{Finite}	-0.135	-0.161	-0.187	0.000	0.000	0.000	
3L3b80m	80	1	3	3	σ_{Finite}	55.149	61.114	65.558	0.000	0.000	0.000	685420
					Δ_{Finite}	-0.109	-0.133	-0.156	0.000	0.000	0.000	
3L3b60m	60	1	3	3	σ_{Finite}	56.256	63.321	70.946	0.000	0.000	0.000	567430
					Δ_{Finite}	-0.078	-0.097	-0.117	0.000	0.000	0.000	
3L3b40m	40	1	3	3	σ_{Finite}	124.028	136.782	144.540	0.000	0.000	0.000	823870
					Δ_{Finite}	-0.093	-0.126	-0.161	0.000	0.000	0.000	
3L3b20m	20	1	3	3	σ_{Finite}	75.230	83.277	86.227	0.000	0.000	0.000	354970
					Δ_{Finite}	-0.022	-0.037	-0.053	0.000	0.000	0.000	
3L4b100m	100	1	4	3	σ_{Finite}	45.217	52.808	58.778	63.876	0.000	0.000	1025500
					Δ_{Finite}	-0.147	-0.173	-0.200	-0.226	0.000	0.000	
3L4b80m	80	1	4	3	σ_{Finite}	50.357	58.638	64.972	70.417	0.000	0.000	858960
					Δ_{Finite}	-0.111	-0.134	-0.156	-0.179	0.000	0.000	
3L4b60m	60	1	4	3	σ_{Finite}	49.895	62.484	68.627	79.896	0.000	0.000	713140
					Δ_{Finite}	-0.079	-0.097	-0.115	-0.134	0.000	0.000	
3L4b40m	40	1	4	3	σ_{Finite}	119.818	137.666	149.444	159.262	0.000	0.000	977630
					Δ_{Finite}	-0.091	-0.120	-0.149	-0.180	0.000	0.000	
3L4b20m	20	1	4	3	σ_{Finite}	75.192	87.758	93.082	97.019	0.000	0.000	415700
					Δ_{Finite}	-0.020	-0.032	-0.046	-0.061	0.000	0.000	
3L5b100m	100	1	5	3	σ_{Finite}	39.567	48.757	56.388	62.854	68.712	0.000	1224500
					Δ_{Finite}	-0.156	-0.182	-0.209	-0.235	-0.262	0.000	
3L5b80m	80	1	5	3	σ_{Finite}	44.384	54.916	63.346	70.336	76.938	0.000	1022800
					Δ_{Finite}	-0.116	-0.139	-0.161	-0.184	-0.208	0.000	
3L5b60m	60	1	5	3	σ_{Finite}	43.769	59.681	68.629	75.624	89.761	0.000	839910
					Δ_{Finite}	-0.081	-0.100	-0.118	-0.137	-0.156	0.000	
3L5b40m	40	1	5	3	σ_{Finite}	114.496	134.734	148.640	158.788	170.132	0.000	1027400
					Δ_{Finite}	-0.089	-0.114	-0.140	-0.167	-0.195	0.000	
3L5b20m	20	1	5	3	σ_{Finite}	71.277	83.671	90.084	92.880	97.772	0.000	414880
					Δ_{Finite}	-0.018	-0.028	-0.038	-0.050	-0.062	0.000	
Note: All stresses are in Mpa, all deflections are in meters												

Table A.2.9 Stresses and deflections under CHBDC full truck load for 4-lane bridges having curvatures of L/R=1.0

Bridge	Span (m)	Curvature	Boxes	Lanes		Average Stress and Deflections Due to CHBDC full Truck Load						Max Axial Force in Bracing (N)
	L	L/R	Nb	NL		B1 (inner)	B2	B3	B4	B5	B6 (outer)	
4L4b100m	100	1	4	4	σ_{Finite}	45.995	52.303	56.980	60.768	0.000	0.000	814840
					Δ_{Finite}	-0.128	-0.154	-0.179	-0.205	0.000	0.000	
4L4b80m	80	1	4	4	σ_{Finite}	51.007	57.734	62.625	66.486	0.000	0.000	696180
					Δ_{Finite}	-0.099	-0.121	-0.143	-0.166	0.000	0.000	
4L4b60m	60	1	4	4	σ_{Finite}	52.737	62.840	67.911	75.272	0.000	0.000	646580
					Δ_{Finite}	-0.072	-0.091	-0.110	-0.129	0.000	0.000	
4L4b40m	40	1	4	4	σ_{Finite}	126.338	136.212	141.420	115.049	0.000	0.000	906960
					Δ_{Finite}	-0.111	-0.136	-0.168	-0.194	0.000	0.000	
4L4b20m	20	1	4	4	σ_{Finite}	77.714	86.367	89.313	70.566	0.000	0.000	403160
					Δ_{Finite}	-0.020	-0.035	-0.053	-0.069	0.000	0.000	
4L5b100m	100	1	5	4	σ_{Finite}	42.932	50.577	56.628	61.690	66.160	0.000	971580
					Δ_{Finite}	-0.133	-0.158	-0.183	-0.208	-0.234	0.000	
4L5b80m	80	1	5	4	σ_{Finite}	47.986	56.080	62.332	67.419	72.004	0.000	819080
					Δ_{Finite}	-0.100	-0.121	-0.142	-0.164	-0.186	0.000	
4L5b60m	60	1	5	4	σ_{Finite}	46.946	58.033	64.809	69.398	78.369	0.000	703860
					Δ_{Finite}	-0.069	-0.087	-0.104	-0.122	-0.140	0.000	
4L5b40m	40	1	5	4	σ_{Finite}	105.196	122.504	134.162	141.984	149.702	0.000	968460
					Δ_{Finite}	-0.074	-0.100	-0.127	-0.156	-0.188	0.000	
4L5b20m	20	1	5	4	σ_{Finite}	73.736	86.850	92.728	94.661	97.637	0.000	436080
					Δ_{Finite}	-0.018	-0.031	-0.045	-0.062	-0.080	0.000	
4L6b100m	100	1	6	4	σ_{Finite}	38.227	46.891	54.008	60.069	65.301	70.140	1089300
					Δ_{Finite}	-0.135	-0.160	-0.184	-0.208	-0.233	-0.259	
4L6b80m	80	1	6	4	σ_{Finite}	42.676	51.683	58.834	64.809	69.853	74.790	889780
					Δ_{Finite}	-0.098	-0.117	-0.137	-0.157	-0.178	-0.199	
4L6b60m	60	1	6	4	σ_{Finite}	41.295	54.454	61.919	68.140	72.698	83.598	763440
					Δ_{Finite}	-0.068	-0.084	-0.100	-0.116	-0.133	-0.150	
4L6b40m	40	1	6	4	σ_{Finite}	83.816	100.491	111.716	119.976	126.240	134.010	982250
					Δ_{Finite}	-0.063	-0.083	-0.105	-0.127	-0.151	-0.177	
4L5620m	20	1	6	4	σ_{Finite}	73.792	85.771	91.101	93.510	94.442	98.109	441670
					Δ_{Finite}	-0.017	-0.027	-0.038	-0.051	-0.065	-0.081	
Note: All stresses are in Mpa, all deflections are in meters												

Table A.2.10 Stresses and deflections under CHBDC full truck load for 2-lane bridges having curvatures of L/R=1.4

Bridge	Span (m)	Curvature	Boxes	Lanes		Average Stress and Deflections Due to CHBDC full Truck Load						Max Axial Force in Bracing (N)
	L	L/R	Nb	NL		B1 (inner)	B2	B3	B4	B5	B6 (outer)	
2L2b100m	100	1.4	2	2	σ_{Finite}	61.104	68.728	0.000	0.000	0.000	0.000	1307300
					Δ_{Finite}	-0.250	-0.300	0.000	0.000	0.000	0.000	
2L2b80m	80	1.4	2	2	σ_{Finite}	66.874	74.815	0.000	0.000	0.000	0.000	1132100
					Δ_{Finite}	-0.189	-0.234	0.000	0.000	0.000	0.000	
2L2b60m	60	1.4	2	2	σ_{Finite}	66.995	82.053	0.000	0.000	0.000	0.000	975800
					Δ_{Finite}	-0.136	-0.175	0.000	0.000	0.000	0.000	
2L2b40m	40	1.4	2	2	σ_{Finite}	157.102	171.252	0.000	0.000	0.000	0.000	1318800
					Δ_{Finite}	-0.163	-0.229	0.000	0.000	0.000	0.000	
2L2b20m	20	1.4	2	2	σ_{Finite}	98.925	103.254	0.000	0.000	0.000	0.000	487520
					Δ_{Finite}	-0.040	-0.073	0.000	0.000	0.000	0.000	
2L3b100m	100	1.4	3	2	σ_{Finite}	55.206	66.753	75.458	0.000	0.000	0.000	1726600
					Δ_{Finite}	-0.300	-0.349	-0.398	0.000	0.000	0.000	
2L3b80m	80	1.4	3	2	σ_{Finite}	62.326	75.431	85.117	0.000	0.000	0.000	1405800
					Δ_{Finite}	-0.220	-0.263	-0.306	0.000	0.000	0.000	
2L3b60m	60	1.4	3	2	σ_{Finite}	59.198	79.591	98.649	0.000	0.000	0.000	1113700
					Δ_{Finite}	-0.151	-0.186	0.000	0.000	0.000	0.000	
2L3b40m	40	1.4	3	2	σ_{Finite}	142.848	170.762	187.456	0.000	0.000	0.000	1481100
					Δ_{Finite}	-0.161	-0.215	-0.271	0.000	0.000	0.000	
2L3b20m	20	1.4	3	2	σ_{Finite}	92.615	105.170	108.661	0.000	0.000	0.000	540170
					Δ_{Finite}	-0.034	-0.057	-0.081	0.000	0.000	0.000	
2L4b100m	100	1.4	4	2	σ_{Finite}	47.256	63.618	76.599	87.859	0.000	0.000	2072200
					Δ_{Finite}	-0.373	-0.426	-0.479	-0.533	0.000	0.000	
2L4b80m	80	1.4	4	2	σ_{Finite}	52.748	71.499	85.311	97.742	0.000	0.000	1605500
					Δ_{Finite}	-0.260	-0.305	-0.349	-0.394	0.000	0.000	
2L4b60m	60	1.4	4	2	σ_{Finite}	48.519	77.906	89.636	114.939	0.000	0.000	1189800
					Δ_{Finite}	-0.166	-0.199	-0.232	-0.266	0.000	0.000	
2L4b40m	40	1.4	4	2	σ_{Finite}	122.592	161.830	182.888	203.902	0.000	0.000	1588400
					Δ_{Finite}	-0.163	-0.211	-0.261	-0.311	0.000	0.000	
2L4b20m	20	1.4	4	2	σ_{Finite}	89.877	106.740	110.375	114.604	0.000	0.000	551760
					Δ_{Finite}	-0.032	-0.049	-0.067	-0.086	0.000	0.000	
Note: All stresses are in Mpa, all deflections are in meters												

Table A.2.11 Stresses and deflections under CHBDC full truck load for 3-lane bridges having curvatures of L/R=1.4

Bridge	Span (m)	Curvature	Boxes	Lanes		Average Stress and Deflections Due to CHBDC full Truck Load						Max Axial Force in Bracing (N)
	L	L/R	Nb	NL		B1 (inner)	B2	B3	B4	B5	B6 (outer)	
3L3b100m	100	1.4	3	3	σ_{Finite}	54.137	62.324	67.659	0.000	0.000	0.000	1355300
					Δ_{Finite}	-0.221	-0.267	-0.312	0.000	0.000	0.000	
3L3b80m	80	1.4	3	3	σ_{Finite}	62.683	71.625	77.065	0.000	0.000	0.000	1156900
					Δ_{Finite}	-0.172	-0.213	-0.255	0.000	0.000	0.000	
3L3b60m	60	1.4	3	3	σ_{Finite}	62.317	73.576	83.625	0.000	0.000	0.000	936150
					Δ_{Finite}	-0.119	-0.153	-0.188	0.000	0.000	0.000	
3L3b40m	40	1.4	3	3	σ_{Finite}	142.846	160.286	166.158	0.000	0.000	0.000	1331800
					Δ_{Finite}	-0.132	-0.189	-0.250	0.000	0.000	0.000	
3L3b20m	20	1.4	3	3	σ_{Finite}	90.082	97.881	96.014	0.000	0.000	0.000	515390
					Δ_{Finite}	-0.027	-0.054	-0.083	0.000	0.000	0.000	
3L4b100m	100	1.4	4	3	σ_{Finite}	49.466	61.466	69.979	76.631	0.000	0.000	1672900
					Δ_{Finite}	-0.256	-0.302	-0.348	-0.395	0.000	0.000	
3L4b80m	80	1.4	4	3	σ_{Finite}	55.268	68.382	77.183	84.030	0.000	0.000	1386800
					Δ_{Finite}	-0.184	-0.223	-0.263	-0.303	0.000	0.000	
3L4b60m	60	1.4	4	3	σ_{Finite}	53.369	73.098	81.128	96.410	0.000	0.000	1119200
					Δ_{Finite}	-0.126	-0.157	-0.190	-0.222	0.000	0.000	
3L4b40m	40	1.4	4	3	σ_{Finite}	135.110	162.472	175.526	184.616	0.000	0.000	1515300
					Δ_{Finite}	-0.131	-0.181	-0.232	-0.287	0.000	0.000	
3L4b20m	20	1.4	4	3	σ_{Finite}	90.783	106.800	107.817	107.596	0.000	0.000	615180
					Δ_{Finite}	-0.025	-0.046	-0.070	-0.097	0.000	0.000	
3L5b100m	100	1.4	5	3	σ_{Finite}	40.477	55.393	66.864	75.916	83.694	0.000	1911600
					Δ_{Finite}	-0.286	-0.332	-0.379	-0.426	-0.473	0.000	
3L5b80m	80	1.4	5	3	σ_{Finite}	45.325	62.522	75.011	84.521	93.077	0.000	1558200
					Δ_{Finite}	-0.202	-0.242	-0.282	-0.322	-0.363	0.000	
3L5b60m	60	1.4	5	3	σ_{Finite}	41.376	67.878	80.751	89.899	109.390	0.000	1264300
					Δ_{Finite}	-0.135	-0.167	-0.200	-0.233	-0.267	0.000	
3L5b40m	40	1.4	5	3	σ_{Finite}	126.174	158.854	176.624	186.740	198.746	0.000	1570400
					Δ_{Finite}	-0.130	-0.173	-0.218	-0.265	-0.314	0.000	
3L5b20m	20	1.4	5	3	σ_{Finite}	85.746	103.558	107.331	105.691	108.168	0.000	617650
					Δ_{Finite}	-0.022	-0.038	-0.057	-0.077	-0.099	0.000	
Note: All stresses are in Mpa, all deflections are in meters												

Table A.2.12 Stresses and deflections under CHBDC full truck load for 4-lane bridges having curvatures of L/R=1.4

Bridge	Span (m)	Curvature	Boxes	Lanes		Average Stress and Deflections Due to CHBDC full Truck Load						Max Axial Force in Bracing (N)
	L	L/R	Nb	NL		B1 (inner)	B2	B3	B4	B5	B6 (outer)	
4L4b100m	100	1.4	4	4	σ_{Finite}	51.075	61.016	67.369	71.858	0.000	0.000	1431800
					Δ_{Finite}	-0.209	-0.253	-0.298	-0.343	0.000	0.000	
4L4b80m	80	1.4	4	4	σ_{Finite}	56.998	67.509	73.839	78.084	0.000	0.000	1209900
					Δ_{Finite}	-0.153	-0.192	-0.231	-0.272	0.000	0.000	
4L4b60m	60	1.4	4	4	σ_{Finite}	58.477	73.802	79.787	88.919	0.000	0.000	1044100
					Δ_{Finite}	-0.109	-0.142	-0.176	-0.211	0.000	0.000	
4L4b40m	40	1.4	4	4	σ_{Finite}	134.828	155.710	163.078	165.510	0.000	0.000	1523100
					Δ_{Finite}	-0.109	-0.161	-0.218	-0.278	0.000	0.000	
4L4b20m	20	1.4	4	4	σ_{Finite}	88.066	102.483	100.951	97.914	0.000	0.000	716440
					Δ_{Finite}	-0.019	-0.042	-0.072	-0.107	0.000	0.000	
4L5b100m	100	1.4	5	4	σ_{Finite}	45.727	58.292	67.203	73.888	79.339	0.000	1642400
					Δ_{Finite}	-0.226	-0.269	-0.313	-0.357	-0.402	0.000	
4L5b80m	80	1.4	5	4	σ_{Finite}	51.713	65.016	73.942	80.305	85.604	0.000	1376200
					Δ_{Finite}	-0.160	-0.197	-0.234	-0.273	-0.311	0.000	
4L5b60m	60	1.4	5	4	σ_{Finite}	48.771	67.030	76.265	81.492	93.255	0.000	1150600
					Δ_{Finite}	-0.107	-0.137	-0.168	-0.199	-0.232	0.000	
4L5b40m	40	1.4	5	4	σ_{Finite}	118.426	146.114	159.272	165.030	170.920	0.000	1603600
					Δ_{Finite}	-0.103	-0.148	-0.195	-0.246	-0.300	0.000	
4L5b20m	20	1.4	5	4	σ_{Finite}	86.538	101.674	101.755	98.225	97.233	0.000	732370
					Δ_{Finite}	-0.016	-0.033	-0.055	-0.081	-0.110	0.000	
4L6b100m	100	1.4	6	4	σ_{Finite}	38.257	52.759	63.684	72.238	79.083	85.141	1770600
					Δ_{Finite}	-0.240	-0.282	-0.325	-0.368	-0.412	-0.456	
4L6b80m	80	1.4	6	4	σ_{Finite}	41.225	57.267	69.563	78.819	85.457	90.689	1504600
					Δ_{Finite}	-0.167	-0.203	-0.239	-0.276	-0.314	-0.352	
4L6b60m	60	1.4	6	4	σ_{Finite}	39.763	61.866	72.745	80.738	85.834	100.625	1217500
					Δ_{Finite}	-0.108	-0.135	-0.164	-0.193	-0.222	-0.253	
4L6b40m	40	1.4	6	4	σ_{Finite}	91.786	119.508	133.784	141.614	145.936	153.200	1626800
					Δ_{Finite}	-0.089	-0.124	-0.161	-0.200	-0.242	-0.287	
4L5620m	20	1.4	6	4	σ_{Finite}	83.638	100.073	101.149	98.938	95.721	97.105	719520
					Δ_{Finite}	-0.014	-0.028	-0.044	-0.064	-0.086	-0.111	
Note: All stresses are in Mpa, all deflections are in meters												

Table A.2.13 Stresses and deflections under CHBDC full truck load for 2-lane bridges having curvatures of L/R=2.0

Bridge	Span (m)	Curvature	Boxes	Lanes		Average Stress and Deflections Due to CHBDC full Truck Load						Max Axial Force in Bracing (N)
	L	L/R	Nb	NL		B1 (inner)	B2	B3	B4	B5	B6 (outer)	
2L2b100m	100	2	2	2	σ_{Finite}	86.082	97.697	0.000	0.000	0.000	0.000	2455900
					Δ_{Finite}	-0.686	-0.816	0.000	0.000	0.000	0.000	
2L2b80m	80	2	2	2	σ_{Finite}	94.034	105.662	0.000	0.000	0.000	0.000	2108800
					Δ_{Finite}	-0.499	-0.615	0.000	0.000	0.000	0.000	
2L2b60m	60	2	2	2	σ_{FInite}	91.308	116.565	0.000	0.000	0.000	0.000	1800800
					Δ_{Finite}	-0.350	-0.452	0.000	0.000	0.000	0.000	
2L2b40m	40	2	2	2	σ_{Finite}	223.216	235.666	0.000	0.000	0.000	0.000	2349600
					Δ_{Finite}	-0.384	-0.557	0.000	0.000	0.000	0.000	
2L2b20m	20	2	2	2	σ_{Finite}	145.934	135.564	0.000	0.000	0.000	0.000	823690
					Δ_{Finite}	-0.087	-0.170	0.000	0.000	0.000	0.000	
2L3b100m	100	2	3	2	σ_{Finite}	61.202	95.786	120.890	0.000	0.000	0.000	2669500
					Δ_{Finite}	-0.963	-1.103	-1.243	0.000	0.000	0.000	
2L3b80m	80	2	3	2	σ_{Finite}	84.593	107.778	121.882	0.000	0.000	0.000	2246600
					Δ_{Finite}	-0.626	-0.736	-0.848	0.000	0.000	0.000	
2L3b60m	60	2	3	2	σ_{Finite}	74.734	112.984	143.454	0.000	0.000	0.000	1819300
					Δ_{Finite}	-0.414	-0.507	-0.601	0.000	0.000	0.000	
2L3b40m	40	2	3	2	σ_{Finite}	198.622	243.220	259.222	0.000	0.000	0.000	2479800
					Δ_{Finite}	-0.399	-0.539	-0.682	0.000	0.000	0.000	
2L3b20m	20	2	3	2	σ_{Finite}	138.754	148.418	140.384	0.000	0.000	0.000	894350
					Δ_{Finite}	-0.074	-0.131	-0.192	0.000	0.000	0.000	
2L4b100m	100	2	4	2	σ_{Finite}	58.601	89.428	111.250	128.596	0.000	0.000	3105800
					Δ_{Finite}	-1.182	-1.319	-1.457	-1.596	0.000	0.000	
2L4b80m	80	2	4	2	σ_{Finite}	65.332	100.822	123.380	141.982	0.000	0.000	2499200
					Δ_{Finite}	-0.791	-0.906	-1.021	-1.138	0.000	0.000	
2L4b60m	60	2	4	2	σ_{Finite}	54.679	111.005	129.349	170.832	0.000	0.000	1879300
					Δ_{Finite}	-0.480	-0.567	-0.654	-0.743	0.000	0.000	
2L4b40m	40	2	4	2	σ_{Finite}	162.080	233.504	259.220	283.972	0.000	0.000	2558500
					Δ_{Finite}	-0.425	-0.549	-0.676	-0.805	0.000	0.000	
2L4b20m	20	2	4	2	σ_{Finite}	135.186	157.360	149.920	147.134	0.000	0.000	949970
					Δ_{Finite}	-0.067	-0.111	-0.157	-0.206	0.000	0.000	
Note: All stresses are in Mpa, all deflections are in meters												

Table A.2.14 Stresses and deflections under CHBDC full truck load for 3-lane bridges having curvatures of L/R=2.0

Bridge	Span (m)	Curvature	Boxes	Lanes		Average Stress and Deflections Due to CHBDC full Truck Load						Max Axial Force in Bracing (N)
	L	L/R	Nb	NL		B1 (inner)	B2	B3	B4	B5	B6 (outer)	
3L3b100m	100	2	3	3	σ_{Finite}	75.316	89.252	95.760	0.000	0.000	0.000	2418300
					Δ_{Finite}	-0.607	-0.724	-0.843	0.000	0.000	0.000	
3L3b80m	80	2	3	3	σ_{Finite}	87.562	102.354	108.092	0.000	0.000	0.000	2166500
					Δ_{Finite}	-0.449	-0.557	-0.666	0.000	0.000	0.000	
3L3b60m	60	2	3	3	σ_{Finite}	84.091	103.855	117.523	0.000	0.000	0.000	1840100
					Δ_{Finite}	-0.300	-0.392	-0.485	0.000	0.000	0.000	
3L3b40m	40	2	3	3	σ_{Finite}	207.996	228.578	223.124	0.000	0.000	0.000	2546900
					Δ_{Finite}	-0.303	-0.452	-0.610	0.000	0.000	0.000	
3L3b20m	20	2	3	3	σ_{Finite}	146.232	136.482	118.241	0.000	0.000	0.000	983150
					Δ_{Finite}	-0.053	-0.120	-0.197	0.000	0.000	0.000	
3L4b100m	100	2	4	3	σ_{Finite}	65.504	87.951	101.086	109.734	0.000	0.000	2936100
					Δ_{Finite}	-0.747	-0.866	-0.985	-1.106	0.000	0.000	
3L4b80m	80	2	4	3	σ_{Finite}	73.845	98.212	110.938	119.100	0.000	0.000	2432900
					Δ_{Finite}	-0.511	-0.612	-0.715	-0.819	0.000	0.000	
3L4b60m	60	2	4	3	σ_{Finite}	68.988	105.508	115.681	138.594	0.000	0.000	1964700
					Δ_{Finite}	-0.335	-0.418	-0.504	-0.591	0.000	0.000	
3L4b40m	40	2	4	3	σ_{Finite}	193.868	238.780	246.412	248.298	0.000	0.000	2822400
					Δ_{Finite}	-0.310	-0.438	-0.571	-0.710	0.000	0.000	
3L4b20m	20	2	4	3	σ_{Finite}	153.754	160.936	142.874	130.785	0.000	0.000	1196700
					Δ_{Finite}	-0.048	-0.101	-0.162	-0.229	0.000	0.000	
3L5b100m	100	2	5	3	σ_{Finite}	48.276	77.501	97.099	110.616	121.232	0.000	3214700
					Δ_{Finite}	-0.881	-1.000	-1.121	-1.242	-1.364	0.000	
3L5b80m	80	2	5	3	σ_{Finite}	54.314	88.092	108.708	121.972	133.120	0.000	2668700
					Δ_{Finite}	-0.595	-0.697	-0.800	-0.904	-1.009	0.000	
3L5b60m	60	2	5	3	σ_{Finite}	43.059	95.703	116.002	127.691	157.776	0.000	2145200
					Δ_{Finite}	-0.379	-0.463	-0.548	-0.634	-0.723	0.000	
3L5b40m	40	2	5	3	σ_{Finite}	177.204	237.234	256.270	259.060	268.182	0.000	2923200
					Δ_{Finite}	-0.315	-0.426	-0.541	-0.661	-0.785	0.000	
3L5b20m	20	2	5	3	σ_{Finite}	148.286	164.586	151.358	134.624	130.336	0.000	1240700
					Δ_{Finite}	-0.041	-0.083	-0.128	-0.179	-0.233	0.000	
Note: All stresses are in Mpa, all deflections are in meters												

Table A.2.15 Stresses and deflections under CHBDC full truck load for 4-lane bridges having curvatures of L/R=2.0

Bridge	Span (m)	Curvature	Boxes	Lanes		Average Stress and Deflections Due to CHBDC full Truck Load						Max Axial Force in Bracing (N)
	L	L/R	Nb	NL		B1 (inner)	B2	B3	B4	B5	B6 (outer)	
4L4b100m	100	2	4	4	σ_{Finite}	69.818	88.048	96.658	101.010	0.000	0.000	2707800
					Δ_{Finite}	-0.570	-0.685	-0.801	-0.918	0.000	0.000	
4L4b80m	80	2	4	4	σ_{Finite}	79.041	97.792	105.216	108.272	0.000	0.000	2304300
					Δ_{Finite}	-0.398	-0.498	-0.600	-0.705	0.000	0.000	
4L4b60m	60	2	4	4	σ_{Finite}	80.867	107.604	112.705	124.120	0.000	0.000	2084400
					Δ_{Finite}	-0.273	-0.360	-0.450	-0.543	0.000	0.000	
4L4b40m	40	2	4	4	σ_{Finite}	205.108	232.230	226.090	215.464	0.000	0.000	2975800
					Δ_{Finite}	-0.242	-0.377	-0.521	-0.674	0.000	0.000	
4L4b20m	20	2	4	4	σ_{Finite}	172.556	156.198	128.976	112.516	0.000	0.000	1437600
					Δ_{Finite}	-0.030	-0.090	-0.164	-0.249	0.000	0.000	
4L5b100m	100	2	5	4	σ_{Finite}	58.837	83.597	97.965	106.614	112.620	0.000	3045300
					Δ_{Finite}	-0.648	-0.760	-0.873	-0.988	-1.103	0.000	
4L5b80m	80	2	5	4	σ_{Finite}	68.293	94.248	107.582	114.610	119.636	0.000	2551800
					Δ_{Finite}	-0.436	-0.531	-0.627	-0.724	-0.824	0.000	
4L5b60m	60	2	5	4	σ_{Finite}	61.524	96.999	109.596	113.605	130.316	0.000	2178700
					Δ_{Finite}	-0.277	-0.356	-0.437	-0.520	-0.605	0.000	
4L5b40m	40	2	5	4	σ_{Finite}	176.510	223.666	230.488	224.092	221.842	0.000	3237900
					Δ_{Finite}	-0.234	-0.349	-0.470	-0.599	-0.734	0.000	
4L5b20m	20	2	5	4	σ_{Finite}	176.990	166.958	139.624	119.048	109.698	0.000	1523600
					Δ_{Finite}	-0.024	-0.068	-0.122	-0.184	-0.253	0.000	
4L6b100m	100	2	6	4	σ_{Finite}	44.437	74.022	93.130	105.904	114.664	121.910	3231900
					Δ_{Finite}	-0.719	-0.828	-0.938	-1.049	-1.161	-1.274	
4L6b80m	80	2	6	4	σ_{Finite}	53.705	84.463	102.320	113.234	120.054	126.624	2676900
					Δ_{Finite}	-0.460	-0.548	-0.638	-0.728	-0.820	-0.914	
4L6b60m	60	2	6	4	σ_{Finite}	44.331	88.848	106.030	115.441	119.379	141.777	2209800
					Δ_{Finite}	-0.289	-0.362	-0.436	-0.512	-0.590	-0.670	
4L6b40m	40	2	6	4	σ_{Finite}	135.030	187.126	200.562	200.286	194.988	198.226	3377800
					Δ_{Finite}	-0.208	-0.298	-0.393	-0.493	-0.599	-0.709	
4L5620m	20	2	6	4	σ_{Finite}	178.240	174.716	147.844	127.416	111.672	108.414	1542300
					Δ_{Finite}	-0.020	-0.055	-0.095	-0.143	-0.197	-0.254	
Note: All stresses are in Mpa, all deflections are in meters												

APPENDIX A.3

Load Distribution Factors for all Modeled Bridges Under Dead Load

Table A.3.1 Load distribution factors under dead load for 2-lane straight bridges

Bridge	Span (m)	Curvature	Boxes	Lanes	Stress Distribution Factor					
	L	L/R	Nb	NL	$D_{\sigma 1inner}$	$D_{\sigma 2}$	$D_{\sigma 3}$	$D_{\sigma 4}$	$D_{\sigma 5}$	$D_{\sigma 6outer}$
2L2b100m	100	0	2	2	1.02	1.02	0.00	0.00	0.00	0.00
2L2b80m	80	0	2	2	1.02	1.02	0.00	0.00	0.00	0.00
2L2b60m	60	0	2	2	1.01	1.01	0.00	0.00	0.00	0.00
2L2b40m	40	0	2	2	1.01	1.01	0.00	0.00	0.00	0.00
2L2b20m	20	0	2	2	0.94	0.94	0.00	0.00	0.00	0.00
2L3b100m	100	0	3	2	1.02	1.02	1.02	0.00	0.00	0.00
2L3b80m	80	0	3	2	1.03	1.03	1.03	0.00	0.00	0.00
2L3b60m	60	0	3	2	0.00	0.00	0.00	0.00	0.00	0.00
2L3b40m	40	0	3	2	1.03	1.03	1.03	0.00	0.00	0.00
2L3b20m	20	0	3	2	0.99	0.98	0.99	0.00	0.00	0.00
2L4b100m	100	0	4	2	1.02	1.01	1.01	1.02	0.00	0.00
2L4b80m	80	0	4	2	1.03	1.03	1.03	1.03	0.00	0.00
2L4b60m	60	0	4	2	1.02	1.02	1.02	1.02	0.00	0.00
2L4b40m	40	0	4	2	1.04	1.03	1.03	1.04	0.00	0.00
2L4b20m	20	0	4	2	1.01	1.00	1.00	1.01	0.00	0.00

Table A.3.2 Load distribution factors under dead load for 3-lane straight bridges

Bridge	Span (m)	Curvature	Boxes	Lanes	Stress Distribution Factor					
	L	L/R	Nb	NL	$D_{\sigma 1inner}$	$D_{\sigma 2}$	$D_{\sigma 3}$	$D_{\sigma 4}$	$D_{\sigma 5}$	$D_{\sigma 6outer}$
3L3b100m	100	0	3	3	1.02	1.02	1.02	0.00	0.00	0.00
3L3b80m	80	0	3	3	1.02	1.02	1.02	0.00	0.00	0.00
3L3b60m	60	0	3	3	1.02	1.01	1.01	0.00	0.00	0.00
3L3b40m	40	0	3	3	1.02	1.01	1.02	0.00	0.00	0.00
3L3b20m	20	0	3	3	0.96	0.94	0.96	0.00	0.00	0.00
3L4b100m	100	0	4	3	1.02	1.02	1.02	1.02	0.00	0.00
3L4b80m	80	0	4	3	1.03	1.02	1.02	1.03	0.00	0.00
3L4b60m	60	0	4	3	1.02	1.01	1.01	1.02	0.00	0.00
3L4b40m	40	0	4	3	1.03	1.02	1.02	1.03	0.00	0.00
3L4b20m	20	0	4	3	0.99	0.97	0.97	0.99	0.00	0.00
3L5b100m	100	0	5	3	1.02	1.01	1.01	1.01	1.02	0.00
3L5b80m	80	0	5	3	1.03	1.02	1.02	1.02	1.03	0.00
3L5b60m	60	0	5	3	1.02	1.02	1.02	1.02	1.02	0.00
3L5b40m	40	0	5	3	1.04	1.03	1.03	1.03	1.04	0.00
3L5b20m	20	0	5	3	1.02	0.99	0.99	0.99	1.02	0.00

Table A.3.3 Load distribution factors under dead load for 4-lane straight bridges

Bridge	Span (m)	Curvature	Boxes	Lanes		Stress Distribution Factor					
	L	L/R	Nb	NL		$D_{\sigma 1inner}$	$D_{\sigma 2}$	$D_{\sigma 3}$	$D_{\sigma 4}$	$D_{\sigma 5}$	$D_{\sigma 6outer}$
4L4b100m	100	0	4	4	D_σ	1.02	1.01	1.01	1.02	0.00	0.00
4L4b80m	80	0	4	4	D_σ	1.03	1.02	1.02	1.03	0.00	0.00
4L4b60m	60	0	4	4	D_σ	1.02	1.01	1.01	1.02	0.00	0.00
4L4b40m	40	0	4	4	D_σ	1.03	1.01	1.01	1.03	0.00	0.00
4L4b20m	20	0	4	4	D_σ	0.97	0.94	0.94	0.97	0.00	0.00
4L5b100m	100	0	5	4	D_σ	1.02	1.01	1.01	1.01	1.02	0.00
4L5b80m	80	0	5	4	D_σ	1.03	1.02	1.02	1.02	1.03	0.00
4L5b60m	60	0	5	4	D_σ	1.02	1.01	1.01	1.01	1.02	0.00
4L5b40m	40	0	5	4	D_σ	1.04	1.02	1.02	1.02	1.04	0.00
4L5b20m	20	0	5	4	D_σ	1.00	0.97	0.96	0.97	1.00	0.00
4L6b100m	100	0	6	4	D_σ	1.02	1.02	1.01	1.01	1.02	1.02
4L6b80m	80	0	6	4	D_σ	1.03	1.03	1.02	1.02	1.03	1.03
4L6b60m	60	0	6	4	D_σ	1.03	1.02	1.01	1.01	1.02	1.03
4L6b40m	40	0	6	4	D_σ	0.94	0.93	0.92	0.92	0.93	0.94
4L5620m	20	0	6	4	D_σ	1.02	0.99	0.98	0.98	0.99	1.02

Table A.3.4 Load distribution factors under dead load for 2-lane bridges having curvatures of L/R=0.4

Bridge	Span (m)	Curvature	Boxes	Lanes	Stress Distribution Factor					
	L	L/R	Nb	NL	$D_{\sigma 1inner}$	$D_{\sigma 2}$	$D_{\sigma 3}$	$D_{\sigma 4}$	$D_{\sigma 5}$	$D_{\sigma 6outer}$
2L2b100m	100	0.4	2	2	1.03	1.08	0.00	0.00	0.00	0.00
2L2b80m	80	0.4	2	2	1.03	1.08	0.00	0.00	0.00	0.00
2L2b60m	60	0.4	2	2	1.00	1.08	0.00	0.00	0.00	0.00
2L2b40m	40	0.4	2	2	1.02	1.07	0.00	0.00	0.00	0.00
2L2b20m	20	0.4	2	2	0.94	1.00	0.00	0.00	0.00	0.00
2L3b100m	100	0.4	3	2	1.00	1.06	1.12	0.00	0.00	0.00
2L3b80m	80	0.4	3	2	1.01	1.07	1.13	0.00	0.00	0.00
2L3b60m	60	0.4	3	2	0.00	0.00	0.00	0.00	0.00	0.00
2L3b40m	40	0.4	3	2	1.00	1.06	1.12	0.00	0.00	0.00
2L3b20m	20	0.4	3	2	0.95	1.01	1.07	0.00	0.00	0.00
2L4b100m	100	0.4	4	2	0.96	1.04	1.12	1.19	0.00	0.00
2L4b80m	80	0.4	4	2	0.97	1.05	1.12	1.20	0.00	0.00
2L4b60m	60	0.4	4	2	0.92	1.05	1.11	1.23	0.00	0.00
2L4b40m	40	0.4	4	2	0.97	1.04	1.11	1.18	0.00	0.00
2L4b20m	20	0.4	4	2	0.95	1.01	1.06	1.12	0.00	0.00

Table A.3.5 Load distribution factors under dead load for 3-lane bridges having curvatures of L/R=0.4

Bridge	Span (m)	Curvature	Boxes	Lanes	Stress Distribution Factor					
	L	L/R	Nb	NL	$D_{\sigma 1inner}$	$D_{\sigma 2}$	$D_{\sigma 3}$	$D_{\sigma 4}$	$D_{\sigma 5}$	$D_{\sigma 6outer}$
3L3b100m	100	0.4	3	3	1.00	1.05	1.09	0.00	0.00	0.00
3L3b80m	80	0.4	3	3	0.00	0.00	0.00	0.00	0.00	0.00
3L3b60m	60	0.4	3	3	0.98	1.04	1.11	0.00	0.00	0.00
3L3b40m	40	0.4	3	3	1.00	1.05	1.10	0.00	0.00	0.00
3L3b20m	20	0.4	3	3	0.91	0.98	1.05	0.00	0.00	0.00
3L4b100m	100	0.4	4	3	0.97	1.03	1.08	1.14	0.00	0.00
3L4b80m	80	0.4	4	3	0.98	1.04	1.09	1.15	0.00	0.00
3L4b60m	60	0.4	4	3	0.95	1.03	1.08	1.17	0.00	0.00
3L4b40m	40	0.4	4	3	0.98	1.03	1.09	1.14	0.00	0.00
3L4b20m	20	0.4	4	3	0.91	0.98	1.04	1.11	0.00	0.00
3L5b100m	100	0.4	5	3	0.93	1.00	1.06	1.13	1.19	0.00
3L5b80m	80	0.4	5	3	0.94	1.01	1.07	1.14	1.20	0.00
3L5b60m	60	0.4	5	3	0.90	1.00	1.06	1.13	1.23	0.00
3L5b40m	40	0.4	5	3	0.97	1.02	1.07	1.12	1.18	0.00
3L5b20m	20	0.4	5	3	0.92	0.97	1.03	1.08	1.15	0.00

Table A.3.6 Load distribution factors under dead load for 4-lane bridges having curvatures of L/R=0.4

Bridge	Span (m)	Curvature	Boxes	Lanes	Stress Distribution Factor					
	L	L/R	Nb	NL	$D_{\sigma 1inner}$	$D_{\sigma 2}$	$D_{\sigma 3}$	$D_{\sigma 4}$	$D_{\sigma 5}$	$D_{\sigma 6outer}$
4L4b100m	100	0.4	4	4	0.98	1.03	1.07	1.12	0.00	0.00
4L4b80m	80	0.4	4	4	0.99	1.03	1.08	1.12	0.00	0.00
4L4b60m	60	0.4	4	4	0.97	1.02	1.07	1.14	0.00	0.00
4L4b40m	40	0.4	4	4	0.98	1.02	1.07	1.12	0.00	0.00
4L4b20m	20	0.4	4	4	0.87	0.94	1.03	1.11	0.00	0.00
4L5b100m	100	0.4	5	4	0.95	1.00	1.05	1.10	1.16	0.00
4L5b80m	80	0.4	5	4	0.96	1.01	1.06	1.11	1.16	0.00
4L5b60m	60	0.4	5	4	0.93	1.00	1.05	1.10	1.18	0.00
4L5b40m	40	0.4	5	4	0.96	1.01	1.06	1.11	1.17	0.00
4L5b20m	20	0.4	5	4	0.89	0.95	1.01	1.08	1.16	0.00
4L6b100m	100	0.4	6	4	0.91	0.98	1.03	1.09	1.14	1.20
4L6b80m	80	0.4	6	4	0.92	0.98	1.04	1.10	1.16	1.21
4L6b60m	60	0.4	6	4	0.89	0.98	1.03	1.08	1.14	1.23
4L6b40m	40	0.4	6	4	0.84	0.89	0.93	0.98	1.02	1.08
4L5620m	20	0.4	6	4	0.89	0.94	1.00	1.06	1.12	1.19

Table A.3.7 Load distribution factors under dead load for 2-lane bridges having curvatures of L/R=1.0

Bridge	Span (m)	Curvature	Boxes	Lanes	Stress Distribution Factor					
	L	L/R	Nb	NL	$D_{\sigma 1inner}$	$D_{\sigma 2}$	$D_{\sigma 3}$	$D_{\sigma 4}$	$D_{\sigma 5}$	$D_{\sigma 6outer}$
2L2b100m	100	1	2	2	1.17	1.29	0.00	0.00	0.00	0.00
2L2b80m	80	1	2	2	1.17	1.29	0.00	0.00	0.00	0.00
2L2b60m	60	1	2	2	1.11	1.30	0.00	0.00	0.00	0.00
2L2b40m	40	1	2	2	1.15	1.25	0.00	0.00	0.00	0.00
2L2b20m	20	1	2	2	1.06	1.16	0.00	0.00	0.00	0.00
2L3b100m	100	1	3	2	1.10	1.27	1.41	0.00	0.00	0.00
2L3b80m	80	1	3	2	1.11	1.28	1.42	0.00	0.00	0.00
2L3b60m	60	1	3	2	0.99	1.25	1.48	0.00	0.00	0.00
2L3b40m	40	1	3	2	1.08	1.24	1.36	0.00	0.00	0.00
2L3b20m	20	1	3	2	1.03	1.19	1.26	0.00	0.00	0.00
2L4b100m	100	1	4	2	0.99	1.20	1.37	1.51	0.00	0.00
2L4b80m	80	1	4	2	0.99	1.22	1.41	1.59	0.00	0.00
2L4b60m	60	1	4	2	0.87	1.23	1.38	1.68	0.00	0.00
2L4b40m	40	1	4	2	0.98	1.20	1.34	1.48	0.00	0.00
2L4b20m	20	1	4	2	1.00	1.17	1.25	1.32	0.00	0.00

Table A.3.8 Load distribution factors under dead load for 3-lane bridges having curvatures of L/R=1.0

Bridge	Span (m)	Curvature	Boxes	Lanes	Stress Distribution Factor					
	L	L/R	Nb	NL	$D_{\sigma 1inner}$	$D_{\sigma 2}$	$D_{\sigma 3}$	$D_{\sigma 4}$	$D_{\sigma 5}$	$D_{\sigma 6outer}$
3L3b100m	100	1	3	3	1.10	1.23	1.32	0.00	0.00	0.00
3L3b80m	80	1	3	3	1.11	1.24	1.33	0.00	0.00	0.00
3L3b60m	60	1	3	3	1.05	1.21	1.35	0.00	0.00	0.00
3L3b40m	40	1	3	3	1.10	1.22	1.29	0.00	0.00	0.00
3L3b20m	20	1	3	3	1.00	1.18	1.25	0.00	0.00	0.00
3L4b100m	100	1	4	3	1.02	1.19	1.32	1.44	0.00	0.00
3L4b80m	80	1	4	3	1.03	1.20	1.33	1.44	0.00	0.00
3L4b60m	60	1	4	3	0.95	1.19	1.31	1.51	0.00	0.00
3L4b40m	40	1	4	3	1.04	1.19	1.30	1.38	0.00	0.00
3L4b20m	20	1	4	3	0.98	1.17	1.26	1.32	0.00	0.00
3L5b100m	100	1	5	3	0.90	1.11	1.28	1.43	1.57	0.00
3L5b80m	80	1	5	3	0.90	1.12	1.30	1.44	1.58	0.00
3L5b60m	60	1	5	3	0.78	1.11	1.27	1.41	1.65	0.00
3L5b40m	40	1	5	3	0.98	1.16	1.28	1.37	1.46	0.00
3L5b20m	20	1	5	3	0.96	1.15	1.25	1.30	1.37	0.00

Table A.3.9 Load distribution factors under dead load for 4-lane bridges having curvatures of L/R=1.0

Bridge	Span (m)	Curvature	Boxes	Lanes	Stress Distribution Factor					
	L	L/R	Nb	NL	$D_{\sigma 1inner}$	$D_{\sigma 2}$	$D_{\sigma 3}$	$D_{\sigma 4}$	$D_{\sigma 5}$	$D_{\sigma 6outer}$
4L4b100m	100	1	4	4	1.03	1.17	1.28	1.37	0.00	0.00
4L4b80m	80	1	4	4	1.05	1.19	1.29	1.37	0.00	0.00
4L4b60m	60	1	4	4	1.00	1.18	1.28	1.42	0.00	0.00
4L4b40m	40	1	4	4	1.14	1.23	1.30	1.09	0.00	0.00
4L4b20m	20	1	4	4	1.07	1.22	1.34	1.16	0.00	0.00
4L5b100m	100	1	5	4	0.95	1.12	1.26	1.37	1.47	0.00
4L5b80m	80	1	5	4	0.97	1.14	1.27	1.37	1.47	0.00
4L5b60m	60	1	5	4	0.88	1.11	1.24	1.34	1.51	0.00
4L5b40m	40	1	5	4	0.98	1.15	1.26	1.34	1.41	0.00
4L5b20m	20	1	5	4	1.03	1.26	1.37	1.44	1.50	0.00
4L6b100m	100	1	6	4	0.85	1.05	1.21	1.35	1.47	1.58
4L6b80m	80	1	6	4	0.88	1.07	1.23	1.35	1.46	1.57
4L6b60m	60	1	6	4	0.78	1.05	1.20	1.33	1.42	1.62
4L6b40m	40	1	6	4	0.81	0.98	1.09	1.17	1.24	1.32
4L5620m	20	1	6	4	1.07	1.27	1.37	1.43	1.47	1.54

Table A.3.10 Load distribution factors under dead load for 2-lane bridges having curvatures of L/R=1.4

Bridge	Span (m)	Curvature	Boxes	Lanes	Stress Distribution Factor					
	L	L/R	Nb	NL	$D_{\sigma 1inner}$	$D_{\sigma 2}$	$D_{\sigma 3}$	$D_{\sigma 4}$	$D_{\sigma 5}$	$D_{\sigma 6outer}$
2L2b100m	100	1.4	2	2	1.36	1.52	0.00	0.00	0.00	0.00
2L2b80m	80	1.4	2	2	1.36	1.52	0.00	0.00	0.00	0.00
2L2b60m	60	1.4	2	2	1.26	1.54	0.00	0.00	0.00	0.00
2L2b40m	40	1.4	2	2	1.33	1.45	0.00	0.00	0.00	0.00
2L2b20m	20	1.4	2	2	1.26	1.34	0.00	0.00	0.00	0.00
2L3b100m	100	1.4	3	2	1.24	1.50	1.69	0.00	0.00	0.00
2L3b80m	80	1.4	3	2	1.25	1.52	1.71	0.00	0.00	0.00
2L3b60m	60	1.4	3	2	1.07	1.47	1.80	0.00	0.00	0.00
2L3b40m	40	1.4	3	2	1.22	1.46	1.60	0.00	0.00	0.00
2L3b20m	20	1.4	3	2	1.21	1.41	1.44	0.00	0.00	0.00
2L4b100m	100	1.4	4	2	1.04	1.41	1.70	1.94	0.00	0.00
2L4b80m	80	1.4	4	2	1.05	1.42	1.70	1.94	0.00	0.00
2L4b60m	60	1.4	4	2	0.88	1.44	1.66	2.10	0.00	0.00
2L4b40m	40	1.4	4	2	1.06	1.40	1.59	1.77	0.00	0.00
2L4b20m	20	1.4	4	2	1.16	1.40	1.46	1.51	0.00	0.00

Table A.3.11 Load distribution factors under dead load for 3-lane bridges having curvatures of L/R=1. 4

Bridge	Span (m)	Curvature	Boxes	Lanes	Stress Distribution Factor					
	L	L/R	Nb	NL	$D_{\sigma 1inner}$	$D_{\sigma 2}$	$D_{\sigma 3}$	$D_{\sigma 4}$	$D_{\sigma 5}$	$D_{\sigma 6outer}$
3L3b100m	100	1.4	3	3	1.26	1.45	1.57	0.00	0.00	0.00
3L3b80m	80	1.4	3	3	1.28	1.46	1.57	0.00	0.00	0.00
3L3b60m	60	1.4	3	3	1.17	1.42	1.60	0.00	0.00	0.00
3L3b40m	40	1.4	3	3	1.27	1.44	1.49	0.00	0.00	0.00
3L3b20m	20	1.4	3	3	1.24	1.42	1.41	0.00	0.00	0.00
3L4b100m	100	1.4	4	3	1.12	1.39	1.58	1.73	0.00	0.00
3L4b80m	80	1.4	4	3	1.14	1.41	1.59	1.73	0.00	0.00
3L4b60m	60	1.4	4	3	1.02	1.41	1.56	1.84	0.00	0.00
3L4b40m	40	1.4	4	3	1.17	1.42	1.53	1.61	0.00	0.00
3L4b20m	20	1.4	4	3	1.20	1.45	1.49	1.48	0.00	0.00
3L5b100m	100	1.4	5	3	0.92	1.27	1.53	1.74	1.92	0.00
3L5b80m	80	1.4	5	3	0.93	1.29	1.55	1.74	1.92	0.00
3L5b60m	60	1.4	5	3	0.74	1.27	1.51	1.69	2.03	0.00
3L5b40m	40	1.4	5	3	1.08	1.37	1.52	1.61	1.71	0.00
3L5b20m	20	1.4	5	3	1.17	1.45	1.51	1.51	1.53	0.00

Table A.3.12 Load distribution factors under dead load for 4-lane bridges having curvatures of L/R=1.4

Bridge	Span (m)	Curvature	Boxes	Lanes	Stress Distribution Factor					
	L	L/R	Nb	NL	$D_{\sigma 1inner}$	$D_{\sigma 2}$	$D_{\sigma 3}$	$D_{\sigma 4}$	$D_{\sigma 5}$	$D_{\sigma 6outer}$
4L4b100m	100	1.4	4	4	1.16	1.38	1.52	1.62	0.00	0.00
4L4b80m	80	1.4	4	4	1.18	1.40	1.53	1.62	0.00	0.00
4L4b60m	60	1.4	4	4	1.11	1.41	1.52	1.68	0.00	0.00
4L4b40m	40	1.4	4	4	1.23	1.43	1.50	1.52	0.00	0.00
4L4b20m	20	1.4	4	4	1.24	1.50	1.52	1.50	0.00	0.00
4L5b100m	100	1.4	5	4	1.02	1.30	1.50	1.65	1.77	0.00
4L5b80m	80	1.4	5	4	1.05	1.33	1.52	1.65	1.75	0.00
4L5b60m	60	1.4	5	4	0.92	1.30	1.48	1.59	1.80	0.00
4L5b40m	40	1.4	5	4	1.11	1.38	1.51	1.57	1.62	0.00
4L5b20m	20	1.4	5	4	1.25	1.52	1.55	1.53	1.53	0.00
4L6b100m	100	1.4	6	4	0.85	1.19	1.44	1.63	1.79	1.92
4L6b80m	80	1.4	6	4	0.85	1.20	1.46	1.66	1.80	1.91
4L6b60m	60	1.4	6	4	0.75	1.21	1.42	1.59	1.69	1.96
4L6b40m	40	1.4	6	4	0.89	1.17	1.31	1.39	1.44	1.51
4L5620m	20	1.4	6	4	1.25	1.53	1.57	1.56	1.53	1.56

Table A.3.13 Load distribution factors under dead load for 4-lane bridges having curvatures of L/R=2.0

Bridge	Span (m)	Curvature	Boxes	Lanes	Stress Distribution Factor					
	L	L/R	Nb	NL	$D_{\sigma 1inner}$	$D_{\sigma 2}$	$D_{\sigma 3}$	$D_{\sigma 4}$	$D_{\sigma 5}$	$D_{\sigma 6outer}$
2L2b100m	100	2	2	2	1.93	2.18	0.00	0.00	0.00	0.00
2L2b80m	80	2	2	2	1.94	2.17	0.00	0.00	0.00	0.00
2L2b60m	60	2	2	2	1.73	2.22	0.00	0.00	0.00	0.00
2L2b40m	40	2	2	2	1.90	2.01	0.00	0.00	0.00	0.00
2L2b20m	20	2	2	2	1.89	1.78	0.00	0.00	0.00	0.00
2L3b100m	100	2	3	2	1.39	2.19	2.77	0.00	0.00	0.00
2L3b80m	80	2	3	2	1.72	2.19	2.46	0.00	0.00	0.00
2L3b60m	60	2	3	2	1.37	2.11	2.65	0.00	0.00	0.00
2L3b40m	40	2	3	2	1.71	2.10	2.23	0.00	0.00	0.00
2L3b20m	20	2	3	2	1.85	2.01	1.88	0.00	0.00	0.00
2L4b100m	100	2	4	2	1.31	2.00	2.49	2.87	0.00	0.00
2L4b80m	80	2	4	2	1.31	2.03	2.48	2.85	0.00	0.00
2L4b60m	60	2	4	2	1.00	2.07	2.41	3.16	0.00	0.00
2L4b40m	40	2	4	2	1.41	2.04	2.26	2.47	0.00	0.00
2L4b20m	20	2	4	2	1.78	2.09	2.00	1.96	0.00	0.00

Table A.3.14 Load distribution factors under dead load for 4-lane bridges having curvatures of L/R=2.0

Bridge	Span (m)	Curvature	Boxes	Lanes	Stress Distribution Factor					
	L	L/R	Nb	NL	$D_{\sigma 1inner}$	$D_{\sigma 2}$	$D_{\sigma 3}$	$D_{\sigma 4}$	$D_{\sigma 5}$	$D_{\sigma 6outer}$
3L3b100m	100	2	3	3	1.77	2.10	2.24	0.00	0.00	0.00
3L3b80m	80	2	3	3	1.81	2.11	2.22	0.00	0.00	0.00
3L3b60m	60	2	3	3	1.62	2.04	2.28	0.00	0.00	0.00
3L3b40m	40	2	3	3	1.88	2.07	2.02	0.00	0.00	0.00
3L3b20m	20	2	3	3	2.15	2.06	1.78	0.00	0.00	0.00
3L4b100m	100	2	4	3	1.50	2.01	2.30	2.49	0.00	0.00
3L4b80m	80	2	4	3	1.54	2.05	2.31	2.47	0.00	0.00
3L4b60m	60	2	4	3	1.34	2.06	2.26	2.68	0.00	0.00
3L4b40m	40	2	4	3	1.71	2.11	2.17	2.18	0.00	0.00
3L4b20m	20	2	4	3	2.13	2.26	2.02	1.84	0.00	0.00
3L5b100m	100	2	5	3	1.11	1.79	2.25	2.56	2.80	0.00
3L5b80m	80	2	5	3	1.13	1.84	2.27	2.54	2.77	0.00
3L5b60m	60	2	5	3	0.78	1.81	2.20	2.42	2.96	0.00
3L5b40m	40	2	5	3	1.54	2.07	2.23	2.25	2.33	0.00
3L5b20m	20	2	5	3	2.11	2.37	2.19	1.96	1.88	0.00

Table A.3.15 Load distribution factors under dead load for 4-lane bridges having curvatures of L/R=2.0

Bridge	Span (m)	Curvature	Boxes	Lanes	Stress Distribution Factor					
	L	L/R	Nb	NL	$D_{\sigma 1inner}$	$D_{\sigma 2}$	$D_{\sigma 3}$	$D_{\sigma 4}$	$D_{\sigma 5}$	$D_{\sigma 6outer}$
4L4b100m	100	2	4	4	1.60	2.01	2.21	2.30	0.00	0.00
4L4b80m	80	2	4	4	1.66	2.06	2.21	2.26	0.00	0.00
4L4b60m	60	2	4	4	1.57	2.09	2.19	2.39	0.00	0.00
4L4b40m	40	2	4	4	1.91	2.17	2.11	2.01	0.00	0.00
4L4b20m	20	2	4	4	2.64	2.41	2.03	1.77	0.00	0.00
4L5b100m	100	2	5	4	1.33	1.89	2.22	2.41	2.54	0.00
4L5b80m	80	2	5	4	1.41	1.96	2.24	2.38	2.47	0.00
4L5b60m	60	2	5	4	1.19	1.92	2.16	2.25	2.55	0.00
4L5b40m	40	2	5	4	1.68	2.15	2.21	2.15	2.13	0.00
4L5b20m	20	2	5	4	2.77	2.64	2.23	1.92	1.77	0.00
4L6b100m	100	2	6	4	1.00	1.69	2.13	2.42	2.62	2.78
4L6b80m	80	2	6	4	1.13	1.80	2.18	2.41	2.55	2.68
4L6b60m	60	2	6	4	0.85	1.77	2.12	2.31	2.39	2.80
4L6b40m	40	2	6	4	1.34	1.86	2.00	2.00	1.94	1.97
4L5620m	20	2	6	4	2.86	2.82	2.41	2.09	1.84	1.78

APPENDIX A.4

Load Distribution Factors for all Modeled Bridges Under Full CHBDC Truck Load

Table A.4.1 Load distribution factors under CHDBC full truck load for 2-lane straight bridges

Bridge	Span (m)	Curvature	Boxes	Lanes	Stress Distribution Factor					
	L	L/R	Nb	NL	$D_{\sigma 1inner}$	$D_{\sigma 2}$	$D_{\sigma 3}$	$D_{\sigma 4}$	$D_{\sigma 5}$	$D_{\sigma 6outer}$
2L2b100m	100	0	2	2	1.01	1.01	0.00	0.00	0.00	0.00
2L2b80m	80	0	2	2	1.01	1.01	0.00	0.00	0.00	0.00
2L2b60m	60	0	2	2	1.02	1.02	0.00	0.00	0.00	0.00
2L2b40m	40	0	2	2	2.47	2.47	0.00	0.00	0.00	0.00
2L2b20m	20	0	2	2	1.95	1.95	0.00	0.00	0.00	0.00
2L3b100m	100	0	3	2	0.67	0.67	0.67	0.00	0.00	0.00
2L3b80m	80	0	3	2	0.67	0.67	0.67	0.00	0.00	0.00
2L3b60m	60	0	3	2	0.00	0.00	0.00	0.00	0.00	0.00
2L3b40m	40	0	3	2	1.68	1.67	1.68	0.00	0.00	0.00
2L3b20m	20	0	3	2	1.35	1.32	1.35	0.00	0.00	0.00
2L4b100m	100	0	4	2	0.50	0.50	0.50	0.50	0.00	0.00
2L4b80m	80	0	4	2	0.51	0.50	0.50	0.51	0.00	0.00
2L4b60m	60	0	4	2	0.51	0.50	0.50	0.52	0.00	0.00
2L4b40m	40	0	4	2	1.27	1.26	1.26	1.27	0.00	0.00
2L4b20m	20	0	4	2	1.03	1.01	1.01	1.03	0.00	0.00

Table A.4.2 Load distribution factors under CHDBC full truck load for 3-lane straight bridges

Bridge	Span (m)	Curvature	Boxes	Lanes	Stress Distribution Factor					
	L	L/R	Nb	NL	$D_{\sigma 1inner}$	$D_{\sigma 2}$	$D_{\sigma 3}$	$D_{\sigma 4}$	$D_{\sigma 5}$	$D_{\sigma 6outer}$
3L3b100m	100	0	3	3	0.97	0.97	0.97	0.00	0.00	0.00
3L3b80m	80	0	3	3	1.01	1.01	1.01	0.00	0.00	0.00
3L3b60m	60	0	3	3	1.03	1.00	1.01	0.00	0.00	0.00
3L3b40m	40	0	3	3	2.42	2.39	2.41	0.00	0.00	0.00
3L3b20m	20	0	3	3	1.97	1.89	1.86	0.00	0.00	0.00
3L4b100m	100	0	4	3	0.76	0.76	0.76	0.76	0.00	0.00
3L4b80m	80	0	4	3	0.76	0.76	0.76	0.76	0.00	0.00
3L4b60m	60	0	4	3	0.76	0.75	0.76	0.77	0.00	0.00
3L4b40m	40	0	4	3	1.83	1.81	1.81	1.83	0.00	0.00
3L4b20m	20	0	4	3	1.46	1.44	1.43	1.46	0.00	0.00
3L5b100m	100	0	5	3	0.60	0.60	0.61	0.60	0.60	0.00
3L5b80m	80	0	5	3	0.61	0.61	0.61	0.61	0.61	0.00
3L5b60m	60	0	5	3	0.62	0.61	0.61	0.61	0.62	0.00
3L5b40m	40	0	5	3	1.48	1.46	1.46	1.46	1.48	0.00
3L5b20m	20	0	5	3	1.20	1.17	1.17	1.17	1.20	0.00

Table A.4.3 Load distribution factors under CHDBC full truck load for 4-lane straight bridges

Bridge	Span (m)	Curvature	Boxes	Lanes	Stress Distribution Factor					
	L	L/R	Nb	NL	$D_{\sigma 1inner}$	$D_{\sigma 2}$	$D_{\sigma 3}$	$D_{\sigma 4}$	$D_{\sigma 5}$	$D_{\sigma 6outer}$
4L4b100m	100	0	4	4	1.01	1.01	1.01	1.01	0.00	0.00
4L4b80m	80	0	4	4	1.01	1.01	1.01	1.01	0.00	0.00
4L4b60m	60	0	4	4	1.02	1.01	1.01	1.03	0.00	0.00
4L4b40m	40	0	4	4	2.39	2.36	2.36	2.39	0.00	0.00
4L4b20m	20	0	4	4	1.89	1.88	1.88	1.89	0.00	0.00
4L5b100m	100	0	5	4	0.81	0.81	0.80	0.81	0.81	0.00
4L5b80m	80	0	5	4	0.81	0.80	0.80	0.80	0.81	0.00
4L5b60m	60	0	5	4	0.82	0.81	0.81	0.81	0.82	0.00
4L5b40m	40	0	5	4	1.93	1.90	1.90	1.90	1.93	0.00
4L5b20m	20	0	5	4	1.56	1.53	1.53	1.53	1.56	0.00
4L6b100m	100	0	6	4	0.67	0.67	0.67	0.67	0.67	0.67
4L6b80m	80	0	6	4	0.67	0.67	0.67	0.67	0.67	0.67
4L6b60m	60	0	6	4	0.69	0.67	0.67	0.67	0.67	0.69
4L6b40m	40	0	6	4	1.39	1.38	1.37	1.37	1.38	1.39
4L5620m	20	0	6	4	1.32	1.29	1.29	1.29	1.29	1.32

Table A.4.4 Load distribution factors under CHDBC full truck load for 2-lane bridges having curvatures of L/R=0.4

Bridge	Span (m)	Curvature	Boxes	Lanes	Stress Distribution Factor					
	L	L/R	Nb	NL	$D_{\sigma 1inner}$	$D_{\sigma 2}$	$D_{\sigma 3}$	$D_{\sigma 4}$	$D_{\sigma 5}$	$D_{\sigma 6outer}$
2L2b100m	100	0.4	2	2	1.02	1.07	0.00	0.00	0.00	0.00
2L2b80m	80	0.4	2	2	1.02	1.07	0.00	0.00	0.00	0.00
2L2b60m	60	0.4	2	2	1.01	1.08	0.00	0.00	0.00	0.00
2L2b40m	40	0.4	2	2	2.48	2.59	0.00	0.00	0.00	0.00
2L2b20m	20	0.4	2	2	1.95	2.05	0.00	0.00	0.00	0.00
2L3b100m	100	0.4	3	2	0.66	0.70	0.74	0.00	0.00	0.00
2L3b80m	80	0.4	3	2	0.66	0.70	0.74	0.00	0.00	0.00
2L3b60m	60	0.4	3	2	0.00	0.00	0.00	0.00	0.00	0.00
2L3b40m	40	0.4	3	2	1.63	1.73	1.83	0.00	0.00	0.00
2L3b20m	20	0.4	3	2	1.30	1.36	1.45	0.00	0.00	0.00
2L4b100m	100	0.4	4	2	0.48	0.52	0.55	0.59	0.00	0.00
2L4b80m	80	0.4	4	2	0.48	0.52	0.55	0.59	0.00	0.00
2L4b60m	60	0.4	4	2	0.46	0.52	0.55	0.62	0.00	0.00
2L4b40m	40	0.4	4	2	1.19	1.27	1.35	1.44	0.00	0.00
2L4b20m	20	0.4	4	2	0.97	1.02	1.06	1.13	0.00	0.00

Table A.4.5 Load distribution factors under CHDBC full truck load for 3-lane bridges having curvatures of L/R=0.4

Bridge	Span (m)	Curvature	Boxes	Lanes	Stress Distribution Factor					
	L	L/R	Nb	NL	$D_{\sigma 1inner}$	$D_{\sigma 2}$	$D_{\sigma 3}$	$D_{\sigma 4}$	$D_{\sigma 5}$	$D_{\sigma 6outer}$
3L3b100m	100	0.4	3	3	0.96	1.00	1.04	0.00	0.00	0.00
3L3b80m	80	0.4	3	3	0.00	0.00	0.00	0.00	0.00	0.00
3L3b60m	60	0.4	3	3	1.00	1.03	1.10	0.00	0.00	0.00
3L3b40m	40	0.4	3	3	2.38	2.47	2.57	0.00	0.00	0.00
3L3b20m	20	0.4	3	3	1.88	1.93	2.01	0.00	0.00	0.00
3L4b100m	100	0.4	4	3	0.72	0.77	0.81	0.84	0.00	0.00
3L4b80m	80	0.4	4	3	0.72	0.77	0.80	0.84	0.00	0.00
3L4b60m	60	0.4	4	3	0.71	0.77	0.81	0.88	0.00	0.00
3L4b40m	40	0.4	4	3	1.74	1.83	1.91	2.01	0.00	0.00
3L4b20m	20	0.4	4	3	1.37	1.45	1.52	1.62	0.00	0.00
3L5b100m	100	0.4	5	3	0.55	0.60	0.63	0.67	0.71	0.00
3L5b80m	80	0.4	5	3	0.56	0.60	0.64	0.67	0.71	0.00
3L5b60m	60	0.4	5	3	0.55	0.60	0.64	0.67	0.74	0.00
3L5b40m	40	0.4	5	3	1.37	1.45	1.52	1.59	1.67	0.00
3L5b20m	20	0.4	5	3	1.10	1.15	1.21	1.26	1.34	0.00

Table A.4.6 Load distribution factors under CHDBC full truck load for 4-lane bridges having curvatures of L/R=0.4

Bridge	Span (m)	Curvature	Boxes	Lanes	Stress Distribution Factor					
	L	L/R	Nb	NL	$D_{\sigma 1inner}$	$D_{\sigma 2}$	$D_{\sigma 3}$	$D_{\sigma 4}$	$D_{\sigma 5}$	$D_{\sigma 6outer}$
4L4b100m	100	0.4	4	4	0.97	1.02	1.06	1.10	0.00	0.00
4L4b80m	80	0.4	4	4	0.97	1.02	1.06	1.10	0.00	0.00
4L4b60m	60	0.4	4	4	0.96	1.02	1.07	1.14	0.00	0.00
4L4b40m	40	0.4	4	4	2.29	2.38	2.49	2.60	0.00	0.00
4L4b20m	20	0.4	4	4	1.75	1.89	2.01	2.11	0.00	0.00
4L5b100m	100	0.4	5	4	0.75	0.80	0.84	0.88	0.91	0.00
4L5b80m	80	0.4	5	4	0.76	0.80	0.84	0.87	0.91	0.00
4L5b60m	60	0.4	5	4	0.75	0.80	0.84	0.87	0.94	0.00
4L5b40m	40	0.4	5	4	1.80	1.88	1.97	2.06	2.16	0.00
4L5b20m	20	0.4	5	4	1.42	1.50	1.59	1.66	1.75	0.00
4L6b100m	100	0.4	6	4	0.61	0.65	0.68	0.72	0.75	0.79
4L6b80m	80	0.4	6	4	0.61	0.64	0.68	0.72	0.75	0.79
4L6b60m	60	0.4	6	4	0.60	0.65	0.68	0.72	0.75	0.82
4L6b40m	40	0.4	6	4	1.26	1.32	1.38	1.45	1.51	1.59
4L5620m	20	0.4	6	4	1.19	1.25	1.31	1.37	1.42	1.49

Table A.4.7 Load distribution factors under CHDBC full truck load for 2-lane bridges having curvatures of L/R=1.0

Bridge	Span (m)	Curvature	Boxes	Lanes	Stress Distribution Factor					
	L	L/R	Nb	NL	$D_{\sigma 1inner}$	$D_{\sigma 2}$	$D_{\sigma 3}$	$D_{\sigma 4}$	$D_{\sigma 5}$	$D_{\sigma 6outer}$
2L2b100m	100	1	2	2	1.15	1.27	0.00	0.00	0.00	0.00
2L2b80m	80	1	2	2	1.15	1.26	0.00	0.00	0.00	0.00
2L2b60m	60	1	2	2	1.10	1.29	0.00	0.00	0.00	0.00
2L2b40m	40	1	2	2	2.77	3.02	0.00	0.00	0.00	0.00
2L2b20m	20	1	2	2	2.18	2.35	0.00	0.00	0.00	0.00
2L3b100m	100	1	3	2	0.72	0.84	0.93	0.00	0.00	0.00
2L3b80m	80	1	3	2	0.72	0.84	0.93	0.00	0.00	0.00
2L3b60m	60	1	3	2	0.67	0.82	0.98	0.00	0.00	0.00
2L3b40m	40	1	3	2	1.75	2.01	2.21	0.00	0.00	0.00
2L3b20m	20	1	3	2	1.40	1.58	1.69	0.00	0.00	0.00
2L4b100m	100	1	4	2	0.48	0.58	0.66	0.73	0.00	0.00
2L4b80m	80	1	4	2	0.49	0.60	0.69	0.78	0.00	0.00
2L4b60m	60	1	4	2	0.44	0.60	0.68	0.84	0.00	0.00
2L4b40m	40	1	4	2	1.19	1.46	1.63	1.80	0.00	0.00
2L4b20m	20	1	4	2	1.02	1.17	1.25	1.33	0.00	0.00

Table A.4.8 Load distribution factors under CHDBC full truck load for 3-lane bridges having curvatures of L/R=1.0

Bridge	Span (m)	Curvature	Boxes	Lanes	Stress Distribution Factor					
	L	L/R	Nb	NL	$D_{\sigma 1inner}$	$D_{\sigma 2}$	$D_{\sigma 3}$	$D_{\sigma 4}$	$D_{\sigma 5}$	$D_{\sigma 6outer}$
3L3b100m	100	1	3	3	1.05	1.17	1.26	0.00	0.00	0.00
3L3b80m	80	1	3	3	1.09	1.21	1.30	0.00	0.00	0.00
3L3b60m	60	1	3	3	1.05	1.18	1.33	0.00	0.00	0.00
3L3b40m	40	1	3	3	2.59	2.85	3.02	0.00	0.00	0.00
3L3b20m	20	1	3	3	2.03	2.25	2.32	0.00	0.00	0.00
3L4b100m	100	1	4	3	0.75	0.88	0.98	1.06	0.00	0.00
3L4b80m	80	1	4	3	0.75	0.88	0.97	1.05	0.00	0.00
3L4b60m	60	1	4	3	0.71	0.88	0.97	1.13	0.00	0.00
3L4b40m	40	1	4	3	1.83	2.10	2.28	2.43	0.00	0.00
3L4b20m	20	1	4	3	1.46	1.70	1.80	1.88	0.00	0.00
3L5b100m	100	1	5	3	0.53	0.66	0.76	0.85	0.93	0.00
3L5b80m	80	1	5	3	0.53	0.66	0.76	0.85	0.93	0.00
3L5b60m	60	1	5	3	0.48	0.65	0.75	0.83	0.99	0.00
3L5b40m	40	1	5	3	1.39	1.63	1.80	1.93	2.06	0.00
3L5b20m	20	1	5	3	1.14	1.34	1.44	1.49	1.56	0.00

Table A.4.9 Load distribution factors under CHDBC full truck load for 4-lane bridges having curvatures of L/R=1.0

Bridge	Span (m)	Curvature	Boxes	Lanes	Stress Distribution Factor					
	L	L/R	Nb	NL	$D_{\sigma 1inner}$	$D_{\sigma 2}$	$D_{\sigma 3}$	$D_{\sigma 4}$	$D_{\sigma 5}$	$D_{\sigma 6outer}$
4L4b100m	100	1	4	4	1.02	1.16	1.26	1.35	0.00	0.00
4L4b80m	80	1	4	4	1.02	1.16	1.26	1.34	0.00	0.00
4L4b60m	60	1	4	4	0.98	1.17	1.27	1.41	0.00	0.00
4L4b40m	40	1	4	4	2.65	2.86	2.97	2.42	0.00	0.00
4L4b20m	20	1	4	4	2.13	2.37	2.45	1.93	0.00	0.00
4L5b100m	100	1	5	4	0.75	0.89	0.99	1.08	1.16	0.00
4L5b80m	80	1	5	4	0.76	0.89	0.99	1.07	1.14	0.00
4L5b60m	60	1	5	4	0.71	0.88	0.98	1.05	1.19	0.00
4L5b40m	40	1	5	4	1.82	2.12	2.32	2.46	2.59	0.00
4L5b20m	20	1	5	4	1.66	1.95	2.09	2.13	2.20	0.00
4L6b100m	100	1	6	4	0.56	0.69	0.80	0.89	0.96	1.03
4L6b80m	80	1	6	4	0.58	0.70	0.80	0.88	0.95	1.01
4L6b60m	60	1	6	4	0.53	0.69	0.79	0.87	0.93	1.07
4L6b40m	40	1	6	4	1.20	1.44	1.61	1.72	1.81	1.93
4L5620m	20	1	6	4	1.42	1.65	1.75	1.80	1.82	1.89

Table A.4.10 Load distribution factors under CHDBC full truck load for 2-lane bridges having curvatures of L/R=1.4

Bridge	Span (m)	Curvature	Boxes	Lanes	Stress Distribution Factor					
	L	L/R	Nb	NL	$D_{\sigma 1inner}$	$D_{\sigma 2}$	$D_{\sigma 3}$	$D_{\sigma 4}$	$D_{\sigma 5}$	$D_{\sigma 6outer}$
2L2b100m	100	0	2	2	1.33	1.50	0.00	0.00	0.00	0.00
2L2b80m	80	0	2	2	1.33	1.48	0.00	0.00	0.00	0.00
2L2b60m	60	0	2	2	1.25	1.53	0.00	0.00	0.00	0.00
2L2b40m	40	0	2	2	3.20	3.49	0.00	0.00	0.00	0.00
2L2b20m	20	0	2	2	2.56	2.67	0.00	0.00	0.00	0.00
2L3b100m	100	0	3	2	0.81	0.98	1.11	0.00	0.00	0.00
2L3b80m	80	0	3	2	0.81	0.98	1.11	0.00	0.00	0.00
2L3b60m	60	0	3	2	0.71	0.96	1.19	0.00	0.00	0.00
2L3b40m	40	0	3	2	1.97	2.36	2.59	0.00	0.00	0.00
2L3b20m	20	0	3	2	1.63	1.85	1.92	0.00	0.00	0.00
2L4b100m	100	0	4	2	0.51	0.69	0.83	0.96	0.00	0.00
2L4b80m	80	0	4	2	0.51	0.69	0.83	0.95	0.00	0.00
2L4b60m	60	0	4	2	0.44	0.71	0.81	1.04	0.00	0.00
2L4b40m	40	0	4	2	1.29	1.70	1.92	2.14	0.00	0.00
2L4b20m	20	0	4	2	1.18	1.40	1.45	1.50	0.00	0.00

Table A.4.11 Load distribution factors under CHDBC full truck load for 3-lane bridges having curvatures of L/R=1.4

Bridge	Span (m)	Curvature	Boxes	Lanes	Stress Distribution Factor					
	L	L/R	Nb	NL	$D_{\sigma 1inner}$	$D_{\sigma 2}$	$D_{\sigma 3}$	$D_{\sigma 4}$	$D_{\sigma 5}$	$D_{\sigma 6outer}$
3L3b100m	100	1.4	3	3	1.19	1.37	1.49	0.00	0.00	0.00
3L3b80m	80	1.4	3	3	1.24	1.42	1.52	0.00	0.00	0.00
3L3b60m	60	1.4	3	3	1.16	1.37	1.56	0.00	0.00	0.00
3L3b40m	40	1.4	3	3	2.98	3.34	3.47	0.00	0.00	0.00
3L3b20m	20	1.4	3	3	2.43	2.64	2.59	0.00	0.00	0.00
3L4b100m	100	1.4	4	3	0.82	1.02	1.16	1.27	0.00	0.00
3L4b80m	80	1.4	4	3	0.83	1.02	1.16	1.26	0.00	0.00
3L4b60m	60	1.4	4	3	0.75	1.03	1.15	1.36	0.00	0.00
3L4b40m	40	1.4	4	3	2.06	2.47	2.67	2.81	0.00	0.00
3L4b20m	20	1.4	4	3	1.76	2.07	2.09	2.09	0.00	0.00
3L5b100m	100	1.4	5	3	0.55	0.75	0.90	1.02	1.13	0.00
3L5b80m	80	1.4	5	3	0.55	0.75	0.90	1.02	1.12	0.00
3L5b60m	60	1.4	5	3	0.45	0.74	0.89	0.99	1.20	0.00
3L5b40m	40	1.4	5	3	1.53	1.93	2.14	2.26	2.41	0.00
3L5b20m	20	1.4	5	3	1.37	1.66	1.72	1.69	1.73	0.00

Table A.4.12 Load distribution factors under CHDBC full truck load for 4-lane bridges having curvatures of L/R=1.4

Bridge	Span (m)	Curvature	Boxes	Lanes	Stress Distribution Factor					
	L	L/R	Nb	NL	$D_{\sigma 1inner}$	$D_{\sigma 2}$	$D_{\sigma 3}$	$D_{\sigma 4}$	$D_{\sigma 5}$	$D_{\sigma 6outer}$
4L4b100m	100	1.4	4	4	1.13	1.35	1.49	1.59	0.00	0.00
4L4b80m	80	1.4	4	4	1.14	1.36	1.48	1.57	0.00	0.00
4L4b60m	60	1.4	4	4	1.09	1.38	1.49	1.66	0.00	0.00
4L4b40m	40	1.4	4	4	2.83	3.27	3.43	3.48	0.00	0.00
4L4b20m	20	1.4	4	4	2.41	2.81	2.76	2.68	0.00	0.00
4L5b100m	100	1.4	5	4	0.80	1.02	1.18	1.29	1.39	0.00
4L5b80m	80	1.4	5	4	0.82	1.03	1.17	1.28	1.36	0.00
4L5b60m	60	1.4	5	4	0.74	1.02	1.16	1.24	1.42	0.00
4L5b40m	40	1.4	5	4	2.05	2.53	2.76	2.86	2.96	0.00
4L5b20m	20	1.4	5	4	1.95	2.29	2.29	2.21	2.19	0.00
4L6b100m	100	1.4	6	4	0.56	0.78	0.94	1.07	1.17	1.26
4L6b80m	80	1.4	6	4	0.56	0.78	0.94	1.07	1.16	1.23
4L6b60m	60	1.4	6	4	0.51	0.79	0.93	1.03	1.09	1.28
4L6b40m	40	1.4	6	4	1.32	1.72	1.92	2.04	2.10	2.20
4L5620m	20	1.4	6	4	1.61	1.93	1.95	1.90	1.84	1.87

Table A.4.13 Load distribution factors under CHDBC full truck load for 2-lane bridges having curvatures of L/R=2.0

Bridge	Span (m)	Curvature	Boxes	Lanes	Stress Distribution Factor					
	L	L/R	Nb	NL	$D_{\sigma 1inner}$	$D_{\sigma 2}$	$D_{\sigma 3}$	$D_{\sigma 4}$	$D_{\sigma 5}$	$D_{\sigma 6outer}$
2L2b100m	100	2	2	2	1.88	2.13	0.00	0.00	0.00	0.00
2L2b80m	80	2	2	2	1.86	2.10	0.00	0.00	0.00	0.00
2L2b60m	60	2	2	2	1.70	2.17	0.00	0.00	0.00	0.00
2L2b40m	40	2	2	2	4.55	4.81	0.00	0.00	0.00	0.00
2L2b20m	20	2	2	2	3.77	3.50	0.00	0.00	0.00	0.00
2L3b100m	100	2	3	2	0.90	1.41	1.78	0.00	0.00	0.00
2L3b80m	80	2	3	2	1.10	1.41	1.59	0.00	0.00	0.00
2L3b60m	60	2	3	2	0.90	1.36	1.73	0.00	0.00	0.00
2L3b40m	40	2	3	2	2.74	3.36	3.58	0.00	0.00	0.00
2L3b20m	20	2	3	2	2.45	2.62	2.48	0.00	0.00	0.00
2L4b100m	100	2	4	2	0.64	0.97	1.21	1.40	0.00	0.00
2L4b80m	80	2	4	2	0.63	0.98	1.20	1.38	0.00	0.00
2L4b60m	60	2	4	2	0.50	1.01	1.17	1.55	0.00	0.00
2L4b40m	40	2	4	2	1.70	2.45	2.72	2.98	0.00	0.00
2L4b20m	20	2	4	2	1.77	2.06	1.97	1.93	0.00	0.00

Table A.4.14 Load distribution factors under CHDBC full truck load for 3-lane bridges having curvatures of L/R=2.0

Bridge	Span (m)	Curvature	Boxes	Lanes	Stress Distribution Factor					
	L	L/R	Nb	NL	$D_{\sigma 1inner}$	$D_{\sigma 2}$	$D_{\sigma 3}$	$D_{\sigma 4}$	$D_{\sigma 5}$	$D_{\sigma 6outer}$
3L3b100m	100	2	3	3	1.65	1.96	2.10	0.00	0.00	0.00
3L3b80m	80	2	3	3	1.73	2.02	2.14	0.00	0.00	0.00
3L3b60m	60	2	3	3	1.57	1.94	2.20	0.00	0.00	0.00
3L3b40m	40	2	3	3	4.34	4.77	4.65	0.00	0.00	0.00
3L3b20m	20	2	3	3	3.94	3.68	3.19	0.00	0.00	0.00
3L4b100m	100	2	4	3	1.09	1.46	1.68	1.82	0.00	0.00
3L4b80m	80	2	4	3	1.11	1.47	1.66	1.78	0.00	0.00
3L4b60m	60	2	4	3	0.98	1.49	1.64	1.96	0.00	0.00
3L4b40m	40	2	4	3	2.95	3.64	3.75	3.78	0.00	0.00
3L4b20m	20	2	4	3	2.98	3.12	2.77	2.54	0.00	0.00
3L5b100m	100	2	5	3	0.65	1.05	1.31	1.49	1.64	0.00
3L5b80m	80	2	5	3	0.65	1.06	1.31	1.47	1.60	0.00
3L5b60m	60	2	5	3	0.47	1.05	1.27	1.40	1.73	0.00
3L5b40m	40	2	5	3	2.15	2.88	3.11	3.14	3.25	0.00
3L5b20m	20	2	5	3	2.37	2.63	2.42	2.15	2.09	0.00

Table A.4.15 Load distribution factors under CHDBC full truck load for 4-lane bridges having curvatures of L/R=2.0

Bridge	Span (m)	Curvature	Boxes	Lanes	Stress Distribution Factor					
	L	L/R	Nb	NL	$D_{\sigma 1inner}$	$D_{\sigma 2}$	$D_{\sigma 3}$	$D_{\sigma 4}$	$D_{\sigma 5}$	$D_{\sigma 6outer}$
4L4b100m	100	2	4	4	1.55	1.95	2.14	2.24	0.00	0.00
4L4b80m	80	2	4	4	1.59	1.96	2.11	2.18	0.00	0.00
4L4b60m	60	2	4	4	1.51	2.01	2.10	2.32	0.00	0.00
4L4b40m	40	2	4	4	4.31	4.88	4.75	4.53	0.00	0.00
4L4b20m	20	2	4	4	4.73	4.28	3.53	3.08	0.00	0.00
4L5b100m	100	2	5	4	1.03	1.46	1.72	1.87	1.97	0.00
4L5b80m	80	2	5	4	1.08	1.50	1.71	1.82	1.90	0.00
4L5b60m	60	2	5	4	0.93	1.47	1.66	1.73	1.98	0.00
4L5b40m	40	2	5	4	3.06	3.87	3.99	3.88	3.84	0.00
4L5b20m	20	2	5	4	3.98	3.76	3.14	2.68	2.47	0.00
4L6b100m	100	2	6	4	0.66	1.09	1.37	1.56	1.69	1.80
4L6b80m	80	2	6	4	0.73	1.14	1.39	1.53	1.63	1.72
4L6b60m	60	2	6	4	0.57	1.13	1.35	1.47	1.52	1.81
4L6b40m	40	2	6	4	1.94	2.69	2.88	2.88	2.80	2.85
4L5620m	20	2	6	4	3.43	3.36	2.85	2.45	2.15	2.09

APPENDIX A.5

Section Properties and Stresses from Beam Theory for prototype bridges

Table A.5.1 Section Properties and Stresses from Beam Theory for 20 meter prototype bridges

Bridge Prototype	Span (m)	No. of Lanes	No. of Boxes	Neutral Axis Y_b (mm)	Moment of Inertia Ic (mm^4)	Live Load Moment (N*mm)	Live Load σ_{simple} (N/mm^2)	Dead Load Moment (N*mm)	Dead Load σ_{simple} (N/mm^2)
2L2B20m	20	2	2	723.2684	26478266823	1417400000	38.71706	1.461E+09	39.898315
2L3B20m	20	2	3	718.9448	17966574593	1417400000	56.71823	982680061	39.322616
2L4B20m	20	2	4	718.3625	13359966692	1417400000	76.21329	748413140	40.242011
3L3B20m	20	3	3	707.1705	27026840932	1417400000	37.08696	1.389E+09	36.345568
3L4B20m	20	3	4	713.0967	19595267670	1417400000	51.58098	1.039E+09	37.800406
3L5B20m	20	3	5	707.1343	16042911682	1417400000	62.4757	841530838	37.092726
4L4B20m	20	4	4	699.4236	27149156238	1417400000	36.51543	1.352E+09	34.841252
4L5B20m	20	4	5	694.0591	22138445613	1417400000	44.4367	1.094E+09	34.308578
4L6B20m	20	4	6	688.8806	18790189906	1417400000	51.96431	922294998	33.812915

Table A.5.2 Section Properties and Stresses from Beam Theory for 40 meter prototype bridges

Bridge Prototype	Span (m)	No. of Lanes	No. of Boxes	Neutral Axis Y_b (mm)	Moment of Inertia Ic (mm^4)	Live Load Moment (N*mm)	Live Load σ_{simple} (N/mm^2)	Dead Load Moment (N*mm)	Dead Load σ_{simple} (N/mm^2)
2L2B40m	40	2	2	1276.39	1.18227E+11	4542400000	49.04012	6.554E+09	70.760796
2L3B40m	40	2	3	1271.849	79752137896	4542400000	72.44001	4.408E+09	70.293873
2L4B40m	40	2	4	1266.693	60394007548	4542400000	95.27148	3.327E+09	69.789438
3L3B40m	40	3	3	1251.338	1.18571E+11	4542400000	47.93832	6.261E+09	66.074058
3L4B40m	40	3	4	1258.775	87093074073	4542400000	65.65229	4.697E+09	67.883247
3L5B40m	40	3	5	1258.448	69307027767	4542400000	82.479	3.799E+09	68.97789
4L4B40m	40	4	4	1239.294	1.18274E+11	4542400000	47.59594	6.111E+09	64.028662
4L5B40m	40	4	5	1230.5	96788643729	4542400000	57.74874	4.902E+09	62.318601
4L6B40m	40	4	6	1233.162	80526079268	4542400000	69.56152	4.085E+09	62.563422

Table A.5.3 Section Properties and Stresses from Beam Theory for 60 meter prototype bridges

Bridge Prototype	Span (m)	No. of Lanes	No. of Boxes	Neutral Axis Y_b (mm)	Moment of Inertia Ic (mm^4)	Live Load Moment (N*mm)	Live Load σ_{simple} (N/mm^2)	Dead Load Moment (N*mm)	Dead Load σ_{simple} (N/mm^2)
2L2B60m	60	2	2	1764.187	3.33993E+11	10183920000	53.7926	1.728E+10	91.290776
2L3B60m	60	2	3	1778.804	2.1825E+11	10183920000	83.00206	1.149E+10	93.666327
2L4B60m	60	2	4	1775.066	1.63711E+11	10183920000	110.421	8.736E+09	94.718727
3L3B60m	60	3	3	1736.949	3.3044E+11	10183920000	53.53156	1.66E+10	87.238464
3L4B60m	60	3	4	1733.373	2.49596E+11	10183920000	70.72444	1.254E+10	87.060666
3L5B60m	60	3	5	1749.659	1.95554E+11	10183920000	91.11771	9.84E+09	88.04236
4L4B60m	60	4	4	1723.949	3.27812E+11	10183920000	53.5568	1.625E+10	85.433357
4L5B60m	60	4	5	1717.973	2.65695E+11	10183920000	65.8488	1.3E+10	84.035122
4L6B60m	60	4	6	1725.297	2.24135E+11	10183920000	78.39152	1.101E+10	84.731166

Table A.5.4 Section Properties and Stresses from Beam Theory for 80 meter prototype bridges

Bridge Prototype	Span (m)	No. of Lanes	No. of Boxes	Neutral Axis Y_b (mm)	Moment of Inertia Ic (mm^4)	Live Load Moment (N*mm)	Live Load σ_{simple} (N/mm^2)	Dead Load Moment (N*mm)	Dead Load σsimple (N/mm^2)
2L2B80m	80	2	2	2223.124	6.97957E+11	15833920000	50.43403	3.519E+10	112.08609
2L3B80m	80	2	3	2234.63	4.6126E+11	15833920000	76.70941	2.355E+10	114.07669
2L4B80m	80	2	4	2240.541	3.43628E+11	15833920000	103.2412	1.756E+10	114.47132
3L3B80m	80	3	3	2193.942	6.87165E+11	15833920000	50.55363	3.394E+10	108.36347
3L4B80m	80	3	4	2193.516	5.203E+11	15833920000	66.7537	2.573E+10	108.49167
3L5B80m	80	3	5	2188.3	4.17081E+11	15833920000	83.07594	2.039E+10	106.96294
4L4B80m	80	4	4	2168.864	6.89865E+11	15833920000	49.78023	3.343E+10	105.09432
4L5B80m	80	4	5	2178.539	5.4802E+11	15833920000	62.94445	2.684E+10	106.70668
4L6B80m	80	4	6	2177.542	4.67278E+11	15833920000	73.78693	2.295E+10	106.96832

Table A.5.5 Section Properties and Stresses from Beam Theory for 100 meter prototype bridges

Bridge Prototype	Span (m)	No. of Lanes	No. of Boxes	Neutral Axis Y_b (mm)	Moment of Inertia Ic (mm^4)	Live Load Moment (N*mm)	Live Load σ_{simple} (N/mm^2)	Dead Load Moment (N*mm)	Dead Load σ_{simple} (N/mm^2)
2L2B100m	100	2	2	2666.388	1.30125E+12	22383920000	45.86684	6.424E+10	131.62468
2L3B100m	100	2	3	2661.926	8.78475E+11	22383920000	67.82704	4.343E+10	131.60725
2L4B100m	100	2	4	2673.832	6.51449E+11	22383920000	91.87347	3.219E+10	132.12244
3L3B100m	100	3	3	2627.525	1.29195E+12	22383920000	45.52359	6.243E+10	126.96309
3L4B100m	100	3	4	2624.609	9.76352E+11	22383920000	60.172	4.725E+10	127.02009
3L5B100m	100	3	5	2613.44	7.89433E+11	22383920000	74.10257	3.791E+10	125.50433
4L4B100m	100	4	4	2604.046	1.29117E+12	22383920000	45.14399	6.159E+10	124.21389
4L5B100m	100	4	5	2614.298	1.02525E+12	22383920000	57.07721	4.929E+10	125.69427
4L6B100m	100	4	6	2606.496	8.60328E+11	22383920000	67.81555	4.143E+10	125.50618

APPENDIX A.6

Typical ABAQUS Input File for 2-lane 4-box girder, 100 m span curved bridges, L/R = 1.0

```
*HEADING
4 BOX CURVED SIMPLY SUPPORTED LINEAR CASE
**DATA CHECK
*PREPRINT,ECHO=YES,MODEL=NO,HISTORY=NO
*Restart,write
***REFERENCE NODE COORDINATES 2L4b100sc inside between-boxes bracings along the bridge**
*NODE
1,0,0,0
8001,0,0,-0.136500
56001,0,0,-4.096000
2,-44.814297,82.032028,0.000000
66,-51.070801,93.484489,0.000000
7202,44.814297,82.032028,0.000000
7266,51.070801,93.484489,0.000000
8006,-45.205330,82.747810,-0.136500
56006,-45.205330,82.747810,-4.096000
15206,45.205330,82.747810,-0.136500
63206,45.205330,82.747810,-4.096000
8062,-50.679768,92.768707,-0.136500
56062,-50.679768,92.768707,-4.096000
15262,50.679768,92.768707,-0.136500
63262,50.679768,92.768707,-4.096000
*********NODE GENERATION FOR END DIAPHRAM***********
*NGEN,NSET=ORIGIN
8001,56001,8000
*NGEN,NSET=NEND
***left end****
2,66,2
8006,56006,8000
8062,56062,8000
8006,8062,2
16006,16062,2
24006,24062,2
32006,32062,2
40006,40062,2
48006,48062,2
56006,56062,2
***right end****
7202,7266,2
15206,63206,8000
15262,63262,8000
15206,15262,2
23206,23262,2
31206,31262,2
39206,39262,2
47206,47262,2
55206,55262,2
63206,63262,2
**********************
```

```
*NSET,NSET=LEFT7
56014,56022,56030,56038,56046,56054,56062
*NSET,NSET=RIGHT7
63214,63222,63230,63238,63246,63254,63262
*****************************NODE GEN. FOR TOP SLAB ************
*NGEN,NSET=NPLATET,LINE=C
2,7202,100,1
4,7204,100,1
6,7206,100,1
8,7208,100,1
10,7210,100,1
12,7212,100,1
14,7214,100,1
16,7216,100,1
18,7218,100,1
20,7220,100,1
22,7222,100,1
24,7224,100,1
26,7226,100,1
28,7228,100,1
30,7230,100,1
32,7232,100,1
34,7234,100,1
36,7236,100,1
38,7238,100,1
40,7240,100,1
42,7242,100,1
44,7244,100,1
46,7246,100,1
48,7248,100,1
50,7250,100,1
52,7252,100,1
54,7254,100,1
56,7256,100,1
58,7258,100,1
60,7260,100,1
62,7262,100,1
64,7264,100,1
66,7266,100,1
*****************************NODE GEN FOR TOP FLANGE **************
*NGEN,NSET=NTOPFLNG,LINE=C
8006,15206,100,8001
8014,15214,100,8001
8022,15222,100,8001
8030,15230,100,8001
8038,15238,100,8001
8046,15246,100,8001
8054,15254,100,8001
8062,15262,100,8001
*****************************NODE GEN. FOR WEBS ******************
*NGEN,NSET=NWEB,LINE=C
16006,23206,100,16001
16014,23214,100,16001
16022,23222,100,16001
16030,23230,100,16001
16038,23238,100,16001
```

16046,23246,100,16001
16054,23254,100,16001
16062,23262,100,16001
****
24006,31206,100,24001
24014,31214,100,24001
24022,31222,100,24001
24030,31230,100,24001
24038,31238,100,24001
24046,31246,100,24001
24054,31254,100,24001
24062,31262,100,24001
****
32006,39206,100,32001
32014,39214,100,32001
32022,39222,100,32001
32030,39230,100,32001
32038,39238,100,32001
32046,39246,100,32001
32054,39254,100,32001
32062,39262,100,32001
****
40006,47206,100,40001
40014,47214,100,40001
40022,47222,100,40001
40030,47230,100,40001
40038,47238,100,40001
40046,47246,100,40001
40054,47254,100,40001
40062,47262,100,40001
****
48006,55206,100,48001
48014,55214,100,48001
48022,55222,100,48001
48030,55230,100,48001
48038,55238,100,48001
48046,55246,100,48001
48054,55254,100,48001
48062,55262,100,48001
****
56006,63206,100,56001
56014,63214,100,56001
56022,63222,100,56001
56030,63230,100,56001
56038,63238,100,56001
56046,63246,100,56001
56054,63254,100,56001
56062,63262,100,56001
**********NODE GEN FOR BOTTOM FLANGE **********
*NGEN,NSET=NPLATEB,LINE=C
56008,63208,100,56001
56010,63210,100,56001
56012,63212,100,56001
56014,63214,100,56001
56016,63216,100,56001
56018,63218,100,56001

```
56020,63220,100,56001
56022,63222,100,56001
56024,63224,100,56001
56026,63226,100,56001
56028,63228,100,56001
56030,63230,100,56001
56032,63232,100,56001
56034,63234,100,56001
56036,63236,100,56001
56038,63238,100,56001
56040,63240,100,56001
56042,63242,100,56001
56044,63244,100,56001
56046,63246,100,56001
56048,63248,100,56001
56050,63250,100,56001
56052,63252,100,56001
56054,63254,100,56001
56056,63256,100,56001
56058,63258,100,56001
56060,63260,100,56001
*****************************ELEMENT GEN FOR TOP SLAB *********************
*ELEMENT,TYPE=S4R
1,2,102,104,4
*ELGEN,ELSET=ESLABT
1,72,100,32,32,2,1
*************************ELEMENT GEN FOR BOTTOM FLANGE *****************
*ELEMENT,TYPE=S4R
2305,56006,56106,56108,56008
2593,56022,56122,56124,56024
2881,56038,56138,56140,56040
3169,56054,56154,56156,56056
*ELGEN,ELSET=FLANGEB
2305,72,100,4,4,2,1
2593,72,100,4,4,2,1
2881,72,100,4,4,2,1
3169,72,100,4,4,2,1
*************************ELEMENT GEN FOR TOP FLANGE ******************
*ELEMENT,TYPE=B31H
3457,8006,8106
3529,8014,8114
3601,8022,8122
3673,8030,8130
3745,8038,8138
3817,8046,8146
3889,8054,8154
3961,8062,8162
*ELGEN,ELSET=TOPFL
3457,72,100,1
3529,72,100,1
3601,72,100,1
3673,72,100,1
3745,72,100,1
3817,72,100,1
3889,72,100,1
3961,72,100,1
```

```
**************************ELEMENT GEN FOR WEBS ********************
*ELEMENT,TYPE=S4R
4033,16006,16106,8106,8006
4465,16014,16114,8114,8014
4897,16022,16122,8122,8022
5329,16030,16130,8130,8030
5761,16038,16138,8138,8038
6193,16046,16146,8146,8046
6625,16054,16154,8154,8054
7057,16062,16162,8162,8062
*ELGEN,ELSET=WEB
4033,72,100,6,6,8000,1
4465,72,100,6,6,8000,1
4897,72,100,6,6,8000,1
5329,72,100,6,6,8000,1
5761,72,100,6,6,8000,1
6193,72,100,6,6,8000,1
6625,72,100,6,6,8000,1
7057,72,100,6,6,8000,1
**************************ELEMENT GEN FOR END DIAPHRAGM ***************
*ELEMENT,TYPE=S4R
7489,16006,16008,8008,8006
7513,16022,16024,8024,8022
7537,16038,16040,8040,8038
7561,16054,16056,8056,8054
7585,23206,23208,15208,15206
7609,23222,23224,15224,15222
7633,23238,23240,15240,15238
7657,23254,23256,15256,15254
*ELGEN,ELSET=DIAPH
7489,4,2,6,6,8000,1
7513,4,2,6,6,8000,1
7537,4,2,6,6,8000,1
7561,4,2,6,6,8000,1
7585,4,2,6,6,8000,1
7609,4,2,6,6,8000,1
7633,4,2,6,6,8000,1
7657,4,2,6,6,8000,1
****************************END FLANGE ELEMENTS ******************
*ELEMENT,TYPE=B31H
7681,8006,8008
7685,8022,8024
7689,8038,8040
7693,8054,8056
7697,15206,15208
7701,15222,15224
7705,15238,15240
7709,15254,15256
*ELGEN,ELSET=ENDFL
7681,4,2,1
7685,4,2,1
7689,4,2,1
7693,4,2,1
7697,4,2,1
7701,4,2,1
7705,4,2,1
```

```
7709,4,2,1
*****************************ELEMENT GEN FOR TRUSS ELEMENTS ***********
*NGEN,NSET=XBP,LINE=C
32010,39210,200,32001
32018,39218,200,32001
32026,39226,200,32001
32034,39234,200,32001
32042,39242,200,32001
32050,39250,200,32001
32058,39258,200,32001
*****************************
*ELEMENT,TYPE=B31H
7713,8406,8414
7714,8406,32410
7715,32410,56414
7716,8414,32410
7717,32410,56406
*ELGEN,ELSET=XBRAC
7713,17,400,20,4,16,5
7714,17,400,20,4,16,5
7715,17,400,20,4,16,5
7716,17,400,20,4,16,5
7717,17,400,20,4,16,5
*************************ELEMENT GEN FOR TRUSSES ELEMENTS BETWEEN BOXES *****
*ELEMENT,TYPE=B31H
20001,8014,8022
20002,8014,32018
20003,32018,56022
20004,8022,32018
20005,32018,56014
20006,56014,56022
*ELGEN,ELSET=XBRACb
20001,19,400,18,3,16,6
20002,19,400,18,3,16,6
20003,19,400,18,3,16,6
20004,19,400,18,3,16,6
20005,19,400,18,3,16,6
20006,19,400,18,3,16,6
*********************************MATERIAL PROPERTIES ***************
*BEAM SECTION,SECTION=RECT,ELSET=XBRAC,MATERIAL=STEEL
.1,.1
5,5
*BEAM SECTION,SECTION=RECT,ELSET=XBRACb,MATERIAL=STEEL
.1,.1
5,5
*SHELL SECTION,ELSET=WEB,MATERIAL=STEEL
.013,5
*BEAM SECTION,SECTION=RECT,ELSET=TOPFL,MATERIAL=STEEL
.032,.6
5,5
*BEAM SECTION,SECTION=RECT,ELSET=ENDFL,MATERIAL=STEEL
.032,.6
5,5
*********************************************
*SHELL SECTION,ELSET=DIAPH,MATERIAL=STEEL
.013,5
```

```
*SHELL SECTION,ELSET=FLANGEB,MATERIAL=STEEL
.030,5
*MATERIAL,NAME=STEEL
*DENSITY
7800
*ELASTIC
200000E6,.3
*SHELL SECTION,ELSET=ESLABT,MATERIAL=CON
.225,5
*MATERIAL,NAME=CON
*DENSITY
2400
*ELASTIC
27000E6,.20
**********MULTIPOINT CONSTRAINT **********
*NGEN,NSET=SLABN6,line=c
6,7206,100
*NGEN,NSET=FLANGEN6,line=c
8006,15206,100
*NGEN,NSET=SLABN14,line=c
14,7214,100
*NGEN,NSET=FLANGEN14,line=c
8014,15214,100
*NGEN,NSET=SLABN22,line=c
22,7222,100
*NGEN,NSET=FLANGEN22,line=c
8022,15222,100
*NGEN,NSET=SLABN30,line=c
30,7230,100
*NGEN,NSET=FLANGEN30,line=c
8030,15230,100
*NGEN,NSET=SLABN38,line=c
38,7238,100
*NGEN,NSET=FLANGEN38,line=c
8038,15238,100
*NGEN,NSET=SLABN46,line=c
46,7246,100
*NGEN,NSET=FLANGEN46,line=c
8046,15246,100
*NGEN,NSET=SLABN54,line=c
54,7254,100
*NGEN,NSET=FLANGEN54,line=c
8054,15254,100
*NGEN,NSET=SLABN62,line=c
62,7262,100
*NGEN,NSET=FLANGEN62,line=c
8062,15262,100
**********
*NSET,NSET=LTOP1
8,10,12
*NSET,NSET=LTOP2
24,26,28
*NSET,NSET=LTOP3
40,42,44
*NSET,NSET=LTOP4
56,58,60
```

```
*NSET,NSET=LBOT1
8008,8010,8012
*NSET,NSET=LBOT2
8024,8026,8028
*NSET,NSET=LBOT3
8040,8042,8044
*NSET,NSET=LBOT4
8056,8058,8060
*NSET,NSET=RTOP1
7208,7210,7212
*NSET,NSET=RTOP2
7224,7226,7228
*NSET,NSET=RTOP3
7240,7242,7244
*NSET,NSET=RTOP4
7256,7258,7260
*NSET,NSET=RBOT1
15208,15210,15212
*NSET,NSET=RBOT2
15224,15226,15228
*NSET,NSET=RBOT3
15240,15242,15244
*NSET,NSET=RBOT4
15256,15258,15260
*MPC
BEAM,SLABN6,FLANGEN6
BEAM,SLABN14,FLANGEN14
BEAM,SLABN22,FLANGEN22
BEAM,SLABN30,FLANGEN30
BEAM,SLABN38,FLANGEN38
BEAM,SLABN46,FLANGEN46
BEAM,SLABN54,FLANGEN54
BEAM,SLABN62,FLANGEN62
BEAM,LBOT1,LTOP1
BEAM,LBOT2,LTOP2
BEAM,LBOT3,LTOP3
BEAM,LBOT4,LTOP4
BEAM,RBOT1,RTOP1
BEAM,RBOT2,RTOP2
BEAM,RBOT3,RTOP3
BEAM,RBOT4,RTOP4
**********************************************************
*BOUNDARY
56006,2,3
LEFT7,2,3
63206,1,3
RIGHT7,1,3
**************Element set for Moment**************
*ELSET,ELSET=MIDSLAB,GEN
1121,1184
*ELSET,ELSET=MIDBOTFLANGE,GEN
2445,2452
2733,2740
3021,3028
3309,3316
*NGEN,NSET=MID
```

```
59606,59662,8
**********************************DEAD LOAD**********************
*STEP
*STATIC
*ELSET,ELSET=LANE,GENERATE
1,2273,32
2,2274,32
3,2275,32
4,2276,32
5,2277,32
6,2278,32
7,2279,32
8,2280,32
9,2281,32
10,2282,32
11,2283,32
12,2284,32
13,2285,32
14,2286,32
15,2287,32
16,2288,32
17,2289,32
18,2290,32
19,2291,32
20,2292,32
21,2293,32
22,2294,32
23,2295,32
24,2296,32
25,2297,32
26,2298,32
27,2299,32
28,2300,32
29,2301,32
30,2302,32
31,2303,32
32,2304,32
*DLOAD
LANE,GRAV,9.81,0,0,-1
FLANGEB,GRAV,9.81,0,0,-1
TOPFL,GRAV,9.81,0,0,-1
WEB,GRAV,9.81,0,0,-1
************Moment Strains************
*ELPRINT,POSITION=AVERAGED AT NODES,ELSET=MIDBOTFLANGE
S11
*ELPRINT,ELSET=XBRAC
SF1
*ELPRINT,ELSET=XBRACb
SF1
*NODEPRINT,NSET=MID
U3
************************************
*ENDSTEP
*STEP
*STATIC
**********************************CONCNTRIC TRUCK LOADING *************
```

```
*ELSET,ELSET=CTRUCK,GENERATE
4,2276,32
5,2277,32
6,2278,32
7,2279,32
8,2280,32
9,2281,32
10,2282,32
11,2283,32
12,2284,32
13,2285,32
14,2286,32
15,2287,32
16,2288,32
17,2289,32
18,2290,32
19,2291,32
20,2292,32
21,2293,32
22,2294,32
23,2295,32
24,2296,32
25,2297,32
26,2298,32
27,2299,32
28,2300,32
29,2301,32
*DLOAD,OP=NEW
CTRUCK,P,-2382
*NSET,NSET=C1TRUCK
3014,3026,3042,3054
*NSET,NSET=C2TRUCK
3514,3526,3542,3554
*NSET,NSET=C3TRUCK
4014,4026,4042,4054
*NSET,NSET=C4TRUCK
4114,4126,4142,4154
*NSET,NSET=C5TRUCK
4314,4326,4342,4354
*CLOAD,OP=NEW
C1TRUCK,3,-60000
C2TRUCK,3,-70000
C3TRUCK,3,-50000
C4TRUCK,3,-50000
C5TRUCK,3,-20000
**********Moment Strains**********
*ELPRINT,POSITION=AVERAGED AT NODES,ELSET=MIDBOTFLANGE
S11
*ELPRINT,ELSET=XBRAC
SF1
*ELPRINT,ELSET=XBRACb
SF1
*NODEPRINT,NSET=MID
U3
**********
*ENDSTEP
```

APPENDIX A.7

Typical ABAQUS Input File for 4-lane 6-box girder, 60 m span curved bridges, L/R = 2.0

```
*HEADING
6BOX CURVED SIMPLY SUPPORTED LINEAR CASE
**DATA CHECK
*PREPRINT,ECHO=YES,MODEL=NO,HISTORY=NO
*Restart,write
***REFERENCE NODE COORDINATES 4L6b60sc inside between-boxes bracings along the bridge**
*NODE
1,0,0,0
8001,0,0,-0.127500
56001,0,0,-2.499000
2,-18.175774,11.670529,0.000000
98,-32.312489,20.747608,0.000000
7202,18.175774,11.670529,0.000000
7298,32.312489,20.747608,0.000000
8006,-18.764805,12.048741,-0.127500
56006,-18.764805,12.048741,-2.499000
15206,18.764805,12.048741,-0.127500
63206,18.764805,12.048741,-2.499000
8094,-31.723457,20.369396,-0.127500
56094,-31.723457,20.369396,-2.499000
15294,31.723457,20.369396,-0.127500
63294,31.723457,20.369396,-2.499000
*********NODE GENERATION FOR END DIAPHRAM***********
*NGEN,NSET=ORIGIN
8001,56001,8000
*NGEN,NSET=NEND
***left end****
2,98,2
8006,56006,8000
8094,56094,8000
8006,8094,2
16006,16094,2
24006,24094,2
32006,32094,2
40006,40094,2
48006,48094,2
56006,56094,2
***right end****
7202,7298,2
15206,63206,8000
15294,63294,8000
15206,15294,2
23206,23294,2
31206,31294,2
39206,39294,2
47206,47294,2
55206,55294,2
63206,63294,2
**********************
```

```
*NSET,NSET=LEFT11
56014,56022,56030,56038,56046,56054,56062,56070,56078,56086,56094
*NSET,NSET=RIGHT11
63214,63222,63230,63238,63246,63254,63262,63270,63278,63286,63294
*********************************NODE GEN. FOR TOP SLAB ************
*NGEN,NSET=NPLATET,LINE=C
2,7202,100,1
4,7204,100,1
6,7206,100,1
8,7208,100,1
10,7210,100,1
12,7212,100,1
14,7214,100,1
16,7216,100,1
18,7218,100,1
20,7220,100,1
22,7222,100,1
24,7224,100,1
26,7226,100,1
28,7228,100,1
30,7230,100,1
32,7232,100,1
34,7234,100,1
36,7236,100,1
38,7238,100,1
40,7240,100,1
42,7242,100,1
44,7244,100,1
46,7246,100,1
48,7248,100,1
50,7250,100,1
52,7252,100,1
54,7254,100,1
56,7256,100,1
58,7258,100,1
60,7260,100,1
62,7262,100,1
64,7264,100,1
66,7266,100,1
68,7268,100,1
70,7270,100,1
72,7272,100,1
74,7274,100,1
76,7276,100,1
78,7278,100,1
80,7280,100,1
82,7282,100,1
84,7284,100,1
86,7286,100,1
88,7288,100,1
90,7290,100,1
92,7292,100,1
94,7294,100,1
96,7296,100,1
98,7298,100,1
*****************************NODE GEN FOR TOP FLANGE **************
```

```
*NGEN,NSET=NTOPFLNG,LINE=C
8006,15206,100,8001
8014,15214,100,8001
8022,15222,100,8001
8030,15230,100,8001
8038,15238,100,8001
8046,15246,100,8001
8054,15254,100,8001
8062,15262,100,8001
8070,15270,100,8001
8078,15278,100,8001
8086,15286,100,8001
8094,15294,100,8001
**********NODE GEN. FOR WEBS **********
*NGEN,NSET=NWEB,LINE=C
16006,23206,100,16001
16014,23214,100,16001
16022,23222,100,16001
16030,23230,100,16001
16038,23238,100,16001
16046,23246,100,16001
16054,23254,100,16001
16062,23262,100,16001
16070,23270,100,16001
16078,23278,100,16001
16086,23286,100,16001
16094,23294,100,16001
**********
24006,31206,100,24001
24014,31214,100,24001
24022,31222,100,24001
24030,31230,100,24001
24038,31238,100,24001
24046,31246,100,24001
24054,31254,100,24001
24062,31262,100,24001
24070,31270,100,24001
24078,31278,100,24001
24086,31286,100,24001
24094,31294,100,24001
**********
32006,39206,100,32001
32014,39214,100,32001
32022,39222,100,32001
32030,39230,100,32001
32038,39238,100,32001
32046,39246,100,32001
32054,39254,100,32001
32062,39262,100,32001
32070,39270,100,32001
32078,39278,100,32001
32086,39286,100,32001
32094,39294,100,32001
**********
40006,47206,100,40001
40014,47214,100,40001
```

```
40022,47222,100,40001
40030,47230,100,40001
40038,47238,100,40001
40046,47246,100,40001
40054,47254,100,40001
40062,47262,100,40001
40070,47270,100,40001
40078,47278,100,40001
40086,47286,100,40001
40094,47294,100,40001
************************
48006,55206,100,48001
48014,55214,100,48001
48022,55222,100,48001
48030,55230,100,48001
48038,55238,100,48001
48046,55246,100,48001
48054,55254,100,48001
48062,55262,100,48001
48070,55270,100,48001
48078,55278,100,48001
48086,55286,100,48001
48094,55294,100,48001
*****************************
56006,63206,100,56001
56014,63214,100,56001
56022,63222,100,56001
56030,63230,100,56001
56038,63238,100,56001
56046,63246,100,56001
56054,63254,100,56001
56062,63262,100,56001
56070,63270,100,56001
56078,63278,100,56001
56086,63286,100,56001
56094,63294,100,56001
*****************************NODE GEN FOR BOTTOM FLANGE ******************
*NGEN,NSET=NPLATEB,LINE=C
56008,63208,100,56001
56010,63210,100,56001
56012,63212,100,56001
56014,63214,100,56001
56016,63216,100,56001
56018,63218,100,56001
56020,63220,100,56001
56022,63222,100,56001
56024,63224,100,56001
56026,63226,100,56001
56028,63228,100,56001
56030,63230,100,56001
56032,63232,100,56001
56034,63234,100,56001
56036,63236,100,56001
56038,63238,100,56001
56040,63240,100,56001
56042,63242,100,56001
```

```
56044,63244,100,56001
56046,63246,100,56001
56048,63248,100,56001
56050,63250,100,56001
56052,63252,100,56001
56054,63254,100,56001
56056,63256,100,56001
56058,63258,100,56001
56060,63260,100,56001
56062,63262,100,56001
56064,63264,100,56001
56066,63266,100,56001
56068,63268,100,56001
56070,63270,100,56001
56072,63272,100,56001
56074,63274,100,56001
56076,63276,100,56001
56078,63278,100,56001
56080,63280,100,56001
56082,63282,100,56001
56084,63284,100,56001
56086,63286,100,56001
56088,63288,100,56001
56090,63290,100,56001
56092,63292,100,56001
*****************************ELEMENT GEN FOR TOP SLAB *********************
*ELEMENT,TYPE=S4R
1,2,102,104,4
*ELGEN,ELSET=ESLABT
1,72,100,48,48,2,1
*************************ELEMENT GEN FOR BOTTOM FLANGE *****************
*ELEMENT,TYPE=S4R
3457,56006,56106,56108,56008
3745,56022,56122,56124,56024
4033,56038,56138,56140,56040
4321,56054,56154,56156,56056
4609,56070,56170,56172,56072
4897,56086,56186,56188,56088
*ELGEN,ELSET=FLANGEB
3457,72,100,4,4,2,1
3745,72,100,4,4,2,1
4033,72,100,4,4,2,1
4321,72,100,4,4,2,1
4609,72,100,4,4,2,1
4897,72,100,4,4,2,1
*************************ELEMENT GEN FOR TOP FLANGE ******************
*ELEMENT,TYPE=B31H
5185,8006,8106
5257,8014,8114
5329,8022,8122
5401,8030,8130
5473,8038,8138
5545,8046,8146
5617,8054,8154
5689,8062,8162
5761,8070,8170
```

```
5833,8078,8178
5905,8086,8186
5977,8094,8194
*ELGEN,ELSET=TOPFL
5185,72,100,1
5257,72,100,1
5329,72,100,1
5401,72,100,1
5473,72,100,1
5545,72,100,1
5617,72,100,1
5689,72,100,1
5761,72,100,1
5833,72,100,1
5905,72,100,1
5977,72,100,1
**********ELEMENT GEN FOR WEBS **********
*ELEMENT,TYPE=S4R
6049,16006,16106,8106,8006
6481,16014,16114,8114,8014
6913,16022,16122,8122,8022
7345,16030,16130,8130,8030
7777,16038,16138,8138,8038
8209,16046,16146,8146,8046
8641,16054,16154,8154,8054
9073,16062,16162,8162,8062
9505,16070,16170,8170,8070
9937,16078,16178,8178,8078
10369,16086,16186,8186,8086
10801,16094,16194,8194,8094
*ELGEN,ELSET=WEB
6049,72,100,6,6,8000,1
6481,72,100,6,6,8000,1
6913,72,100,6,6,8000,1
7345,72,100,6,6,8000,1
7777,72,100,6,6,8000,1
8209,72,100,6,6,8000,1
8641,72,100,6,6,8000,1
9073,72,100,6,6,8000,1
9505,72,100,6,6,8000,1
9937,72,100,6,6,8000,1
10369,72,100,6,6,8000,1
10801,72,100,6,6,8000,1
**********ELEMENT GEN FOR END DIAPHRAGM **********
*ELEMENT,TYPE=S4R
11233,16006,16008,8008,8006
11257,16022,16024,8024,8022
11281,16038,16040,8040,8038
11305,16054,16056,8056,8054
11329,16070,16072,8072,8070
11353,16086,16088,8088,8086
11377,23206,23208,15208,15206
11401,23222,23224,15224,15222
11425,23238,23240,15240,15238
11449,23254,23256,15256,15254
11473,23270,23272,15272,15270
```

```
11497,23286,23288,15288,15286
*ELGEN,ELSET=DIAPH
11233,4,2,6,6,8000,1
11257,4,2,6,6,8000,1
11281,4,2,6,6,8000,1
11305,4,2,6,6,8000,1
11329,4,2,6,6,8000,1
11353,4,2,6,6,8000,1
11377,4,2,6,6,8000,1
11401,4,2,6,6,8000,1
11425,4,2,6,6,8000,1
11449,4,2,6,6,8000,1
11473,4,2,6,6,8000,1
11497,4,2,6,6,8000,1
*****************************END FLANGE ELEMENTS ****************
*ELEMENT,TYPE=B31H
11521,8006,8008
11525,8022,8024
11529,8038,8040
11533,8054,8056
11537,8070,8072
11541,8086,8088
11545,15206,15208
11549,15222,15224
11553,15238,15240
11557,15254,15256
11561,15270,15272
11565,15286,15288
*ELGEN,ELSET=ENDFL
11521,4,2,1
11525,4,2,1
11529,4,2,1
11533,4,2,1
11537,4,2,1
11541,4,2,1
11545,4,2,1
11549,4,2,1
11553,4,2,1
11557,4,2,1
11561,4,2,1
11565,4,2,1
*******************************ELEMENT GEN FOR TRUSS ELEMENTS ***********
*NGEN,NSET=XBP,LINE=C
32010,39210,200,32001
32018,39218,200,32001
32026,39226,200,32001
32034,39234,200,32001
32042,39242,200,32001
32050,39250,200,32001
32058,39258,200,32001
32066,39266,200,32001
32074,39274,200,32001
32082,39282,200,32001
32090,39290,200,32001
*****************************
*ELEMENT,TYPE=B31H
```

```
11569,8906,8914
11570,8906,32910
11571,32910,56914
11572,8914,32910
11573,32910,56906
*ELGEN,ELSET=XBRAC
11569,7,900,30,6,16,5
11570,7,900,30,6,16,5
11571,7,900,30,6,16,5
11572,7,900,30,6,16,5
11573,7,900,30,6,16,5
**************************ELEMENT GEN FOR TRUSSES ELEMENTS BETWEEN BOXES *****
*ELEMENT,TYPE=B31H
20001,8014,8022
20002,8014,32018
20003,32018,56022
20004,8022,32018
20005,32018,56014
20006,56014,56022
*ELGEN,ELSET=XBRACb
20001,9,900,30,5,16,6
20002,9,900,30,5,16,6
20003,9,900,30,5,16,6
20004,9,900,30,5,16,6
20005,9,900,30,5,16,6
20006,9,900,30,5,16,6
**********************************MATERIAL PROPERTIES ****************
*BEAM SECTION,SECTION=RECT,ELSET=XBRAC,MATERIAL=STEEL
.1,.1
5,5
*BEAM SECTION,SECTION=RECT,ELSET=XBRACb,MATERIAL=STEEL
.1,.1
5,5
*SHELL SECTION,ELSET=WEB,MATERIAL=STEEL
.012,5
*BEAM SECTION,SECTION=RECT,ELSET=TOPFL,MATERIAL=STEEL
.030,.6
5,5
*BEAM SECTION,SECTION=RECT,ELSET=ENDFL,MATERIAL=STEEL
.030,.6
5,5
**********************************************
*SHELL SECTION,ELSET=DIAPH,MATERIAL=STEEL
.012,5
*SHELL SECTION,ELSET=FLANGEB,MATERIAL=STEEL
.027,5
*MATERIAL,NAME=STEEL
*DENSITY
7800
*ELASTIC
200000E6,.3
*SHELL SECTION,ELSET=ESLABT,MATERIAL=CON
.225,5
*MATERIAL,NAME=CON
*DENSITY
2400
```

```
*ELASTIC
27000E6,.20
*****************MULTIPOINT CONSTRAINT ***************
*NGEN,NSET=SLABN6,line=c
6,7206,100
*NGEN,NSET=FLANGEN6,line=c
8006,15206,100
*NGEN,NSET=SLABN14,line=c
14,7214,100
*NGEN,NSET=FLANGEN14,line=c
8014,15214,100
*NGEN,NSET=SLABN22,line=c
22,7222,100
*NGEN,NSET=FLANGEN22,line=c
8022,15222,100
*NGEN,NSET=SLABN30,line=c
30,7230,100
*NGEN,NSET=FLANGEN30,line=c
8030,15230,100
*NGEN,NSET=SLABN38,line=c
38,7238,100
*NGEN,NSET=FLANGEN38,line=c
8038,15238,100
*NGEN,NSET=SLABN46,line=c
46,7246,100
*NGEN,NSET=FLANGEN46,line=c
8046,15246,100
*NGEN,NSET=SLABN54,line=c
54,7254,100
*NGEN,NSET=FLANGEN54,line=c
8054,15254,100
*NGEN,NSET=SLABN62,line=c
62,7262,100
*NGEN,NSET=FLANGEN62,line=c
8062,15262,100
*NGEN,NSET=SLABN70,line=c
70,7270,100
*NGEN,NSET=FLANGEN70,line=c
8070,15270,100
*NGEN,NSET=SLABN78,line=c
78,7278,100
*NGEN,NSET=FLANGEN78,line=c
8078,15278,100
*NGEN,NSET=SLABN86,line=c
86,7286,100
*NGEN,NSET=FLANGEN86,line=c
8086,15286,100
*NGEN,NSET=SLABN94,line=c
94,7294,100
*NGEN,NSET=FLANGEN94,line=c
8094,15294,100
****************************************
*NSET,NSET=LTOP1
8,10,12
*NSET,NSET=LTOP2
24,26,28
```

```
*NSET,NSET=LTOP3
40,42,44
*NSET,NSET=LTOP4
56,58,60
*NSET,NSET=LTOP5
72,74,76
*NSET,NSET=LTOP6
88,90,92
*NSET,NSET=LBOT1
8008,8010,8012
*NSET,NSET=LBOT2
8024,8026,8028
*NSET,NSET=LBOT3
8040,8042,8044
*NSET,NSET=LBOT4
8056,8058,8060
*NSET,NSET=LBOT5
8072,8074,8076
*NSET,NSET=LBOT6
8088,8090,8092
*NSET,NSET=RTOP1
7208,7210,7212
*NSET,NSET=RTOP2
7224,7226,7228
*NSET,NSET=RTOP3
7240,7242,7244
*NSET,NSET=RTOP4
7256,7258,7260
*NSET,NSET=RTOP5
7272,7274,7276
*NSET,NSET=RTOP6
7288,7290,7292
*NSET,NSET=RBOT1
15208,15210,15212
*NSET,NSET=RBOT2
15224,15226,15228
*NSET,NSET=RBOT3
15240,15242,15244
*NSET,NSET=RBOT4
15256,15258,15260
*NSET,NSET=RBOT5
15272,15274,15276
*NSET,NSET=RBOT6
15288,15290,15292
*MPC
BEAM,SLABN6,FLANGEN6
BEAM,SLABN14,FLANGEN14
BEAM,SLABN22,FLANGEN22
BEAM,SLABN30,FLANGEN30
BEAM,SLABN38,FLANGEN38
BEAM,SLABN46,FLANGEN46
BEAM,SLABN54,FLANGEN54
BEAM,SLABN62,FLANGEN62
BEAM,SLABN70,FLANGEN70
BEAM,SLABN78,FLANGEN78
BEAM,SLABN86,FLANGEN86
```

```
BEAM,SLABN94,FLANGEN94
BEAM,LBOT1,LTOP1
BEAM,LBOT2,LTOP2
BEAM,LBOT3,LTOP3
BEAM,LBOT4,LTOP4
BEAM,LBOT5,LTOP5
BEAM,LBOT6,LTOP6
BEAM,RBOT1,RTOP1
BEAM,RBOT2,RTOP2
BEAM,RBOT3,RTOP3
BEAM,RBOT4,RTOP4
BEAM,RBOT5,RTOP5
BEAM,RBOT6,RTOP6
**********************************************************
*BOUNDARY
56006,2,3
LEFT11,2,3
63206,1,3
RIGHT11,1,3
**************Element set for Moment**************
*ELSET,ELSET=MIDSLAB,GEN
1681,1776
*ELSET,ELSET=MIDBOTFLANGE,GEN
3597,3604
3885,3892
4173,4180
4461,4468
4749,4758
5037,5044
*NGEN,NSET=MID
59606,59694,8
************************************
**********************************DEAD LOAD***********************
*STEP
*STATIC
*ELSET,ELSET=LANE,GENERATE
1,3409,48
2,3410,48
3,3411,48
4,3412,48
5,3413,48
6,3414,48
7,3415,48
8,3416,48
9,3417,48
10,3418,48
11,3419,48
12,3420,48
13,3421,48
14,3422,48
15,3423,48
16,3424,48
17,3425,48
18,3426,48
19,3427,48
20,3428,48
```

```
21,3429,48
22,3430,48
23,3431,48
24,3432,48
25,3433,48
26,3434,48
27,3435,48
28,3436,48
29,3437,48
30,3438,48
31,3439,48
32,3440,48
33,3441,48
34,3442,48
35,3443,48
36,3444,48
37,3445,48
38,3446,48
39,3447,48
40,3448,48
41,3449,48
42,3450,48
43,3451,48
44,3452,48
45,3453,48
46,3454,48
47,3455,48
48,3456,48
*DLOAD
LANE,GRAV,9.81,0,0,-1
FLANGEB,GRAV,9.81,0,0,-1
TOPFL,GRAV,9.81,0,0,-1
WEB,GRAV,9.81,0,0,-1
**********Moment Strains**********
*ELPRINT,POSITION=AVERAGED AT NODES,ELSET=MIDBOTFLANGE
S11
*ELPRINT,ELSET=XBRAC
SF1
*ELPRINT,ELSET=XBRACb
SF1
*NODEPRINT,NSET=MID
U3
**********
*ENDSTEP
*STEP
*STATIC
**********CONCNTRIC TRUCK LOADING **********
*ELSET,ELSET=CTRUCK,GENERATE
4,3412,48
5,3413,48
6,3414,48
7,3415,48
8,3416,48
9,3417,48
10,3418,48
11,3419,48
```

```
12,3420,48
13,3421,48
14,3422,48
15,3423,48
16,3424,48
17,3425,48
18,3426,48
19,3427,48
20,3428,48
21,3429,48
22,3430,48
23,3431,48
24,3432,48
25,3433,48
26,3434,48
27,3435,48
28,3436,48
29,3437,48
30,3438,48
31,3439,48
32,3440,48
33,3441,48
34,3442,48
35,3443,48
36,3444,48
37,3445,48
38,3446,48
39,3447,48
40,3448,48
41,3449,48
42,3450,48
43,3451,48
44,3452,48
45,3453,48
*DLOAD,OP=NEW
CTRUCK,P,-2449
*NSET,NSET=C1TRUCK
2712,2722,2734,2744,2756,2766,2778,2788
*NSET,NSET=C2TRUCK
3512,3522,3534,3544,3556,3566,3578,3588
*NSET,NSET=C3TRUCK
4212,4222,4234,4244,4256,4266,4278,4288
*NSET,NSET=C4TRUCK
4312,4322,4334,4344,4356,4366,4378,4388
*NSET,NSET=C5TRUCK
4712,4722,4734,4744,4756,4766,4778,4788
*CLOAD,OP=NEW
C1TRUCK,3,-60000
C2TRUCK,3,-70000
C3TRUCK,3,-50000
C4TRUCK,3,-50000
C5TRUCK,3,-20000
**********Moment Strains**********
*ELPRINT,POSITION=AVERAGED AT NODES,ELSET=MIDBOTFLANGE
S11
*ELPRINT,ELSET=XBRAC
```

```
SF1
*ELPRINT,ELSET=XBRACb
SF1
*NODEPRINT,NSET=MID
U3
**********************************
*ENDSTEP
```

APPENDIX A.8

Geometries of prototype bridges

Table A8.1 Geometries of bridge prototypes of 20m span

Span (m)	No. of lanes	No. of boxes	Cross-sectional dimensions, mm								
			A	B	C	D	F	t_1	t_2	t_3	t_4
20	2	2	9300	2325	300	800	1025	16	10	15	225
20	2	3	9300	1550	300	800	1025	11	8	15	225
20	2	4	9300	1160	300	800	1025	10	8	14	225
20	3	3	13050	2175	300	800	1025	16	10	17	225
20	3	4	13050	1630	300	800	1025	12	8	16	225
20	3	5	13050	1305	300	800	1025	10	8	16	225
20	4	4	16800	2100	300	800	1025	16	10	18	225
20	4	5	16800	1680	300	800	1025	13	10	18	225
20	4	6	16800	1400	300	800	1025	11	10	18	225

Table A.8.2 Geometries of bridge prototypes of 40 m span

Span (m)	No. of lanes	No. of boxes	Cross-sectional dimensions, mm								
			A	B	C	D	F	t_1	t_2	t_3	t_4
40	2	2	9300	2325	375	1600	1825	28	14	18	225
40	2	3	9300	1550	375	1600	1825	19	10	18	225
40	2	4	9300	1160	375	1600	1825	14	8	18	225
40	3	3	13050	2175	375	1600	1825	28	14	20	225
40	3	4	13050	1630	375	1600	1825	21	11	19	225
40	3	5	13050	1305	375	1600	1825	17	10	18	225
40	4	4	16800	2100	375	1600	1825	28	14	21	225
40	4	5	16800	1680	375	1600	1825	22	11	22	225
40	4	6	16800	1400	375	1600	1825	19	9	22	225

Table A.8.3 Geometries of bridge prototypes of 60 m span

Span (m)	No. of lanes	No. of boxes	Cross-sectional dimensions, mm								
			A	B	C	D	F	t_1	t_2	t_3	t_4
60	2	2	9300	2325	450	2400	2625	40	18	23	225
60	2	3	9300	1550	450	2400	2625	27	12	22	225
60	2	4	9300	1160	450	2400	2625	20	10	21	225
60	3	3	13050	2175	450	2400	2625	40	18	25	225
60	3	4	13050	1630	450	2400	2625	30	14	25	225
60	3	5	13050	1305	450	2400	2625	24	10	25	225
60	4	4	16800	2100	450	2400	2625	40	18	26	225
60	4	5	16800	1680	450	2400	2625	32	14	27	225
60	4	6	16800	1400	450	2400	2625	30	12	27	225

Table A.8.4 Geometries of bridge prototypes of 80 m span

Span (m)	No. of lanes	No. of boxes	Cross-sectional dimensions, mm								
			A	B	C	D	F	t_1	t_2	t_3	t_4
80	2	2	9300	2325	450	3200	3425	52	22	26	225
80	2	3	9300	1550	450	3200	3425	35	15	25	225
80	2	4	9300	1160	450	3200	3425	26	11	25	225
80	3	3	13050	2175	450	3200	3425	52	22	28	225
80	3	4	13050	1630	450	3200	3425	40	17	28	225
80	3	5	13050	1305	450	3200	3425	31	13	29	225
80	4	4	16800	2100	450	3200	3425	52	22	30	225
80	4	5	16800	1680	450	3200	3425	42	18	29	225
80	4	6	16800	1400	450	3200	3425	38	16	29	225

Table A.8.5 Geometries of bridge prototypes of 100 m span

Span (m)	No. of lanes	No. of boxes	Cross-sectional dimensions, mm								
			A	B	C	D	F	t_1	t_2	t_3	t_4
100	2	2	9300	2325	600	4000	4225	64	26	30	225
100	2	3	9300	1550	600	4000	4225	43	18	30	225
100	2	4	9300	1160	600	4000	4225	32	13	30	225
100	3	3	13050	2175	600	4000	4225	64	26	33	225
100	3	4	13050	1630	600	4000	4225	48	20	33	225
100	3	5	13050	1305	600	4000	4225	38	16	34	225
100	4	4	16800	2100	600	4000	4225	64	26	35	225
100	4	5	16800	1680	600	4000	4225	51	21	34	225
00	4	6	16800	1400	600	4000	4225	42	18	34	225